Iowa Research Online
The University of Iowa's Institutional Repository

University of Iowa
Iowa Research Online

Theses and Dissertations

Summer 2016

Surge free added resistance tests in oblique wave headings for the KRISO container ship model

Mark Ryan Stocker
University of Iowa

Follow this and additional works at: https://ir.uiowa.edu/etd

 Part of the Mechanical Engineering Commons

Copyright 2016 Mark Ryan Stocker

This thesis is available at Iowa Research Online: https://ir.uiowa.edu/etd/2148

Recommended Citation

Stocker, Mark Ryan. "Surge free added resistance tests in oblique wave headings for the KRISO container ship model." MS (Master of Science) thesis, University of Iowa, 2016.
https://doi.org/10.17077/etd.augghs5m

Follow this and additional works at: https://ir.uiowa.edu/etd

 Part of the Mechanical Engineering Commons

www.manaraa.com

SURGE FREE ADDED RESISTANCE TESTS IN OBLIQUE WAVE HEADINGS FOR THE KRISO CONTAINER SHIP MODEL

by

Mark Ryan Stocker

A thesis submitted in partial fulfillment
of the requirements for the Master of Science
degree in Mechanical Engineering in the
Graduate College of
The University of Iowa

August 2016

Thesis Supervisors: Professor Frederick Stern
Associate Research Scientist Yugo Sanada

www.manaraa.com

Copyright by

MARK RYAN STOCKER

2016

All Rights Reserved

www.manaraa.com

Graduate College
The University of Iowa
Iowa City, Iowa

CERTIFICATE OF APPROVAL

_____

MASTER'S THESIS

_____

This is to certify that the Master's thesis of

Mark Ryan Stocker

has been approved by the Examining Committee for
the thesis requirement for the Master of Science degree
in Mechanical Engineering at the August 2016 graduation.

Thesis Committee: _____
Frederick Stern, Thesis Supervisor

_____
Yugo Sanada, Thesis Supervisor

_____
Albert Ratner

www.manaraa.com

To my beloved Amanda for the unwavering support throughout my studies and research.

www.manaraa.com

ACKNOWLEDGEMENTS

I would like to thank Dr. Frederick Stern, my thesis co-supervisor, and Dr. Yugo Sanada, my thesis co-supervisor, for their guidance, support, and patience with me during the completion of my research and thesis. I greatly appreciate the opportunity to work with and learn from someone as well respected as Dr. Frederick Stern in the hydrodynamics community. I am very grateful for the dedication Dr. Yugo Sanada has provided as a supervisor and a teacher through the research process. His expertise, breadth of knowledge, and willingness to teach were paramount to the success of this research.

Several test cases are used for the NATO RTO Task Group AVT-216 and Tokyo 2015 CFD Workshop. I would like to thank the Office of Naval Research, who sponsored this research under the grants N00014-01-1-0073 and NICOP N00014-06-1-064 administered by Drs. Thomas Fu. Also, Naval Engineering Education Consortium (NEEC) granted partial sponsorship of this research administered by Prof. Steven Ceccio.

The KCS research at IIHR was done as part of a joint study with FORCE Technologies under support of ONR Global Grant N629091217081 from Naval International Cooperative Opportunities in Science and Technology Program (NICOP). I would like to thank Drs. Claus Simonsen and Janne Otzen for the collaborative effort between facilities.

I would like to thank the support faculty at IIHR-Hydroscience & Engineering for committing their time to help with technical support and experimental set up.

www.manaraa.com

ABSTRACT

Surge Free Added Resistance testing in variable head wave conditions were completed for a container ship model. The added resistance experiments include calm water, head wave, and oblique wave cases with a focus on establishing a validation benchmark for CFD codes computing the added resistance and motions of the ship model during maneuvering. The ship used is a 1/85.19 scale KRISO Container Ship, KCS, model with a length of 2.70 m. Tests were performed at the IIHR wave basin. The 20 x 40 x 4.5 m wave basin is equipped with 6 inline plunger type wave makers and a 3 degrees of freedom carriage. A 4 degrees of freedom, surge, heave, roll, and pitch free mount with a mass spring damper system was used to tow the model. Calm water tests were performed for 13 Froude numbers between 0.0867 and 0.2817. The resistance coefficients, sinkage, and trim were found for each test. The calm water results were obtained and compared to results from towing tank facilities, with traditional mounts, to estimate facility biases at the IIHR wave basin. The results show that the size difference of the IIHR model and surge free motion create magnitude differences between facilities. Head and oblique wave tests were performed at Froude number 0.26 and wave height to wavelength ratio, H/λ, of 0.0167. For all wave tests, time histories of wave amplitude, resistance, and 4 DOF were measured. Fourier analysis was completed for all time histories of waves, forces, and motions and the 0^{th}, 1^{st}, and 2^{nd} harmonic amplitudes and phases are presented. All head wave results are compared to other facilities data taken in a towing tank with a traditional mount. The data from all wave heading data was analyzed with a focus on the trends with incremented wave encounter angle. Most harmonic amplitudes show good agreement between all facilities, but removal of the small model used by IIHR shows even better agreement between facilities. The oblique wave heading data shows good agreement with the only other experimental oblique wave added resistance testing. Complete uncertainty analysis was completed for select cases for calm water, head wave, and oblique wave conditions. The uncertainty showed accurate data form most wavelength settings.

www.manaraa.com

PUBLIC ABSTRACT

In an effort to reduce the global warming impact of the maritime industry, the International Maritime Organization has created the Energy Efficiency Design Index encouraging technology and design advancements that reduce green house gas emissions. A major factor of ship emissions is wave encounter resistance determined by the ship's hull design. In order to reduce wave encounter resistance and meet the emission regulations, the hull design process must utilize accurate experimental and simulation methods.

Though a large portion of the ship hull design process is completed using computer models, physical experiments are necessary for model validation and final design stages. The focus of this thesis is surge free variable wave heading tests, which have little experimental data due to limitations of the traditional towing tank. In order for the data to be used to validate simulations, the data must be very accurate. The accuracy of the data is assessed by the uncertainty associated with each measurement and calculating the influence on the result.

The effect of the extra free motions of the mounting system is studied by comparing the calm water and head wave tests to other facilities with mounting systems that allow less free motions. The results show that the model size and the mounting system have large effects on the results. The variable heading results show expected trends and good accuracy. The added resistance in variable headings shows agreement in trend to another variable heading study. The variable heading results are as benchmark data for a computer model.

www.manaraa.com

TABLE OF CONTENTS

www.manaraa.com

www.manaraa.com

LIST OF TABLES

www.manaraa.com

www.manaraa.com

www.manaraa.com

www.manaraa.com

LIST OF FIGURES

www.manaraa.com

www.manaraa.com

www.manaraa.com

www.manaraa.com

www.manaraa.com

www.manaraa.com

www.manaraa.com

LIST OF SYMBOLS

A	= Desired Wave Amplitude	k	= Wave Number	s_x	= Standard Deviation
A_w	= Waterline Area	k_s	= Spring Constant	$s_{\bar{x}}$	= Random Standard Uncertainty
b_x	= Systematic Standard Deviation	kxx	= Horizontal Radius of Gyration	S	= Total Wetted Surface
B_x	= Bias Limit	kyy	= Longitudinal Radius of Gyration	SW	= Wetted Surface of Hull
B	= Beam	K	= Form Factor	SR	= Wetted Surface of Rudder
c_S	= Damper Constant	KCS	= KRISO Container Ship Model	t	= Time
CB	= Block Coefficient	KG	= Distance from ship bottom to center	t_{95}	= Confidence Interval
C_F	= Frictional Resistance Coefficient	KO	= Distance from bottom of ship to swing origin	T	= Draft
CM	= Maximum Section Coefficient	LCB	= Longitudinal Center of Buoyancy	T_m	= Period of swing with the ship model
C_R	= Residuary Resistance Coefficient	$L_{pp,}$ L	= Length Between Perpendiculars	T_e	= Wave Encounter Period
C_T	= Total Resistance Coefficient	Lwl	= Length at Waterline	$T_{hz/\theta}$	= Natural Heave/Pitch Period
DR	= Dynamic Range	λ	= Wavelength	$T_{h\phi}$	= Natural Roll Period
∇	= Volume	m	= Mass of Counter Weight	T_S	= Period of swing without the ship model
χ	= Wave Encounter Angle (Head Waves, $\chi = 0°$)	M	= Model Mass	T_{water}	= Water Temperature
f_e	= Wave Encounter Frequency	m_x	= Added Mass of Ship	u	= Total Systematic Uncertainty
$f_{hz/\theta}$	= Natural Heave/Pitch Frequency	M_l	= Load Cell Mass	U_{95}	= Expanded Standard Uncertainty
$f_{h\phi}$	= Natural Roll Frequency	M_c	= Lightweight Carriage Mass	V	= Carriage Velocity
f_w	= Wave Frequency	M_s	= Mass of Swing	x	= Modified Surge
F_0	= Initial Load of Mass Spring Damper	ν	= Kinematic Viscosity	x_{meas}	= Measured Surge
F_E	= Inertial Force	$\overline{OG}$	= Distance from origin to center of gravity	x_0	= Inner Center Position Counter Weights
F_H	= Hydrodynamic Force	θ, τ	= Pitch	x_1	= Outer Position of the Counter Weights
FP	= Forward Perpendicular	θ_x	= Sensitivity Coefficient	XG	= Longitudinal Center of Gravity
GM	= Metacentric Height	R	= Result of specified motions/forces	X_T	= Measured X-Force
I_a	= Added Mass Moment of Area Around y-axis	R_{add}	= Mean Added Resistance	γ	= Incident Wave Phase at Bow when t=0
I_m	= Moment of Inertia of Ship Model	Re	= Reynolds Number	z,σ	= Heave
I_s	= Moment of Inertia of Swing	ρ	= Density	ζ_{FP},ζ	= Wave Amplitude at Forward Perpendicular
I_y	= Waterline Second Moment of Area	ϕ	= Roll	ζ_s	= Wave Amplitude at Stationary Position

www.manaraa.com

CHAPTER 1 INTRODUCTION

Due to the increasing global interest in reducing the effects of global warming, the transportation industries are under pressure to reduce their greenhouse gas emissions, specifically carbon dioxide. The maritime industry accounts for approximately 3% of the annual global carbon dioxide emissions, which is more than the total annual amount of emissions from Germany (IMO 2015). The International Maritime Organization (IMO) has proposed emission regulations that include the Energy Efficiency Operational Index (EEOI) and Energy Efficiency Design Index (EEDI). The EEOI index is used to assess the efficiency of the ship's operational procedures, as in speed and course. The EEDI is used to assess the efficiency of the ship's technology and design quality in regards to carbon dioxide emissions. The EEDI is defined as the carbon emissions per transport work. The increasingly stringent EEDI regulations, for ships built after January 1, 2013, encourage technological developments. Prior to implementation of EEDI, designers were only concerned with the ship's performance in calm water, but with the implementation of EEDI it is necessary to accurately predict the ship's design efficiency in calm water, head wave, and oblique wave conditions. In regards to the ship's design, the efficiency is assessed based on the resistance of the ship during route conditions. Predicting the resistance on a ship hull requires development of accurate experimental methods and simulation models. The ideal prediction of the propulsion model is achieved with added powering tests because they are fully appended, free running, and have 6 degrees of freedom. Yet, added resistance testing with a captive ship model is a necessary step to understand the hydrodynamic effects in calm water and wave conditions. These effects are calculated using potential flow theory (PF), computational fluid dynamics (CFD), and experimental fluid dynamics (EFD).

Recently potential flow and computational fluid dynamics have developed at a very rapid pace, vastly changing the ship hydrodynamics industry. Simulation Based Design (SBD) has become the standard development procedure, greatly reducing the cost of the design process by eliminating the need to build a new hull model after redesign. This requires both the numerical or computational methods to be accurate as well as the experimental methods used for validation to be accurate. The PF method has the ability to compute resistance and motion predictions over many conditions quickly. However,

www.manaraa.com

potential theory neglects the viscous effects, turbulent flow around the hull effects, and the wave breaking. These limitations limit the accuracy of its prediction of forces and moments acting on the ship (Simonsen et al. 2014). With the increase in computing power, use of CFD analysis has increased. The Reynolds Averaging Navier Stokes (RANS) model is the most common CFD method. Even with the advancement of potential flow and CFD added resistance prediction, the EFD approach is vital to the final stages of ship development.

Highly accurate EFD studies are necessary for further model development and CFD validation. Typical experimental added resistance studies are conducted in a long narrow towing tank, where a bare hull scale ship model is towed in calm water and regular head waves to obtain the added resistance and 2 DOF motions (Heave and Pitch). Resistance and 2 DOF calm water tests were completed for a 7.279 m KCS model at MOERI and NMRI (Zou et. al. 2013). The resistance, sinkage, and trim results from the two facilities were investigated to better estimate the total uncertainty of EFD results presented in (Gothenburg 2010). The two facilities studied the same size model and showed good agreement. FORCE technologies conducted added resistance and 2 DOF experiments for a L = 4.376 m (Simonsen et al. 2013), 6.070 m (Simonsen et al. 2014, Otzen 2013), and 2.700 m (Otzen 2015) KRISO Container Ship model, KCS, in calm water and head wave conditions with a focus on validation of CFD predictive capability and physics. Though many experimental added resistance studies investigate 2 DOF in calm water and head wave conditions, few studies include appendages and additional degrees of freedom such as roll and a soft spring mount. In a study by (Wu et al. 2014), a soft spring mount was used to study added resistance with 4 DOF, including surge, for the KVLCC2 ship model. Also rare are experimental added resistance studies in oblique waves. To perform oblique heading experiments, either multidirectional wave generators or a carriage with transverse direction capabilities are necessary. The only notable added resistance study of added resistance in oblique waves was done by (Fujii & Takahashi 1975). The carriage used allowed 5 DOF, including soft spring controlled surge, heave, soft spring controlled sway, roll, and pitch, by implementing two light weight sub carriages with soft spring systems. Tests were carried out for a container ship and a tanker ship for angles from 0° to 180°, incremented by 30° where 180° is head waves. The study found that added resistance decreases as the wave encounter angle decreases from 180° to 120°. For the wave encounter

www.manaraa.com

angles less than 90° the added resistance was found to be much less than that of head waves. Similar experiments are necessary to validate CFD results in Oblique waves for the KCS container ship model.

In order to validate numerical and computational models, the experimental added resistance testing requires high accuracy for the measurement of the force and motions, as well as the ship ballasting. There have been many formulations of uncertainty analysis methods (Kline & McClintock 1953, Abernethy et al. 1985, Coleman & Steele 1989) proposing improved uncertainty methods. Later, standards have been established to allow comparison of uncertainty results (ASME 1998, AIAA 1999, ASME 2005, JCGM 2008, and ASME 2013). The International Tow Tank Conference, ITTC, has established recommended procedures for resistance testing in tow tanks (ITTC 2008a, ITTC 2014), seakeeping experiments (ITTC 2011), and instrument calibration (ITTC 2008b). Studies by (Longo & Stern 2005) and (Irvine et al. 2008) provide a full uncertainty assessment of typical data sets in calm water and head waves, respectively, following (ASME 1998). To understand the quality of identical test conditions from multiple facilities, (Stern et al. 2005) includes a facility bias calculation in the uncertainty assessment. FORCE technologies presents the uncertainty procedures used for added resistance and motion testing for the KCS 6.07 m model (Otzen 2013), and the 2.70 m model (Otzen 2015) following ISO GUM standards (JCGM 2008). The uncertainty analysis for the present study follows (ASME 2013). (ASME 2013) includes minor changes to (ASME 2005) in order to create uniformity between ASME and ISO GUM standards.

The objective of this present study is to provide benchmark EFD and uncertainty analysis for CFD validation for a 1:85.18 scale (L = 2.70m) model of the KRISO container ship model (KCS) in calm water, head wave, and oblique wave encounter conditions for added resistance and 4 DOF motions (Surge, Heave, Roll, and Pitch). Experiments were conducted at the IIHR wave basin, a facility equipped to do towing tests in calm water, head waves, and oblique waves. RAO's of added resistance and motions, time histories, and uncertainty analysis are included for all of the EFD data. The calm water and head wave data is used to study the facility bias of the IIHR wave basin along with other facilities' results presented in (Zou et al. 2013) and provided by FORCE technologies. The objective of this comparison is to investigate the quality of EFD data used to validate CFD

www.manaraa.com

code (Larrson et al. 2013). The oblique wave data obtained in this study is used to investigate the effect of waves at different encounter angles on the added resistance and motions of a towed ship model. Five wave headings, $\chi = 0°, 45°, 90°, 135°, 180°$, are tested. The regular oblique wave data is also used to validate CFD code, and preliminary results have already been published in (Sadat-Hosseini et al. 2015). A complete uncertainty analysis for select test conditions is included in this study to ensure that the data obtained at IIHR has good quality.

The data was collected as a part of the NATO RTO Task Group AVT-216 "Evaluation of Predictive Methods for Ship Maneuvering and Control", in order to acquire experimental data for evaluation of predictive methods for added resistance for variable heading. The study is part of a joint project with FORCE Technologies under the ONRG NICOP support for FORCE. The test cases were also used for experimental comparison at the Tokyo 2015 CFD Workshop.

www.manaraa.com

CHAPTER 2 EXPERIMENTAL METHODS

2.1 IIHR Wave Basin

The IIHR Hydraulic Wave Basin Facility is a state of the art hydrodynamic test facility designed to conduct local flow measurements, semi-captive, and radio-controlled free-running ship model tests. The basin is 40 m long, 20 m wide, and 4.3 m deep, with a water depth of 3 m. It is equipped with six plunger type wave makers used to create a wide range of wave conditions. The Wave Basin facility utilizes a carriage with three major systems in order to achieve three degrees of freedom above the tank. The main carriage spans the entire width of the wave basin and travels along a rail in the x-direction that spans the entire length of the wave basin. The second carriage system, a sub carriage, is attached to the main carriage and is designed to travel in the y-direction driven by a rack and pinion system. The third system is a turntable fixed to the sub carriage and designed to rotate the ship mount in the x-y plane. The sum of the three carriage systems allows semi-captive ship testing in head waves and oblique waves, along with the capability of tracking a free running model on the horizontal surface of the wave basin. Figure 2.1 and Figure 2.2, show the schematic and a photograph of the wave basin, respectively. The wave makers are aligned at the East end of the wave basin with the capability of creating regular and irregular waves. On the West side of the wave basin is a 7.8 x 20 m^2 flat beach, with a tilt angle of 11.3°, that is designed to reduce wave reflection. In addition, two wave dampers are installed along the length of the wave basin. Immediately after the completion of a test, the dampers are lowered onto the water. The dampers are raised out when the water becomes calm. This procedure greatly reduces the length of time needed to achieve calm water conditions and begin the next test. A trimming tank is located in the southwest corner where ship model ballasting and wave gauge calibration is conducted. The facility is equipped with two operating control panels to manually control the movement of the carriage and the individual wave maker settings. With the three degrees of freedom carriage system, the wave basin is well equipped to conduct oblique wave tests.

www.manaraa.com

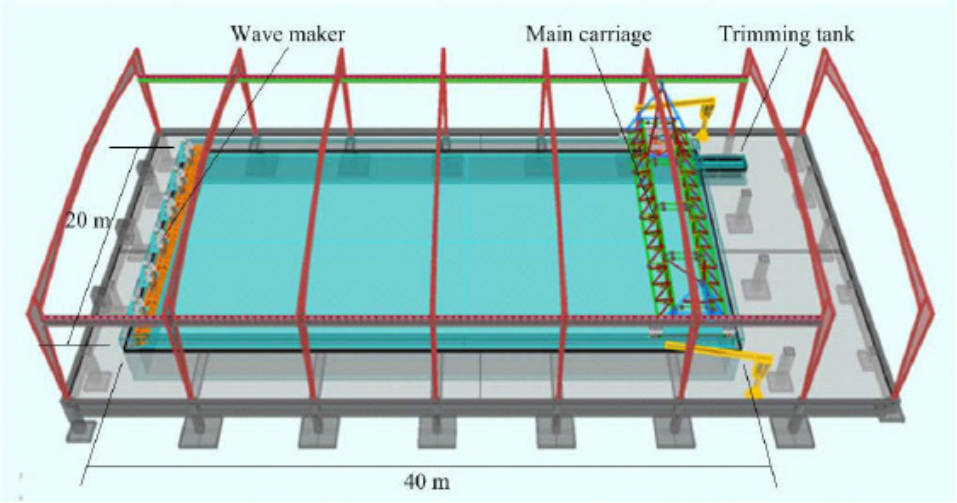

Figure 2.1 Schematic of the IIHR wave basin (Sanada et al. 2013)

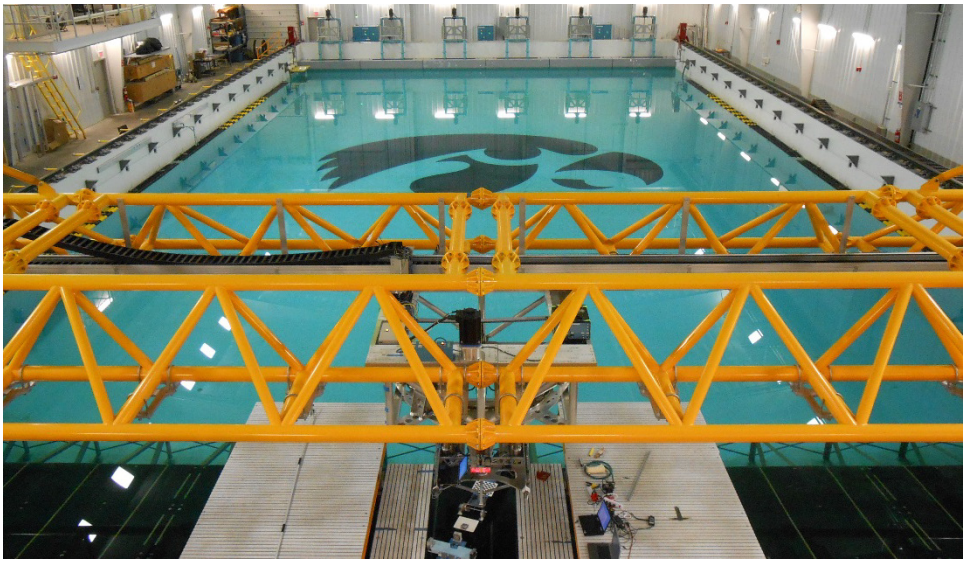
Figure 2.2 Photograph of wave basin from the beach side

Each of the six wave making plungers have the capability of operating at separate amplitude, frequency, and initial phase settings. The plungers are 1.2 m, 3.3 m, and 0.8 m height, weight, and depth, respectively, and have a curvature radius of 100 mm. Figure 2.3 shows the six wave plungers. The maximum plunger stroke is 250 mm when the frequency is set lower than 0.62 Hz. Typically, all six of the plunger's settings are synchronized in order to generate regular waves. The wave maker is capable of creating irregular waves by inputting an analog voltage time series into each plunger (Sanada et al. 2013). To evaluate the accuracy of regular wave generation, calibration determines the relationship between the input wave parameters and generated waves. (Elshiekh 2014) details the wave

www.manaraa.com

calibration method and results at the IIHR wave basin. Figure 2.3 shows the cross sectional schematic of the wave plungers.

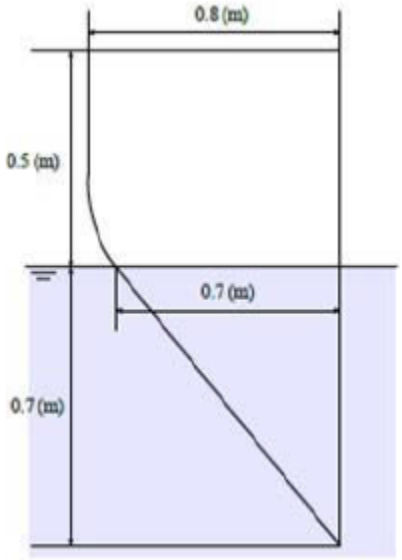

Figure 2.3 Wave plunger set up (Sanada et al. 2013)

The temperature of the atmosphere and water were recorded for the days where testing was conducted. The water temperature is used to calculate the resistance coefficients in calm water and wave cases. Figure A.1 shows the tendency of the atmospheric and water temperature over time. The temperature values are shown in Table A.1 and are used to calculate the resistance coefficients. Some dates include two temperatures for values were taken in the morning and afternoon.

2.2 KRISO Container Ship Model

The present study focuses on the KRISO Container Ship (KCS) a public hull designed for academic use. The KCS model is a modern container ship design with a bulbous bow. The full-scale length is 230 m, though a full-scale ship does not exist. Figure 2.4 shows the ship's body plan and centerline profile. Calm water and head waves were conducted by FORCE technologies, for a L = 4.36 m, 1:52.75 scale, 6.07 m, 1:37.89 scale, model and a 2.70 m, 1:85.19 scale, model. This current study utilizes the same wooden L = 2.70 m model used by FORCE. The model has no propeller, but instead a cap mounted in the propeller position. The model includes a horn-type rudder locked in the zero degree position during testing. For this study, the ship superstructure is not attached to the hull. A

www.manaraa.com

lightweight splashguard is attached to the bow to prevent flooding in the ship. The ship parameters were set according to the model's scale. Table 2.1 lists the principle particulars for the full size and 2.70 m KCS models. The metacentric height above vertical center of gravity (VCG), i.e. GM, the radius of gyration about the x-axis (k_{xx}) and y-axis (k_{yy}), and the natural heave (f_{hz}), roll ($f_{h\phi}$), and pitch ($f_{h\theta}$) frequencies were set in reference to (Otzen 2015). The aforementioned parameters are adjusted by the incline test, pendulum test, and zero speed test.

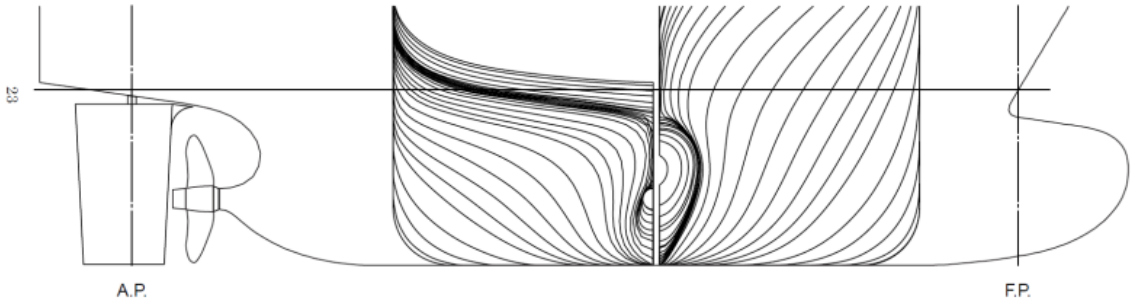

Figure 2.4 The KCS body plan and centerline profile (Fujisawa et al. 2000)

Table 2.1 Principle Particulars of KRISO Container Ship model

	Full Scale	IIHR
Main Particulars		
Lpp,L (m)	230	2.700 ± 0.001
Lwl (m)	232.5	2.729 ± 0.001
B (m)	32.2	0.378 ± 0.001
T (m)	10.8	0.1268 ± 0.0005
∇ (m^3)	52030	0.0842 ± 0.0005
SW (m^2)	9424	1.2987 ± 0.004
SR (m^2)	115	0.0158 ± 0.004
CB	0.6505	0.6505
CM	0.9849	
LCB (%L), fwd+	-1.48	-1.48
GM/L	0.0622	0.0622 ± 0.0047
k_{xx}/B	0.4	0.4 ± 0.005
k_{yy}/L	0.25	0.25 ± 0.001
$T_{h\phi}$ (s)	40	3.571 ± 0.006
T_{hz}, $T_{h\theta}$ (s)	9.09	0.917 ± 0.006
Ship speed		
U (m/s)	12.35	1.34
Re	2.84×10^9	3.613×10^6

The mass properties of the ship model are set using an iterative process where ballast weights were set and then checked using specific tests for each mass property. Three important mass properties were used to adjust ballast weights, $k_{yy}/L = 0.25$, $GM/L = 0.062$,

www.manaraa.com

and $k_{xx}/B = 0.4$, in order of significance. The k_{yy} and k_{xx} are measured by a swing test done on a custom swing built at IIHR, shown in Figure 2.5 in the k_{yy} configuration. In order to test k_{xx}, the ship rest is rotated 90° so the swing rotates the ship about the x axis. For both k_{yy} and k_{xx}, two swing test cases, with and without the model, were done with counter weights centered on the swing and diagonally, as shown in Figure 2.6. The tests are completed by displacing the swing slightly and letting it swing for 10 periods while recording the start and end time of each period. The swing period start and stop time are measured using a laser sensor. The swing period is used to calculate the k_{yy}/L and k_{xx}/L. The GM is measured by placing the boat in the water and setting a 0.5 kg counterweight on the horizontal center of gravity. The counter weight is moved to the portside and then the ship model is allowed to settle. Once settled, the ship's roll angle is measured using a Spi-Tronic Pro 3600 digital protractor. The counter weight is then set on the edge of the starboard side and again the roll angle is recorded. The roll angles are used to calculate the metacentric height, GM. An iterative process was used to set the ballast weights. First the weights were adjusted until $k_{yy}/L = 0.25 \pm 2\%$. Then the GM was measured and if it was not within $GM = 0.0622 \pm 2\%$ the weights were slightly adjusted until it was and then k_{yy}/L was measured again. If k_{yy}/L and GM are within the ± 2% tolerance, k_{xx}/B is measured. If k_{xx}/B was not within $0.4 \pm 2\%$ the weights were slightly adjusted until it was and the process repeats by checking k_{yy}/L and GM, in that order. This iterative process was repeated until all mass properties were within ± 2% of the scale ship values.

In order to get accurate resonance frequency predictions, the natural heave, roll, and pitch frequencies are measured. The natural frequency is not directly measured instead the natural oscillation period of each motion is measured. To measure the motions, a MEMSIC CXTA01 tilt sensor is attached to the ship at the location of the center of gravity. The ship model is placed in calm water and displaced in the negative direction of the specified motion. The ship model is then released and is allowed to heave, roll, or pitch for ten periods. The time history of the motions are analyzed using C++ source code to find the peaks and calculate the natural periods. The frequency is defined as the inverse of the average oscillation period. The natural frequency values in Table 2.1 reflect the measured natural frequencies for heave, roll, and pitch.

www.manaraa.com

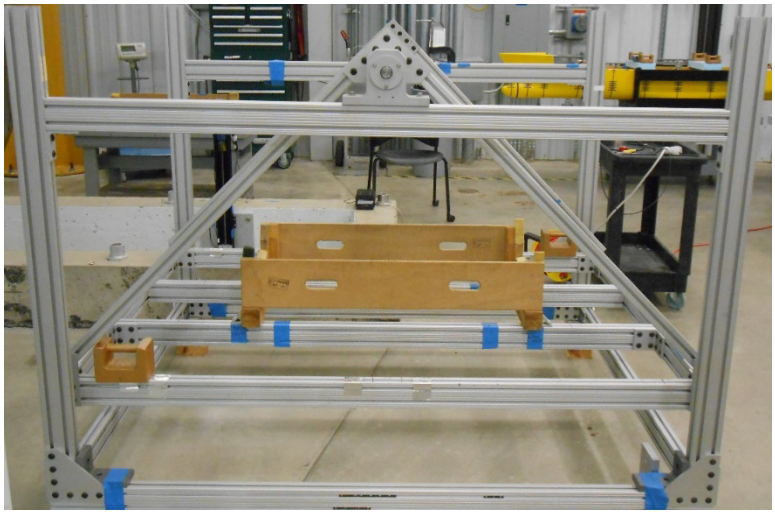

Figure 2.5 Custom swing for the swing test set up for K_{yy}/L

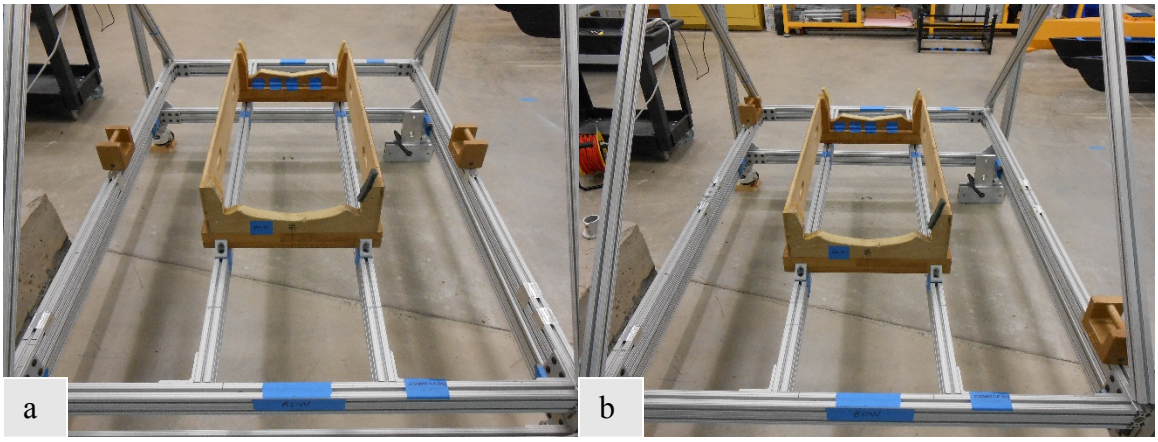

Figure 2.6 Centered (a) and Diagonal (b) counterweight positions, respectively

2.3 Data Acquisition System

A semi-captive surge free mount tows the KCS model. The surge free mount allows the model 4 DOF surge (x), heave (z), roll (ϕ), and pitch (θ). For each run the carriage velocity (V), surge, heave, roll, and pitch motions at the center of gravity, total resistance force (X_T), and wave elevation at a stationary point 15 m from the wave makers (ζ_s) and at the forward perpendicular of the ship (ζ_{FP}, ζ) are recorded. The data is synchronized/acquired as time histories at a sampling rate of 100 Hz. The time series begin at the beginning of wave making. The KCS model mounted to the surge free mount during a test is shown in Figure 2.7.

www.manaraa.com

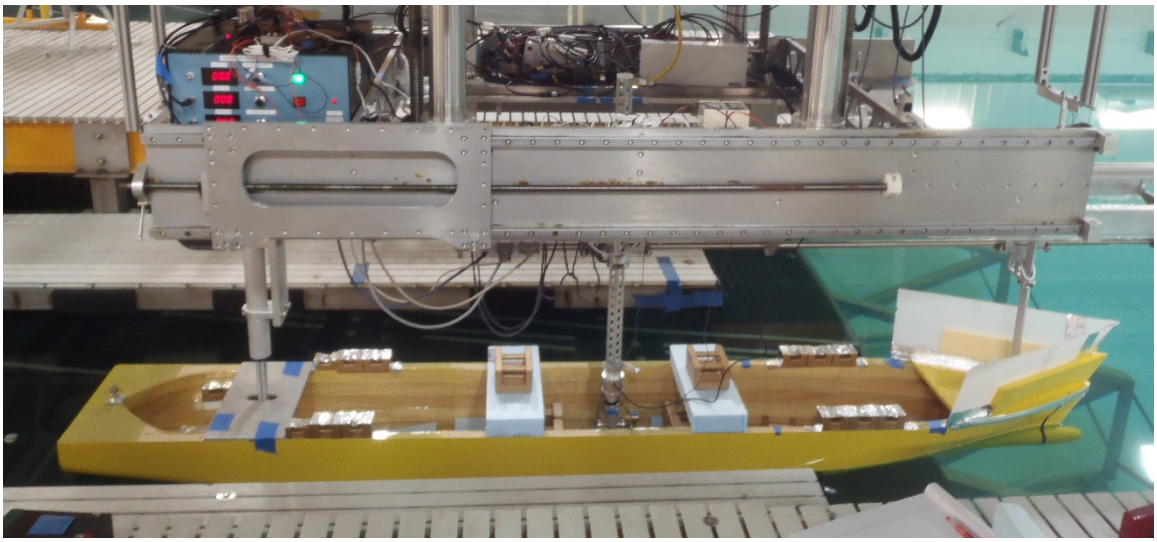

Figure 2.7 KCS model mounted to the surge free mount

2.3.1 Surge Free Mount

The surge free mount system is a lightweight carriage connected to the three-system carriage. Figures 2.8 and 2.9 show a photograph and schematic of the test set up, respectively. The rail alignment allows the lightweight system to move in the surge direction. A potentiometer measures the surge motion, where 0 m is located at the center of the rail. The lightweight carriage is connected to a spring mass damper system allowing control of the inertial surge effects due to ship acceleration. Figure 2.10 shows a close up photograph of the lightweight carriage. The spring mass damper system has an adjustable spring and damper coefficient and surge offset. The use of the mass spring damper system decreases the effect of acceleration on the harmonics of the surge motion, allowing for larger time periods of useful data. This is important because unlike tradition long and narrow towing tanks, the IIHR wave basin has limited run space. The limited run space leads to shorter runs where the acceleration effects are not naturally dampened during the duration of the steady state velocity region. The ideal mass spring damper settings create the longest amount of time where the measured total resistance is at the mean value. Therefore, the appropriate mass spring damper settings were obtained by comparing the effects of various spring mass damper settings in calm water conditions. Based on this study, the spring coefficient of 100 N/m and a damping coefficient of 50 Ns/m are used for every test case. Also, the surge offset of the lightweight carriage is adjusted. The surge offset is set to 30 mm for every test case based on the mean surge value during the steady

www.manaraa.com

state velocity region. Also, a linear actuator is used to lock the surge motion during acceleration to reduce the effect of acceleration on the surge motion. The rod is released at the time where acceleration stops. Figure 2.11 shows a photograph of the surge lock device. The time of release is shown on the velocity time histories for each test in the Figures in Appendix C.

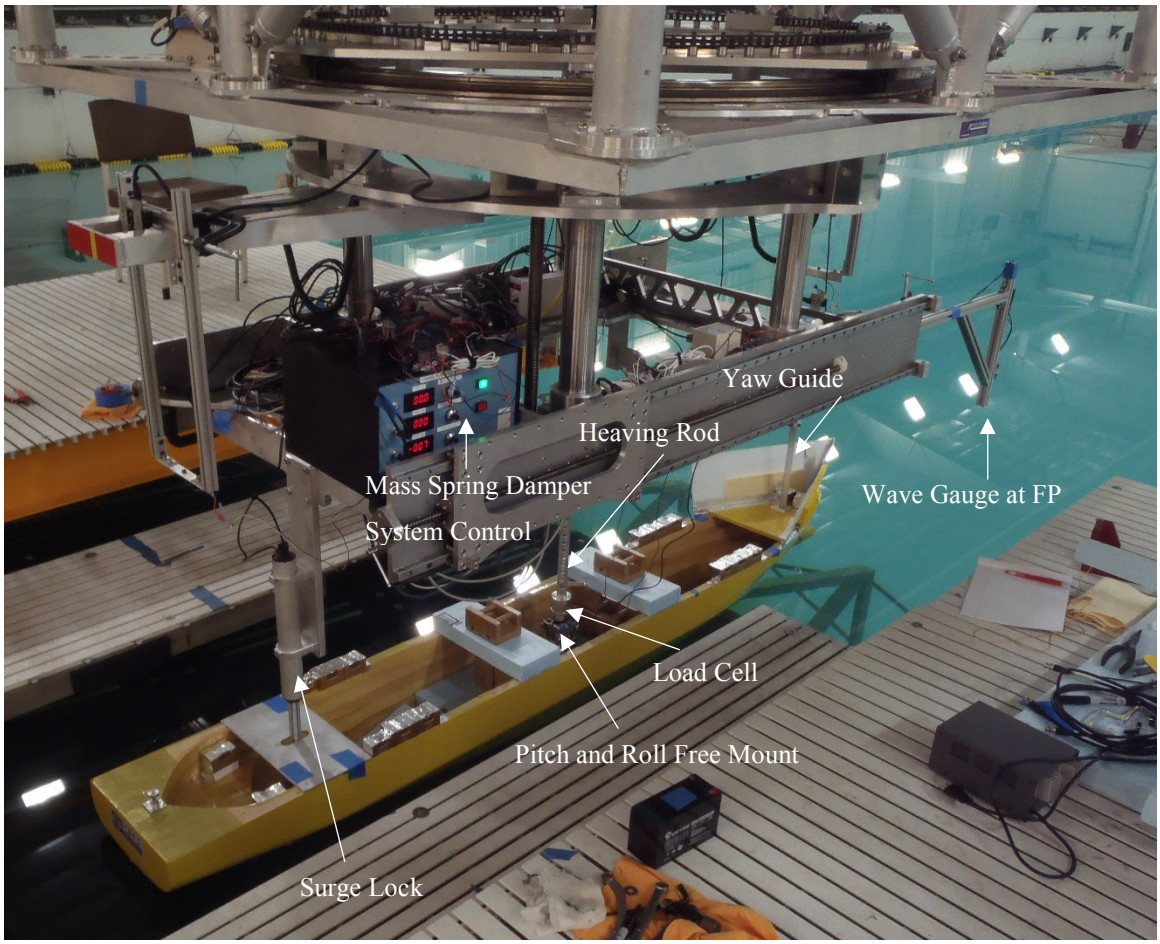

Figure 2.8 Photograph of KCS mounted to Surge Free Mount with key components labeled

www.manaraa.com

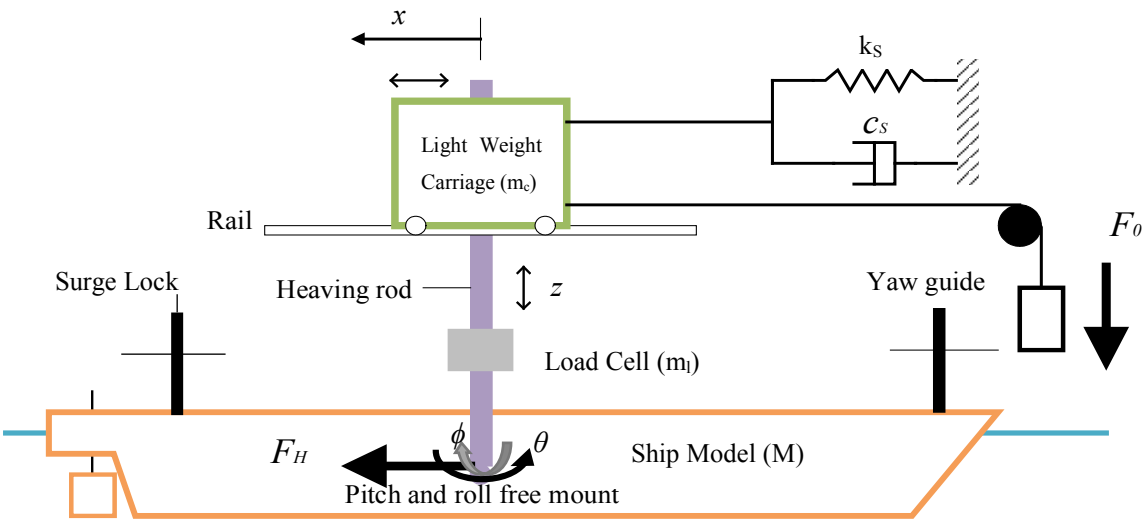

Figure 2.10 Schematic of surge free mount including spring parameters

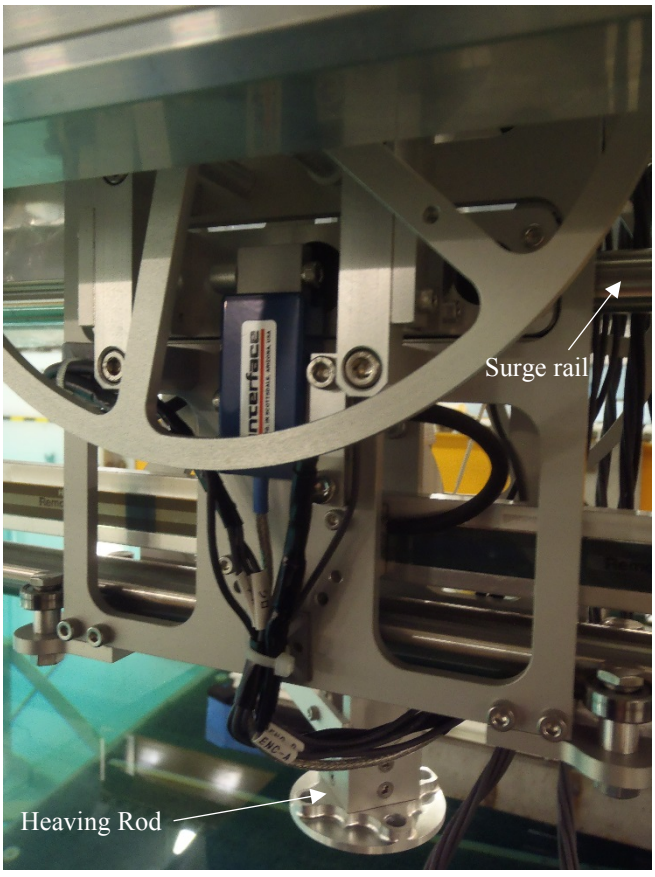

Figure 2.9 Light Weight Carriage

www.manaraa.com

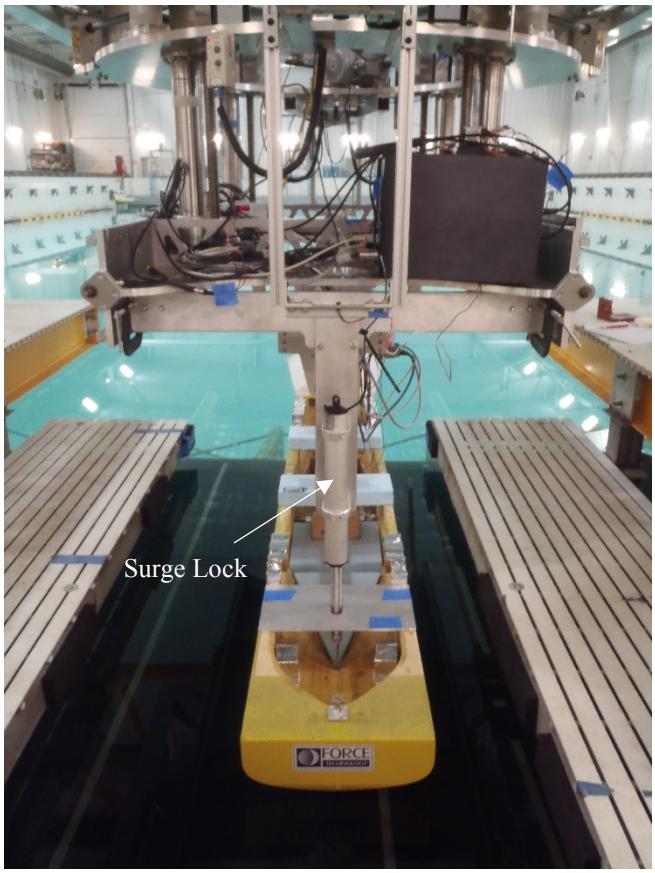

Figure 2.11 Photograph of from stern view of KCS

A lightweight heaving rod connects the ship model to the lightweight carriage allowing a 1DOF, z direction, motion. This connection allows the ship to heave freely. A potentiometer records the time history of the heave motion. A one-component load cell attaches the heaving rod to the center of gravity of the ship. The load cell is an Izumi Sokki ML-FX10 rated for ± 10 kgf. An Izumi Sokki DA-18K amplifier is used to amplify the signal from the load cell. The load cell is aligned to measure the total resistance in the x-direction. One side of the load cell is bolted to the heaving rod while the other side of the load cell is bolted a roll and pitch free mount at the center of gravity of the KCS model. The roll and pitch free mount is a custom mount that has a hinge for both the roll and pitch motions. Potentiometers measure the time histories of the roll and pitch motions. Figure 2.9 shows the heaving rod and the roll and pitch free mount. Attached to the bow of the ship is a yaw guide. The yaw guide is a thin rod attached to the lightweight carriage and is free to heave. The yaw guide is bolted directly to the ship to prevent the yaw and sway motion of the ship during testing.

www.manaraa.com

The wave amplitude is measured at the forward perpendicular of the ship (ζ_{FP}, ζ) and a stationary point 15 m from the wave makers (ζ_S). Keyence UD-100 ultrasonic displacement sensors with a range of 300 to 1300 mm measure both stationary and moving amplitudes. A Keyence UD-501 amplifier amplifies the displacement signal. The ζ_S is used for the wave amplitude result and the phase of ζ_{FP} is used for the phase result.

2.4 Test Conditions

The local coordinate system is defined as in Figure 2.12. Where the system is labeled as surge (x), sway (y), and heave (z). roll (ϕ), pitch (θ), and yaw (ψ) are all defined by the right hand rule and are measured at GM. Experiments were performed for calm water and various wave encounter angle (χ) conditions (χ = 0.0°, 45.0°, 90.0°, 135.0°, 180.0°). The Froude number is set 0.26 for all of the wave cases. The wave slope, the ratio of wave height (H) and wavelength (λ), is set to 1/60 for all wave cases. All wave conditions are regular waves at a specified encounter angle. Figure 2.13 shows the definition of the wave encounter angle.

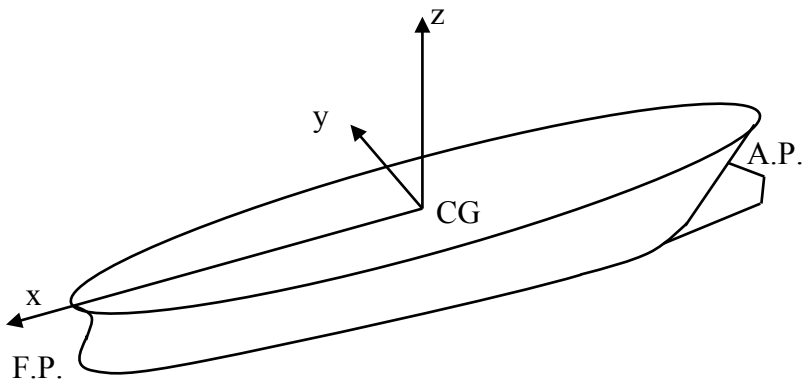

Figure 2.12 Coordinate system for IIHR testing

www.manaraa.com

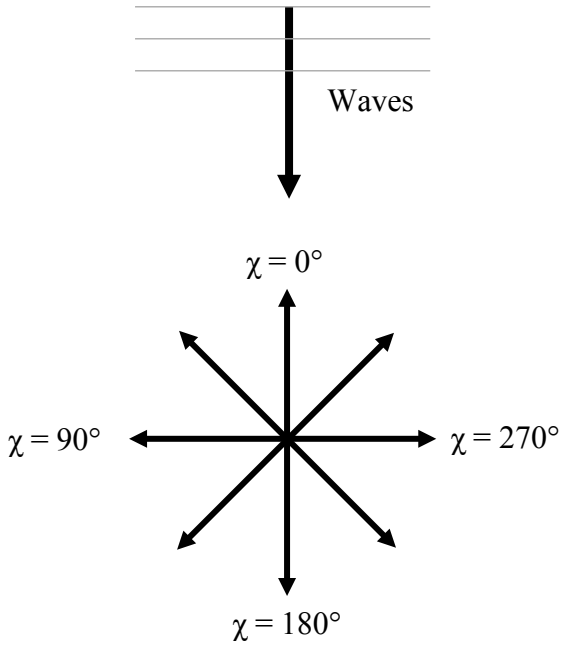

Figure 2.13 Wave encounter angle, χ

Prior to each test run, the ship model is aligned to the correct wave encounter angle. The start location and orientation for each wave encounter angle maximizes the amount of travel space and centers the travel in the middle of the wave basin. The wave encounter angle remains constant throughout the entirety of the test run. The carriage motion is delayed for a set period of time every test run to allow the waves to reach a constant correct amplitude and phase. The delay is set based on the calculated time for the fully developed waves to travel the entire length of the wave basin. The carriage acceleration is set to maximize the length of steady state velocity while limiting the maximum acceleration force put on the load cell. The wave settings, velocity, and carriage starting location are set manually before each test run. To run the test, two triggers are switched on simultaneously to activate the data acquisition system, carriage control, and the wave maker. After the delay time, the carriage begins to accelerate to the set speed. The carriage continues until it reaches the safety boundary of the wave basin. At the safety boundary the carriage will begin to decelerate to zero velocity. After the ships reaches a zero velocity, the triggers shut off the data acquisition and wave makers.

2.4.1 Calm Water Test Conditions

Calm water tests were completed for a Froude number range of 0.0867 to 0.2817. These test cases were completed with a wave encounter angle χ = 0°. Table 2.3 shows the

www.manaraa.com

test conditions for the head direction calm water tests. The calm water tests in head direction with varying Froude numbers were used to validate the surge free mounting system by comparing the results to NMRI (Zou et al. 2014), KRISO (Zou et al. 2014), and FORCE (Stern et al. 2014). Also, calm water tests were performed at the design speed, Fr = 0.26, for each wave encounter angle before each day of testing. The calm water tests at varying wave encounter angles at the design speed, Fr = 0.26, were used to obtain the calm water resistance necessary for the calculation of added resistance.

Table 2.3 Test conditions for calm water cases

k_s [N/m], c_s [N/m^2]	χ [°]	Fr	Numbers of runs
100, 50	0	0.0867	4
		0.1084	3
		0.1300	3
		0.1517	1
		0.1734	1
		0.1950	3
		0.2059	3
		0.2167	3
		0.2276	1
		0.2384	1
		0.2492	1
		0.2601	6
		0.2709	1
		0.2817	1

2.4.2 Head Wave Test Conditions

Added resistance in head waves tests were performed at Fr = 0.26. These cases included a range of wavelength to ship length ratio (λ/L) ratio from 0.50 to 1.95. The wave steepness (H/λ) was held constant at 0.016 for all cases. Table 2.4 shows the test conditions for the head wave tests. Two different data sets are analyzed because they include different wavelength conditions. The data set labeled Aug. was taken in August of 2015 and includes conditions similar to those of the oblique wave condition testing. The data set labeled Nov. was taken in November 2015 and includes wavelength conditions that match tests at FORCE Technologies. The added resistance in head waves tests were used to validate the surge free mounting system by comparing the results to FORCE L = 4.38, 6.07, and 2.70 m models (Simonsen et al. 2008, Simonsen et al. 2013, Simonsen et al. 2014).

www.manaraa.com

Table 2.4 Test conditions for head wave cases

χ [°]	k_s [N/m], c_s [N/m^2]	H/λ	Fr	λ/L	Numbers of runs
0	100, 50	1/60	0.2601		3
				0.50	3
				0.75	1
				1.00	3
				1.25	1
				1.50	3
				2.00	3
0	100, 50	1/60	0.2601		3
				0.50	1
				0.65	1
				0.75	1
				0.85	1
				0.95	1
				1.05	1
				1.15	1
				1.25	1
				1.37	1
				1.50	1
				1.65	1
				1.80	1
				1.95	1

2.4.3 Oblique Wave Test Tests Conditions

Added resistance tests in head, quartering, beam, and following wave conditions were performed at Fr = 0.26. Table 2.5 shows the test conditions for the oblique wave cases. These cases included a range of wavelength to ship length ratio ratios from 0.50 to 2.00. The 5 wave encounter angles studied are $\chi = 0.0°, 45.0°, 90.0°, 135.0°, 180.0°$. The wavelength to ship length ratios were chosen near the heave, pitch, and roll resonance conditions. The dimensionless heave/pitch and roll natural frequencies are $T_{hz/\theta}$ =0.917 s and $T_{h\phi}$ = 3.571 s, respectively, as shown in Table 2.1. Figure 2.14 shows the wave encounter frequency compared to the wave conditions along with the resonance frequencies of heave, roll, and pitch. The wave steepness was held constant at 0.016 for all cases.

www.manaraa.com

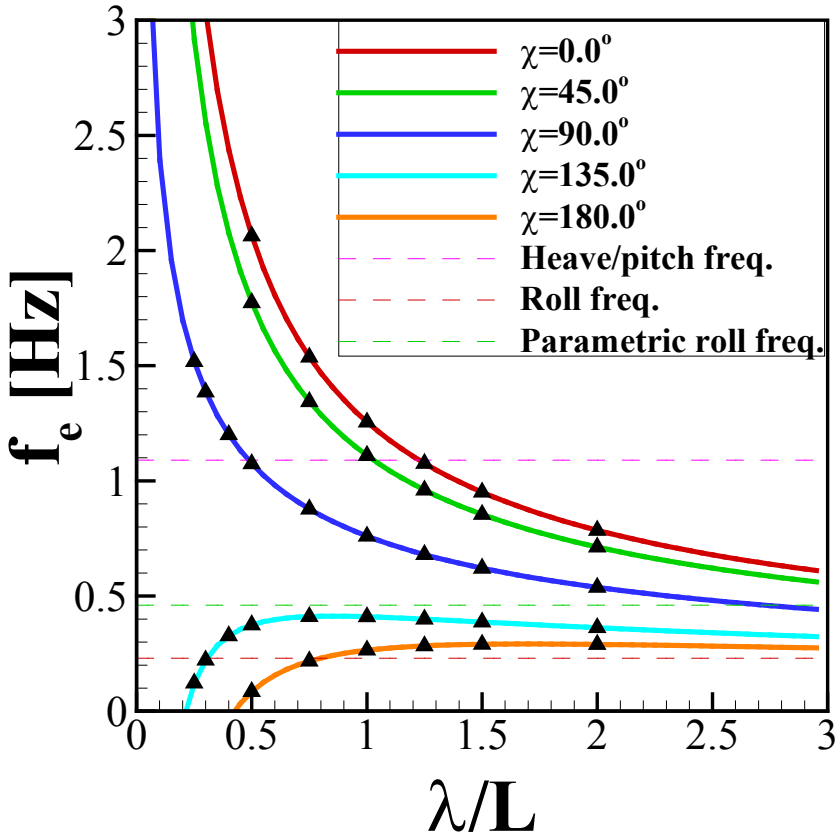

Figure 2.14 Resonance frequencies and wave encounter frequencies

www.manaraa.com

Table 2.5 Test conditions for oblique wave cases

χ [°]	k_s [N/m], c_s [N/m^2]	H/λ	Fr	λ/L	Numbers of runs
45	100, 50	1/60	0.2601		3
				0.50	3
				0.75	1
				1.00	3
				1.25	1
				1.50	1
				2.00	3
90	100, 50	1/60	0.2601		3
				0.25	3
				0.30	3
				0.40	3
				0.50	3
				0.75	1
				1.00	3
				1.25	1
				1.50	1
				2.00	3
135	100, 50	1/60	0.2601		3
				0.25	3
				0.30	3
				0.40	3
				0.50	3
				0.75	1
				1.00	3
				1.25	1
				1.50	1
				2.00	3
180	100, 50	1/60	0.2601		3
				0.50	3
				0.75	1
				1.00	3
				1.25	1
				1.50	1
				2.00	3

2.5 Data Reduction and Analysis Methods

For each test, data from eight instruments was collected and synchronized using a data acquisition device. The data sampling rate for every instrument is 100 Hz. Synchronizing software is used to synchronize all data from each run into one file. C++

www.manaraa.com

codes are used to convert these synchronized files to compatible Tec plot asci format files. The raw analog voltage signal data is converted from voltage to the measured dimensions based on calibration of the each measuring instrument. The calibrations were completed following (ITTC 2014). Time histories of the velocity, resistance, and motions for each case are included in Appendix C.

2.5.1 Surge Modification

Typically, a surge free added resistance test is completed in a long narrow towing tank, where the testing time period with uniform velocity is very long. Therefore, the added inertial effects from acceleration will dampen over time, leaving a large portion of the data unaffected by the inertial effects. However, the tests completed at the IIHR Wave Basin have very short testing time periods with uniform velocity due to the space constraints. Therefore, the data must be modified to eliminate the added inertial effects. Figure 2.15 shows the overview of the surge modification process.

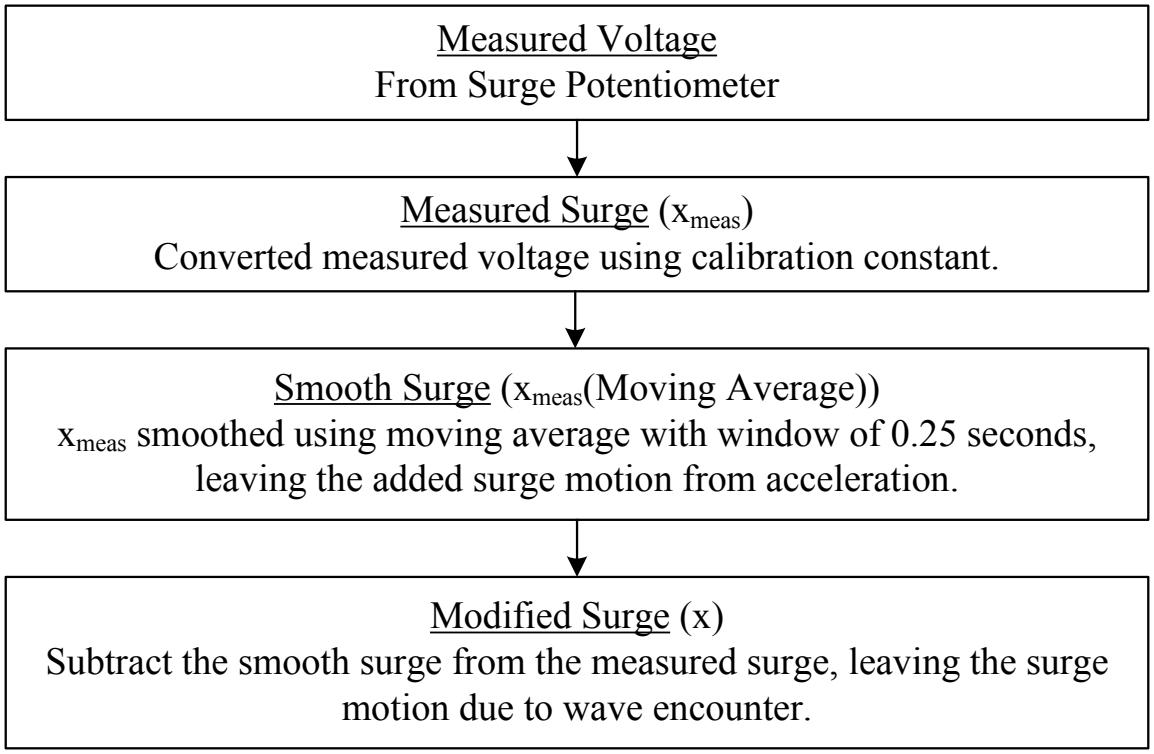

Figure 2.15 Flow chart of the surge modification process

www.manaraa.com

The measured surge (x_{meas}) time history is the raw measured surge that includes the added effects of the mass spring damper system and acceleration. A moving average filter, with a mean window size of 0.25 seconds, is applied to the surge data to calculate a time history of the effect of the added effects on the surge motion. The moving averaged surge time history is then subtracted from the unmodified surge time history. The result of the subtraction is a surge motion due to the wave encounter, henceforth referred to as surge (x). Figure 2.16 shows the time histories of the measured, moving average, and modified surge for $\chi = 0°$ and $\lambda/L = 2.00$.

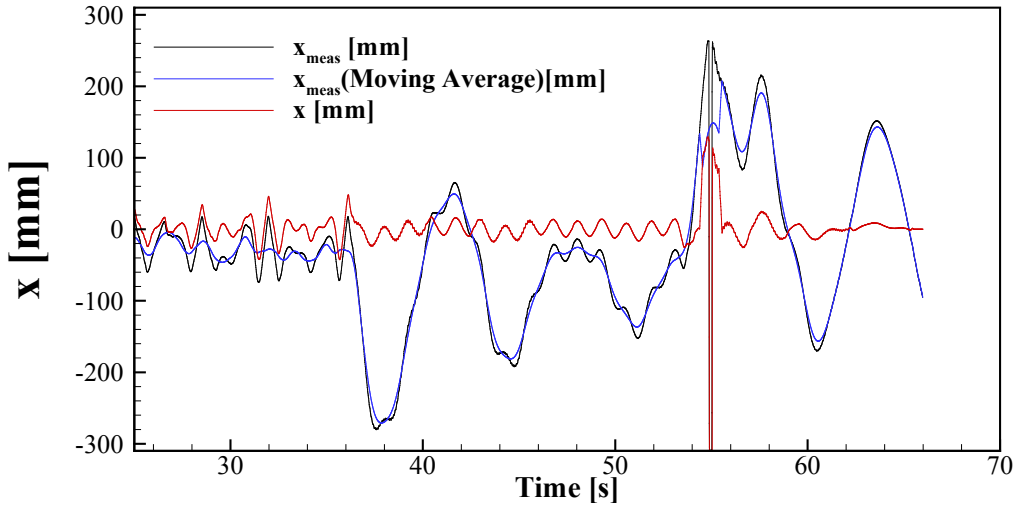

Figure 2.16 Time History of measured, moving average, and modified surge

2.5.2 Hydrodynamic Force Calculation

The added inertial effects of acceleration and the spring mass damper not only effect the surge motion, they also effect the total resistance. Like with the surge motion, this is a concern at the IIHR Wave Basin due to small testing time periods as a result of space constraints. To compensate, the inertial effects are removed from the X-force. Figure 2.17 shows the raw measured total resistance for head wave conditions where $\lambda/L = 1.00$. From the figure, it is clear that there are large fluctuations along with very high frequency noise. This is due to noise from the instrumentation, as well as surge inertial effects due to acceleration. Figure 2.18 shows the overview of the hydrodynamic force calculation.

www.manaraa.com

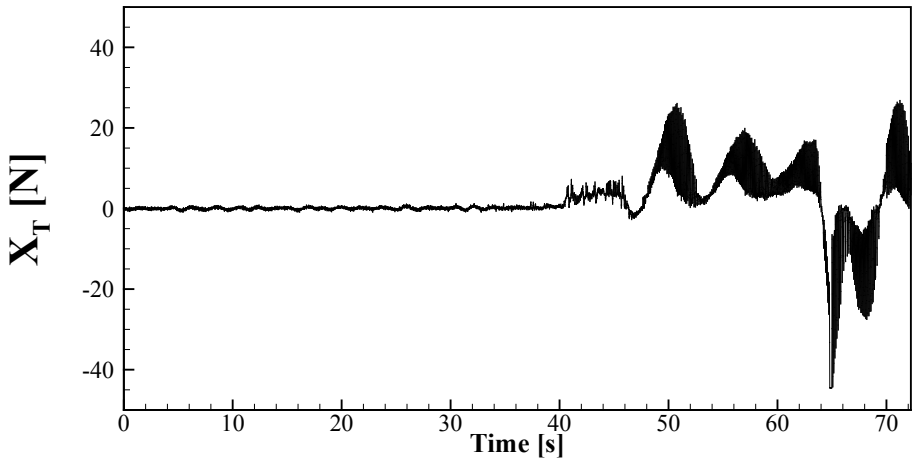

Figure 2.17 Raw time history of total resistance

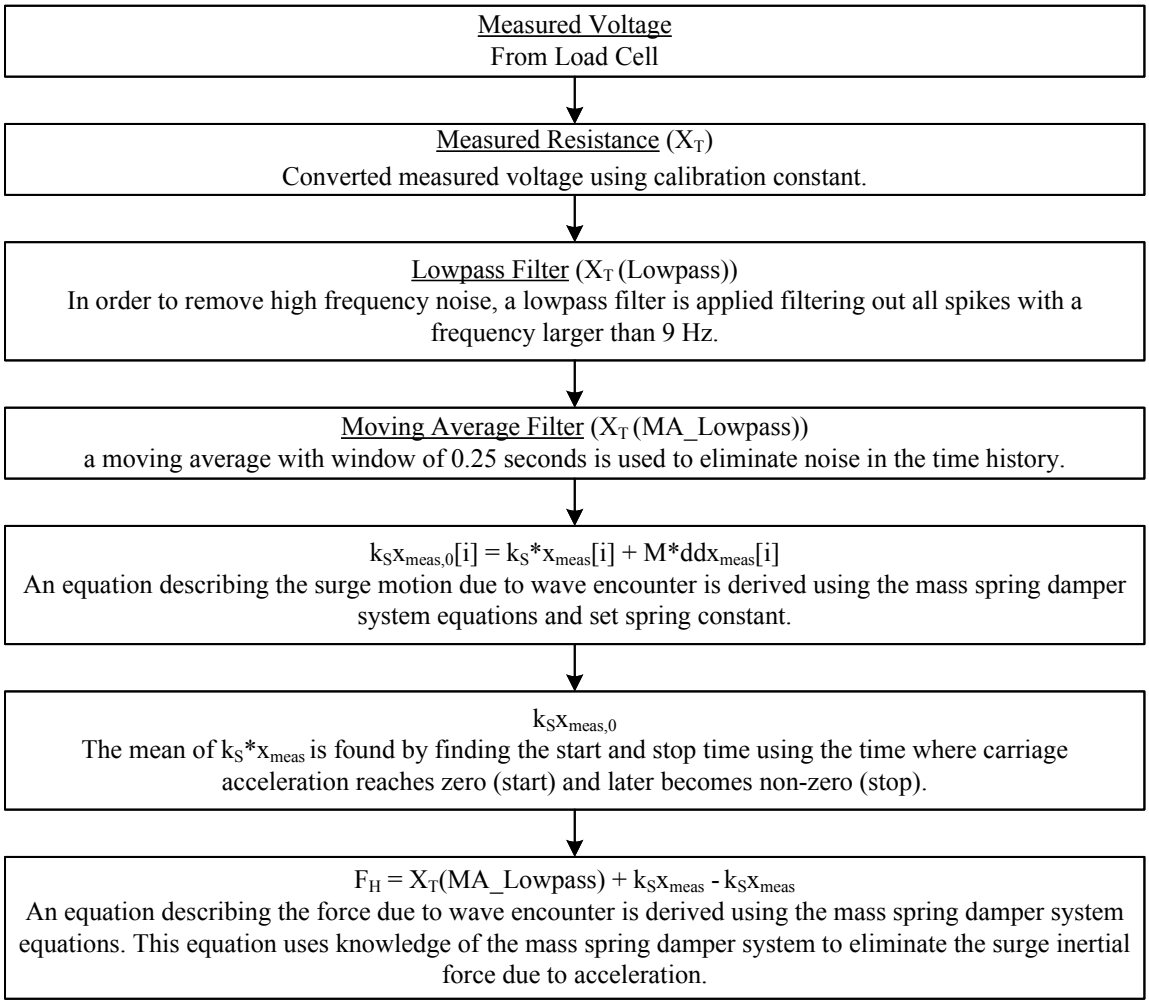

Figure 2.18 Flow chart of hydrodynamic force calculation

www.manaraa.com

In order to improve the quality, the data is filtered twice. Figure 2.19 shows the time histories of the total resistance data after the lowpass filter (a) and after the moving average filter (b). The first filter is a lowpass filter that filters out any oscillations with a frequency higher than 9 Hz. The second filter is a moving average filter that utilizes a window size of 0.25 seconds. With the application of the filters, the data excludes high frequency noise from instrumentation and test set up. It is at a stage where the added resistance may be removed.

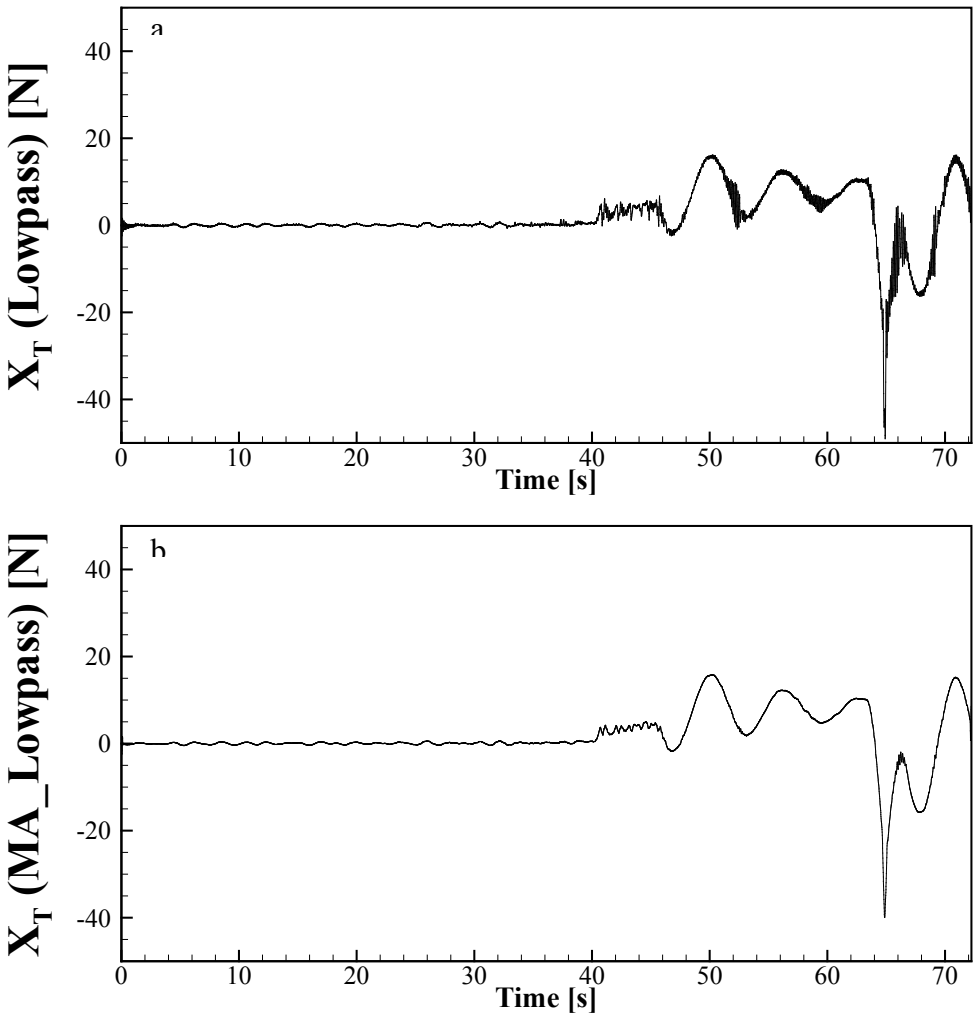

Figure 2.19 Total resistance after (a) lowpass and (b) moving average filters

In order to remove the added inertial force, the wave encounter frequency must be calculated. The waves are produced at specific frequency (f_w), matching the frequency of the wave plungers. Equation 2.1 is used to calculate the wave encounter frequency (f_e). The wave encounter period (T_e) is the inverse of the wave encounter frequency.

www.manaraa.com

$$f_e = f_w + \frac{V}{\lambda}\cos(\chi + 180°) \tag{2.1}$$

The measured X-force is modified to eliminate the effect of the mass spring damper system and acceleration, referred to as the inertial force. The resulting force is defined as the hydrodynamic force (F_H). General mass spring system principles are used to define the mass spring damper system. Figure 2.8 shows the important parameters describing the mass spring system. Equation 2.2 describes the mass spring damper system. Equation 2.3 defines the measured force by the load cell (X_T). Equations 2.4 and 2.5 are used to define the hydrodynamic force and the wave excitation force (F_E).

$$\left(M + m_l + m_c\right)\ddot{x}_{meas} = F_0 - k_s x_{meas} - c_s \dot{x}_{meas} - F_H \tag{2.2}$$

$$X_T = F_0 - k_s x_{meas} - c_s \dot{x}_{meas} \tag{2.3}$$

$$F_H = m_x \ddot{x}_{meas} + c_s \dot{x}_{meas} + \frac{1}{2}\rho S C_T \left(V + \dot{x}_{meas}\right)^2 + R_{add} + F_E \tag{2.4}$$

$$F_E = \sum A \sin\left(2\pi n f_e t\right) \tag{2.5}$$

Several assumptions are applied to Equations 2.2 through 2.5 to simplify the set of equations. It is assumed that the mass of the ship (M) is much larger than the mass of the load cell (m_l), mass of the surge-free mount carriage (m_c), and the added mass of the ship. Therefore, all of the masses are neglected besides the ship's mass. The damper constant of the surge free mount and the hydrodynamic damper constant are negligible. The velocity is assumed to be much larger than the first derivative of surge, therefore the first derivative of surge can be neglected. Equation 2.6 is used to describe the steady force on the ship. Equation 2.7 is used to define the hydrodynamic force, when considering the above assumptions and substituting Equations 2.5 and 2.6 into Equation 2.4. Equation 2.8 and 2.9 reflect Equations 2.2 and 2.3, respectively, after applying the above assumptions.

$$R_s = \frac{1}{2}\rho S C_T V^2 + R_{add} \tag{2.6}$$

$$F_H = R_s + \sum A \sin\left(2\pi n f_e t\right) \tag{2.7}$$

$$M\ddot{x} = F_0 - k_s - R_s - \sum A \sin\left(2\pi n f_e t\right) \tag{2.8}$$

$$X_T = F_0 - k_s x_{meas} \tag{2.9}$$

www.manaraa.com

Equation 2.10 defines the hydrodynamic force in terms of the measured force and the ship mass and second derivative of surge.

$$F_H = X_T - M\ddot{x}_{meas} \tag{2.10}$$

The second derivative of surge cannot be used for calculating the hydrodynamic force due to high frequency noise in the data signal. To find the hydrodynamic force, the second derivative of surge is estimated using the mass spring damper principles. Equation 2.11 is used to define the average surge over the constant velocity period (x_0). The average surge is substituted into Equation 2.8 to obtain Equation 2.12.

$$x_0 = \frac{F_0 - R_s}{k_s} \tag{2.11}$$

$$M\ddot{x} + k_s\left(x - x_0\right) = -\sum A\sin\left(2\pi n f_e t\right) \tag{2.12}$$

The modified surge used in equation 2.12 is used to eliminate the surge inertial force. Since the right side of Equation 2.12 defines the surge inertial force, it can be set to zero. Therefore, Equation 2.12 reduces to Equation 2.13. Equation 2.14 is used to calculate the hydrodynamic force.

$$M\ddot{x}_{meas} = k_s x_{meas} - k_s x_{meas,0} \tag{2.13}$$

$$F_H = X_T + k_s x_{meas} - k_s x_{meas,0} \tag{2.14}$$

Equation 2.14 eliminates the inertial force of the mass spring damper because the spring constant times the mean surge is approximately equal to the measured force. Figure 2.20 shows the total resistance after low pass and moving average filtering, the spring constant times surge, the spring constant times the average surge, and the hydrodynamic force. From Figure 2.20, it is evident that the negative of spring constant times the surge motion shows very little variation from the total resistance. Therefore, the two cancel each other out when used in Equation 2.14. What is left is the term with the average surge times the spring constant. This average value is determined from a window shortly after the end of acceleration until slightly before deceleration. Figure 2.20 indicates the start and stop time of mean calculation.

www.manaraa.com

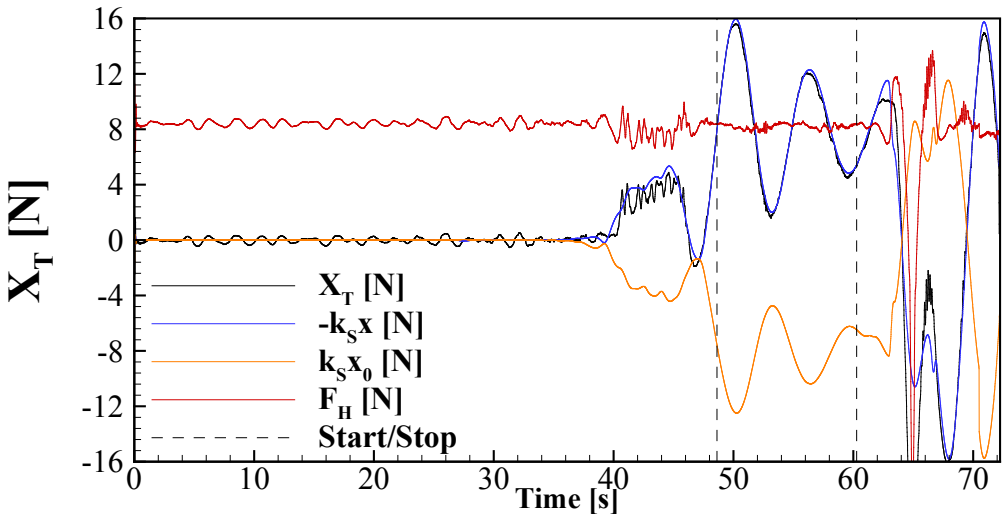

Figure 2.20 Total resistance, mass spring damper values, and hydrodynamic force

2.5.3 Calm Water Data Reduction Equations

Calm water testing was completed for the KCS model in calm water conditions. After testing, the signals for each variable needed to be conditioned. The Reynolds number was then calculated for the temperature of the water test conditions and 15℃, which was used for a total standard added resistance calculation. Equation 2.15 is used to calculate the total resistance coefficient (C_T).

$$C_T = \frac{F_{H,calm}}{\frac{1}{2}\rho S V^2} \tag{2.15}$$

Where $F_{H,calm}$ is the calm water total resistance, S is the wetted surface, and V is the velocity. Equation 2.16 is used to calculate the frictional resistance coefficient (C_F), following (ITTC 2014).

$$C_F = \frac{0.075}{(\log_{10} \mathrm{Re} - 2)^2} \tag{2.16}$$

Where Re is the Reynolds number at the temperature during a given run. Equations 2.17 and 2.18 are used to calculate the residuary resistance coefficient (C_R) with and without the Prohaska method, respectively.

$$C_R = C_T - (1+K)C_F \tag{2.17}$$

$$C_R = C_T - C_F \tag{2.18}$$

www.manaraa.com

Where K is calculated using the Pohaska method as in (Larsson et al. 2014). Equation 2.19 is used to calculate the Froude number to be used in the Prohaska method.

$$F_r = \frac{V}{\sqrt{gL}} \tag{2.19}$$

For the Prohaska method, F_R^4/C_F vs. C_T/C_F is plotted and a linear fit is found. The y intercept of the aforementioned linear fit was used for the Prohaska method K value. In order to compare total resistance between runs with different water temperatures, the total resistance coefficient is calculated for a temperature of 15℃. Equations 2.20 and 2.21 are used to calculate the total resistance coefficient at 15℃ with and without the Prohaska method, respectively. The sinkage and trim motions were also calculated for the calm water tests. The length of the ship is used to nondimensionalize the sinkage (σ/L) and the trim (τ) is reported in degrees.

$$C_T^{15^\circ} = C_R + (1+K)C_F^{15^\circ} \tag{2.20}$$

$$C_T^{15^\circ} = C_R + C_F^{15^\circ} \tag{2.21}$$

2.5.4 Head and Oblique Wave Data Reduction Equations

Testing in wave conditions with varying wave encounter angles was completed for the KCS model. The wave encounter angles tested were, 0°, 45°, 90°, 135°, and 180°, where 0° represents head waves as in Figure 2.11. The wave encounter angles 0°, 45°, 90°, 135°, and 180° are referred to as head, bow quartering, beam, stern quartering, and following waves, respectively. For each case, there are variables that are dependent on the set carriage speed and the measured water temperature. Values of water density and viscosity from (ITTC 2006) are used for analysis. These results are determined via a computer code based on the temperature of the water. The density and viscosity of water is dependent on the measured temperature of the water. According to (ITTC 2006), the density and viscosity are computed from a computer code from the NIST (National Institute of Standards and Technology) and the NMI (National Meteorological Institute). The Reynolds number is the carriage velocity non-dimensionalized by multiplying it by the length and dividing by the kinematic viscosity. Equation 2.22 is used to define the Reynolds number. The Froude number, Equation 2.19, is also used to non-dimensionalize the carriage velocity.

www.manaraa.com

$$\mathrm{Re} = \frac{VL}{\nu} \tag{2.22}$$

The results are non-dimensionalized in order to compare scale model results. Equation 2.23 is used to calculate the total resistance coefficient, the non-dimensional hydrodynamic force. The hydrodynamic force is non-dimensionalized by the water density, wetted surface, and the velocity.

$$C_T(t) = \frac{F_H(t)}{1/2\rho S V^2} \tag{2.23}$$

Equation 2.24 is used to non-dimensionalize the wave elevation at the forward perpendicular. The wave elevation is non-dimensoinalized by the ship length.

$$\frac{\zeta(t)}{L} \tag{2.24}$$

Equations 2.25 and 2.26 are used to non-dimensionalize the surge and heave motions, respectively. The surge and heave motions are non-dimensionalized by dividing by the target wave amplitude.

$$\frac{x(t)}{A} \tag{2.25}$$

$$\frac{z(t)}{A} \tag{2.26}$$

Equations 2.27 and 2.28 are used to non-dimensionalize the roll and pitch motions, respectively. The motions are non-dimensionalized by dividing by the target wave amplitude and the wave number. Equation 2.29 is used to calculate the target wave number, k. While the wavelength is not directly measured, it is calculated based on the set $\lambda/L=1/60$. The uncertainty of this calculation is addressed in the uncertainty analysis.

$$\frac{\phi(t)}{Ak} \tag{2.27}$$

$$\frac{\theta(t)}{Ak} \tag{2.28}$$

$$k = \frac{2\pi}{\lambda} \tag{2.29}$$

Equation 2.30 is used to calculate the added resistance in head waves. This value represents the non-dimensional force due to wave encounter. The added resistance is the difference between the 0^{th} harmonic of the hydrodynamic force for a specific run and the

www.manaraa.com

mean calm water hydrodynamic force with the same wave encounter angle divided by the water density, gravitational constant, the measured 1st harmonic wave amplitude squared, and the ship's beam squared divided by the ship's length.

$$\sigma_{aw} = \frac{F_{H_0} - F_{H,calm}}{\rho g \zeta_{S_1}^2 B^2 / L} \tag{2.30}$$

Fourier analysis is used to convert the wave, hydrodynamic force, surge, heave, roll, and pitch results from the time domain into the frequency domain. The encounter of the forward perpendicular of the ship with a wave peak is chosen as the start time for the Fourier analysis. This encounter point is located at t/Te = 0 in the time histories. The analysis frame for each case is 10 full wave encounter periods during the steady state velocity period. For several cases the number of periods is less than 10 due to space constraints limiting run length. In those cases, the maximum amount of periods are analyzed. The 0th through 4th harmonic amplitudes were calculated along with the 1st through 4th phases for the force and all four motions. Equations 2.31 through 2.35 are used to calculate the harmonic amplitudes and phases for hydrodynamic force, motions, and waves.

$$R(t) = \frac{R_0}{2} + \sum_{n=1}^{N} R_n \cos(2\pi f_e t + R_{\varepsilon n}) \tag{2.31}$$

$$a_n = \frac{2}{T}\int_0^T R(t)\cos(2\pi f_e t)dt \tag{2.32}$$

$$b_n = \frac{2}{T}\int_0^T R(t)\sin(2\pi f_e t)dt \tag{2.33}$$

$$R_n = \sqrt{a_n^2 + b_n^2} \tag{2.34}$$

$$R_{\varepsilon n} = tan^{-1}\left(-\frac{b_n}{a_n}\right) - \gamma_I \tag{2.35}$$

Where R_0 is the mean value, R_n is the n-th harmonic amplitude, $R_{\varepsilon n}$ is the phase of the n-th harmonic, and γ_I is the incident wave phase at the bow at t=0.

www.manaraa.com

CHAPTER 3 UNCERTAINTY ANALYSIS

The uncertainty analysis follows on (ASME 2013) Standard. The (ASME 2013) standard is an update to (ASME 2005). The update creates more uniformity between the ASME and ISO gum standards.

3.1 Standard Total and Expanded Uncertainty

The total uncertainty of a results has two components. These components are the systematic and random standard uncertainties associated with measurements. The systematic standard uncertainty is due to measuring system limitations. The random standard uncertainties are due to the repeatability of measurements over multiple tests. Equation 3.1 is used to calculate the total uncertainty a specific variable R.

$$u_R = \sqrt{b_R^2 + s_{\bar{R}}^2} \tag{3.1}$$

Where $s_{\bar{R}}$ and b_R represent the random standard uncertainty and systematic standard uncertainty for the variable R. The approach presented in (ASME 2013) is followed in order to calculate the random and systematic standard uncertainty for each variable.

A common way of expressing uncertainty is an interval about the measurement result that the true answer lies within, given a certain confidence. This interval is calculated by multiplying the standard total uncertainty by a coverage factor. The coverage factor determines the confidence that the true result lies within the interval. For the present study, a confidence level of 95% will be used for the expanded uncertainty. Although M < 10, a large sample size is assumed. Therefore, the coverage factor for a normal t-distribution is 2. Equation 3.2 is used to calculate the expanded uncertainty.

$$U_{R,95} = t_{95} \cdot u_R = 2 \cdot u_R \tag{3.2}$$

The total uncertainty is presented as a percentage of the result and the dynamic range. The result is the mean of the results of the specified variable. Equation 3.3 defines the dynamic range (DR) of a group of results, (c).

$$DR = \left(Max(c) - Min(c)\right)/2 \tag{3.3}$$

www.manaraa.com

3.2 Random Standard Uncertainty

The random standard uncertainty is calculated using the deviation results from the expected value based on a finite number of repeated runs. The expected quantity for a given variable is defined as the mean value of measured variables. The mean value is found by dividing the sum of all of the measured quantities by the number of runs. Equation 3.4 is used to calculate the mean value.

$$\overline{R} = \frac{1}{M}\sum_{m=1}^{M} R_m \tag{3.4}$$

Where $\overline{R}$ is the mean result, M is the number of runs, and q_n is the individual result of the run. The standard deviation is a measure of the variance of individual results from the mean value. Equation 3.5 is used to calculate the standard deviation. Equation 3.6 is used to calculate the random standard uncertainty.

$$s_R = \sqrt{\frac{\sum_{m=1}^{M}\left(R_m - \overline{R}\right)^2}{M-1}} \tag{3.5}$$

$$s_{\overline{R}} = \frac{s_R}{\sqrt{M}} \tag{3.6}$$

3.3 Systematic Standard Uncertainty

When measurement results are non-dimensionalized, the final result is a function of the variables used in the calculation as in Equation 3.7.

$$R = R\left(x_1, x_2, ..., x_j\right) \tag{3.7}$$

Where x_i, represents the variables used to calculate R and i is a counter 1 through j. A combined systematic standard uncertainty is calculated to define the uncertainty of R in terms of uncertainties of the data reduction variables. Equation 3.8 is used to calculate the total systematic standard uncertainty. If all of the individual measurements are uncorrelated, the total systematic standard uncertainty calculation reduces to Equation 3.9.

$$b_R^2 = \sum_{i=1}^{j}\left(\frac{\partial R}{\partial x_i}\right)^2 b^2(x_i) + 2\sum_{i=1}^{J-1}\sum_{k=i+1}^{J}\frac{\partial R}{\partial x_i}\frac{\partial R}{\partial x_k} b^2(x_i, x_k) \tag{3.8}$$

$$b_R = \sqrt{\sum_{i=1}^{J}\left(\theta_{x_i} b_{x_i}\right)^2} \tag{3.9}$$

www.manaraa.com

3.3.1 Sensitivity Coefficients and Systematic Uncertainty for Calm Water Tests

The systematic standard uncertainty of a result is the sum of the contributing systematic uncertainties of the measured variables. Figure 3.1 shows the schematic of the uncertainty sources and their effect on the non-dimensionalized results, similar to the recommended formatting of (ITTC 2014). The bold boxes indicate the major contributor to the uncertainty. Though the systematic uncertainty of the principle particulars, geometric uncertainty, do not directly effect the RAO, they can effect the results if the uncertainty is large and the true values cannot be determined. Likewise, the installation set up does not directly effect the non-dimensionalized result, but if the model were to be mounted not at the center of gravity, the results would be inaccurate. This is why the installation uncertainty is considered. Every instrument is calibrated following (ITTC 2014). The uncertainty of calibration is calculated using the standard deviation of linear regression analysis, SEE. This category also includes manufacturer's uncertainty of the calibration standard. Repeat measurements are completed, but the random uncertainty is only determined for the non-dimensionalized results.

For all results the major contributor to the total standard uncertainty was the systematic standard uncertainty. For the total resistance coefficients and the residual resistance coefficients, the major source of systematic uncertainty is the load cell. The major source of systematic uncertainty of the friction coefficient is the Reynolds number. The Reynolds number has a majority of the systematic uncertainty attributed to the viscosity. For both sinkage and trim the major source of uncertainty is the systematic uncertainty of the measured motion.

www.manaraa.com

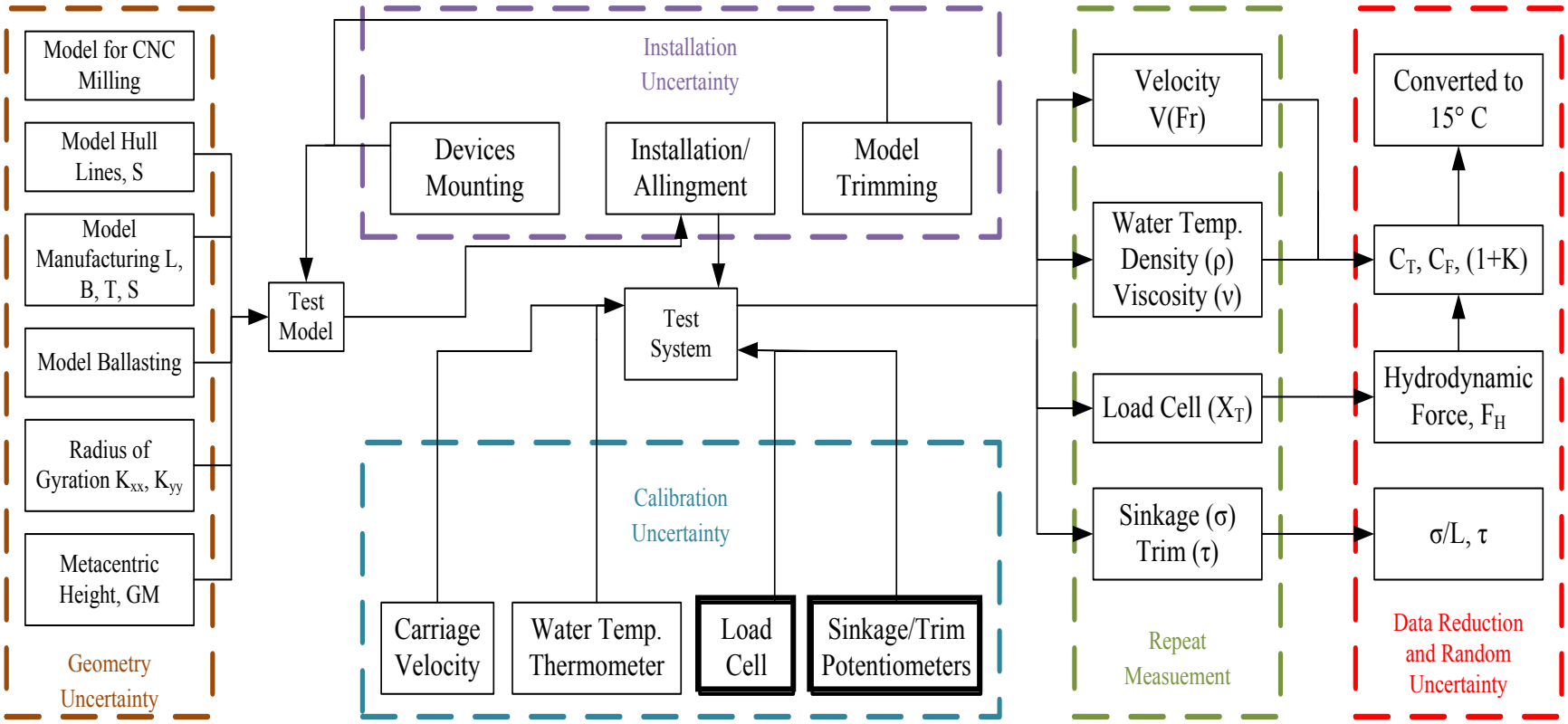

Figure 3.1 Systematic uncertainty sources in calm water test conditions (bold border indicates main sources of uncertainty)

www.manaraa.com

Values of water density and viscosity from (ITTC 2006) are used for analysis. These results are determined via a computer code based on the temperature of the water. The uncertainty of the density and viscosity of water is dependent on the uncertainty of the density calculation and the uncertainty of the temperature measurement. According to (ITTC 2006), the density and viscosity are computed from a computer code from NIST (National Institute of Standards and Technology), the NMI (National Meteorological Institute) for the United States. According to (ITTC 2006), the computer code has uncertainties of ± 0.0001 % and ± 1 %, for the density and kinematic viscosity respectively. The bias limit of the temperature is 0.06 °C based upon the variance of the thermometer resolution. Equation 3.10 and 3.11 are used to calculate the systematic standard uncertainties of density and viscosity respectively.

$$b_\rho = \frac{\sqrt{B_{\rho,Code}^2 + \left(\theta_T B_T\right)^2}}{2} \tag{3.10}$$

$$b_\nu = \frac{\sqrt{B_{\nu,Code}^2 + \left(\theta_T B_T\right)^2}}{2} \tag{3.11}$$

Equations 3.12 and 3.13 are used to calculate the total systematic standard uncertainty of Reynolds number and Froude number, respectively. The uncertainty of gravity is neglected because the gravitational constant is used. Equations 3.14 through and 3.18 are used to calculate the sensitivity coefficients used for the Reynolds number and Froude number systematic standard uncertainty calculation.

$$b_{\mathrm{Re}} = \sqrt{(\theta_V b_V)^2 + (\theta_L b_L)^2 + (\theta_\nu b_\nu)^2} \tag{3.12}$$

$$b_{Fr} = \sqrt{(\theta_V b_V)^2 + (\theta_L b_L)^2} \tag{3.13}$$

$$\theta_{V,\mathrm{Re}} = \frac{\partial \mathrm{Re}}{\partial V} = \frac{L}{\nu} \tag{3.14}$$

$$\theta_{L,\mathrm{Re}} = \frac{\partial \mathrm{Re}}{\partial L} = \frac{V}{\nu} \tag{3.15}$$

$$\theta_{\nu,\mathrm{Re}} \frac{\partial \mathrm{Re}}{\partial \nu} = -\frac{VL}{\nu^2} \tag{3.16}$$

$$\theta_{V,Fr} = \frac{\partial Fr}{\partial V} = \frac{1}{\sqrt{gL}} \tag{3.17}$$

www.manaraa.com

$$\theta_{V,Fr} = \frac{\partial Fr}{\partial V} = -\frac{1}{2\sqrt{g}L^{3/2}} \tag{3.18}$$

Equation 3.19 is used to calculate the systematic standard uncertainty for total resistance coefficient. Equation 3.20 through 3.23 are used to calculate the sensitivity coefficients for total resistance coefficient.

$$b_{C_T} = \sqrt{\left(\theta_{F_{H,calm}} b_{F_{H,calm}}\right)^2 + \left(\theta_\rho b_\rho\right)^2 + \left(\theta_S b_S\right)^2 + \left(\theta_V b_V\right)^2} \tag{3.19}$$

$$\theta_{F_{H,calm}} = \frac{\partial C_T}{\partial F_{H,calm}} = \frac{2}{\rho S V^2} \tag{3.20}$$

$$\theta_\rho = \frac{\partial C_T}{\partial \rho} = -\frac{2F_{H,calm}}{\rho^2 S V^2} \tag{3.21}$$

$$\theta_S = \frac{\partial C_T}{\partial S} = -\frac{2F_{H,calm}}{\rho S^2 V^2} \tag{3.22}$$

$$\theta_V = \frac{\partial C_T}{\partial V} = -\frac{4F_{H,calm}}{\rho S V^3} \tag{3.23}$$

Equation 3.24 is used to calculate the systematic standard uncertainty of the frictional resistance coefficient. Equation 3.25 is used to calculate the sensitivity coefficient for frictional resistance coefficient.

$$b_{C_F} = \sqrt{\left(\theta_{\mathrm{Re}} b_{\mathrm{Re}}\right)^2} \tag{3.24}$$

$$\theta_{\mathrm{Re}} = \frac{\partial C_F}{\partial \mathrm{Re}} = \frac{0.15\log^2(10)}{\mathrm{Re}(2\log(10) - \log(\mathrm{Re}))^2} \tag{3.25}$$

Equation 3.26 is used to calculate the systematic standard uncertainty for residual resistance coefficient. Equations 3.27 through 3.29 are used to calculate the sensitivity coefficients of residual resistance coefficient.

$$b_{C_R} = \sqrt{\left(\theta_{C_T} b_{C_T}\right)^2 + \left(\theta_{C_F} b_{C_F}\right)^2 + \left(\theta_K b_K\right)^2} \tag{3.26}$$

$$\theta_{C_T} = \frac{\partial C_R}{\partial C_T} = 1 \tag{3.27}$$

$$\theta_{C_F} = \frac{\partial C_R}{\partial C_F} = -(1+K) \tag{3.28}$$

www.manaraa.com

$$\theta_K = \frac{\partial C_R}{\partial K} = -C_F \tag{3.29}$$

Equation 3.30 is used to calculate the systematic standard uncertainty for trim coefficient.Equations 3.31 through 3.32 are used to calculate the sensitivity coefficients for the trim coefficient.

$$b_{\frac{\sigma}{L}} = \sqrt{\left(\theta_\sigma b_\sigma\right)^2 + \left(\theta_L b_L\right)^2} \tag{3.30}$$

$$\theta_\sigma = \frac{\partial \frac{\sigma}{L}}{\partial \sigma} = \frac{1}{L} \tag{3.31}$$

$$\theta_L = \frac{\partial \frac{\sigma}{L}}{\partial L} = -\frac{\sigma}{L^2} \tag{3.32}$$

3.3.2 Sensitivity Coefficients and Systematic Standard Uncertainty for Wave Tests

Like the uncertainty schematic for calm water, Figure 3.2 shows the schematic of the uncertainty sources and their effect on the non-dimensionalized results similar to the formatting of (ITTC 2014). The bold boxes indicate the major contributor to the uncertainty. Though the systematic uncertainty of the principle particulars, geometric uncertainty, do not directly effect the RAO, they can effect the results if the uncertainty is large and the true values cannot be determined. Likewise, the installation set up does not directly effect the non-dimensionalized result, but if the model were to be mounted not at the center of gravity, the results would be inaccurate. This is why the installation uncertainty is considered. Every instrument is calibrated following (ITTC 2014). For every result, the systematic standard uncertainty is the major contributor to the uncertainty. Also, the major contributor to each total systematic standard uncertianty is due to the directe measurement of the motion or resistance. Repeat measurements are completed, but the random uncertainty is only determined for the non-dimensionalized results.

www.manaraa.com

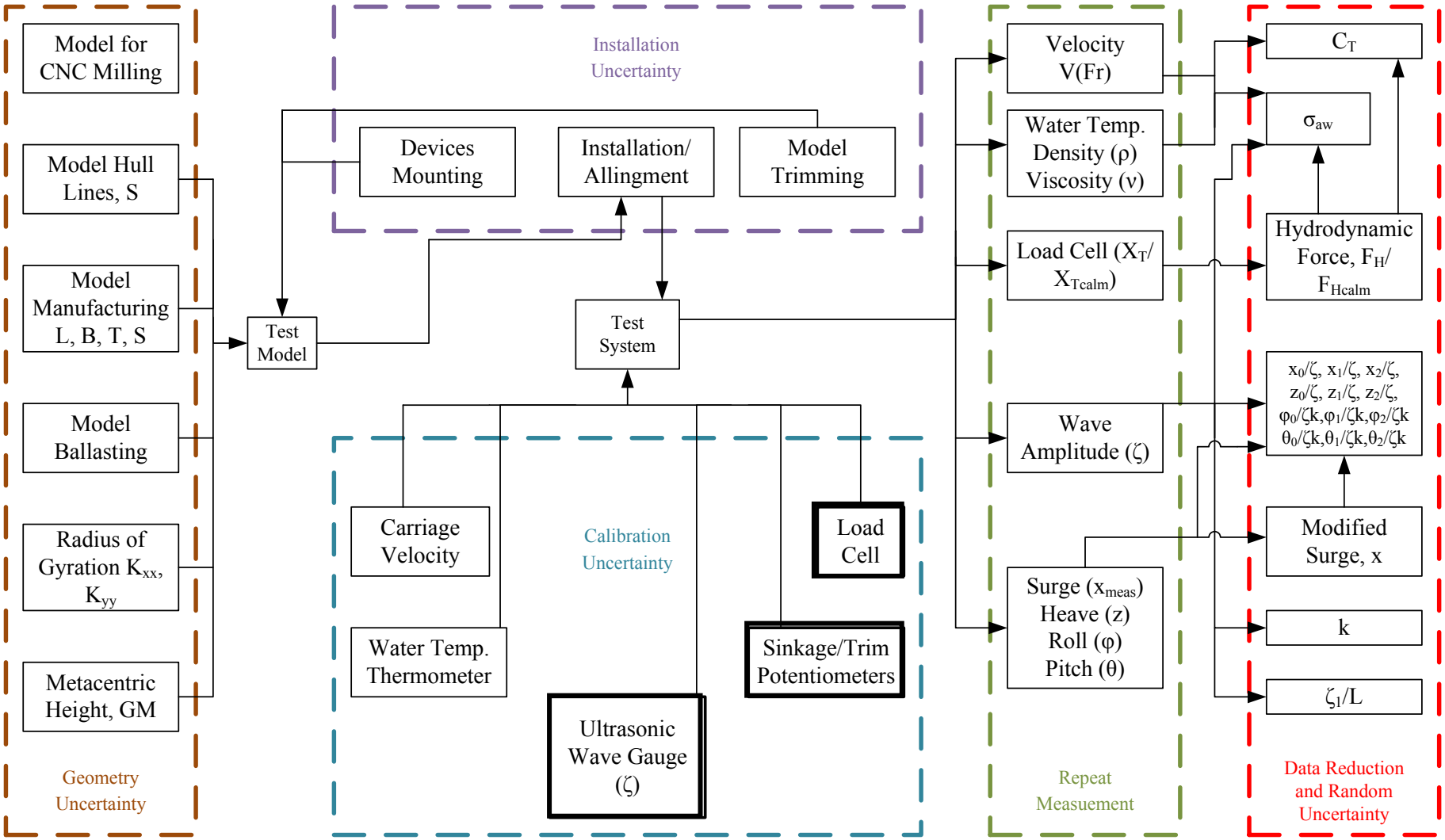

Figure 3.2 Systematic uncertainty sources in wave test conditions (bold border indicates main sources of uncertainty)

www.manaraa.com

Values of water density and viscosity from (ITTC 2006) are used for analysis. These results are determined via a computer code as described in the calm water methods. The systematic uncertainty of density and viscosity are calculated using the same methods as calm water, Equations 3.10 and 3.11.

Equations 3.33 and 3.34 are used to calculate the systematic standard uncertainty of Reynolds number and Froude number, respectively. The uncertainty of gravity is neglected because the gravitational constant is used. Equations 3.35 through and 3.39 are used to calculate the sensitivity coefficients used for the Reynolds number and Froude number total bias calculations.

$$b_{\mathrm{Re}} = \sqrt{(\theta_V b_V)^2 + (\theta_L b_L)^2 + (\theta_\nu b_\nu)^2} \tag{3.33}$$

$$b_{Fr} = \sqrt{(\theta_V b_V)^2 + (\theta_L b_L)^2} \tag{3.34}$$

$$\theta_{V,\mathrm{Re}} = \frac{\partial \mathrm{Re}}{\partial V} = \frac{L}{\nu} \tag{3.35}$$

$$\theta_{L,\mathrm{Re}} = \frac{\partial \mathrm{Re}}{\partial L} = \frac{V}{\nu} \tag{3.36}$$

$$\theta_{\nu,\mathrm{Re}} \frac{\partial \mathrm{Re}}{\partial \nu} = -\frac{VL}{\nu^2} \tag{3.37}$$

$$\theta_{V,Fr} = \frac{\partial Fr}{\partial V} = \frac{1}{\sqrt{gL}} \tag{3.38}$$

$$\theta_{V,Fr} = \frac{\partial Fr}{\partial V} = -\frac{1}{2\sqrt{g}L^{3/2}} \tag{3.39}$$

Equation 3.40 shows the total systematic standard uncertainty for total resistance coefficient. Equation 3.41 through 3.44 are used to calculate the sensitivity coefficients for total resistance coefficient.

$$b_{C_T} = \sqrt{\left(\theta_{F_H} b_{F_H}\right)^2 + \left(\theta_\rho b_\rho\right)^2 + \left(\theta_S b_S\right)^2 + \left(\theta_V b_V\right)^2} \tag{3.40}$$

$$\theta_{F_H} = \frac{\partial C_T}{\partial F_H} = \frac{2}{\rho S V^2} \tag{3.41}$$

$$\theta_\rho = \frac{\partial C_T}{\partial \rho} = -\frac{2F_{H,calm}}{\rho^2 S V^2} \tag{3.42}$$

www.manaraa.com

$$\theta_S = \frac{\partial C_T}{\partial S} = -\frac{2F_H}{\rho S^2 V^2} \tag{3.43}$$

$$\theta_V = \frac{\partial C_T}{\partial V} = -\frac{4F_H}{\rho S V^3} \tag{3.44}$$

Equation 3.45 is used to calculate the systematic standard uncertainty for added resistance. Equations 3.46 through 3.51 are used to calculate the sensitivity coefficients used for added resistance.

$$b_{\sigma_{aw}} = \sqrt{\left(\theta_{F_{H0}} b_{F_{H0}}\right)^2 + \left(\theta_{F_{HCalm}} b_{F_{HCalm}}\right)^2 + \left(\theta_\rho b_\rho\right)^2 + \left(\theta_{\zeta_1} b_{\zeta_1}\right)^2 + \left(\theta_B b_B\right)^2 + \left(\theta_L b_L\right)^2} \tag{3.45}$$

$$\theta_{F_{H0}} = \frac{\partial \sigma_{aw}}{\partial F_{H0}} = \frac{1}{\rho g \zeta_{S1}^2 B^2 / L} \tag{3.46}$$

$$\theta_{F_{H,calm}} = \frac{\partial \sigma_{aw}}{\partial F_{H,calm}} = \frac{-1}{\rho g \zeta_{S1}^2 B^2 / L} \tag{3.47}$$

$$\theta_\rho = \frac{\partial \sigma_{aw}}{\partial \rho} = -\frac{F_{H0} - F_{H,calm}}{\rho^2 g \zeta_{S1}^2 B^2 / L} \tag{3.48}$$

$$\theta_{\zeta_{1I}} = \frac{\partial \sigma_{aw}}{\partial \zeta_{FP1}} = -2\frac{F_{H0} - F_{H,calm}}{\rho g \zeta_{S1}^3 B^2 / L} \tag{3.49}$$

$$\theta_B = \frac{\partial \sigma_{aw}}{\partial B} = -2\frac{F_{H0} - F_{H,calm}}{\rho g \zeta_{S1}^2 B^3 / L} \tag{3.50}$$

$$\theta_L = \frac{\partial \sigma_{aw}}{\partial L} = \frac{F_{H0} - F_{H,calm}}{\rho g \zeta_{S1}^2 B^2} \tag{3.51}$$

Equation 3.52 is used to calculate the systematic standard uncertainty for surge transfer function. Equations 3.53 through 3.54 are used to calculate the sensitivity coefficients for the surge transfer function.

$$b_{x/A} = \sqrt{\left(\theta_x b_x\right)^2 + \left(\theta_A b_A\right)^2} \tag{3.52}$$

$$\theta_x = \frac{\partial x/A}{\partial x} = \frac{1}{A} \tag{3.53}$$

$$\theta_A = \frac{\partial x/A}{\partial A} = -\frac{x}{A^2} \tag{3.54}$$

www.manaraa.com

Equation 3.55 is used to calculate the systematic standard uncertainty for heave transfer function. Equations 3.56 and 3.57 are used to calculate the sensitivity coefficients for the heave transfer function.

$$b_{z/A} = \sqrt{\left(\theta_z b_z\right)^2 + \left(\theta_A b_A\right)^2} \tag{3.55}$$

$$\theta_z = \frac{\partial z / A}{\partial z} = \frac{1}{A} \tag{3.56}$$

$$\theta_A = \frac{\partial z / A}{\partial A} = -\frac{z}{A^2} \tag{3.57}$$

Equation 3.58 is used to calculate the systematic standard uncertainty for roll transfer function. Equations 3.59 and 3.61 are used to calculate the sensitivity coefficients for the roll heave transfer function.

$$b_{\frac{\phi(t)}{Ak}} = \sqrt{\left(\theta_\phi b_\phi\right)^2 + \left(\theta_A b_A\right)^2 + \left(\theta_k b_k\right)^2} \tag{3.58}$$

$$\theta_\phi = \frac{\partial \frac{\phi}{Ak}}{\partial \phi} = \frac{1}{Ak} \tag{3.59}$$

$$\theta_A = \frac{\partial \frac{\phi}{Ak}}{\partial A} = -\frac{\phi}{A^2 k} \tag{3.60}$$

$$\theta_k = \frac{\partial \frac{\phi}{kA}}{\partial k} = -\frac{\phi}{Ak^2} \tag{3.61}$$

Equation 3.62 is used to calculate the systematic standard uncertainty for pitch transfer function. Equations 3.63 and 3.65 are used to calculate the sensitivity coefficients for the roll heave transfer function.

$$b_{\frac{\theta(t)}{Ak}} = \sqrt{\left(\theta_\theta b_\theta\right)^2 + \left(\theta_A b_A\right)^2 + \left(\theta_k b_k\right)^2} \tag{3.62}$$

$$\theta_\theta = \frac{\partial \frac{\theta}{Ak}}{\partial \theta} = \frac{1}{Ak} \tag{3.63}$$

$$\theta_A = \frac{\partial \frac{\phi}{Ak}}{\partial A} = -\frac{\phi}{A^2 k} \tag{3.64}$$

www.manaraa.com

$$\theta_{\lambda} = \frac{\partial \frac{\phi}{kA}}{\partial \lambda} = -\frac{\phi}{Ak} \tag{3.65}$$

3.3.3 Systematic Standard Uncertainties of Measurements and Mass Properties

Every individual measurement has a systematic standard uncertainty associated with the instrument used to acquire it. The systematic standard uncertainty of measurements effect the non-dimensional results and their uncertainties. Therefore, the systematic standard uncertainty of each measurement is necessary to calculate the total systematic standard uncertainty of the non-dimensionalized result. Procedures from (ASME 2013), (Otzen 2013), and (Otzen 2015) are used to calculate the individual systematic standard uncertainties where they apply. Appendix B shows the procedure for calculating the systematic uncertainty of each measurement. Table 3.1 shows the estimated systematic standard uncertainties for the measured variables. Following (ASME 2013) the 95 % confidence of the individual bias limits must be removed before being factored into the results. This is achieved by dividing the bias limit by the coverage factor of 2, yielding the systematic standard uncertainties.

www.manaraa.com

Table 3.1 Systematic uncertainty of measurements

Variable	Name	Systematic Uncertainty	Units	Magnitude
T_w	Water Temperature	b_{Tw}	kg/m^3	0.05
L	Length Between Perpendiculars	b_L	m	0.001
B	Beam	b_B	m	0.001
T	Draft	b_T	m	0.0005
S	Wetted Surface	b_S	m^2	0.004
M	Model Mass	b_M	kg	0.05
X_T	Measured X-Force	b_{XT}	N	0.04
V	Carriage Velocity	b_V	m/s	0.0007
x	Surge	b_x	mm	0.2
z,σ	Heave	b_z	mm	0.2
ϕ	Roll	b_ϕ	deg	0.04
θ,τ	Pitch	b_θ	deg	0.04
χ	Wave Encounter Angle	b_χ	deg	0.005
A	Desired Wave Amplitude	b_A	m	0
ζ,ζ_s	Wave Amplitude	b_ζ	mm	0.1
λ	Wavelength	b_λ	mm	0.2
T_e	Period of Encounter	b_{Te}	s	-
XG	Longitudinal Center of Gravity	b_{XG}	m	0.003
GM	Metacentric Height	b_{GM}	m	0.00006
KG	Vertical Center of Gravity	b_{KG}	m	0.004
kyy/L	Longitudinal Radius of Gyration	$b_{kyy/L}$	-	0.001
kxx/B	Horizontal Radius of Gyration	$b_{kxx/B}$	-	0.005
T_{hz}, $T_{h\phi}$, $T_{h\theta}$	Natural Heave, Roll, and Pitch Period	b_{fhz}, $b_{fh\phi}$, $b_{fh\theta}$	s	0.006

www.manaraa.com

3.4 Uncertainty Results

3.4.1 Uncertainty in Calm Water

Complete uncertainty analysis was completed for for C_T^{15}, C_R, sinkage, and trim in calm water. The average expanded uncertainty of the total resistance coefficient is 5.2 $\%C_T^{15}$, where larger values occur at lower Froude numbers due to small nominal values. The major contributor to total expanded uncertainty of C_T^{15} comes from the systematic uncertainty. The largest contribution to the systematic uncertainty is the uncertainty of the measured resistance due to the other measured values having relatively small systematic uncertainties. The average expanded uncertainty of the residual resistance coefficient is 635.2 $\%C_R$, where the Froude numbers with low nominal values significantly increase the average percent uncertainty. The major contributor to total expanded uncertainty of C_R is the systematic uncertainty. The systematic uncertainty of the total resistance coefficient heavily influences the total systematic uncertainty, with decreasing percent contribution with increasing wave heights. The average expanded uncertainties of sinkage and trim are 12.4 $\%\sigma/L$ and 691.1 $\%\tau$. The major contributor to the total expanded uncertainty of sinkage is the random uncertainty. The major contributor to the total expanded uncertainty of trim is the total systematic uncertainty. The total systematic uncertainty is large due to the nominal values being much smaller than the range of the instrument. As with the resistance coefficients the sinkage and trim the small nominal values significantly increase the average percent expanded uncertainties. Another reason for the large uncertainties is that the nominal values are lower than what the range of values the experiment was designed for at IIHR Wave Basin. In calm water conditions, the surge free mount and ship size have a large bias when comparing to traditional surge locked experiments with larger ship models.

www.manaraa.com

Table 3.2 Systematic uncertainty analysis for water density

Variable (X)	X	b_{Tw} %T_w	b_X,code	$\theta_{Tw}^2 b_{Tw}^2$ %b_X^2	$b_{X.code}^2$ %b_X^2	b_X %X
ν [m^2/s]	9.99E-07	0.2	1.0E-08	1.4	98.6	1.0
ρ [kg/m^3]	998.2	0.2	0.001	99.1	0.9	0.0

Table 3.3 Uncertainty analysis for total resistance coefficient, C_T^{15}

Fr	Number of runs (M)	C_T^{15}x10^3	$\theta_{F_H}^2 b_{F_H}^2$ %$b_{C_T}^2$	$\theta_\rho^2 b_\rho^2$ %$b_{C_T}^2$	$\theta_S^2 b_S^2$ %$b_{C_T}^2$	$\theta_V^2 b_V^2$ %$b_{C_T}^2$	b_{C_T} %$\overline{C_T}$	$s_{\overline{C_T}}$ %$\overline{C_T}$	u_{C_T} %$\overline{C_T}$	$b_{C_T}^2$ %$u_{C_T}^2$	$s_{\overline{C_T}}^2$ %$u_{C_T}^2$	U_{95,C_T} %$\overline{C_T}$	U_{95,C_T} %DR
0.087	4	4.919	99.4	0.0	0.4	0.2	6.2	0.3	6.2	99.8	0.2	**12.4**	**60.6**
0.108	3	5.072	98.6	0.0	1.0	0.4	3.9	0.7	4.0	96.8	3.2	**7.9**	**39.9**
0.130	3	4.882	97.6	0.0	1.8	0.6	2.8	0.1	2.8	99.9	0.1	**5.7**	**27.5**
0.194	3	4.529	91.6	0.0	7.4	1.0	1.4	1.0	1.7	67.3	32.7	**3.4**	**15.5**
0.205	3	4.638	89.4	0.0	9.4	1.1	1.2	0.3	1.3	94.3	5.7	**2.6**	**11.8**
0.217	3	4.646	87.4	0.0	11.4	1.2	1.1	0.6	1.3	78.3	21.7	**2.5**	**11.8**
0.260	6	4.824	76.2	0.0	22.1	1.7	0.8	0.6	1.0	63.0	37.0	**2.0**	**9.8**
Ave.			**91.5**	**0.0**	**7.6**	**0.9**	**2.5**	**0.5**	**2.6**	**85.6**	**14.4**	**5.2**	**25.3**

*DR=1.148

Table 3.4 Uncertainty analysis for residual resistance coefficient, C_R

Fr	Number of runs (M)	C_Rx10^3	$\theta_{C_T}^2 b_{C_T}^2$ %$b_{C_R}^2$	$\theta_{C_F}^2 b_{C_F}^2$ %$b_{C_R}^2$	$\theta_K^2 b_K^2$ %$b_{C_R}^2$	b_{C_R} %$\overline{C_R}$	$s_{\overline{C_R}}$ %$\overline{C_R}$	u_{C_R} %$\overline{C_R}$	$b_{C_R}^2$ %$u_{C_R}^2$	$s_{\overline{C_R}}^2$ %$u_{C_R}^2$	U_{95,C_R} %$\overline{C_R}$	U_{95,C_R} %DR
0.087	4	0.015	95.9	4.1	0.0	2085.0	100.4	2087.4	99.8	0.2	**4174.8**	**37.4**
0.108	3	0.393	92.6	7.4	0.0	50.3	9.1	51.1	96.8	3.2	**102.2**	**24.6**
0.130	3	0.374	88.2	11.8	0.0	36.9	1.2	37.0	99.9	0.1	**73.9**	**17.0**
0.194	3	0.373	70.5	29.5	0.0	17.2	12.0	20.9	67.3	32.7	**41.8**	**9.6**
0.205	3	0.526	67.3	32.7	0.0	11.0	2.7	11.3	94.3	5.7	**22.6**	**7.3**
0.217	3	0.574	63.9	36.1	0.0	9.1	4.8	10.3	78.3	21.7	**20.6**	**7.2**
0.260	6	0.892	53.9	46.1	0.0	4.4	3.4	5.5	63.0	37.0	**11.0**	**6.0**
Ave.			**76.0**	**24.0**	**0.0**	**316.3**	**19.1**	**317.6**	**85.6**	**14.4**	**635.3**	**15.6**

*DR=1.487

www.manaraa.com

Table 3.5 Uncertainty analysis for sinkage, σ/L

Fr	Number of runs (M)	σ/Lx10^2	$\theta_\sigma^2 b_\sigma^2$ $\%b_{\sigma/L}^2$	$\theta_L^2 b_L^2$ $\%b_{\sigma/L}^2$	$b_{\sigma/L}$ $\%\overline{\sigma/L}$	$s_{\overline{\sigma/L}}$ $\%\overline{\sigma/L}$	$u_{\sigma/L}$ $\%\overline{\sigma/L}$	$b_{\sigma/L}^2$ $\%u_{\sigma/L}^2$	$s_{\overline{\sigma/L}}^2$ $\%u_{\sigma/L}^2$	$U_{95,\sigma/L}$ $\%\overline{\sigma/L}$	$U_{95,\sigma/L}$ $\%DR$
0.087	4	0.200	100.0	0.0	3.7	24.2	24.5	2.3	97.7	**49.0**	**0.5**
0.108	3	-0.600	100.0	0.0	1.2	8.6	8.7	2.0	98.0	**17.3**	**0.5**
0.130	3	-1.700	100.0	0.0	0.4	8.2	8.3	0.3	99.7	**16.5**	**1.3**
0.194	3	-7.700	100.0	0.0	0.1	0.8	0.8	1.5	98.5	**1.6**	**0.6**
0.205	3	-8.800	100.0	0.0	0.1	0.4	0.4	5.0	95.0	**0.8**	**0.3**
0.217	3	-9.800	100.0	0.0	0.1	0.5	0.6	1.9	98.1	**1.1**	**0.5**
0.260	6	-17.300	100.0	0.0	0.0	0.3	0.3	1.9	98.1	**0.6**	**0.5**
Ave.			**100.0**	**0.0**	**0.8**	**6.1**	**6.2**	**2.1**	**97.9**	**12.4**	**0.6**

*DR=0.217

Table 3.6 Uncertainty analysis for trim, τ

Fr	Number of runs (M)	τ [deg]	b_τ $\%\overline{\tau}$	$s_{\overline{\tau}}$ $\%\overline{\tau}$	u_τ $\%\overline{\tau}$	b_τ^2 $\%u_\tau^2$	$s_{\overline{\tau}}^2$ $\%u_\tau^2$	$U_{95,\tau}$ $\%\overline{\tau}$	$U_{95,\tau}$ $\%DR$
0.087	4	0.016	245.4	40.2	248.7	97.4	2.6	**497.3**	**106.4**
0.108	3	0.019	212.8	24.2	214.1	98.7	1.3	**428.3**	**105.7**
0.130	3	0.021	186.9	10.4	187.2	99.7	0.3	**374.4**	**105.2**
0.194	3	0.020	203.0	19.7	204.0	99.1	0.9	**408.0**	**105.5**
0.205	3	-0.004	1111.1	163.3	1123.1	97.9	2.1	**2246.1**	**106.1**
0.217	3	0.020	200.0	27.5	201.9	98.1	1.9	**403.8**	**106.0**
0.260	6	-0.017	239.5	13.5	239.9	99.7	0.3	**479.8**	**105.2**
Ave.			**342.7**	**42.7**	**345.6**	**98.7**	**1.3**	**691.1**	**105.7**

*DR=0.0762

www.manaraa.com

3.4.2 Uncertainty in Waves

Complete uncertainty analysis was completed for ζ/L, σ_{aw}, 0^{th}, 1^{st}, and 2^{nd} harmonic amplitudes of total resistance coefficient, surge, heave, roll, and pitch following (ASME 2013). Table 3.7 through 3.12 show the uncertainty analysis for the 0^{th} harmonic amplitudes of total resistance coefficient, added resistance, surge, heave, roll, and pitch. The 0^{th} harmonic of the total resistance coefficient shows total expanded uncertainty < 5%D for every wave encounter angle. The systematic uncertainty for every wave encounter angle, except χ=0°, is the major contributor to the total expanded uncertainty. The systematic uncertainty of the resistance is the major contributor to the total systematic uncertainty for all wave encounter angles. The added resistance shows very large total expanded uncertainty, in regards to the mean value, due to the mean value being really small or the amplitude of the wave height being very small. The systematic uncertainty for every wave encounter angle is the major contributor to the total expanded uncertainty. The systematic uncertainty of the 0^{th} harmonic resistance and the calm water 0^{th} harmonic resistance are equal major contributors to the total systematic uncertainty for all wave encounter angles.

The 0^{th} harmonic of surge, heave, roll, and pitch show fairly similar uncertainty trends. The average total expanded uncertainty between all wave encounters angles of surge, heave, roll, and pitch are 542.98%D, 20.48%D, 40.02%D, and 81.42%D respectively. The percent uncertainties are inflated due to the relatively small nominal values compared to the range of the instruments. For all 0^{th} harmonic amplitudes, the systematic uncertainty is the significant contributor to the total expanded uncertainty. The significant contributor to the total systematic uncertainty is the measured motion of the given value.

www.manaraa.com

Table 3.7 Uncertainty analysis of 0th harmonic amplitude of total resistance coefficient

χ Dynamic Range	λ/L	Number of Runs (M)	$C_{T0}x10^3$	$\theta^2_{F_{H0}} b^2_{F_{H0}}$ $\%b^2_{C_{T0}}$	$\theta^2_\rho b^2_\rho$ $\%b^2_{C_{T0}}$	$\theta^2_S b^2_S$ $\%b^2_{C_{T0}}$	$\theta^2_V b^2_V$ $\%b^2_{C_{T0}}$	$b_{C_{T0}}$ $\%\overline{C_{T0}}$	$s_{\overline{C_{T0}}}$ $\%\overline{C_{T0}}$	$u_{C_{T0}}$ $\%\overline{C_{T0}}$	$b^2_{C_{T0}}$ $\%u^2_{C_{T0}}$	$s^2_{\overline{C_{T0}}}$ $\%u^2_{C_{T0}}$	$U_{95,C_{T0}}$ $\%\overline{C_{T0}}$	$U_{95,C_{T0}}$ $\%DR$
0^0 DR=1.532	0.50	3	4.97	72.8	0.0	25.2	1.9	0.8	0.2	0.8	92.2	7.8	**1.6**	**5.2**
	1.00	12	6.98	57.6	0.0	39.4	3.0	0.6	0.5	0.8	62.4	37.6	**1.5**	**7.0**
	1.50	3	7.41	54.6	0.0	42.2	3.2	0.6	1.1	1.2	22.3	77.7	**2.5**	**12.1**
	2.00	3	5.73	66.9	0.0	30.8	2.3	0.7	2.1	2.2	9.5	90.5	**4.5**	**16.7**
	Ave.			**63.0**	**0.0**	**34.3**	**2.7**	**0.7**	**1.1**	**1.4**	**38.4**	**61.6**	**2.7**	**11.1**
45^0 DR=0.959	0.50	3	4.83	73.8	0.0	24.4	1.8	0.8	0.2	0.8	92.2	7.8	**1.6**	**8.1**
	1.00	3	6.35	62.1	0.0	35.3	2.7	0.6	0.2	0.7	89.2	10.8	**1.4**	**9.1**
	2.00	3	6.37	62.0	0.0	35.3	2.7	0.6	0.5	0.8	66.2	33.8	**1.6**	**10.5**
	Ave.			**66.0**	**0.0**	**31.5**	**2.4**	**0.7**	**0.4**	**0.8**	**71.3**	**28.7**	**1.7**	**9.8**
90^0 DR=0.701	0.25	3	2.29	92.7	0.0	6.8	0.5	1.5	0.6	1.6	85.3	14.7	**3.2**	**10.4**
	0.30	3	2.86	89.0	0.0	10.2	0.8	1.2	0.8	1.5	67.9	32.1	**2.9**	**11.9**
	0.40	3	2.90	88.8	0.0	10.4	0.8	1.2	0.5	1.3	84.1	15.9	**2.6**	**10.7**
	0.50	3	2.81	89.4	0.0	9.9	0.7	1.2	0.3	1.3	94.3	5.7	**2.5**	**10.1**
	1.00	3	3.43	85.0	0.0	14.0	1.1	1.0	1.3	1.7	36.9	63.1	**3.4**	**16.5**
	2.00	3	3.16	86.9	0.0	12.2	0.9	1.1	0.8	1.3	67.2	32.8	**2.7**	**12.1**
	Ave.			**88.7**	**0.0**	**10.5**	**0.8**	**1.2**	**1.1**	**1.8**	**67.9**	**32.1**	**3.5**	**14.9**
135^0 DR=0.165	0.25	3	4.41	77.4	0.0	21.0	1.6	0.8	0.4	0.9	78.7	21.3	**1.9**	**50.2**
	1.00	3	4.43	77.1	0.0	21.2	1.6	0.8	0.4	0.9	84.5	15.5	**1.8**	**48.4**
	0.40	3	4.50	76.8	0.0	21.6	1.6	0.8	0.2	0.8	96.6	3.4	**1.7**	**45.6**
	0.50	3	4.49	76.9	0.0	21.5	1.6	0.8	0.2	0.9	93.1	6.9	**1.7**	**46.5**
	1.00	3	4.65	75.4	0.0	22.8	1.7	0.8	0.2	0.8	94.7	5.3	**1.6**	**46.3**
	2.00	3	4.62	75.7	0.0	22.6	1.7	0.8	0.5	1.0	71.6	28.4	**1.9**	**53.1**
	Ave.			**77.6**	**0.0**	**20.8**	**1.6**	**0.8**	**0.4**	**0.9**	**79.0**	**21.0**	**1.9**	**29.4**
180^0 DR=0.148	0.50	3	4.59	75.9	0.0	22.4	1.7	0.8	0.1	0.8	97.9	2.1	**1.6**	**50.7**
	1.00	3	4.65	75.4	0.0	22.8	1.7	0.8	0.1	0.8	98.3	1.7	**1.6**	**50.8**
	2.00	3	4.89	73.5	0.0	24.6	1.9	0.8	1.0	1.3	37.8	62.2	**2.5**	**83.0**
	Ave.			**76.2**	**0.0**	**22.1**	**1.7**	**0.8**	**0.6**	**1.1**	**66.9**	**33.1**	**2.1**	**27.8**

www.manaraa.com

Table 3.8 Uncertainty analysis of added resistance coefficient

χ Dynamic Range	λ/L	Number of Runs (M)	σ_{aw}	$\theta^2_{F_{H0}} b^2_{F_{H0}}$ $\%b^2_{\sigma_{aw}}$	$\theta^2_{F_{H\_calm}} b^2_{F_{H\_calm}}$ $\%b^2_{\sigma_{aw}}$	$\theta^2_\rho b^2_\rho$ $\%b^2_{\sigma_{aw}}$	$\theta^2_\zeta b^2_\zeta$ $\%b^2_{\sigma_{aw}}$	$\theta^2_B b^2_B$ $\%b^2_{\sigma_{aw}}$	$\theta^2_L b^2_L$ $\%b^2_{\sigma_{aw}}$	$b_{\sigma_{aw}}$ $\%\overline{\sigma_{aw}}$	$s_{\overline{\sigma_{aw}}}$ $\%\overline{\sigma_{aw}}$	$u_{\sigma_{aw}}$ $\%\overline{\sigma_{aw}}$	$b^2_{\sigma_{aw}}$ $\%u^2_{\sigma_{aw}}$	$s^2_{\overline{\sigma_{aw}}}$ $\%u^2_{\sigma_{aw}}$	$U_{95,\sigma_{aw}}$ $\%\sigma_{aw}$	$U_{95,\sigma_{aw}}$ $\%DR$
0^0 DR=4.592	0.50	3.00	5.16	48.9	49.1	0.0	1.9	0.1	0.0	16.0	3.2	16.3	96.2	3.8	**32.7**	**36.7**
	1.00	12.00	10.36	36.3	36.4	0.0	22.1	5.2	0.0	2.3	1.4	2.7	73.9	26.1	**5.4**	**12.2**
	1.50	3.00	5.50	38.5	38.7	0.0	14.9	7.9	0.0	1.9	3.0	3.5	28.5	71.5	**7.1**	**8.4**
	2.00	3.00	1.18	48.4	48.6	0.0	1.5	1.4	0.0	4.4	11.3	12.1	13.2	86.8	**24.3**	**6.2**
	Ave.			**43.1**	**43.2**	**0.0**	**10.1**	**3.7**	**0.0**	**6.2**	**4.7**	**8.7**	**53.0**	**47.0**	**17.4**	**15.9**
45^0 DR=3.002	0.50	3.00	4.92	49.0	49.2	0.0	1.7	0.1	0.0	16.8	4.0	17.3	94.6	5.4	**34.5**	**56.6**
	1.00	3.00	8.02	40.7	40.9	0.0	14.9	3.5	0.0	2.8	1.0	3.0	88.9	11.1	**6.0**	**16.0**
	2.00	3.00	2.02	45.8	45.9	0.0	4.2	4.0	0.0	2.6	1.6	3.1	73.6	26.4	**6.2**	**4.2**
	Ave.			**45.2**	**45.3**	**0.0**	**6.9**	**2.5**	**0.0**	**7.4**	**2.2**	**7.8**	**85.7**	**14.3**	**15.6**	**25.6**
90^0 DR=16.58	0.25	3.0	8.22	49.3	49.5	0.0	1.2	0.0	0.0	40.1	10.2	41.4	93.9	6.1	**82.8**	**41.0**
	0.30	3.0	34.28	38.2	38.3	0.0	23.0	0.5	0.0	7.6	3.4	8.3	83.4	16.6	**16.6**	**34.3**
	0.40	3.0	20.10	41.9	42.1	0.0	15.4	0.6	0.0	6.9	2.5	7.4	88.5	11.5	**14.8**	**17.9**
	0.50	3.0	11.34	45.5	45.7	0.0	8.3	0.5	0.0	7.6	1.3	7.7	97.1	2.9	**15.3**	**10.5**
	1.00	3.0	5.62	44.9	45.1	0.0	8.1	1.9	0.0	3.8	3.5	5.2	55.2	44.8	**10.3**	**3.5**
	2.00	3.0	1.11	48.6	48.7	0.0	1.4	1.3	0.0	4.7	2.2	5.2	81.6	18.4	**10.3**	**0.7**
	Ave.			**44.8**	**44.9**	**0.0**	**9.6**	**0.8**	**0.0**	**11.8**	**3.9**	**12.5**	**83.3**	**16.7**	**25.0**	**18.0**
135^0 DR=1.257	0.25	3.0	1.25	49.9	50.1	0.0	0.0	0.0	0.0	261.4	150.8	301.8	75.0	25.0	**603.6**	**601.9**
	0.30	3.0	2.57	49.8	50.0	0.0	0.2	0.0	0.0	88.7	29.6	93.5	90.0	10.0	**187.0**	**382.0**
	0.40	3.0	2.78	49.7	49.9	0.0	0.3	0.0	0.0	46.1	8.4	46.9	96.8	3.2	**93.8**	**207.4**
	0.50	3.0	1.55	49.8	50.0	0.0	0.2	0.0	0.0	52.9	1.4	52.9	99.9	0.1	**105.8**	**130.5**
	1.00	3.0	1.20	49.7	49.8	0.0	0.4	0.1	0.0	17.2	1.0	17.2	99.6	0.4	**34.4**	**32.7**
	2.00	3.0	0.27	49.8	50.0	0.0	0.1	0.1	0.0	19.3	9.4	21.4	80.9	19.1	**42.9**	**9.1**
	Ave.			**49.8**	**50.0**	**0.0**	**0.2**	**0.0**	**0.0**	**80.9**	**33.4**	**89.0**	**90.4**	**9.6**	**177.9**	**227.3**
180^0 DR=0.279	0.50	3.00	0.92	49.9	50.0	0.0	0.1	0.0	0.0	89.3	10.5	89.9	98.6	1.4	**179.9**	**592.2**
	1.00	3.00	0.48	49.9	50.0	0.0	0.1	0.0	0.0	42.7	5.8	43.1	98.2	1.8	**86.1**	**148.4**
	2.00	3.00	0.39	49.8	49.9	0.0	0.2	0.2	0.0	13.3	15.4	20.3	42.6	57.4	**40.7**	**56.4**
	Ave.			**49.8**	**50.0**	**0.0**	**0.1**	**0.1**	**0.0**	**48.4**	**10.6**	**51.1**	**79.8**	**20.2**	**102.2**	**265.7**

www.manaraa.com

Table 3.9 Uncertainty analysis of 0th harmonic amplitude of surge

χ Dynamic Range	λ/L	Number of Runs (M)	x_0/A	$\theta_{x_0}^2 b_{x_0}^2$ $\%b_{x_0/A}^2$	$\theta_A^2 b_A^2$ $\%b_{x_0/A}^2$	$b_{x_0/A}$ $\%\overline{x_0/A}$	$s_{\overline{x_0/A}}$ $\%\overline{x_0/A}$	$u_{x_0/A}$ $\%\overline{x_0/A}$	$b_{x_0/A}^2$ $\%u_{x_0/A}^2$	$s_{\overline{x_0/A}}^2$ $\%u_{x_0/A}^2$	$U_{95,x_0/A}$ $\%\overline{x_0/A}$	$U_{95,x_0/A}$ $\%DR$
0^0 DR=0.005	0.50	3	0.010	100.0	0.0	183.3	6.3	183.4	99.9	0.1	**366.9**	**822.4**
	1.00	12	0.002	100.0	0.0	563.1	25.9	563.7	99.8	0.2	**1127.4**	**411.4**
	1.50	3	0.007	100.0	0.0	85.5	38.3	93.7	83.3	16.7	**187.4**	**300.2**
	2.00	3	0.011	100.0	0.0	43.4	12.4	45.2	92.4	7.6	**90.4**	**213.7**
	Ave.			**100.0**	**0.0**	**218.8**	**20.7**	**221.5**	**93.8**	**6.2**	**443.0**	**436.9**
45^0 DR=0.006	0.50	3	0.015	100.0	0.0	124.4	7.1	124.6	99.7	0.3	**249.2**	**604.7**
	1.00	3	0.007	100.0	0.0	128.8	0.5	128.8	100.0	0.0	**257.6**	**301.9**
	2.00	3	0.005	100.0	0.0	96.0	15.3	97.2	97.5	2.5	**194.4**	**152.9**
	Ave.			**100.0**	**0.0**	**116.4**	**7.6**	**116.9**	**99.1**	**0.9**	**233.7**	**353.2**
90^0 DR=0.019	0.25	3	0.039	100.0	0.0	98.2	1.9	98.2	100.0	0.0	**196.4**	**394.7**
	0.30	3	0.012	100.0	0.0	258.1	16.3	258.6	99.6	0.4	**517.3**	**329.5**
	0.40	3	0.007	100.0	0.0	345.8	2.5	345.8	100.0	0.0	**691.7**	**246.7**
	0.50	3	0.006	100.0	0.0	323.1	8.8	323.3	99.9	0.1	**646.5**	**197.4**
	1.00	3	0.002	100.0	0.0	386.2	12.3	386.4	99.9	0.1	**772.7**	**98.7**
	2.00	3	0.001	100.0	0.0	587.6	5.4	587.7	100.0	0.0	**1175.3**	**49.3**
	Ave.			**100.0**	**0.0**	**333.2**	**7.9**	**333.3**	**99.9**	**0.1**	**666.7**	**219.4**
135^0 DR=0.149	0.25	3	0.002	100.0	0.0	1874.0	33.7	1874.3	100.0	0.0	**3748.5**	**512.0**
	0.30	3	0.032	100.0	0.0	99.8	4.3	99.9	99.8	0.2	**199.9**	**427.0**
	0.40	3	0.013	100.0	0.0	185.6	2.3	185.6	100.0	0.0	**371.1**	**320.0**
	0.50	3	0.009	100.0	0.0	214.7	1.7	214.7	100.0	0.0	**429.4**	**256.0**
	1.00	3	0.022	100.0	0.0	44.5	0.7	44.5	100.0	0.0	**89.0**	**128.0**
	2.00	3	0.006	100.0	0.0	78.7	12.8	79.7	97.4	2.6	**159.5**	**64.8**
	Ave.			**100.0**	**0.0**	**416.2**	**9.3**	**416.5**	**99.5**	**0.5**	**832.9**	**284.6**
180^0 DR=0.003	0.50	3	0.007	100.0	0.0	276.5	0.7	276.5	100.0	0.0	**553.0**	**1280.0**
	1.00	3	0.005	100.0	0.0	191.7	2.5	191.7	100.0	0.0	**383.4**	**640.0**
	2.00	3	0.001	100.0	0.0	337.3	39.6	339.7	98.6	1.4	**679.3**	**322.2**
	Ave.			**100.0**	**0.0**	**268.5**	**14.3**	**269.3**	**99.5**	**0.5**	**538.6**	**747.4**

www.manaraa.com

Table 3.10 Uncertainty analysis of 0th harmonic amplitude of heave

χ Dynamic Range	λ/L	Number of Runs (M)	z_0/A	$\theta_{z_0}^2 b_{z_0}^2$ $\%b_{z_0/A}^2$	$\theta_A^2 b_A^2$ $\%b_{z_0/A}^2$	$b_{z_0/A}$ $\%\overline{z_0/A}$	$s_{\overline{z_0/A}}$ $\%\overline{z_0/A}$	$u_{z_0/A}$ $\%\overline{z_0/A}$	$b_{z_0/A}^2$ $\%u_{z_0/A}^2$	$s_{\overline{z_0/A}}^2$ $\%u_{z_0/A}^2$	$U_{95,z_0/A}$ $\%\overline{z_0/A}$	$U_{95,z_0/A}$ $\%DR$
0^0 DR=0.291	0.50	3	0.420	100.0	0.0	3.3	0.2	3.3	99.6	0.4	**6.6**	**16.2**
	1.00	12	0.163	100.0	0.0	4.2	1.3	4.4	91.1	8.9	**8.9**	**8.5**
	1.50	3	0.097	100.0	0.0	4.7	1.9	5.1	86.4	13.6	**10.2**	**5.8**
	2.00	3	0.078	100.0	0.0	4.4	1.6	4.7	89.0	11.0	**9.4**	**4.3**
	Ave.			**100.0**	**0.0**	**4.2**	**1.2**	**4.4**	**91.6**	**8.4**	**8.7**	**8.7**
45^0 DR=0.169	0.50	3	0.419	100.0	0.0	3.3	1.5	3.6	83.3	16.7	**7.2**	**17.9**
	1.00	3	0.082	100.0	0.0	8.5	0.4	8.5	99.8	0.2	**16.9**	**8.2**
	2.00	3	0.090	100.0	0.0	3.8	0.3	3.8	99.4	0.6	**7.7**	**4.1**
	Ave.			**100.0**	**0.0**	**5.2**	**0.7**	**5.3**	**94.2**	**5.8**	**10.6**	**10.1**
90^0 DR=0.197	0.25	3	0.399	100.0	0.0	6.9	1.1	7.0	97.4	2.6	**14.0**	**28.4**
	0.30	3	0.294	100.0	0.0	7.8	2.0	8.1	93.8	6.2	**16.2**	**24.1**
	0.40	3	0.273	100.0	0.0	6.3	1.3	6.4	96.2	3.8	**12.9**	**17.9**
	0.50	3	0.202	100.0	0.0	6.8	0.5	6.9	99.5	0.5	**13.7**	**14.1**
	1.00	3	0.032	100.0	0.0	21.6	7.5	22.9	89.3	10.7	**45.8**	**7.4**
	2.00	3	0.011	100.0	0.0	31.2	5.9	31.7	96.6	3.4	**63.4**	**3.6**
	Ave.			**100.0**	**0.0**	**13.4**	**3.0**	**13.8**	**95.5**	**4.5**	**27.7**	**15.9**
135^0 DR=0.068	0.25	3	0.047	100.0	0.0	58.6	8.6	59.2	97.9	2.1	**118.4**	**81.5**
	0.30	3	0.161	100.0	0.0	14.3	1.0	14.4	99.5	0.5	**28.7**	**67.4**
	0.40	3	0.092	100.0	0.0	18.7	3.7	19.1	96.3	3.7	**38.2**	**51.4**
	0.50	3	0.104	100.0	0.0	13.2	1.0	13.3	99.4	0.6	**26.5**	**40.5**
	1.00	3	0.029	100.0	0.0	23.9	6.8	24.8	92.5	7.5	**49.6**	**21.0**
	2.00	3	0.024	100.0	0.0	14.5	3.0	14.8	96.0	4.0	**29.7**	**10.3**
	Ave.			**100.0**	**0.0**	**23.9**	**4.0**	**24.3**	**96.9**	**3.1**	**48.5**	**45.3**
180^0 DR=0.219	0.50	3	0.526	100.0	0.0	2.6	0.3	2.6	98.6	1.4	**5.3**	**12.7**
	1.00	3	0.228	100.0	0.0	3.0	1.8	3.5	74.8	25.2	**7.0**	**7.3**
	2.00	3	0.087	100.0	0.0	3.9	1.4	4.2	88.4	11.6	**8.4**	**3.3**
	Ave.			**100.0**	**0.0**	**3.2**	**1.2**	**3.4**	**87.2**	**12.8**	**6.9**	**7.8**

www.manaraa.com

Table 3.11 Uncertainty analysis of 0th harmonic amplitude of roll

χ Dynamic Range	λ/L	Number of Runs (M)	ϕ_0/Ak	$\theta_{\phi_0}^2 b_{\phi_0}^2$ $\%b_{\phi_0/A}^2$	$\theta_A^2 b_A^2$ $\%b_{\phi_0/A}^2$	$\theta_k^2 b_k^2$ $\%b_{\phi_0/A}^2$	$b_{\phi_0/Ak}$ $\%\overline{\phi_0/Ak}$	$s_{\overline{\phi_0/Ak}}$ $\%\overline{\phi_0/Ak}$	$u_{\phi_0/Ak}$ $\%\overline{\phi_0/Ak}$	$b_{\phi_0/Ak}^2$ $\%u_{\phi_0/Ak}^2$	$s_{\overline{\phi_0/Ak}}^2$ $\%u_{\phi_0/Ak}^2$	$U_{95,\phi_0/Ak}$ $\%\overline{\phi_0/Ak}$	$U_{95,\phi_0/Ak}$ %DR
0^0 DR=0.198	0.50	3	0.080	100.0	0.0	0.0	17.7	19.6	26.4	44.8	55.2	**52.9**	**21.5**
	1.00	12	0.125	100.0	0.0	0.0	11.3	9.7	15.0	57.5	42.5	**29.9**	**19.0**
	1.50	3	0.343	100.0	0.0	0.0	4.1	3.7	5.5	55.7	44.3	**11.1**	**19.3**
	2.00	3	0.418	100.0	0.0	0.0	3.4	7.6	8.4	16.5	83.5	**16.7**	**35.5**
	Ave.			**100.0**	**0.0**	**0.0**	**9.1**	**10.2**	**13.8**	**43.6**	**56.4**	**27.6**	**23.8**
45^0 DR=0.369	0.50	3	0.148	100.0	0.0	0.0	9.6	1.1	9.7	98.8	1.2	**19.3**	**3.0**
	1.00	3	0.642	100.0	0.0	0.0	2.2	0.5	2.3	95.2	4.8	**4.5**	**3.1**
	2.00	3	2.039	99.9	0.0	0.1	0.7	0.4	0.8	75.1	24.9	**1.6**	**3.5**
	Ave.			**100.0**	**0.0**	**0.0**	**10.0**	**7.0**	**12.4**	**52.7**	**47.3**	**24.7**	**11.0**
90^0 DR=0.366	0.25	3	0.030	100.0	0.0	0.0	48.0	21.9	52.7	82.7	17.3	**105.5**	**8.5**
	0.30	3	0.032	100.0	0.0	0.0	44.2	10.9	45.5	94.3	5.7	**91.0**	**8.0**
	0.40	3	0.111	100.0	0.0	0.0	12.8	27.7	30.5	17.6	82.4	**60.9**	**18.5**
	0.50	3	0.244	100.0	0.0	0.0	5.8	8.8	10.6	30.4	69.6	**21.1**	**14.1**
	1.00	3	0.326	100.0	0.0	0.0	4.4	6.2	7.6	33.1	66.9	**15.2**	**13.5**
	2.00	3	0.762	100.0	0.0	0.0	1.9	1.6	2.4	58.7	41.3	**4.9**	**10.1**
	Ave.			**100.0**	**0.0**	**0.0**	**19.5**	**12.8**	**24.9**	**52.8**	**47.2**	**49.8**	**12.1**
135^0 DR=0.232	0.25	3	0.014	100.0	0.0	0.0	103.5	9.2	103.9	99.2	0.8	**207.8**	**12.3**
	0.30	3	0.153	100.0	0.0	0.0	9.3	16.3	18.7	24.7	75.3	**37.5**	**24.6**
	0.40	3	0.264	100.0	0.0	0.0	5.4	22.6	23.2	5.4	94.6	**46.4**	**52.8**
	0.50	3	0.228	100.0	0.0	0.0	6.2	18.8	19.8	9.9	90.1	**39.6**	**38.9**
	1.00	3	0.396	100.0	0.0	0.0	3.6	11.9	12.4	8.3	91.7	**24.9**	**42.4**
	2.00	3	0.479	100.0	0.0	0.0	3.0	3.2	4.3	46.9	53.1	**8.7**	**17.8**
	Ave.			**100.0**	**0.0**	**0.0**	**21.8**	**13.6**	**30.4**	**32.4**	**67.6**	**60.8**	**31.5**
180^0 DR=0.060	0.50	3	0.092	100.0	0.0	0.0	15.4	11.5	19.2	63.9	36.1	**38.4**	**59.2**
	1.00	3	0.089	100.0	0.0	0.0	15.9	5.3	16.8	90.1	9.9	**33.6**	**49.8**
	2.00	3	0.147	100.0	0.0	0.0	9.7	17.3	19.8	23.8	76.2	**39.7**	**96.9**
	Ave.			**100.0**	**0.0**	**0.0**	**13.7**	**11.4**	**18.6**	**59.3**	**40.7**	**37.2**	**68.6**

www.manaraa.com

Table 3.12 Uncertainty analysis of 0th harmonic amplitude of pitch

χ Dynamic Range	λ/L	Number of Runs (M)	θ0/Ak	$\theta_{\theta_0}^2 b_{\theta_0}^2$ $\%b_{\theta_0/A}^2$	$\theta_A^2 b_A^2$ $\%b_{\theta_0/A}^2$	$\theta_k^2 b_k^2$ $\%b_{\theta_0/A}^2$	$b_{\theta_0/Ak}$ $\%\overline{\theta_0/A}$	$s_{\overline{\theta_0/Ak}}$ $\%\overline{\theta_0/A}$	$u_{\theta_0/Ak}$ $\%\overline{\theta_0/Ak}$	$b_{\theta_0/Ak}^2$ $\%u_{\theta_0/Ak}^2$	$s_{\overline{\theta_0/Ak}}^2$ $\%u_{\theta_0/Ak}^2$	$U_{95,\theta_0/Ak}$ $\%\overline{\theta_0/Ak}$	$U_{95,\theta_0/Ak}$ $\%DR$
0^0 DR=0.0373	0.50	3	0.053	100.0	0.0	0.0	26.7	2.6	26.8	99.1	0.9	**53.6**	**51.8**
	1.00	12	0.164	100.0	0.0	0.0	8.7	1.1	8.8	98.3	1.7	**17.5**	**52.0**
	1.50	3	0.112	100.0	0.0	0.0	12.7	2.9	13.0	95.1	4.9	**26.0**	**52.9**
	2.00	3	0.057	100.0	0.0	0.0	24.9	4.7	25.3	96.6	3.4	**50.7**	**52.5**
	Ave.			**100.0**	**0.0**	**0.0**	**18.2**	**2.8**	**18.5**	**97.3**	**2.7**	**36.9**	**52.3**
45^0 DR=0.016	0.50	3	0.031	100.0	0.0	0.0	45.4	10.2	46.5	95.2	4.8	**93.0**	**182.1**
	1.00	3	0.014	100.0	0.0	0.0	98.4	0.5	98.4	100.0	0.0	**196.8**	**177.6**
	2.00	3	0.027	100.0	0.0	0.0	53.1	16.3	55.5	91.3	8.7	**111.0**	**185.9**
	Ave.			**100.0**	**0.0**	**0.0**	**65.6**	**9.0**	**66.8**	**95.5**	**4.5**	**133.6**	**181.9**
90^0 DR=0.034	0.25	3	0.027	100.0	0.0	0.0	52.2	14.0	54.1	93.3	6.7	**108.1**	**86.7**
	0.30	3	0.075	100.0	0.0	0.0	19.0	1.4	19.1	99.5	0.5	**38.2**	**84.0**
	0.40	3	0.066	100.0	0.0	0.0	21.4	2.6	21.5	98.5	1.5	**43.1**	**84.4**
	0.50	3	0.041	100.0	0.0	0.0	34.8	2.5	34.8	99.5	0.5	**69.7**	**84.0**
	1.00	3	0.085	100.0	0.0	0.0	16.7	0.0	16.7	100.0	0.0	**33.4**	**83.8**
	2.00	3	0.043	100.0	0.0	0.0	33.3	3.7	33.5	98.8	1.2	**66.9**	**84.3**
	Ave.			**100.0**	**0.0**	**0.0**	**29.6**	**4.0**	**30.0**	**98.3**	**1.7**	**59.9**	**84.5**
135^0 DR=0.077	0.25	3	0.070	100.0	0.0	0.0	20.3	1.1	20.3	99.7	0.3	**40.6**	**37.0**
	0.30	3	0.051	100.0	0.0	0.0	27.7	11.5	30.0	85.2	14.8	**60.0**	**40.0**
	0.40	3	0.091	100.0	0.0	0.0	15.6	6.6	16.9	84.8	15.2	**33.8**	**40.1**
	0.50	3	0.075	100.0	0.0	0.0	18.9	0.6	18.9	99.9	0.1	**37.8**	**37.0**
	1.00	3	0.164	100.0	0.0	0.0	8.7	5.8	10.4	69.1	30.9	**20.9**	**44.4**
	2.00	3	0.019	100.0	0.0	0.0	73.5	18.2	75.7	94.2	5.8	**151.4**	**38.0**
	Ave.			**100.0**	**0.0**	**0.0**	**27.4**	**7.3**	**28.7**	**88.8**	**11.2**	**57.4**	**39.4**
180^0 DR=0.069	0.50	3	0.024	100.0	0.0	0.0	58.6	3.5	58.7	99.6	0.4	**117.3**	**234.9**
	1.00	3	0.017	100.0	0.0	0.0	84.0	6.5	84.3	99.4	0.6	**168.6**	**235.2**
	2.00	3	0.040	100.0	0.0	0.0	35.9	1.2	35.9	99.9	0.1	**71.9**	**234.6**
	Ave.			**100.0**	**0.0**	**0.0**	**59.5**	**3.7**	**59.6**	**99.6**	**0.4**	**119.3**	**234.9**

www.manaraa.com

Table 3.13 through 3.18 show the uncertainty analysis for the 1st harmonic amplitudes of wave amplitude, total resistance coefficient, surge, heave, roll, and pitch. The average total uncertainty of the 1st harmonic amplitude of wave amplitude is < 10%D for all wave encounter angles where the largest total expanded uncertainties occur at χ = 90° and 135°. Wave encounter angles χ = 90°, 135°, and 180° have larger contributions to the total uncertainty from the random uncertainty as opposed to the large contribution from the systematic uncertainty for χ = 0° and 45°. The major contributor to the large average total expanded uncertainties χ = 90° and 135° is that very small wave lengths were tested for beam and bow quartering. The wavelengths are very small relative to the range of the ultrasonic wave gauges.

The 1st harmonic of the total resistance coefficient have very large total expanded uncertainty for every wave encounter angle due to small nominal values. The total systematic uncertainty for every wave encounter angle is the major contributor to the total expanded uncertainty. The systematic uncertainty of the resistance is the major contributor to the total systematic uncertainty for all wave encounter angles. The small nominal values are due to the inertial forces being removed from the hydraulic force.

The 1st harmonic of surge, heave, roll, and pitch show fairly similar uncertainty trends. The average total expanded uncertainty between all wave encounters angles of surge, heave, roll, and pitch are 49.8%D, 19.5%D, 93.1%D, and 75.2%D respectively. The large average uncertainty of surge is due to small nominal vales. The larger average uncertainty of heave is due to small nominal vales at lower wavelengths. The larger average uncertainties of roll are due to very small nominal values in head wave conditions. The larger average uncertainties of pitch are due to very small nominal values in small wavelength cases. For all 1st harmonic amplitudes, the systematic uncertainty is the significant contributor to the total expanded uncertainty. The significant contributor to the total systematic uncertainty is the measured motion of the given value. Therefore, the data quality could be improved by increasing the accuracy of the motions measuring device.

www.manaraa.com

Table 3.13 Uncertainty analysis of 1st harmonic amplitude of wave amplitude

χ Dynamic Range	λ/L	Number of Runs (M)	$\overline{\zeta_1 / L}$	$\theta_{\zeta_1}^2 \cdot b_{\zeta_1}^2$ $\%b_{\zeta_1/L}^2$	$\theta_L^2 \cdot b_L^2$ $\%b_{\zeta_1/L}^2$	$b_{\zeta_1/L}$ $\%\overline{\zeta_1 / L}$	$s_{\overline{\zeta_1/L}}$ $\%\overline{\zeta_1 / L}$	$u_{\zeta_1/L}$ $\%\overline{\zeta_1 / L}$	$b_{\zeta_1/L}^2$ $\%u_{\zeta_1/L}^2$	$s_{\overline{\zeta_1/L}}^2$ $\%u_{\zeta_1/L}^2$	$U_{95,\overline{\zeta_1/L}}$ $\%\overline{\zeta_1 / L}$	$U_{95,\overline{\zeta_1/L}}$ $\%DR$
0^0 DR=0.006	0.50	3.00	0.004	99.9	0.1	1.1	0.1	1.1	98.9	1.1	**2.2**	**1.5**
	1.00	12.00	0.008	99.6	0.4	0.6	0.4	0.7	60.6	39.4	**1.4**	**1.9**
	1.50	3.00	0.013	98.9	1.1	0.4	0.1	0.4	91.8	8.2	**0.7**	**1.6**
	2.00	3.00	0.017	98.2	1.8	0.3	0.1	0.3	93.0	7.0	**0.6**	**1.5**
	Ave.			**99.1**	**0.9**	**0.6**	**0.6**	**86.1**	**13.9**	**1.2**	**1.6**	**0.0**
45^0 DR=0.006	0.50	3	0.004	99.9	0.1	1.1	1.2	1.6	45.2	54.8	**3.3**	**2.1**
	1.00	3	0.008	99.6	0.4	0.6	0.6	0.8	45.3	54.7	**1.6**	**2.1**
	2.00	3	0.017	98.1	1.9	0.3	0.0	0.3	100.0	0.0	**0.5**	**1.4**
	Ave.			**99.2**	**0.8**	**0.6**	**0.6**	**0.9**	**63.5**	**36.5**	**1.8**	**1.9**
90^0 DR=0.006	0.25	3	0.002	100.0	0.0	2.2	2.3	3.1	47.4	52.6	**6.3**	**1.8**
	0.30	3	0.003	100.0	0.0	1.8	1.2	2.2	70.8	29.2	**4.3**	**1.5**
	0.40	3	0.003	99.9	0.1	1.4	1.5	2.0	47.3	52.7	**4.1**	**1.8**
	0.50	3	0.004	99.9	0.1	1.1	1.1	1.5	50.8	49.2	**3.0**	**1.7**
	1.00	3	0.008	99.5	0.5	0.6	0.7	0.9	37.3	62.7	**1.8**	**2.0**
	2.00	3	0.017	98.1	1.9	0.3	1.3	1.4	3.9	96.1	**2.7**	**6.2**
	Ave.			**99.6**	**0.4**	**1.2**	**1.3**	**1.9**	**42.9**	**57.1**	**3.7**	**2.5**
135^0 DR=0.007	0.25	3	0.002	100.0	0.0	2.1	1.4	2.6	69.0	31.0	**5.2**	**1.5**
	0.30	3	0.003	100.0	0.0	1.8	1.0	2.0	77.5	22.5	**4.1**	**1.4**
	0.40	3	0.003	99.9	0.1	1.4	0.2	1.4	97.2	2.8	**2.8**	**1.3**
	0.50	3	0.004	99.9	0.1	1.1	0.3	1.1	93.6	6.4	**2.2**	**1.3**
	1.00	3	0.008	99.6	0.4	0.6	0.1	0.6	98.4	1.6	**1.1**	**1.3**
	2.00	3	0.017	98.2	1.8	0.3	1.5	1.6	3.1	96.9	**3.1**	**7.2**
	Ave.			**99.6**	**0.4**	**1.2**	**0.8**	**1.5**	**73.1**	**26.9**	**3.1**	**2.3**
180^0 DR=0.006	0.50	3	0.004	99.9	0.1	1.1	0.8	1.4	63.3	36.7	**2.7**	**1.8**
	1.00	3	0.008	99.5	0.5	0.5	0.3	0.6	77.1	22.9	**1.2**	**1.7**
	2.00	3	0.017	98.2	1.8	0.3	0.1	0.3	91.3	8.7	**0.6**	**1.5**
	Ave.			**99.2**	**0.8**	**0.6**	**0.4**	**0.8**	**77.2**	**22.8**	**1.5**	**1.7**

www.manaraa.com

Table 3.14 Uncertainty analysis of 1st harmonic amplitude of total resistance coefficient

χ Dynamic Range	λ/L	Number of Runs (M)	$C_{T1}x10^3$	$\theta^2_{F_{H1}} b^2_{F_{H1}}$ $\%b^2_{C_{T1}}$	$\theta^2_\rho b^2_\rho$ $\%b^2_{C_{T1}}$	$\theta^2_S b^2_S$ $\%b^2_{C_{T1}}$	$\theta^2_V b^2_V$ $\%b^2_{C_{T1}}$	$b_{C_{T1}}$ $\%\overline{C_{T1}}$	$s_{\overline{C_{T1}}}$ $\%\overline{C_{T1}}$	$u_{C_{T1}}$ $\%\overline{C_{T1}}$	$b^2_{C_{T1}}$ $\%u^2_{C_{T1}}$	$s^2_{\overline{C_{T1}}}$ $\%u^2_{C_{T1}}$	$U_{95,C_{T1}}$ $\%\overline{C_{T1}}$	$U_{95,C_{T1}}$ $\%DR$
0^0 DR=0.243	0.50	3	0.17	100.0	0.0	0.0	0.0	19.3	4.9	19.9	93.9	6.1	**39.8**	**27.5**
	1.00	12	0.07	100.0	0.0	0.0	0.0	43.7	6.2	44.2	98.1	1.9	**88.3**	**26.9**
	1.50	3	0.08	100.0	0.0	0.0	0.0	39.9	21.6	45.4	77.4	22.6	**90.8**	**30.2**
	2.00	3	0.56	99.5	0.0	0.4	0.0	5.8	2.3	6.2	86.0	14.0	**12.5**	**28.7**
	Ave.			**99.9**	**0.0**	**0.1**	**0.0**	**27.2**	**8.7**	**28.9**	**88.9**	**11.1**	**57.9**	**28.3**
45^0 DR=0.437	0.50	3	0.05	100.0	0.0	0.0	0.0	61.4	9.5	62.1	97.7	2.3	**124.2**	**14.9**
	1.00	3	0.12	100.0	0.0	0.0	0.0	27.2	1.0	27.2	99.9	0.1	**54.3**	**14.8**
	2.00	3	0.93	98.7	0.0	1.2	0.1	3.5	3.4	4.9	51.9	48.1	**9.7**	**20.7**
	Ave.			**99.6**	**0.0**	**0.4**	**0.0**	**30.7**	**4.6**	**31.4**	**83.2**	**16.8**	**62.8**	**16.8**
90^0 DR=0.716	0.25	3	0.02	100.0	0.0	0.0	0.0	141.4	7.1	141.6	99.8	0.2	**283.1**	**9.1**
	0.30	3	0.06	100.0	0.0	0.0	0.0	57.0	5.6	57.3	99.0	1.0	**114.6**	**9.1**
	0.40	3	0.12	100.0	0.0	0.0	0.0	27.5	5.7	28.1	95.9	4.1	**56.2**	**9.3**
	0.50	3	0.17	100.0	0.0	0.0	0.0	19.5	3.9	19.9	96.1	3.9	**39.7**	**9.2**
	1.00	3	0.27	99.9	0.0	0.1	0.0	12.0	9.1	15.0	63.3	36.7	**30.1**	**11.4**
	2.00	3	0.60	99.5	0.0	0.5	0.0	5.4	3.8	6.6	67.2	32.8	**13.2**	**11.1**
	Ave.			**99.9**	**0.0**	**0.1**	**0.0**	**43.8**	**5.9**	**44.7**	**86.9**	**13.1**	**89.5**	**9.8**
135^0 DR=1.005	0.25	3	0.13	100.0	0.0	0.0	0.0	24.3	7.6	25.5	91.2	8.8	**51.0**	**6.8**
	0.30	3	0.11	100.0	0.0	0.0	0.0	28.7	7.1	29.6	94.2	5.8	**59.1**	**6.6**
	0.40	3	0.31	99.9	0.0	0.1	0.0	10.5	1.2	10.6	98.8	1.2	**21.2**	**6.5**
	0.50	3	0.12	100.0	0.0	0.0	0.0	28.2	2.9	28.4	98.9	1.1	**56.7**	**6.5**
	1.00	3	0.99	98.5	0.0	1.4	0.1	3.3	5.6	6.5	25.8	74.2	**13.0**	**12.8**
	2.00	3	2.12	93.7	0.0	5.9	0.4	1.6	0.5	1.7	91.1	8.9	**3.3**	**7.0**
	Ave.			**98.7**	**0.0**	**1.2**	**0.1**	**16.1**	**4.1**	**17.0**	**83.3**	**16.7**	**34.0**	**7.7**
180^0 DR=0.934	0.50	3	0.25	99.9	0.0	0.1	0.0	12.7	1.6	12.8	98.5	1.5	**25.6**	**7.0**
	1.00	3	0.46	99.7	0.0	0.3	0.0	7.0	0.7	7.0	98.9	1.1	**14.1**	**7.0**
	2.00	3	2.03	94.2	0.0	5.4	0.4	1.6	0.5	1.7	91.6	8.4	**3.4**	**7.5**
	Ave.			**97.9**	**0.0**	**1.9**	**0.1**	**7.1**	**0.9**	**7.2**	**96.3**	**3.7**	**14.4**	**7.1**

www.manaraa.com

Table 3.15 Uncertainty analysis of 1st harmonic amplitude of surge

χ Dynamic Range	λ/L	Number of Runs (M)	x_1/A	$\theta_{x_1}^2 b_{x_1}^2$ $\%b_{x_1/A}^2$	$\theta_A^2 b_A^2$ $\%b_{x_1/A}^2$	$b_{x_1/A}$ $\%\overline{x_1/A}$	$s_{\overline{x_1/A}}$ $\%\overline{x_1/A}$	$u_{x_1/A}$ $\%\overline{x_1/A}$	$b_{x_1/A}^2$ $\%u_{x_1/A}^2$	$s_{\overline{x_1/A}}^2$ $\%u_{x_1/A}^2$	$U_{95,x_1/A}$ $\%\overline{x_1/A}$	$U_{95,x_1/A}$ $\%DR$
0^0 DR=0.117	0.50	3	0.024	100.0	0.0	78.6	2.2	78.7	99.9	0.1	**157.4**	**32.9**
	1.00	12	0.040	100.0	0.0	24.2	0.7	24.2	99.9	0.1	**48.4**	**16.4**
	1.50	3	0.181	100.0	0.0	3.5	0.3	3.5	99.3	0.7	**7.1**	**11.0**
	2.00	3	0.258	100.0	0.0	1.9	0.4	1.9	96.5	3.5	**3.8**	**8.4**
	Ave.			**100.0**	**0.0**	**27.1**	**0.9**	**27.1**	**98.9**	**1.1**	**54.1**	**17.2**
45^0 DR=0.085	0.50	3	0.039	100.0	0.0	48.9	4.3	49.0	99.2	0.8	**98.1**	**43.9**
	1.00	3	0.103	100.0	0.0	9.3	0.7	9.3	99.5	0.5	**18.7**	**21.9**
	2.00	3	0.214	100.0	0.0	2.2	0.1	2.2	99.9	0.1	**4.5**	**10.9**
	Ave.			**100.0**	**0.0**	**20.1**	**1.7**	**20.2**	**99.5**	**0.5**	**40.4**	**25.6**
90^0 DR=0.041	0.25	3	0.053	100.0	0.0	71.9	4.4	72.0	99.6	0.4	**144.1**	**185.5**
	0.30	3	0.058	100.0	0.0	55.2	10.5	56.2	96.5	3.5	**112.4**	**157.0**
	0.40	3	0.104	100.0	0.0	23.1	6.8	24.1	92.1	7.9	**48.2**	**120.6**
	0.50	3	0.093	100.0	0.0	20.7	2.9	20.9	98.0	2.0	**41.8**	**93.5**
	1.00	3	0.031	100.0	0.0	31.1	9.7	32.6	91.2	8.8	**65.1**	**48.5**
	2.00	3	0.025	100.0	0.0	19.3	2.0	19.4	98.9	1.1	**38.8**	**23.3**
	Ave.			**100.0**	**0.0**	**36.9**	**6.0**	**37.5**	**96.1**	**3.9**	**75.1**	**104.7**
135^0 DR=0.167	0.25	3	0.130	100.0	0.0	29.5	9.2	30.8	91.2	8.8	**61.7**	**48.1**
	0.30	3	0.134	100.0	0.0	23.9	4.9	24.4	96.0	4.0	**48.8**	**39.0**
	0.40	3	0.149	100.0	0.0	16.0	0.7	16.1	99.8	0.2	**32.1**	**28.7**
	0.50	3	0.037	100.0	0.0	52.4	5.0	52.6	99.1	0.9	**105.3**	**23.0**
	1.00	3	0.348	100.0	0.0	2.7	0.1	2.8	99.7	0.3	**5.5**	**11.5**
	2.00	3	0.337	100.0	0.0	1.4	1.2	1.9	58.1	41.9	**3.7**	**7.5**
	Ave.			**100.0**	**0.0**	**21.0**	**3.5**	**21.4**	**90.6**	**9.4**	**42.9**	**26.3**
180^0 DR=0.200	0.50	3	0.040	100.0	0.0	47.9	4.2	48.1	99.2	0.8	**96.1**	**19.2**
	1.00	3	0.177	100.0	0.0	5.4	2.4	5.9	83.2	16.8	**11.8**	**10.5**
	2.00	3	0.441	100.0	0.0	1.1	0.8	1.3	66.7	33.3	**2.7**	**5.9**
	Ave.			**100.0**	**0.0**	**18.1**	**2.5**	**18.4**	**83.0**	**17.0**	**36.9**	**11.8**

www.manaraa.com

Table 3.16 Uncertainty analysis of 1st harmonic amplitude of heave

χ Dynamic Range	λ/L	Number of Runs (M)	z1/A	$\theta_{z_1}^2 b_{z_1}^2$ $\%b_{z_1/A}^2$	$\theta_A^2 b_A^2$ $\%b_{z_1/A}^2$	$b_{z_1/A}$ $\%\overline{z_1/A}$	$s_{\overline{z_1/A}}$ $\%\overline{z_1/A}$	$u_{z_1/A}$ $\%\overline{z_1/A}$	$b_{z_1/A}^2$ $\%u_{z_1/A}^2$	$s_{\overline{z_1/A}}^2$ $\%u_{z_1/A}^2$	$U_{95,z_1/A}$ $\%\overline{z_1/A}$	$U_{95,z_1/A}$ $\%DR$
0^0 DR=0.465	0.50	3	0.067	100.0	0.0	20.7	0.5	20.7	99.9	0.1	**41.3**	**5.9**
	1.00	12	0.595	100.0	0.0	1.2	1.4	1.8	42.3	57.7	**3.6**	**4.6**
	1.50	3	0.907	100.0	0.0	0.5	0.1	0.5	98.1	1.9	**1.0**	**2.0**
	2.00	3	0.996	100.0	0.0	0.3	0.3	0.4	62.8	37.2	**0.9**	**1.9**
	Ave.			**100.0**	**0.0**	**5.7**	**0.6**	**5.8**	**75.8**	**24.2**	**11.7**	**3.6**
45^0 DR=0.532	0.50	3	0.071	100.0	0.0	19.4	1.2	19.4	99.6	0.4	**38.9**	**5.2**
	1.00	3	1.136	100.0	0.0	0.6	0.2	0.6	92.2	7.8	**1.3**	**2.7**
	2.00	3	1.049	100.0	0.0	0.3	0.0	0.3	98.3	1.7	**0.7**	**1.3**
	Ave.			**100.0**	**0.0**	**6.8**	**0.5**	**6.8**	**96.7**	**3.3**	**13.6**	**3.1**
90^0 DR=0.477	0.25	3	0.228	100.0	0.0	12.1	0.4	12.1	99.9	0.1	**24.2**	**11.6**
	0.30	3	0.412	100.0	0.0	5.6	1.8	5.9	90.7	9.3	**11.7**	**10.1**
	0.40	3	0.861	100.0	0.0	2.0	2.0	2.8	51.1	48.9	**5.6**	**10.1**
	0.50	3	1.181	100.0	0.0	1.2	0.1	1.2	98.4	1.6	**2.4**	**5.8**
	1.00	3	0.950	100.0	0.0	0.7	0.8	1.1	45.0	55.0	**2.2**	**4.3**
	2.00	3	1.157	100.0	0.0	0.3	0.1	0.3	91.4	8.6	**0.6**	**1.5**
	Ave.			**100.0**	**0.0**	**3.6**	**0.9**	**3.9**	**79.4**	**20.6**	**7.8**	**7.3**
135^0 DR=0.155	0.25	3	0.130	100.0	0.0	29.5	9.2	30.8	91.2	8.8	**61.7**	**48.1**
	0.30	3	0.134	100.0	0.0	23.9	4.9	24.4	96.0	4.0	**48.8**	**39.0**
	0.40	3	0.149	100.0	0.0	16.0	0.7	16.1	99.8	0.2	**32.1**	**28.7**
	0.50	3	0.037	100.0	0.0	52.4	5.0	52.6	99.1	0.9	**105.3**	**23.0**
	1.00	3	0.348	100.0	0.0	2.7	0.1	2.8	99.7	0.3	**5.5**	**11.5**
	2.00	3	0.337	100.0	0.0	1.4	1.2	1.9	58.1	41.9	**3.7**	**7.5**
	Ave.			**100.0**	**0.0**	**21.0**	**3.5**	**21.4**	**90.6**	**9.4**	**42.9**	**26.3**
180^0 DR=0.276	0.50	3	0.090	100.0	0.0	15.3	1.1	15.3	99.5	0.5	**30.7**	**10.0**
	1.00	3	0.045	100.0	0.0	15.5	5.3	16.3	89.5	10.5	**32.7**	**5.3**
	2.00	3	0.597	100.0	0.0	0.6	0.1	0.6	97.6	2.4	**1.2**	**2.5**
	Ave.			**100.0**	**0.0**	**10.4**	**2.2**	**10.8**	**95.5**	**4.5**	**21.5**	**5.9**

www.manaraa.com

Table 3.17 Uncertainty analysis of 1st harmonic amplitude of roll

χ Dynamic Range	λ/L	Number of Runs (M)	ϕ_1/Ak	$\theta_{\phi_1}^2 b_{\phi_1}^2$ $\%b_{\phi_1/A}^2$	$\theta_A^2 b_A^2$ $\%b_{\phi_1/A}^2$	$\theta_k^2 b_k^2$ $\%b_{\phi_1/A}^2$	$b_{\phi_1/Ak}$ $\%\overline{\phi_1/Ak}$	$s_{\overline{\phi_1/Ak}}$ $\%\overline{\phi_1/Ak}$	$u_{\phi_1/Ak}$ $\%\overline{\phi_1/Ak}$	$b_{\phi_1/Ak}^2$ $\%u_{\phi_1/Ak}^2$	$s_{\overline{\phi_1/Ak}}^2$ $\%u_{\phi_1/Ak}^2$	$U_{95,\phi_1/Ak}$ $\%\overline{\phi_1/Ak}$	$U_{95,\phi_1/Ak}$ $\%\overline{\phi_1/Ak}$	$U_{95,\phi_1/A}$ $\%DR$
0^0 DR=0.046	0.50	3	0.002	100.0	0.0	0.0	582.1	30.9	17.8	582.3	99.9	0.1	**1164.7**	**61.4**
	1.00	12	0.009	100.0	0.0	0.0	157.3	8.5	2.4	157.3	100.0	0.0	**314.7**	**61.4**
	1.50	3	0.050	100.0	0.0	0.0	28.4	9.9	5.7	29.0	96.1	3.9	**57.9**	**62.7**
	2.00	3	0.074	100.0	0.0	0.0	19.3	10.8	6.3	20.2	90.4	9.6	**40.5**	**64.6**
	Ave.			**100.0**	**0.0**	**0.0**	**196.8**	**15.0**	**8.1**	**197.2**	**96.6**	**3.4**	**394.4**	**62.5**
45^0 DR=0.951	0.50	3	0.148	100.0	0.0	0.0	9.6	1.8	1.1	9.7	98.8	1.2	**19.3**	**3.0**
	1.00	3	0.642	100.0	0.0	0.0	2.2	0.9	0.5	2.3	95.2	4.8	**4.5**	**3.1**
	2.00	3	2.039	99.9	0.0	0.1	0.7	0.7	0.4	0.8	75.1	24.9	**1.6**	**3.5**
	Ave.			**100.0**	**0.0**	**0.0**	**4.2**	**1.1**	**0.7**	**4.2**	**89.7**	**10.3**	**8.5**	**3.2**
90^0 DR=1.363	0.25	3	0.167	100.0	0.0	0.0	8.5	2.0	1.1	8.6	98.3	1.7	**17.2**	**2.1**
	0.30	3	0.224	100.0	0.0	0.0	6.3	2.0	1.2	6.5	96.6	3.4	**12.9**	**2.1**
	0.40	3	0.326	100.0	0.0	0.0	4.4	2.0	1.2	4.5	93.4	6.6	**9.0**	**2.2**
	0.50	3	0.378	100.0	0.0	0.0	3.8	1.3	0.8	3.8	95.9	4.1	**7.7**	**2.1**
	1.00	3	0.325	100.0	0.0	0.0	4.4	3.8	2.2	4.9	79.8	20.2	**9.8**	**2.3**
	2.00	3	2.893	99.9	0.0	0.1	0.5	1.8	1.0	1.1	19.1	80.9	**2.3**	**4.8**
	Ave.			**100.0**	**0.0**	**0.0**	**4.6**	**2.2**	**1.2**	**4.9**	**80.5**	**19.5**	**9.8**	**2.6**
135^0 DR=1.296	0.25	3	0.034	100.0	0.0	0.0	40.8	20.9	0.0	40.8	100.0	0.0	**81.6**	**5.7**
	0.30	3	0.078	100.0	0.0	0.0	31.4	41.8	0.0	31.4	100.0	0.0	**62.8**	**3.7**
	0.40	3	0.446	100.0	0.0	0.0	4.2	13.5	0.0	4.2	100.0	0.0	**8.5**	**2.9**
	0.50	3	0.805	100.0	0.0	0.0	2.4	11.6	0.0	2.4	100.0	0.0	**4.8**	**3.0**
	1.00	3	2.358	100.0	0.0	0.0	0.6	17.6	0.0	0.6	100.0	0.0	**1.1**	**2.1**
	2.00	3	2.700	99.9	0.0	0.1	0.5	3.4	0.0	0.5	100.0	0.0	**1.1**	**2.3**
	Ave.			**100.0**	**0.0**	**0.0**	**13.5**	**3.2**	**1.9**	**14.3**	**63.5**	**36.5**	**28.5**	**4.8**
180^0 DR=0.136	0.50	3	0.123	100.0	0.0	0.0	11.6	2.6	1.5	11.7	98.3	1.7	**23.4**	**21.0**
	1.00	3	0.094	100.0	0.0	0.0	15.1	19.5	11.3	18.8	64.1	35.9	**37.6**	**26.0**
	2.00	3	0.286	100.0	0.0	0.0	5.0	5.4	3.1	5.9	71.4	28.6	**11.8**	**24.7**
	Ave.			**100.0**	**0.0**	**0.0**	**10.5**	**9.2**	**5.3**	**12.1**	**78.0**	**22.0**	**24.2**	**23.9**

www.manaraa.com

Table 3.18 Uncertainty analysis of 1st harmonic amplitude of pitch

χ Dynamic Range	λ/L	Number of Runs (M)	θ1/Ak	$\theta_{\theta_1}^2 b_{\theta_1}^2$ $\%b_{\theta_1/A}^2$	$\theta_A^2 b_A^2$ $\%b_{\theta_1/A}^2$	$\theta_k^2 b_k^2$ $\%b_{\theta_1/A}^2$	$b_{\theta_1/Ak}$ $\%\overline{\theta_1/A}$	$s_{\overline{\theta_1/Ak}}$ $\%\overline{\theta_1/A}$	$u_{\theta_1/Ak}$ $\%\overline{\theta_1/Ak}$	$b_{\theta_1/Ak}^2$ $\%u_{\theta_1/Ak}^2$	$s_{\overline{\theta_1/Ak}}^2$ $\%u_{\theta_1/Ak}^2$	$U_{95,\theta_1/Ak}$ $\%\overline{\theta_1/Ak}$	$U_{95,\theta_1/Ak}$ $\%DR$
0° DR=0.581	0.50	3	0.021	100.0	0.0	0.0	66.4	0.4	66.4	100.0	0.0	**132.7**	**4.9**
	1.00	12	0.472	100.0	0.0	0.0	3.0	1.1	3.2	87.9	12.1	**6.4**	**5.2**
	1.50	3	1.085	100.0	0.0	0.0	1.3	0.1	1.3	98.7	1.3	**2.6**	**4.9**
	2.00	3	1.182	100.0	0.0	0.0	1.2	0.1	1.2	99.6	0.4	**2.4**	**4.9**
	Ave.			**100.0**	**0.0**	**0.0**	**18.0**	**0.4**	**18.0**	**96.6**	**3.4**	**36.0**	**5.0**
45° DR=0.367	0.50	3	0.034	100.0	0.0	0.0	42.3	0.1	42.3	100.0	0.0	**84.5**	**7.8**
	1.00	3	0.659	100.0	0.0	0.0	2.2	0.9	2.3	86.4	13.6	**4.6**	**8.3**
	2.00	3	0.767	100.0	0.0	0.0	1.9	0.1	1.9	99.5	0.5	**3.7**	**7.8**
	Ave.			**100.0**	**0.0**	**0.0**	**15.4**	**0.4**	**15.5**	**95.3**	**4.7**	**31.0**	**8.0**
90° DR=0.040	0.25	3	0.017	100.0	0.0	0.0	81.8	5.2	82.0	99.6	0.4	**163.9**	**71.2**
	0.30	3	0.029	100.0	0.0	0.0	48.8	3.3	48.9	99.6	0.4	**97.8**	**71.2**
	0.40	3	0.072	100.0	0.0	0.0	19.6	1.4	19.7	99.5	0.5	**39.3**	**71.3**
	0.50	3	0.097	100.0	0.0	0.0	14.6	0.8	14.6	99.7	0.3	**29.2**	**71.2**
	1.00	3	0.035	100.0	0.0	0.0	40.1	3.6	40.3	99.2	0.8	**80.5**	**71.4**
	2.00	3	0.035	100.0	0.0	0.0	40.8	2.2	40.9	99.7	0.3	**81.7**	**71.2**
	Ave.			**100.0**	**0.0**	**0.0**	**41.0**	**2.8**	**41.0**	**99.5**	**0.5**	**82.1**	**71.2**
135° DR=0.292	0.25	3	0.023	100.0	0.0	0.0	62.1	11.3	63.1	96.8	3.2	**126.2**	**10.1**
	0.30	3	0.011	100.0	0.0	0.0	134.4	41.6	140.7	91.2	8.8	**281.3**	**10.4**
	0.40	3	0.032	100.0	0.0	0.0	44.3	10.0	45.4	95.1	4.9	**90.8**	**10.1**
	0.50	3	0.021	100.0	0.0	0.0	66.5	4.0	66.6	99.6	0.4	**133.2**	**9.9**
	1.00	3	0.379	100.0	0.0	0.0	3.7	1.3	4.0	88.7	11.3	**8.0**	**10.5**
	2.00	3	0.585	100.0	0.0	0.0	2.4	0.4	2.5	96.9	3.1	**4.9**	**10.0**
	Ave.			**100.0**	**0.0**	**0.0**	**52.2**	**11.5**	**53.7**	**94.7**	**5.3**	**107.4**	**10.2**
180° DR=0.264	0.50	3	0.024	100.0	0.0	0.0	58.6	3.5	58.7	99.6	0.4	**117.3**	**234.9**
	1.00	3	0.017	100.0	0.0	0.0	84.0	6.5	84.3	99.4	0.6	**168.6**	**235.2**
	2.00	3	0.040	100.0	0.0	0.0	35.9	1.2	35.9	99.9	0.1	**71.9**	**234.6**
	Ave.			**100.0**	**0.0**	**0.0**	**59.5**	**3.7**	**59.6**	**99.6**	**0.4**	**119.3**	**234.9**

www.manaraa.com

Table 3.19 through 3.23 show the uncertainty analysis for the 2nd harmonic amplitudes of total resistance coefficient, surge, heave, roll, and pitch. The average total uncertainty of the 2nd harmonic amplitude of the total resistance coefficient have very large total expanded uncertainty for every wave encounter angle due to small nominal values. The total systematic uncertainty for every wave encounter angle is the major contributor to the total expanded uncertainty. The systematic uncertainty of the resistance is the major contributor to the total systematic uncertainty for all wave encounter angles. The small nominal values are due to the inertial forces being removed from the hydraulic force.

The 2nd harmonic of surge, heave, roll, and pitch show fairly similar uncertainty trends. All of the 2nd harmonic amplitudes are very small, therefore the total expanded uncertainty, in regards to %D, are inflated. The average total expanded uncertainty between all wave encounters angles of surge, heave, roll, and pitch are 330.79%D, 141.5%D, 956%D, and 318.88%D respectively. For all 2nd harmonic amplitudes, the systematic uncertainty is the significant contributor to the total expanded uncertainty. The significant contributor to the total systematic uncertainty is the measured motion of the given value. Therefore, the data quality could be improved by increasing the accuracy of the motions measuring device.

www.manaraa.com

Table 3.19 Uncertainty analysis of 2nd harmonic amplitude of total resistance coefficient

χ Dynamic Range	λ/L	Number of Runs (M)	$C_{T2}x10^3$	$\theta^2_{F_{H2}} b^2_{F_{H2}}$ $\%b^2_{C_{T2}}$	$\theta^2_{\rho} b^2_{\rho}$ $\%b^2_{C_{T2}}$	$\theta^2_{S} b^2_{S}$ $\%b^2_{C_{T2}}$	$\theta^2_{V} b^2_{V}$ $\%b^2_{C_{T2}}$	$b_{C_{T2}}$ $\%\overline{C_{T2}}$	$s_{\overline{C_{T2}}}$ $\%\overline{C_{T2}}$	$u_{C_{T2}}$ $\%\overline{C_{T2}}$	$b^2_{C_{T2}}$ $\%u^2_{C_{T2}}$	$s^2_{\overline{C_{T2}}}$ $\%u^2_{C_{T2}}$	$U_{95,C_{T2}}$ $\%\overline{C_{T2}}$	$U_{95,C_{T2}}$ $\%DR$
0^0 DR=0.047	0.50	3	0.14	100.0	0.0	0.0	0.0	22.9	0.9	22.9	99.8	0.2	**45.9**	**138.8**
	1.00	12	0.05	100.0	0.0	0.0	0.0	59.9	4.2	60.1	99.5	0.5	**120.2**	**138.9**
	1.50	3	0.06	100.0	0.0	0.0	0.0	51.9	4.5	52.1	99.3	0.7	**104.2**	**138.8**
	2.00	3	0.06	100.0	0.0	0.0	0.0	51.0	11.9	52.4	94.8	5.2	**104.8**	**142.2**
	Ave.			**100.0**	**0.0**	**0.0**	**0.0**	**46.4**	**5.4**	**46.9**	**98.4**	**1.6**	**93.8**	**139.7**
45^0 DR=0.073	0.50	3	0.06	100.0	0.0	0.0	0.0	55.3	5.2	55.6	99.1	0.9	111.2	89.0
	1.00	3	0.08	100.0	0.0	0.0	0.0	38.5	0.4	38.5	100.0	0.0	76.9	88.9
	2.00	3	0.20	99.9	0.0	0.1	0.0	16.3	2.1	16.4	98.4	1.6	32.8	89.7
	Ave.			**100.0**	**0.0**	**0.0**	**0.0**	**36.7**	**2.6**	**36.8**	**99.2**	**0.8**	**73.6**	**89.2**
90^0 DR=0.068	0.25	3	0.01	100.0	0.0	0.0	0.0	405.7	16.8	406.1	99.8	0.2	**812.1**	**95.5**
	0.30	3	0.01	100.0	0.0	0.0	0.0	289.3	4.4	289.4	100.0	0.0	**578.7**	**95.3**
	0.40	3	0.01	100.0	0.0	0.0	0.0	245.0	4.3	245.0	100.0	0.0	**490.0**	**95.6**
	0.50	3	0.02	100.0	0.0	0.0	0.0	132.0	4.5	132.1	99.9	0.1	**264.2**	**95.4**
	1.00	3	0.12	100.0	0.0	0.0	0.0	26.9	2.3	27.0	99.3	0.7	**54.0**	**95.8**
	2.00	3	0.14	100.0	0.0	0.0	0.0	22.5	2.1	22.6	99.2	0.8	**45.2**	**95.7**
	Ave.			**100.0**	**0.0**	**0.0**	**0.0**	**186.9**	**5.7**	**187.0**	**99.7**	**0.3**	**374.0**	**95.5**
135^0 DR=0.143	0.25	3	0.04	100.0	0.0	0.0	0.0	86.8	8.6	87.2	99.0	1.0	**174.4**	**45.5**
	0.30	3	0.04	100.0	0.0	0.0	0.0	85.0	48.2	97.7	75.6	24.4	**195.4**	**51.9**
	0.40	3	0.14	100.0	0.0	0.0	0.0	22.9	9.3	24.7	86.0	14.0	**49.4**	**48.9**
	0.50	3	0.07	100.0	0.0	0.0	0.0	46.2	18.7	49.8	86.0	14.0	**99.7**	**49.0**
	1.00	3	0.23	99.9	0.0	0.1	0.0	14.3	6.5	15.8	82.8	17.2	**31.5**	**49.7**
	2.00	3	0.11	100.0	0.0	0.0	0.0	28.4	7.7	29.4	93.1	6.9	**58.8**	**46.9**
	Ave.			**100.0**	**0.0**	**0.0**	**0.0**	**47.3**	**16.5**	**50.8**	**87.1**	**12.9**	**101.6**	**48.7**
180^0 DR=0.104	0.50	3	0.31	99.9	0.0	0.1	0.0	10.5	0.9	10.5	99.3	0.7	21.0	62.7
	1.00	3	0.14	100.0	0.0	0.0	0.0	23.3	7.4	24.4	90.9	9.1	48.9	65.5
	2.00	3	0.10	100.0	0.0	0.0	0.0	31.5	9.2	32.8	92.1	7.9	65.6	65.1
	Ave.			**99.9**	**0.0**	**0.1**	**0.0**	**21.7**	**5.8**	**22.6**	**94.1**	**5.9**	**45.2**	**64.5**

www.manaraa.com

Table 3.20 Uncertainty analysis of 2nd harmonic amplitude of surge

χ Dynamic Range	λ/L	Number of Runs (M)	x_2/A	$\theta_{x_2}^2 b_{x_2}^2$ $\%b_{x_2/A}^2$	$\theta_A^2 b_A^2$ $\%b_{x_2/A}^2$	$b_{x_2/A}$ $\%\overline{x_2/A}$	$s_{\overline{x_2/A}}$ $\%\overline{x_2/A}$	$u_{x_2/A}$ $\%\overline{x_2/A}$	$b_{x_2/A}^2$ $\%u_{x_2/A}^2$	$s_{\overline{x_2/A}}^2$ $\%u_{x_2/A}^2$	$U_{95,x_2/A}$ $\%\overline{x_2/A}$	$U_{95,x_2/A}$ $\%DR$
0^0 DR=0.004	0.50	3	0.001	100.0	0.0	1808.1	15.1	1808.1	100.0	0.0	**3616.3**	**1098.2**
	1.00	12	0.002	100.0	0.0	543.2	6.1	543.3	100.0	0.0	**1086.6**	**549.1**
	1.50	3	0.006	100.0	0.0	99.7	5.2	99.9	99.7	0.3	**199.7**	**366.5**
	2.00	3	0.008	100.0	0.0	59.6	12.1	60.8	96.0	4.0	**121.6**	**280.2**
	Ave.			**100.0**	**0.0**	**627.7**	**9.6**	**628.0**	**98.9**	**1.1**	**1256.1**	**573.5**
45^0 DR=0.008	0.50	3	0.017	100.0	0.0	116.0	2.2	116.0	100.0	0.0	**231.9**	**495.8**
	1.00	3	0.031	100.0	0.0	31.2	2.3	31.3	99.5	0.5	**62.6**	**248.5**
	2.00	3	0.022	100.0	0.0	21.9	0.5	21.9	99.9	0.1	**43.8**	**124.0**
	Ave.			**100.0**	**0.0**	**56.4**	**1.7**	**56.4**	**99.8**	**0.2**	**112.8**	**289.4**
90^0 DR=0.025	0.25	3	0.062	100.0	0.0	61.7	9.3	62.4	97.8	2.2	**124.8**	**302.1**
	0.30	3	0.044	100.0	0.0	72.9	9.0	73.4	98.5	1.5	**146.8**	**250.8**
	0.40	3	0.047	100.0	0.0	51.5	9.2	52.3	96.9	3.1	**104.6**	**189.7**
	0.50	3	0.072	100.0	0.0	26.7	1.2	26.7	99.8	0.2	**53.5**	**149.5**
	1.00	3	0.030	100.0	0.0	31.9	7.2	32.7	95.1	4.9	**65.3**	**76.6**
	2.00	3	0.032	100.0	0.0	14.9	0.4	14.9	99.9	0.1	**29.7**	**36.7**
	Ave.			**100.0**	**0.0**	**43.2**	**6.1**	**43.7**	**98.0**	**2.0**	**87.5**	**167.6**
135^0 DR=0.585	0.25	3	0.126	100.0	0.0	30.4	6.3	31.0	95.9	4.1	**62.0**	**133.8**
	0.30	3	0.044	100.0	0.0	72.5	5.0	72.7	99.5	0.5	**145.4**	**109.5**
	0.40	3	0.015	100.0	0.0	162.6	2.9	162.7	100.0	0.0	**325.3**	**81.9**
	0.50	3	0.032	100.0	0.0	59.7	3.6	59.8	99.6	0.4	**119.7**	**65.6**
	1.00	3	0.047	100.0	0.0	20.5	1.4	20.6	99.6	0.4	**41.1**	**32.8**
	2.00	3	0.009	100.0	0.0	52.0	4.5	52.2	99.3	0.7	**104.3**	**16.6**
	Ave.			**100.0**	**0.0**	**66.3**	**3.9**	**66.5**	**99.0**	**1.0**	**133.0**	**73.4**
180^0 DR=0.046	0.50	3	0.111	100.0	0.0	17.3	2.6	17.5	97.8	2.2	**35.1**	**82.9**
	1.00	3	0.019	100.0	0.0	51.0	10.4	52.1	96.0	4.0	**104.1**	**41.8**
	2.00	3	0.018	100.0	0.0	26.8	2.4	26.9	99.2	0.8	**53.8**	**20.6**
	Ave.			**100.0**	**0.0**	**31.7**	**5.1**	**32.2**	**97.7**	**2.3**	**64.3**	**48.4**

www.manaraa.com

Table 3.21 Uncertainty analysis of 2nd harmonic amplitude of heave

χ Dynamic Range	λ/L	Number of Runs (M)	z_2/A	$\theta_{z_2}^2 b_{z_2}^2$ $\%b_{z_2/A}^2$	$\theta_A^2 b_A^2$ $\%b_{z_2/A}^2$	$b_{z_2/A}$ $\%\overline{z_2/A}$	$s_{\overline{z_2/A}}$ $\%\overline{z_2/A}$	$u_{z_2/A}$ $\%\overline{z_2/A}$	$b_{z_2/A}^2$ $\%u_{z_2/A}^2$	$s_{\overline{z_2/A}}^2$ $\%u_{z_2/A}^2$	$U_{95,z_2/A}$ $\%\overline{z_2/A}$	$U_{95,z_2/A}$ $\%DR$
0^0 DR=0.005	0.50	3	0.007	100.0	0.0	192.1	0.5	192.1	100.0	0.0	**384.1**	**559.8**
	1.00	12	0.013	100.0	0.0	51.6	2.5	51.6	99.8	0.2	**103.3**	**280.2**
	1.50	3	0.009	100.0	0.0	53.8	9.9	54.7	96.7	3.3	**109.4**	**189.7**
	2.00	3	0.014	100.0	0.0	24.4	15.1	28.7	72.4	27.6	**57.4**	**164.4**
	Ave.			**100.0**	**0.0**	**80.5**	**7.0**	**81.8**	**92.2**	**7.8**	**163.6**	**298.6**
45^0 DR=0.007	0.50	3	0.012	100.0	0.0	111.1	1.0	111.1	100.0	0.0	**222.2**	**361.1**
	1.00	3	0.006	100.0	0.0	121.7	0.3	121.7	100.0	0.0	**243.5**	**180.6**
	2.00	3	0.021	100.0	0.0	16.5	2.3	16.6	98.1	1.9	**33.2**	**91.1**
	Ave.			**100.0**	**0.0**	**83.1**	**1.2**	**83.1**	**99.4**	**0.6**	**166.3**	**210.9**
90^0 DR=0.027	0.25	3	0.012	100.0	0.0	233.5	6.9	233.6	99.9	0.1	**467.1**	**204.0**
	0.30	3	0.012	100.0	0.0	185.4	1.2	185.4	100.0	0.0	**370.9**	**169.9**
	0.40	3	0.011	100.0	0.0	156.4	10.5	156.8	99.5	0.5	**313.6**	**127.7**
	0.50	3	0.010	100.0	0.0	137.7	7.9	137.9	99.7	0.3	**275.8**	**102.1**
	1.00	3	0.019	100.0	0.0	37.2	7.3	37.9	96.3	3.7	**75.9**	**51.9**
	2.00	3	0.062	100.0	0.0	5.5	0.8	5.6	97.7	2.3	**11.2**	**25.8**
	Ave.			**100.0**	**0.0**	**126.0**	**5.8**	**126.2**	**98.9**	**1.1**	**252.4**	**113.6**
135^0 DR=0.081	0.25	3	0.175	100.0	0.0	15.7	2.3	15.9	97.9	2.1	**31.8**	**69.3**
	0.30	3	0.044	100.0	0.0	52.6	2.1	52.7	99.8	0.2	**105.4**	**57.2**
	0.40	3	0.027	100.0	0.0	64.0	2.2	64.0	99.9	0.1	**128.0**	**42.9**
	0.50	3	0.015	100.0	0.0	90.0	5.3	90.2	99.7	0.3	**180.3**	**34.3**
	1.00	3	0.022	100.0	0.0	31.8	5.1	32.2	97.5	2.5	**64.5**	**17.4**
	2.00	3	0.090	100.0	0.0	3.9	2.0	4.4	78.3	21.7	**8.7**	**9.7**
	Ave.			**100.0**	**0.0**	**43.0**	**3.2**	**43.2**	**95.5**	**4.5**	**86.5**	**38.5**
180^0 DR=0.034	0.50	3	0.070	100.0	0.0	19.7	0.5	19.7	99.9	0.1	**39.5**	**93.4**
	1.00	3	0.023	100.0	0.0	30.5	1.9	30.6	99.6	0.4	**61.2**	**46.7**
	2.00	3	0.045	100.0	0.0	7.6	1.2	7.7	97.6	2.4	**15.4**	**23.6**
	Ave.			**100.0**	**0.0**	**19.3**	**1.2**	**19.3**	**99.1**	**0.9**	**38.7**	**54.6**

www.manaraa.com

Table 3.22 Uncertainty analysis of 2nd harmonic amplitude of roll

χ Dynamic Range	λ/L	Number of Runs (M)	ϕ2/Ak	$\theta_{\phi_0}^2 b_{\phi_0}^2$ $\%b_{\phi_2/A}^2$	$\theta_A^2 b_A^2$ $\%b_{\phi_2/A}^2$	$\theta_k^2 b_k^2$ $\%b_{\phi_2/A}^2$	$b_{\phi_2/Ak}$ $\%\overline{\phi_2/Ak}$	$s_{\overline{\phi_2/Ak}}$ $\%\overline{\phi_2/Ak}$	$u_{\phi_2/Ak}$ $\%\overline{\phi_2/Ak}$	$b_{\phi_2/Ak}^2$ $\%u_{\phi_2/Ak}^2$	$s_{\overline{\phi_2/Ak}}^2$ $\%u_{\phi_2/Ak}^2$	$U_{95,\phi_2/Ak}$ $\%\overline{\phi_2/Ak}$	$U_{95,\phi_2/Ak}$ $\%DR$
0° DR=0.017	0.50	3	0.000	100.0	0.0	0.0	6770.8	6.7	6770.8	100.0	0.0	**13541.7**	**1738.3**
	1.00	12	0.002	100.0	0.0	0.0	828.1	2.9	828.1	100.0	0.0	**1656.1**	**1738.3**
	1.50	3	0.002	100.0	0.0	0.0	610.3	17.9	610.6	99.9	0.1	**1221.1**	**1739.1**
	2.00	3	0.003	100.0	0.0	0.0	408.4	20.5	408.9	99.7	0.3	**817.8**	**1740.5**
	Ave.			**100.0**	**0.0**	**0.0**	**2154.4**	**12.0**	**2154.6**	**99.9**	**0.1**	**4309.2**	**1739.0**
45° DR=0.095	0.50	3	0.005	100.0	0.0	0.0	308.6	6.3	308.7	100.0	0.0	**617.3**	**29.8**
	1.00	3	0.195	100.0	0.0	0.0	7.3	1.1	7.4	97.8	2.2	**14.7**	**30.1**
	2.00	3	0.194	100.0	0.0	0.0	7.3	0.9	7.4	98.4	1.6	**14.8**	**30.1**
	Ave.			**100.0**	**0.0**	**0.0**	**107.7**	**2.8**	**107.8**	**98.7**	**1.3**	**215.6**	**30.0**
90° DR=0.057	0.25	3	0.018	100.0	0.0	0.0	78.4	6.7	78.7	99.3	0.7	**157.5**	**49.3**
	0.30	3	0.032	100.0	0.0	0.0	44.3	1.8	44.3	99.8	0.2	**88.7**	**49.2**
	0.40	3	0.058	100.0	0.0	0.0	24.7	12.7	27.8	79.1	20.9	**55.6**	**55.3**
	0.50	3	0.034	100.0	0.0	0.0	42.4	6.1	42.8	98.0	2.0	**85.6**	**49.7**
	1.00	3	0.070	100.0	0.0	0.0	20.3	8.3	22.0	85.6	14.4	**43.9**	**53.1**
	2.00	3	0.133	100.0	0.0	0.0	10.7	2.3	11.0	95.6	4.4	**21.9**	**50.3**
	Ave.			**100.0**	**0.0**	**0.0**	**36.8**	**6.3**	**37.8**	**92.9**	**7.1**	**75.5**	**51.1**
135° DR=0.173	0.25	3	0.063	100.0	0.0	0.0	22.6	8.5	24.1	87.6	12.4	**48.3**	**17.6**
	0.30	3	0.048	100.0	0.0	0.0	29.7	9.6	31.2	90.6	9.4	**62.4**	**17.3**
	0.40	3	0.030	100.0	0.0	0.0	47.5	30.3	56.3	71.1	28.9	**112.7**	**19.5**
	0.50	3	0.014	100.0	0.0	0.0	99.9	105.8	145.5	47.1	52.9	**291.0**	**23.9**
	1.00	3	0.062	100.0	0.0	0.0	23.1	9.5	25.0	85.6	14.4	**49.9**	**17.8**
	2.00	3	0.360	100.0	0.0	0.0	3.9	1.7	4.3	83.8	16.2	**8.6**	**17.9**
	Ave.			**100.0**	**0.0**	**0.0**	**37.8**	**27.6**	**47.7**	**77.6**	**22.4**	**95.5**	**19.0**
180° DR=0.024	0.50	3	0.073	100.0	0.0	0.0	19.4	8.1	21.1	85.3	14.7	**42.1**	**128.8**
	1.00	3	0.031	100.0	0.0	0.0	45.5	10.5	46.7	94.9	5.1	**93.4**	**122.1**
	2.00	3	0.025	100.0	0.0	0.0	56.2	16.5	58.5	92.1	7.9	**117.1**	**124.0**
	Ave.			**100.0**	**0.0**	**0.0**	**40.4**	**11.7**	**42.1**	**90.8**	**9.2**	**84.2**	**125.0**

www.manaraa.com

Table 3.23 Uncertainty analysis of 2nd harmonic amplitude of pitch

χ Dynamic Range	λ/L	Number of Runs (M)	θ2/Ak	$\theta_{\theta_2}^2 b_{\theta_2}^2$ $\%b_{\theta_2/A}^2$	$\theta_A^2 b_A^2$ $\%b_{\theta_2/A}^2$	$\theta_k^2 b_k^2$ $\%b_{\theta_2/A}^2$	$b_{\theta_2/Ak}$ $\%\overline{\theta_2/Ak}$	$s_{\overline{\theta_2/Ak}}$ $\%\overline{\theta_2/Ak}$	$u_{\theta_2/Ak}$ $\%\overline{\theta_2/Ak}$	$b_{\theta_2/Ak}^2$ $\%u_{\theta_2/Ak}^2$	$s_{\overline{\theta_2/Ak}}^2$ $\%u_{\theta_2/Ak}^2$	$U_{95,\theta_2/Ak}$ $\%\overline{\theta_2/Ak}$	$U_{95,\theta_2/Ak}$ $\%DR$
0^0 DR=0.016	0.50	3	0.001	100.0	0.0	0.0	1086.1	0.3	1086.1	100.0	0.0	**2172.2**	**173.8**
	1.00	12	0.007	100.0	0.0	0.0	216.3	3.2	216.3	100.0	0.0	**432.6**	**173.8**
	1.50	3	0.018	100.0	0.0	0.0	78.3	2.4	78.3	99.9	0.1	**156.6**	**173.9**
	2.00	3	0.034	100.0	0.0	0.0	41.8	4.4	42.0	98.9	1.1	**84.0**	**174.7**
	Ave.			**100.0**	**0.0**	**0.0**	**355.6**	**2.6**	**355.7**	**99.7**	**0.3**	**711.4**	**174.0**
45^0 DR=0.012	0.50	3	0.006	100.0	0.0	0.0	228.2	1.0	228.2	100.0	0.0	**456.4**	**223.8**
	1.00	3	0.028	100.0	0.0	0.0	51.2	1.1	51.3	100.0	0.0	**102.5**	**223.8**
	2.00	3	0.032	100.0	0.0	0.0	44.9	1.7	45.0	99.9	0.1	**89.9**	**223.9**
	Ave.			**100.0**	**0.0**	**0.0**	**108.1**	**1.3**	**108.1**	**99.9**	**0.1**	**216.3**	**223.8**
90^0 DR=0.029	0.25	3	0.011	100.0	0.0	0.0	129.1	8.1	129.3	99.6	0.4	**258.6**	**98.6**
	0.30	3	0.013	100.0	0.0	0.0	110.5	5.9	110.7	99.7	0.3	**221.4**	**98.6**
	0.40	3	0.018	100.0	0.0	0.0	80.4	6.3	80.7	99.4	0.6	**161.3**	**98.7**
	0.50	3	0.031	100.0	0.0	0.0	45.5	1.9	45.6	99.8	0.2	**91.1**	**98.5**
	1.00	3	0.015	100.0	0.0	0.0	95.5	10.7	96.1	98.8	1.2	**192.3**	**99.0**
	2.00	3	0.069	100.0	0.0	0.0	20.7	1.8	20.7	99.3	0.7	**41.5**	**98.8**
	Ave.			**100.0**	**0.0**	**0.0**	**80.3**	**5.8**	**80.5**	**99.4**	**0.6**	**161.0**	**98.7**
135^0 DR=0.023	0.25	3	0.017	100.0	0.0	0.0	84.4	11.1	85.1	98.3	1.7	**170.2**	**139.7**
	0.30	3	0.002	100.0	0.0	0.0	626.0	193.4	655.2	91.3	8.7	**1310.3**	**145.0**
	0.40	3	0.006	100.0	0.0	0.0	247.2	54.9	253.2	95.3	4.7	**506.5**	**141.9**
	0.50	3	0.017	100.0	0.0	0.0	84.5	2.3	84.5	99.9	0.1	**169.0**	**138.6**
	1.00	3	0.030	100.0	0.0	0.0	47.5	3.7	47.6	99.4	0.6	**95.2**	**138.9**
	2.00	3	0.043	100.0	0.0	0.0	32.8	6.9	33.5	95.8	4.2	**67.1**	**141.5**
	Ave.			**100.0**	**0.0**	**0.0**	**187.1**	**45.4**	**193.2**	**96.7**	**3.3**	**386.4**	**140.9**
180^0 DR=0.014	0.50	3	0.024	100.0	0.0	0.0	58.6	3.5	58.7	99.6	0.4	**117.3**	**234.9**
	1.00	3	0.017	100.0	0.0	0.0	84.0	6.5	84.3	99.4	0.6	**168.6**	**235.2**
	2.00	3	0.040	100.0	0.0	0.0	35.9	1.2	35.9	99.9	0.1	**71.9**	**234.6**
	Ave.			**100.0**	**0.0**	**0.0**	**59.5**	**3.7**	**59.6**	**99.6**	**0.4**	**119.3**	**234.9**

www.manaraa.com

CHAPTER 4 TEST RESULTS AND DISCUSSION

4.1 Calm Water

Added Resistance and 4 DOF motion tests were completed in calm water conditions for fourteen Fr conditions, from 0.087 to 0.281. For each test the velocity, V [m/s], total force in the X-direction (X_T) [N], sinkage, (σ) [mm], and trim (τ) [deg]. The force and sinkage are non-dimensionalized resulting in C_T[15], CR, and σ/L. Several conditions were repeated for random uncertainty analysis and Fr = 0.2601 was repeated six times because it is the design speed for KCS. The calm water results are compared to NMRI, KRISO, FORCE[1] (L = 4.38 m), FORCE[2] (L = 6.07 m), FORCE[3] (L = 2.70 m) with similar conditions. The calm water results comparison is essential to confirming the system set up at IIHR.

Figure 4.1 shows the mean and individual test results, with standard deviation, of this study for total resistance coefficient with and without the Prohaska method, residual resistance coefficient with and without the Prohaska method, sinkage, and trim in calm water. The standard deviation values are included in the uncertainty results, Tables 3.3 through 3.6. Figures 4.2 and 4.3 show the total and residual resistance coefficients, respectively, for all facilities and excluding the L = 2.70 m model results calculated with and without the Prohaska method. Figure 4.4 shows the sinkage and trim for all facilities and excluding the L = 2.70 m model results. Tables 4.1 and 4.2 show the total coefficient of resistance results for all facilities calculated with and without the Prohaska method, respectively. The symbol %D represents the percentage of the mean value, while %DR represents the percentage of the dynamic range. Likewise, Tables 4.3 and 4.4 show the residual coefficient of resistance results for all facilities calculated with and without the Prohaska method, respectively. The results of the total and residual resistance coefficients show a large scatter when comparing all models for analysis with and without the Prohaska method. If the smaller 2.70 m model is excluded, the scatter of results is reasonably small. Tables 4.5 and 4.6 show the calm water sinkage and trim. Like the resistance coefficients, the sinkage and trim trends show that the scatter is much larger when including the smaller 2.70 m model.

www.manaraa.com

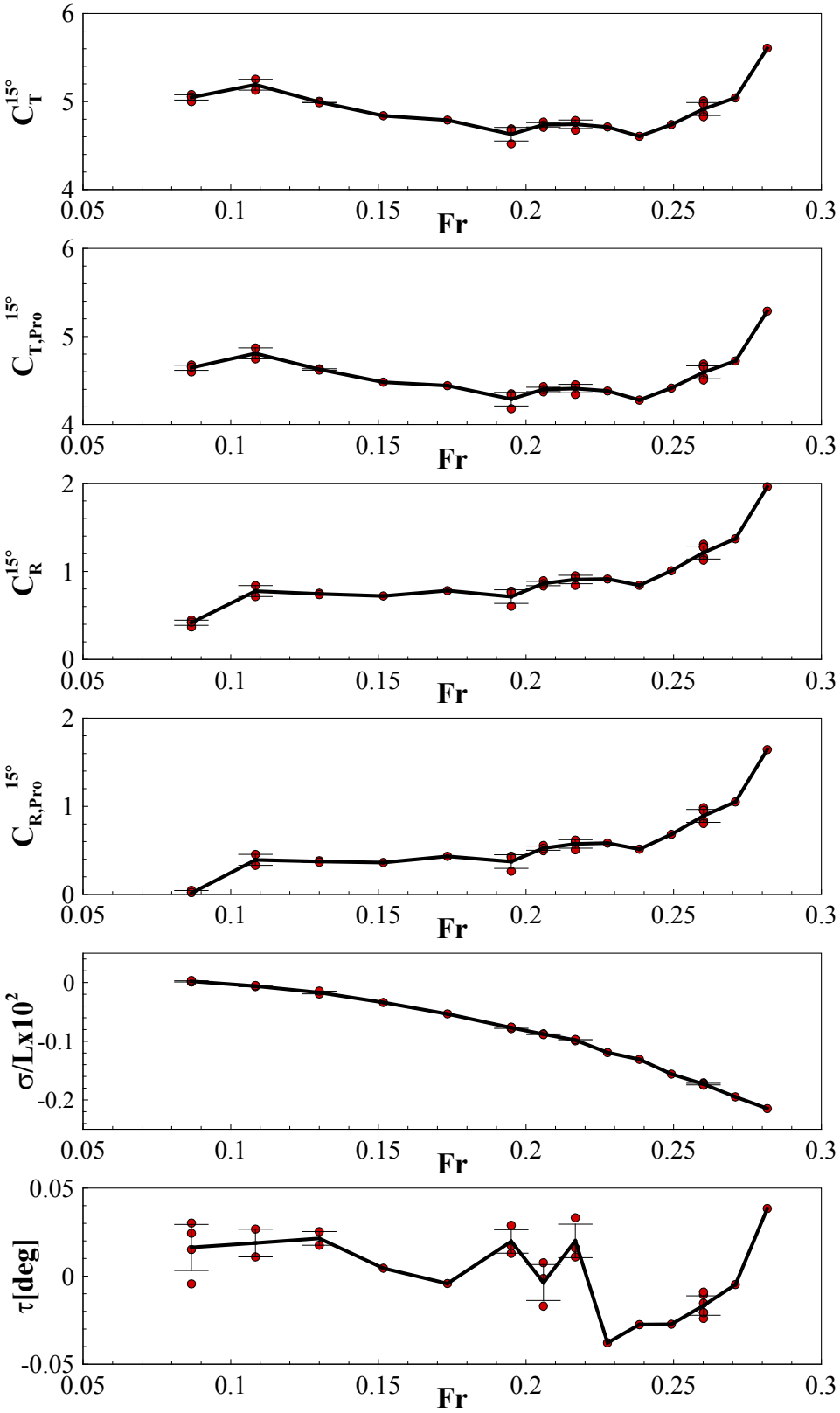

Figure 4.1 Resistance and motion results in calm water with individual tests, mean, and standard deviation

www.manaraa.com

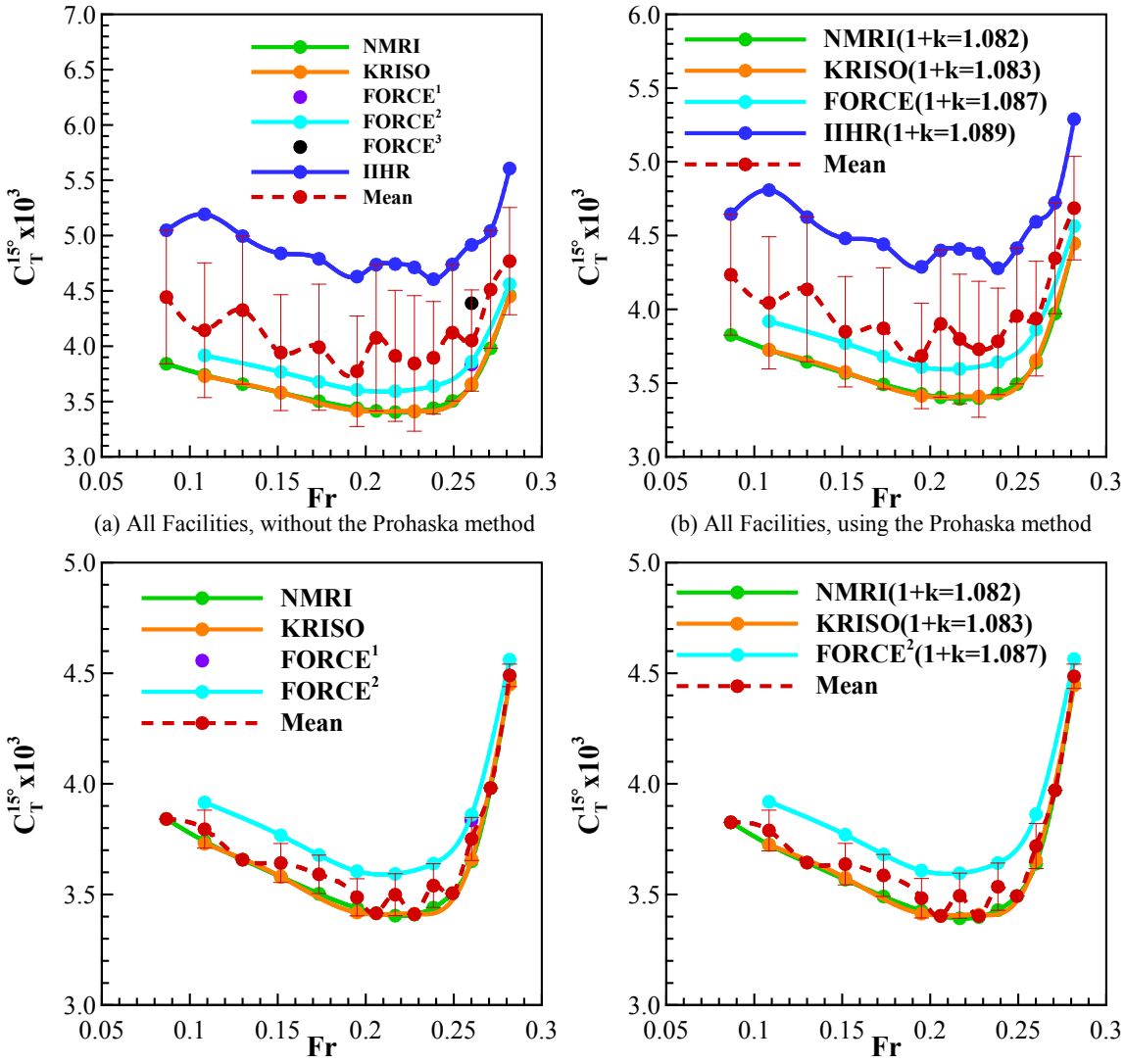

(a) All Facilities, without the Prohaska method

(b) All Facilities, using the Prohaska method

(c) Excluding 2.7m model, without the Prohaska method

(d) Excluding 2.7m model, using the Prohaska method

Figure 4.2 Comparison of C_T calculated with and without the Prohaska method, at NMRI, FORCE models, IIHR, and mean of the facilities (standard deviation between facilities is included with the mean line)

www.manaraa.com

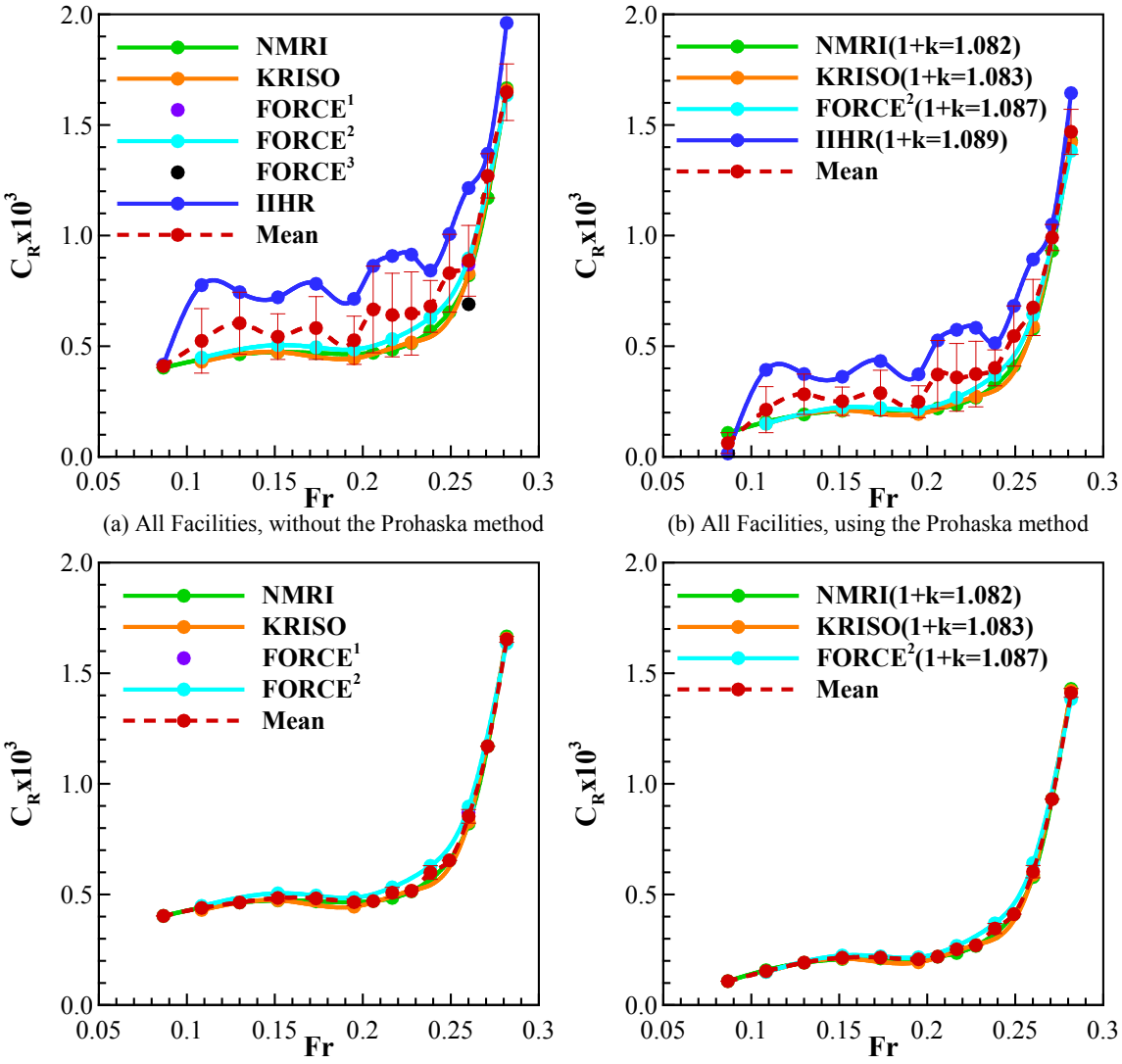

(a) All Facilities, without the Prohaska method

(b) All Facilities, using the Prohaska method

(c) Excluding 2.7m model, without the Prohaska meth

(d) Excluding 2.7m model, using the Prohaska method

Figure 4.3 Comparison of C_R calculated with and without the Prohaska method, at NMRI, FORCE models, IIHR, and mean of the facilities (Standard deviation between facilities is included with the mean line)

www.manaraa.com

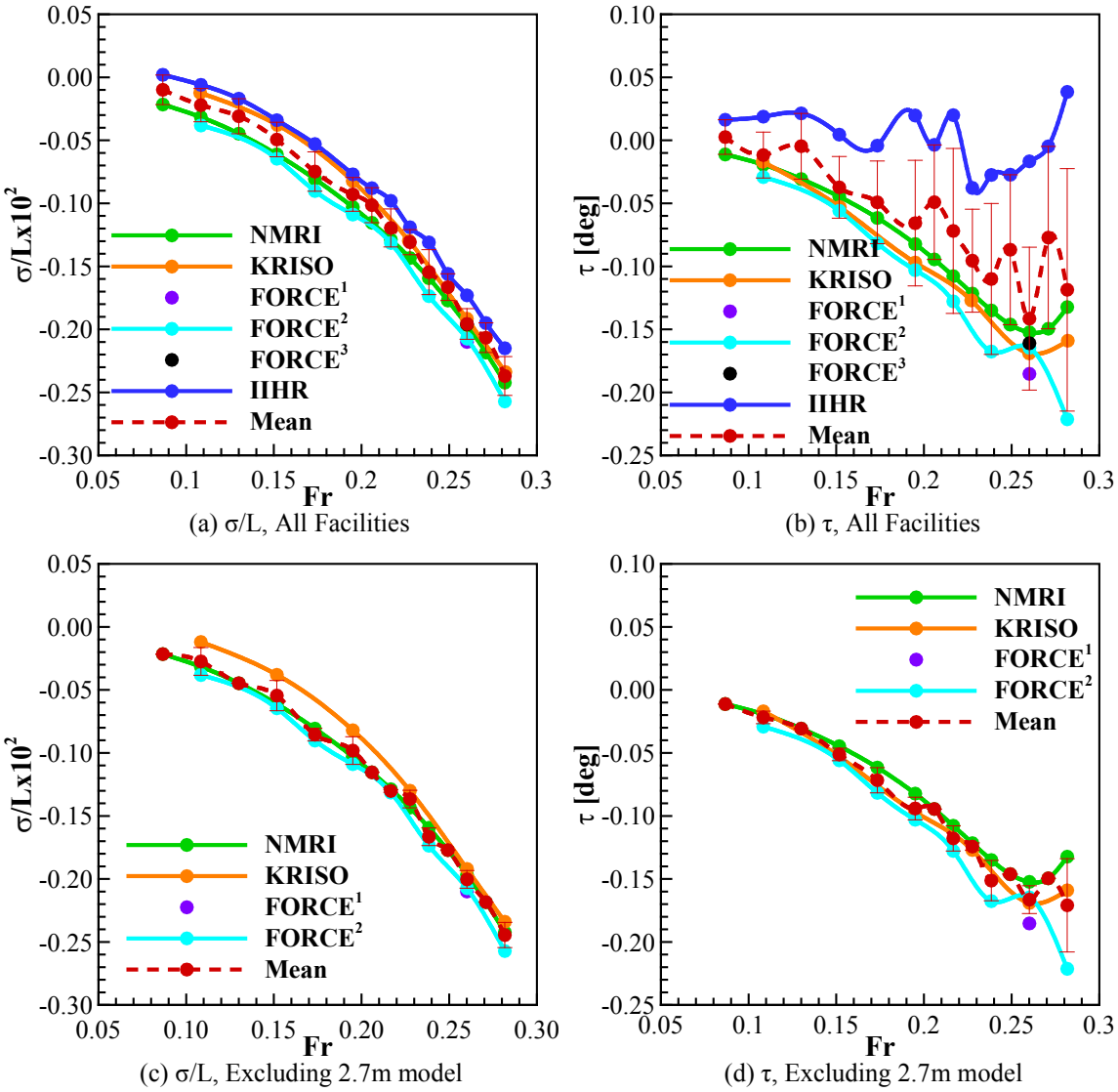

(a) σ/L, All Facilities

(b) τ, All Facilities

(c) σ/L, Excluding 2.7m model

(d) τ, Excluding 2.7m model

Figure 4.4 Comparison of σ/L and τ, at IIHR, NMRI, KRISO, FORCE models, and mean of the facilities (Standard deviation between facilities is included with the mean line)

www.manaraa.com

Table 4.1 Comparison of total resistance coefficient calculated without using the Prohaska method, C_T^{15}, for KCS in calm water

Institute	NMRI	KRISO	FORCE[1]	FORCE[2]	FORCE[3]	IIHR	All Facilities		Without 2.7m model	
Fr	$C_T^{15°} \times 10^3$						Ave ($\overline{D}$)	SD% $\overline{D}$ {SD%DR}	Ave ($\overline{D}$)	SD% $\overline{D}$ {SD%DR}
0.0867	3.841					5.048	**4.444**	**13.6**	**3.841**	
0.1084	3.740	3.729		3.916		5.192	**4.144**	**14.7**	**3.795**	**2.3**
0.1300	3.657					4.995	**4.326**	**15.5**	**3.657**	
0.1517	3.580	3.580		3.767		4.839	**3.942**	**13.3**	**3.642**	**2.4**
0.1734	3.503			3.678		4.790	**3.990**	**14.3**	**3.591**	**2.4**
0.1950	3.438	3.418		3.605		4.629	**3.773**	**13.3**	**3.487**	**2.4**
0.2059	3.415					4.737	**4.076**	**16.2**	**3.415**	
0.2167	3.404			3.593		4.743	**3.913**	**15.1**	**3.499**	**2.7**
0.2276	3.409	3.412				4.712	**3.844**	**16.0**	**3.411**	**0.0**
0.2384	3.440			3.639		4.606	**3.895**	**13.1**	**3.540**	**2.8**
0.2492	3.505					4.739	**4.122**	**15.0**	**3.505**	
0.2601	3.650	3.658	3.835	3.860	4.388	4.916	**4.051**	**11.3**	**3.751**	**2.6**
0.2709	3.981					5.042	**4.512**	**11.8**	**3.981**	
0.2817	4.459	4.449		4.561		5.606	**4.769**	**10.2**	**4.490**	**1.1**
Ave (Total)	**3.644**	**3.708**	**3.835**	**3.827**	**4.388**	**4.899**	**4.129**	**13.8{114.3*}**	**3.686**	**2.1{14.3+}**

* DR=0.498

\+ DR=0.540

www.manaraa.com

Table 4.2 Comparison of total resistance coefficient calculated using the Prohaska method, C_T^{15}, for KCS in calm water

Institute	NMRI	KRISO	FORCE[2]	IIHR	All Facilities		Without 2.7m model	
Fr	$C_T^{15°} \times 10^3$				Ave ($\overline{D}$)	SD% $\overline{D}$ {SD%DR}	Ave ($\overline{D}$)	SD% $\overline{D}$ {SD%DR}
0.0867	3.826			4.645	**4.235**	**9.7**	**3.826**	
0.1084	3.725	3.724	3.919	4.808	**4.044**	**11.1**	**3.789**	**2.4**
0.1300	3.644			4.625	**4.135**	**11.9**	**3.644**	
0.1517	3.567	3.575	3.770	4.481	**3.848**	**9.7**	**3.637**	**2.6**
0.1734	3.491		3.681	4.441	**3.871**	**10.6**	**3.586**	**2.6**
0.1950	3.426	3.413	3.608	4.288	**3.684**	**9.7**	**3.483**	**2.6**
0.2059	3.403			4.399	**3.901**	**12.8**	**3.403**	
0.2167	3.392		3.596	4.409	**3.799**	**11.6**	**3.494**	**2.9**
0.2276	3.398	3.408		4.381	**3.729**	**12.4**	**3.403**	**0.1**
0.2384	3.429		3.642	4.278	**3.783**	**9.5**	**3.535**	**3.0**
0.2492	3.493			4.414	**3.954**	**11.6**	**3.493**	
0.2601	3.639	3.654	3.863	4.593	**3.937**	**9.9**	**3.719**	**2.8**
0.2709	3.971			4.722	**4.346**	**8.6**	**3.971**	
0.2817	4.448	4.445	4.564	5.289	**4.686**	**7.5**	**4.486**	**1.2**
Ave (Total)	**3.632**	**3.703**	**3.830**	**4.555**	**3.997**	**10.5{83.5*}**	**3.676**	**2.3{15.3+}**

* DR=0.501

+ DR=0.541

www.manaraa.com

Table 4.3 Comparison of residual resistance coefficient calculated without using the Prohaska method, $C_{R,}$ for KCS in calm water

Institute	NMRI	KRISO	FORCE[1]	FORCE[2]	FORCE[3]	IIHR	All Facilities		Without 2.7m model	
Fr	$C_R \times 10^3$						Ave ($\overline{D}$)	SD% $\overline{D}$ {SD%DR}	Ave ($\overline{D}$)	SD% $\overline{D}$ {SD%DR}
0.0867	0.403					0.417	**0.410**	**1.7**	**0.403**	
0.1084	0.440	0.430		0.448		0.776	**0.524**	**27.9**	**0.439**	**1.7**
0.1300	0.464					0.744	**0.604**	**23.2**	**0.464**	
0.1517	0.473	0.474		0.505		0.721	**0.543**	**19.0**	**0.484**	**3.1**
0.1734	0.469			0.495		0.782	**0.582**	**24.3**	**0.482**	**2.7**
0.1950	0.465	0.445		0.485		0.714	**0.527**	**20.6**	**0.465**	**3.5**
0.2059	0.470					0.863	**0.666**	**29.5**	**0.470**	
0.2167	0.484			0.532		0.908	**0.641**	**29.5**	**0.508**	**4.7**
0.2276	0.514	0.517				0.914	**0.648**	**28.9**	**0.516**	
0.2384	0.568			0.629		0.842	**0.680**	**17.3**	**0.599**	**5.1**
0.2492	0.654					1.007	**0.830**	**21.3**	**0.654**	
0.2601	0.820	0.828	0.869	0.897	0.690	1.215	**0.886**	**18.1**	**0.853**	**3.7**
0.2709	1.170					1.370	**1.270**	**7.9**	**1.170**	
0.2817	1.666	1.657		1.635		1.961	**1.730**	**7.8**	**1.653**	**0.8**
Ave(Total)	**0.647**	**0.725**	**0.869**	**0.703**	**0.690**	**0.945**	**0.753**	**19.8{22.6*}**	**0.654**	**3.2{3.3+}**

* DR=0.660

\+ DR=0.625

www.manaraa.com

Table 4.4 Comparison of residual resistance coefficient calculated using the Prohaska method, C_R, for KCS in calm water

Institute	NMRI	KRISO	FORCE[2]	IIHR	All Facilities		Without 2.7m model	
Fr	$C_R \times 10^3$				Ave ($\overline{D}$)	SD% $\overline{D}$ {SD%DR}	Ave ($\overline{D}$)	SD% $\overline{D}$ {SD%DR}
0.0867	0.108			0.015	**0.062**	**75.6**	**0.108**	
0.1084	0.158	0.150	0.150	0.393	**0.213**	**49.0**	**0.153**	**2.4**
0.1300	0.192			0.374	**0.283**	**32.3**	**0.192**	
0.1517	0.208	0.211	0.224	0.362	**0.251**	**25.6**	**0.214**	**3.2**
0.1734	0.210		0.220	0.433	**0.288**	**35.7**	**0.215**	**2.3**
0.1950	0.212	0.193	0.216	0.373	**0.249**	**29.1**	**0.207**	**4.7**
0.2059	0.219			0.526	**0.372**	**41.3**	**0.219**	
0.2167	0.235		0.268	0.574	**0.359**	**42.5**	**0.252**	**6.4**
0.2276	0.268	0.272		0.583	**0.374**	**39.4**	**0.270**	
0.2384	0.323		0.369	0.514	**0.402**	**20.2**	**0.346**	**6.7**
0.2492	0.411			0.682	**0.546**	**24.8**	**0.411**	
0.2601	0.579	0.588	0.642	0.892	**0.675**	**18.9**	**0.603**	**4.6**
0.2709	0.931			1.050	**0.991**	**6.0**	**0.931**	
0.2817	1.429	1.420	1.383	1.644	**1.469**	**7.0**	**1.411**	**1.4**
Ave(Total)	**0.392**	**0.473**	**0.434**	**0.601**	**0.467**	**32.0{21.2*}**	**0.395**	**4.0{2.3+}**

* DR=0.704

+ DR=0.673

www.manaraa.com

Table 4.5 Comparison of sinkage for KCS in calm water

Institute	NMRI	KRISO	FORCE[1]	FORCE[2]	FORCE[3]	IIHR	All Facilities		Without 2.7m model	
Fr	σ/L ×10²						Ave ($\overline{D}$)	SD% $\overline{D}$ {SD%DR}	Ave ($\overline{D}$)	SD% $\overline{D}$ {SD%DR}
0.0867	-0.0216					0.0019	**-0.0099**	**119.3**	**-0.0216**	
0.1084	-0.0316	-0.0124		-0.0382		-0.0063	**-0.0221**	**59.5**	**-0.0274**	**39.9**
0.1300	-0.0447					-0.0170	**-0.0309**	**44.9**	**-0.0447**	
0.1517	-0.0612	-0.0378		-0.0646		-0.0339	**-0.0494**	**27.6**	**-0.0545**	**21.8**
0.1734	-0.0807			-0.0902		-0.0534	**-0.0748**	**20.9**	**-0.0855**	**5.6**
0.1950	-0.1030	-0.0823		-0.1089		-0.0772	**-0.0929**	**14.4**	**-0.0981**	**11.6**
0.2059	-0.1154					-0.0876	**-0.1015**	**13.7**	**-0.1154**	
0.2167	-0.1288			-0.1315		-0.0983	**-0.1195**	**12.6**	**-0.1302**	**1.0**
0.2276	-0.1434	-0.1297				-0.1192	**-0.1308**	**7.6**	**-0.1366**	**5.0**
0.2384	-0.1594			-0.1736		-0.1308	**-0.1546**	**11.5**	**-0.1665**	**4.3**
0.2492	-0.1771					-0.1559	**-0.1665**	**6.4**	**-0.1771**	
0.2601	-0.1967	-0.1916	-0.2100	-0.2074	-0.1960	-0.1727	**-0.1957**	**6.2**	**-0.2014**	**3.7**
0.2709	-0.2184					-0.1948	**-0.2066**	**5.7**	**-0.2184**	
0.2817	-0.2423	-0.2339		-0.2572		-0.2147	**-0.2370**	**6.5**	**-0.2445**	**3.9**
Ave(Total)	**-0.1230**	**-0.1146**	**-0.2100**	**-0.1340**	**-0.1960**	**-0.0971**	**-0.1137**	**25.5{25.5*}**	**-0.1230**	**10.8{11.9+}**

* DR=0.114

+ DR=0.111

www.manaraa.com

Table 4.6 Comparison of trim for KCS in calm water

Institute	NMRI	KRISO	FORCE[21]	FORCE[2]	FORCE[3]	IIHR	All Facilities		Without 2.7m model	
Fr	τ [deg]						Ave ($\overline{D}$)	SD% $\overline{D}$ {SD%DR}	Ave ($\overline{D}$)	SD% $\overline{D}$ {SD%DR}
0.0867	-0.011					0.016	**0.003**	**539.2**	**-0.011**	
0.1084	-0.019	-0.017		-0.029		0.019	**-0.012**	**155.7**	**-0.022**	**24.2**
0.1300	-0.031					0.021	**-0.005**	**560.2**	**-0.031**	
0.1517	-0.045	-0.053		-0.056		0.005	**-0.037**	**65.6**	**-0.051**	**9.3**
0.1734	-0.062			-0.082		-0.004	**-0.049**	**66.8**	**-0.072**	**14.0**
0.1950	-0.082	-0.097		-0.103		0.020	**-0.066**	**75.9**	**-0.094**	**9.2**
0.2059	-0.095					-0.004	**-0.049**	**92.7**	**-0.095**	
0.2167	-0.108			-0.128		0.020	**-0.072**	**91.1**	**-0.118**	**8.5**
0.2276	-0.122	-0.127				-0.038	**-0.095**	**42.8**	**-0.124**	**2.2**
0.2384	-0.135			-0.168		-0.028	**-0.110**	**54.4**	**-0.151**	**10.8**
0.2492	-0.146					-0.027	**-0.087**	**68.5**	**-0.146**	
0.2601	-0.152	-0.169	-0.185	-0.165	-0.161	-0.017	**-0.141**	**40.1**	**-0.168**	**7.0**
0.2709	-0.150					-0.005	**-0.077**	**93.8**	**-0.150**	
0.2817	-0.132	-0.159		-0.221		0.038	**-0.119**	**81.1**	**-0.171**	**21.8**
Ave(Total)	**-0.092**	**-0.104**	**-0.185**	**-0.119**	**-0.161**	**0.001**	**-0.065**	**144.9{131.6*}**	**-0.100**	**11.9{14.9+}**

* DR=0.072

+ DR=0.080

www.manaraa.com

4.2 Head Waves

4.2.1 IIHR Head Waves

Added Resistance and 4 DOF motion tests were completed for head wave conditions with Fr = 0.2601, H/λ = 1/60, and wave numbers, λ/L, from 0.50 to 2.00. Time history results of wave amplitude at forward perpendicular, stationary wave amplitude, measured X-force, hydrodynamic X-force, surge, modified surge, heave, pitch, and roll were obtained. The time histories for the waves, forces, and motions are shown in Appendix C, Figures C.1 through C.15. The time histories show very little variation for conditions with multiple tests. For calm water conditions, two data sets were obtained with varying wavelength conditions, as in Table 2.4. The first data set, labeled August, follows similar wavelength conditions as the oblique wave condition tests. The second data set, labeled November, follows wavelength conditions used by FORCE Technologies.

The results for both data sets in head waves are analyzed statistically to ensure good agreement between individual tests. Figure 4.5 shows the mean, individual test, and standard deviation of the 0^{th} harmonic amplitudes of total resistance coefficient, added resistance, and 4 degrees of freedom motions. Figure 4.6 shows the mean, individual test, and standard deviation of the 1^{st} harmonic amplitudes and phases of wave amplitude, total resistance coefficient, and 4 degrees of freedom motions. Figure 4.7 shows the mean, individual test, and standard deviation of the 2^{nd} harmonic amplitudes and phases of total resistance coefficient and 4 degrees of freedom motions. The standard deviation results are shown in Tables 3.7 through 3.23. The results show reasonably small scatter of data points from the mean values for the 0^{th} and 1^{st} harmonic amplitudes. The 2^{nd} harmonic amplitudes show larger scatter at certain wavelengths, especially for mean values with very small magnitudes.

Similar analysis was done for the August data set. Figure 4.8 shows the 0^{th} harmonic amplitudes of total resistance coefficient, added resistance, and 4 degrees of freedom motions. Figure 4.9 shows the 1^{st} harmonic amplitudes and phases of wave amplitude, total resistance coefficient, and 4 degrees of freedom motions. Figure 4.10 the 2^{nd} harmonic amplitudes and phases of total resistance coefficient and 4 degrees of freedom motions.

www.manaraa.com

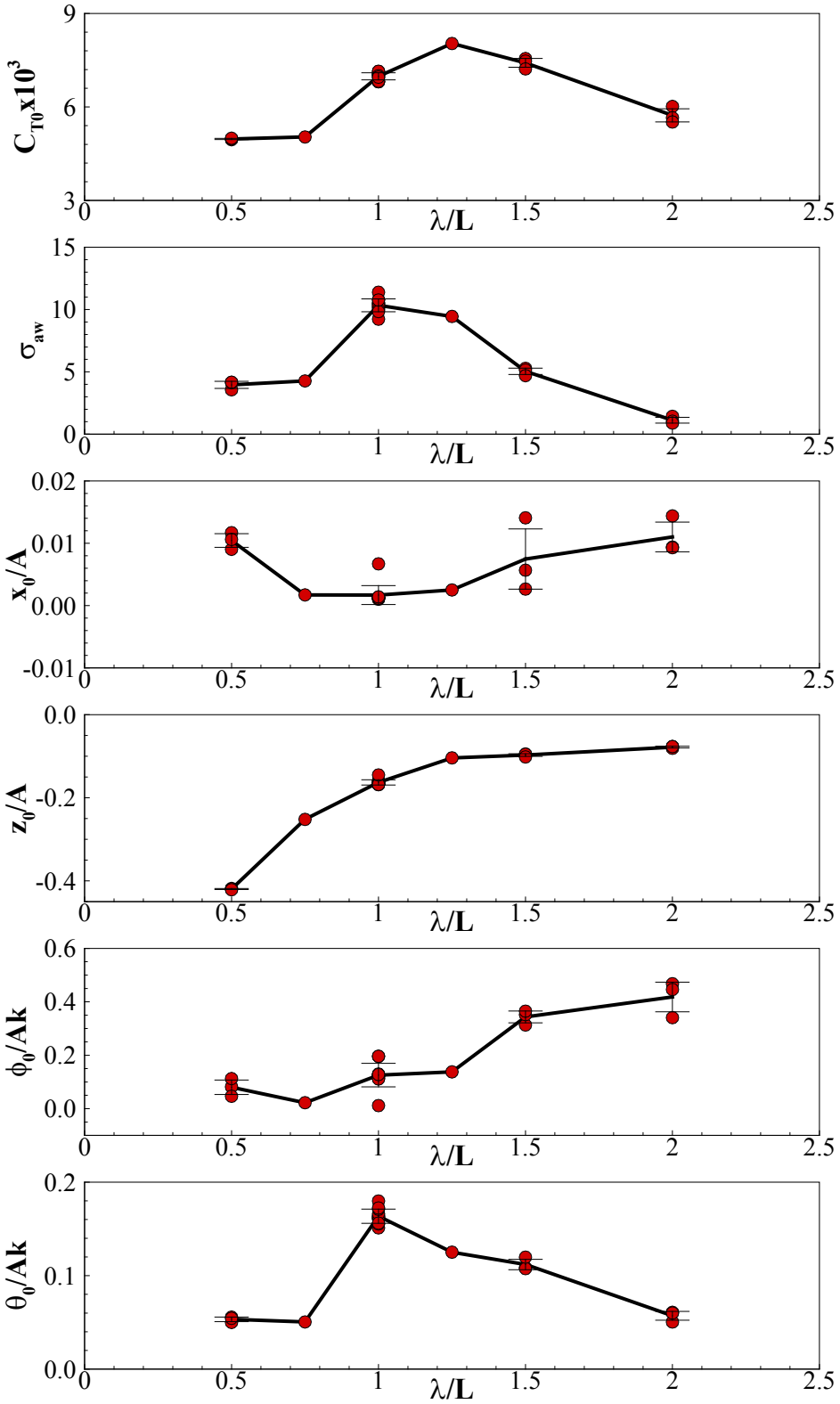

Figure 4.5 Mean, individual results, and standard deviation for 0th harmonic amplitude of resistance and 4 DOF for the August head wave data set

www.manaraa.com

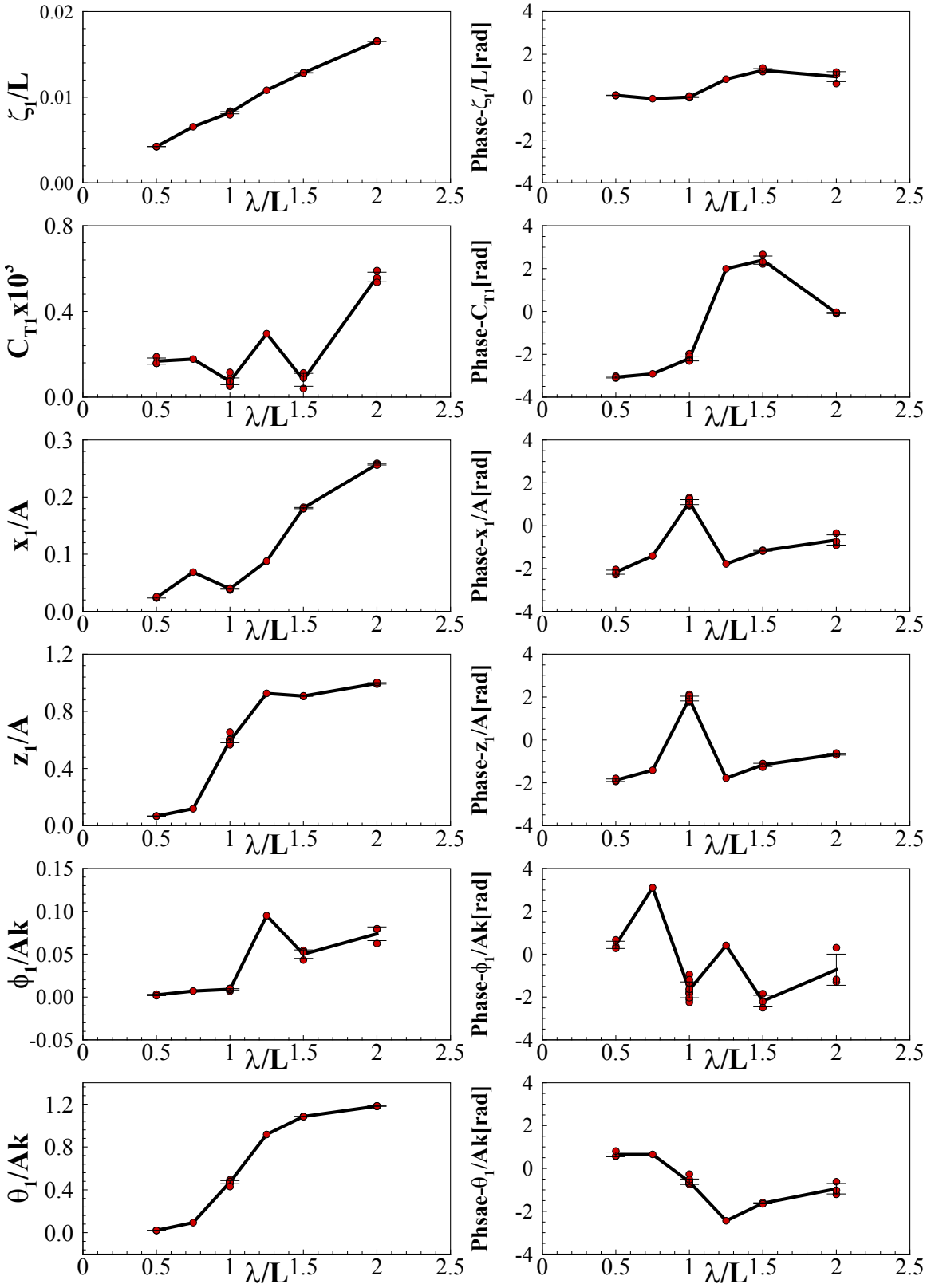

Figure 4.6 Mean, individual results, and standard deviation for 1st harmonic amplitude and phase of resistance and 4 DOF for the August head wave data set

www.manaraa.com

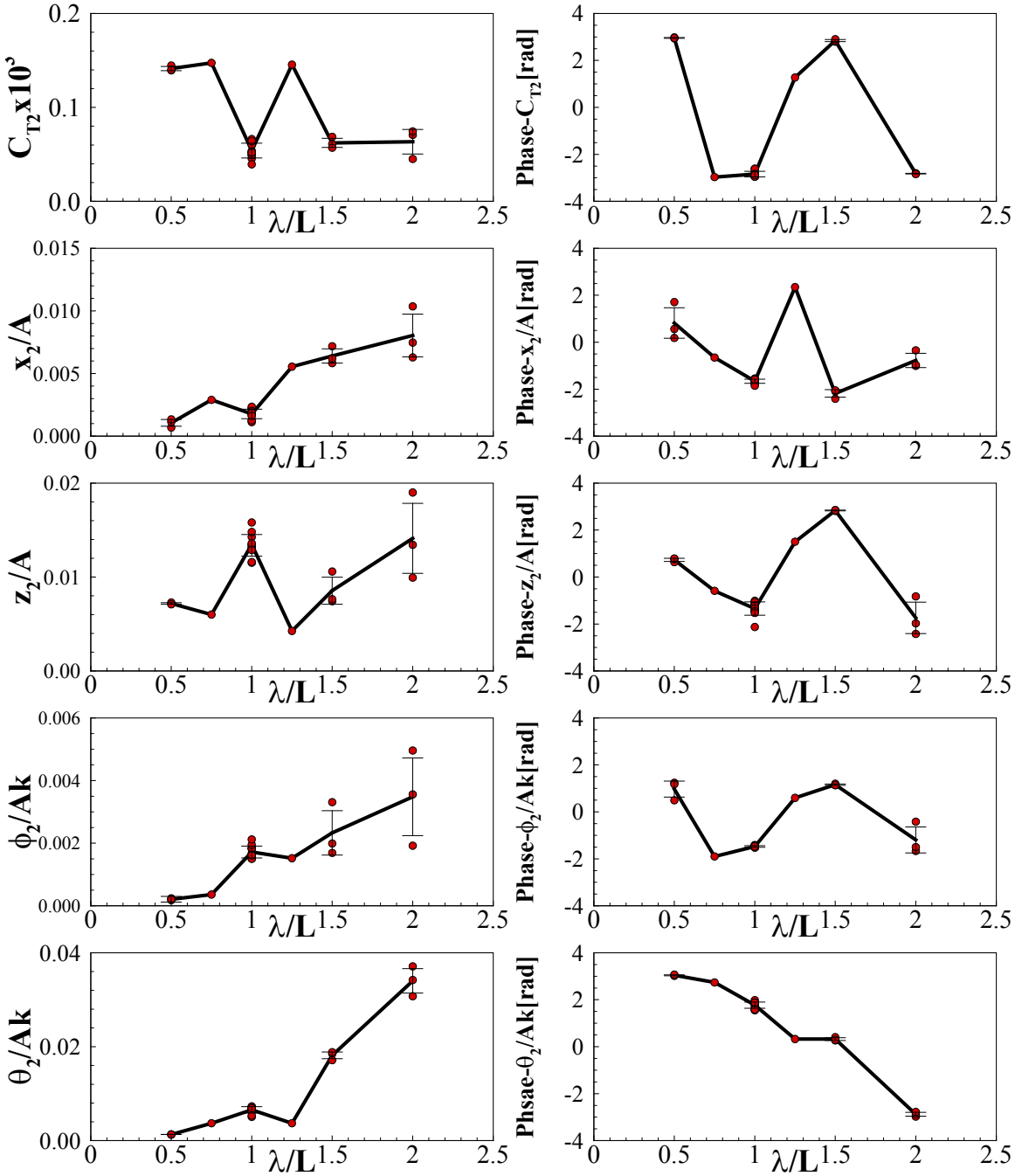

Figure 4.7 Mean, individual results, and standard deviation for 2nd harmonic amplitude and phase of resistance and 4 DOF for the August head wave data set

www.manaraa.com

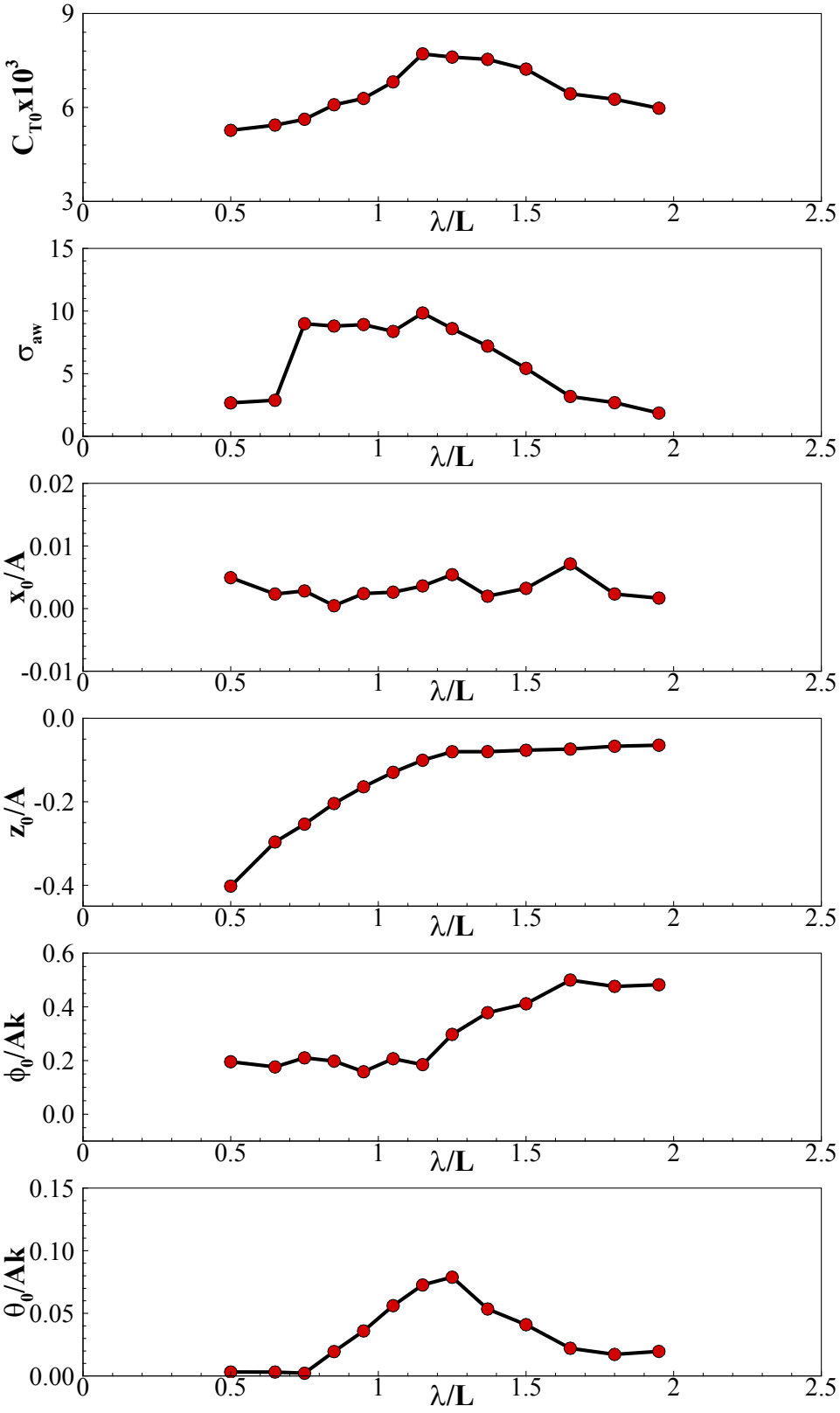

Figure 4.8 Mean, individual results, and standard deviation for 0th harmonic amplitude of resistance and 4 DOF for the November head wave data set

www.manaraa.com

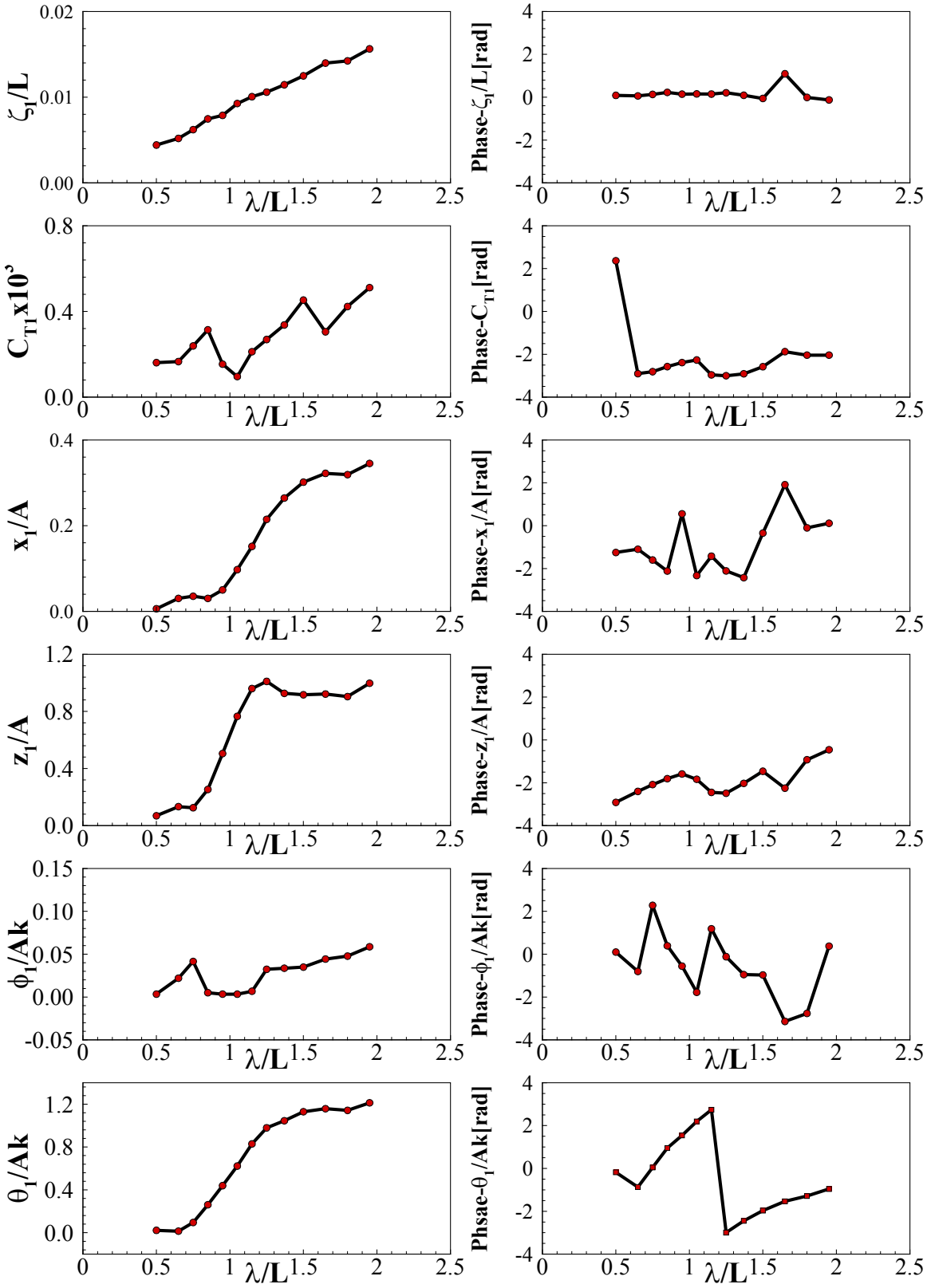

Figure 4.9 Mean, individual results, and standard deviation for 1st harmonic amplitude and phase of resistance and 4 DOF for the November head wave data set

www.manaraa.com

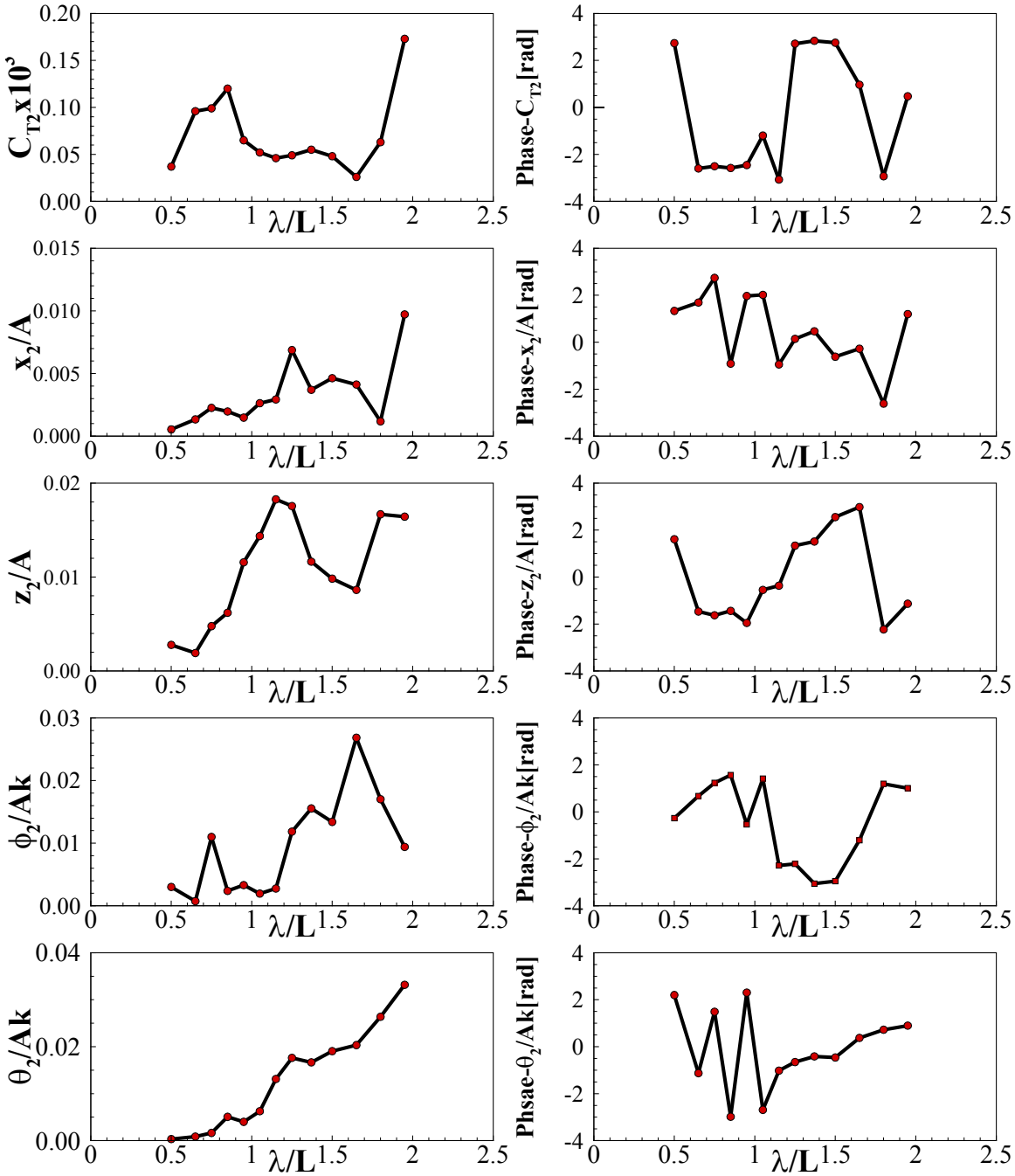

Figure 4.10 Mean, individual results, and standard deviation for 2nd harmonic amplitude and phase of resistance and 4 DOF for the November head wave data set

www.manaraa.com

4.2.2 Facility Comparison of Head Waves

The head wave data is used to validate the surge free mount set up. The surge free mount system is validated by showing good agreement to the results found at FORCE Technologies. Three data sets FORCE[1] L = 4.37 m, FORCE[2] 6.07 m, and FORCE[3] 2.70 m. Figures 4.11 through 4.15 show the time histories of forces and motions from the IIHR August data and FORCE[2] raw and the reconstructed data for λ/L of 0.65, 0.85, 1.15, 1.37, and 1.95. Two reconstructed lines are included from FORCE[2], one from the original analysis (Sadat-Hosseini et al. 2015) and the other from updated analysis. The reconstructed data is reconstructed based on the 0^{th} through 2^{nd} harmonic amplitudes and phases. The time histories show generally good agreement, especially with increasing λ/L. The largest difference between facilities occurs with the total resistance coefficient. This is due to the removal of the added inertial force due to surge motion. This eliminates the large fluctuations of the force and allows for a more accurate estimation of the mean force used to calculate added resistance. Figures 4.11 through 4.15 include the IIHR raw data for total resistance coefficient with a narrowed y-axis range, in order to have better resolution of the time histories.

www.manaraa.com

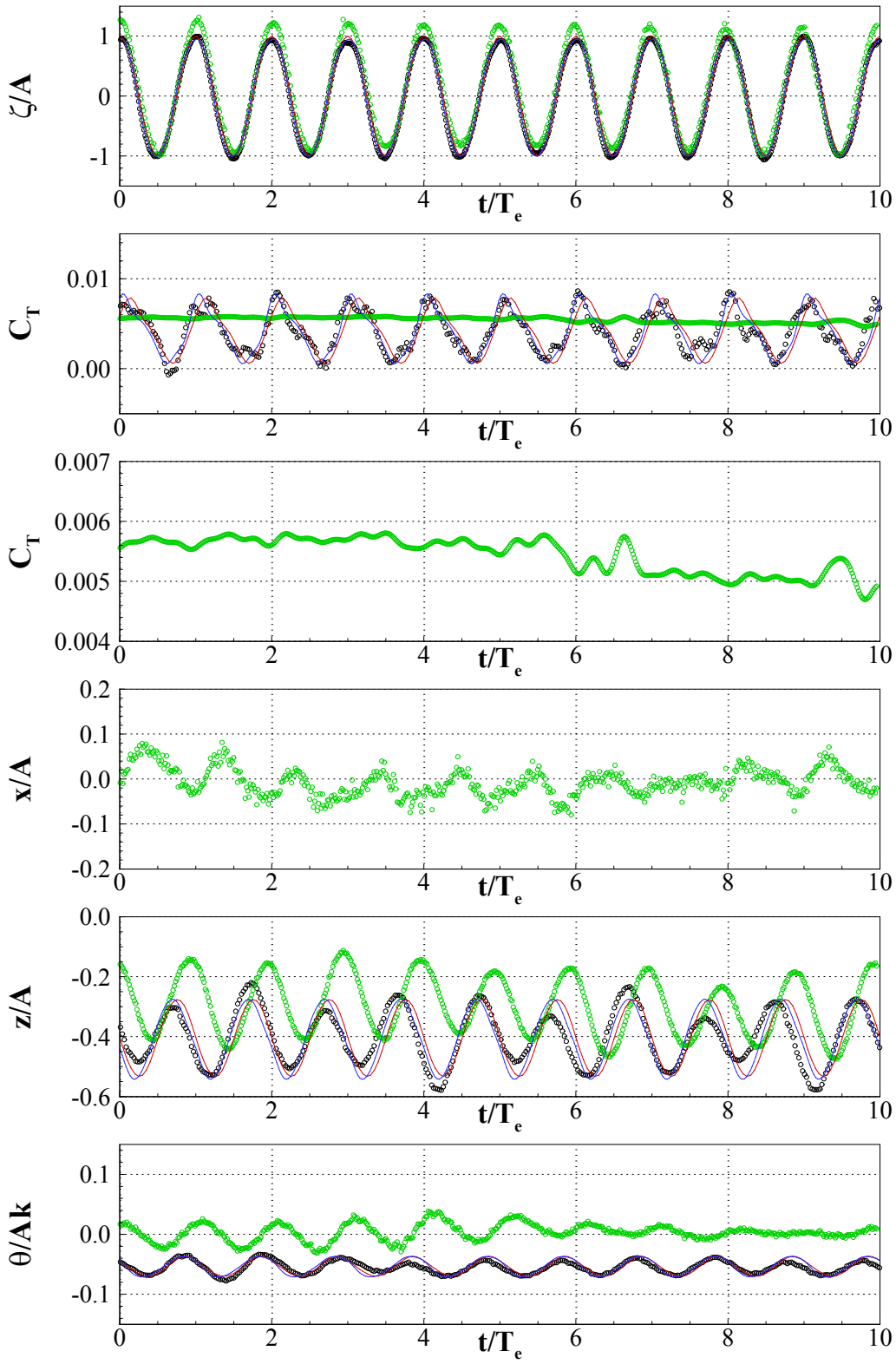

Figure 4.11Time series for force and motions of KCS in regular head waves at λ/L = 0.65 for FORCE[2] EFD (black symbol), reconstructed T2015 (red line) and updated (blue line), and IIHR Nov. (green symbol)

www.manaraa.com

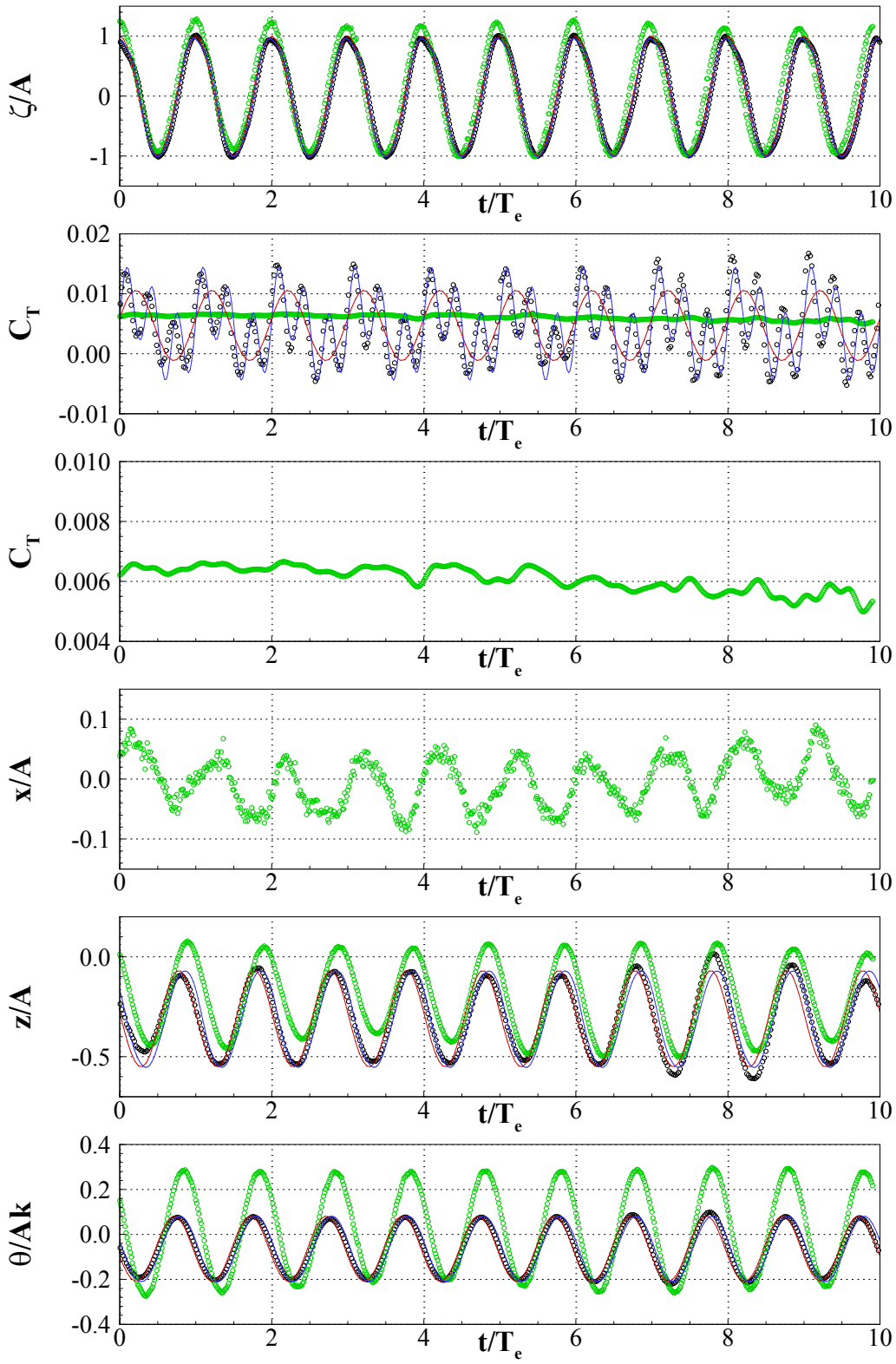

Figure 4.12 Time series for force and motions of KCS in regular head waves at λ/L = 0.85 for FORCE^2 EFD (black symbol), reconstructed T2015 (red line) and updated (blue line), and IIHR Nov. (green symbol)

www.manaraa.com

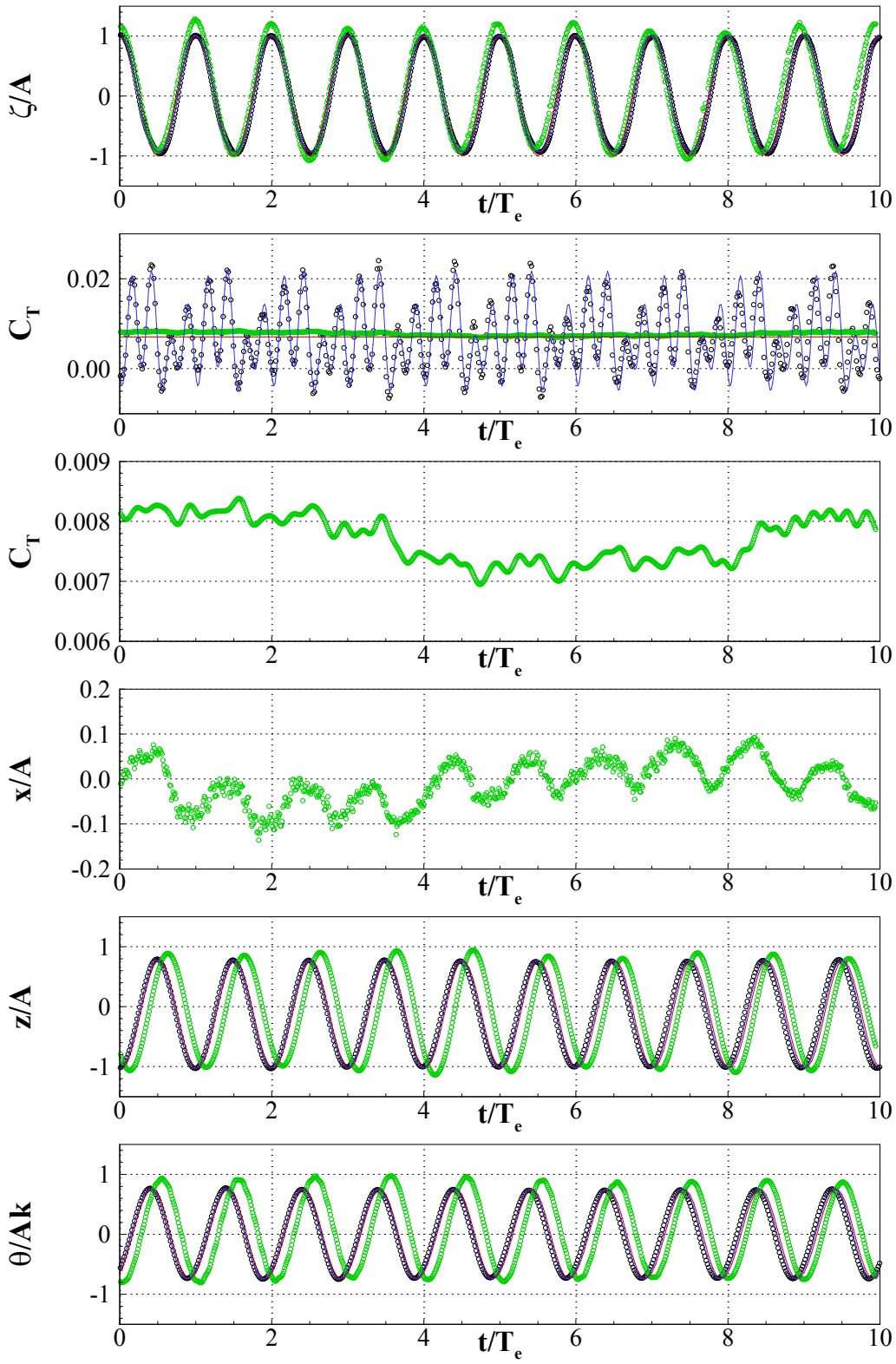

Figure 4.13 Time series for force and motions of KCS in regular head waves at λ/L = 1.15 for FORCE[2] EFD (black symbol), reconstructed T2015 (red line) and updated (blue line), and IIHR Nov. (green symbol)

www.manaraa.com

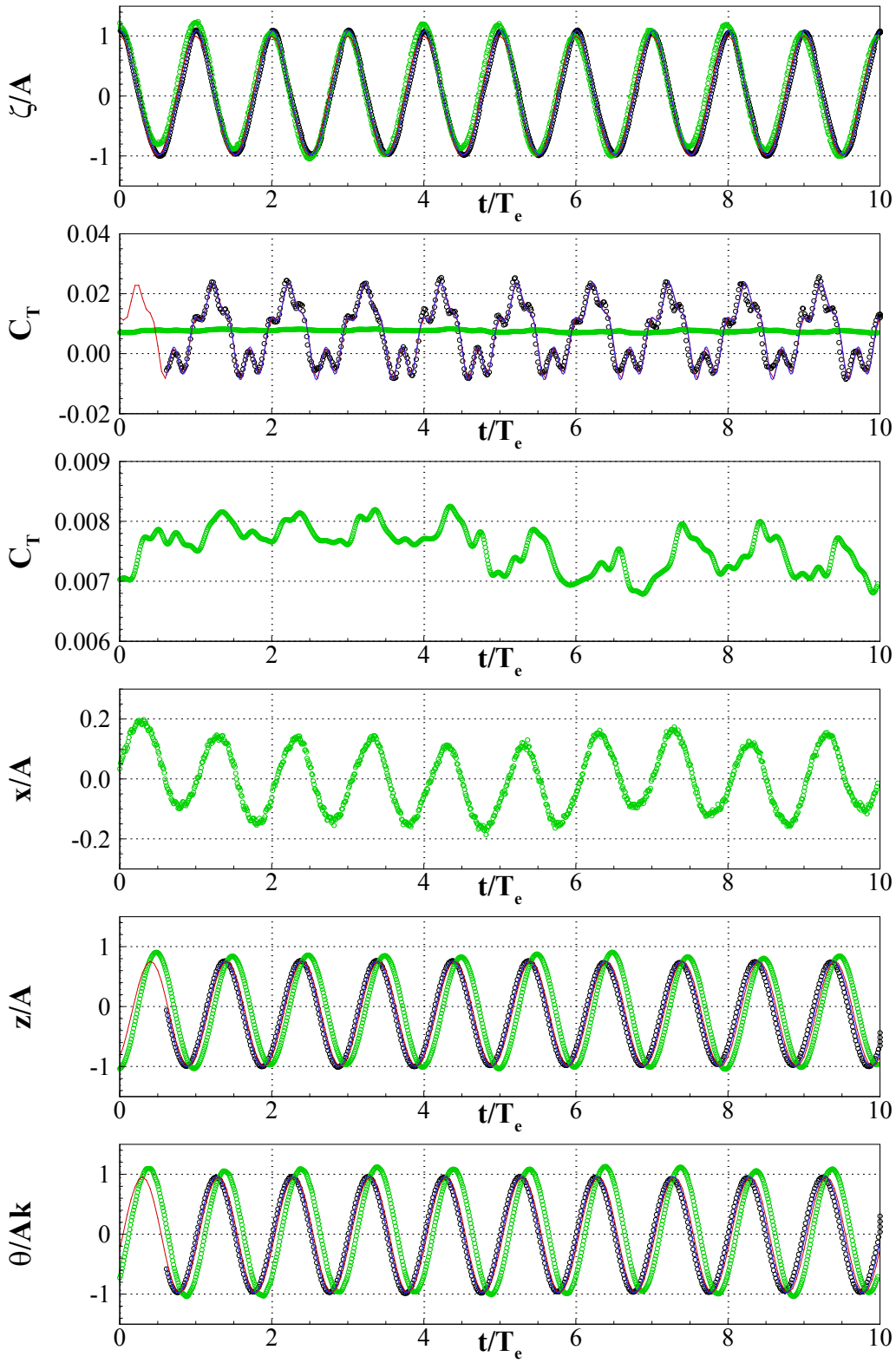

Figure 4.14 Time series for force and motions of KCS in regular head waves at λ/L = 1.37 for FORCE[2] EFD (black symbol), reconstructed T2015 (red line) and updated (blue line), and IIHR Nov. (green symbol)

www.manaraa.com

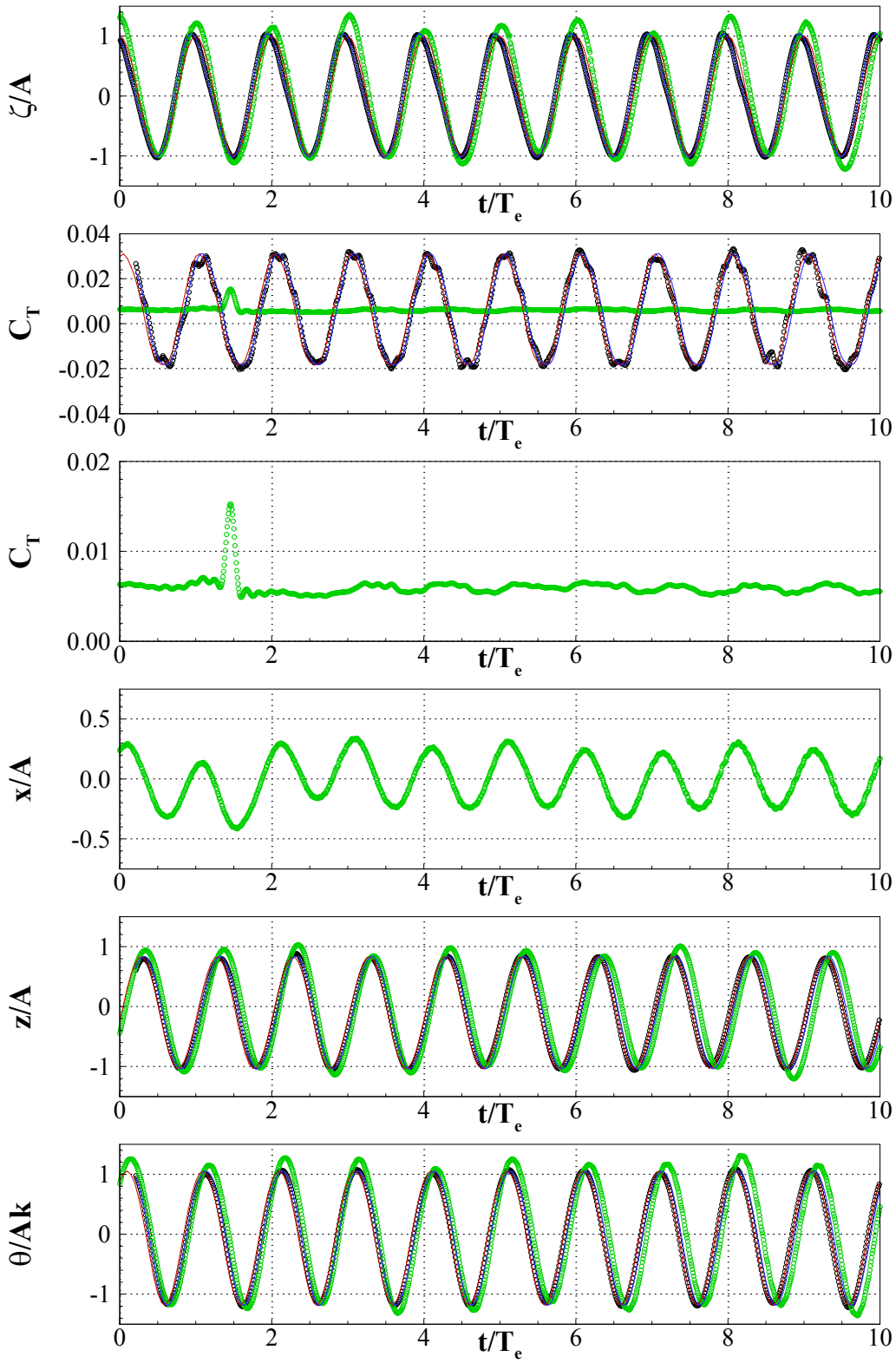

Figure 4.15 Time series for force and motions of KCS in regular head waves at λ/L = 1.95 for FORCE^2 EFD (black symbol), reconstructed T2015 (red line) and updated (blue line), and IIHR Nov. (green symbol)

www.manaraa.com

The 0^{th} harmonic resistance and motion results from FORCE and IIHR are compared. Figure 4.16 shows the 0^{th} harmonic amplitudes of the total resistance coefficient, added resistance, added resistance without the 2.70 m model, heave, and pitch. Figure 4.16 includes the individual facility results and a mean line with standard deviation. Table 4.7 through 4.10 show the 0^{th} harmonic amplitudes of total resistance coefficient, added resistance, heave, and pitch. The tables include the mean and standard deviation between all facilities along with the mean and standard deviation between facilities excluding the 2.70 m model. As with calm water the 2.70 m model increases the scatter found between facilities.

The 0^{th} harmonic amplitude of total resistance coefficient shows an agreement in trend between ship models, but shows magnitude differences. Figure 4.16 shows the added resistance comparison with and without the 2.70 m model. The standard deviations of added resistance without the L = 2.70 m model are slightly smaller, 12.8 %D with L = 2.70 m model and 11.7 %D without. The 0^{th} harmonic amplitude of heave showed a very similar trend at all facilities, with minor magnitude differences and standard deviation of 16.7 %D. The 0^{th} harmonic of pitch showed very large scatter in results between models, mainly due to the sign difference between the 6.07 m model and the 2.70 m model.

www.manaraa.com

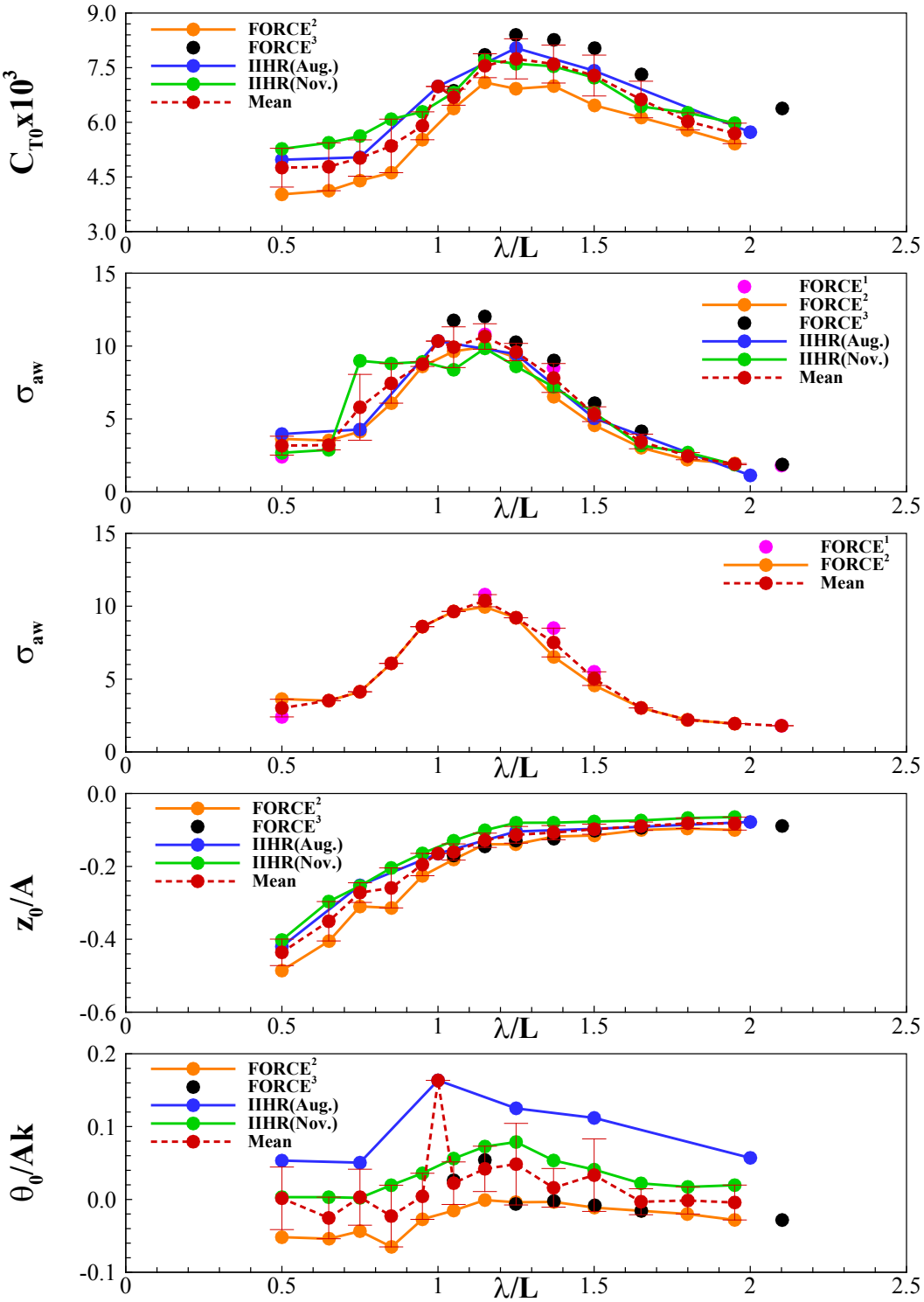

Figure 4.16 Comparison of and 0th harmonic of amplitude of resistance and motions, at Fr=0.26, for FORCE, IIHR (August and November), and mean and standard deviation of the facilities

www.manaraa.com

Table 4.7 Comparison of 0th harmonic amplitudes of total resistance coefficient for KCS in head waves at Fr=0.26

Institute	FORCE[2]	FORCE[3]	IIHR (Aug.)	IIHR (Nov.)	All Facilities	
λ/L	C_{T0} x 10^3				Ave ($\overline{D}$)	SD% $\overline{D}$ {SD%DR}
0.50	4.020		4.973	5.270	**4.754**	**11.2**
0.65	4.122			5.437	**4.780**	**13.8**
0.75	4.399		5.037	5.622	**5.019**	**10.0**
0.85	4.616			6.086	**5.351**	**13.7**
0.95	5.522			6.287	**5.904**	**6.5**
1.00			6.984		**6.984**	
1.05	6.378	6.865		6.816	**6.686**	**3.3**
1.15	7.095	7.850		7.710	**7.552**	**4.3**
1.25	6.921	8.399	8.036	7.608	**7.741**	**7.1**
1.37	6.994	8.263		7.536	**7.598**	**6.8**
1.50	6.463	8.035	7.414	7.224	**7.284**	**7.7**
1.65	6.129	7.314		6.436	**6.626**	**7.6**
1.80	5.787			6.261	**6.024**	**3.9**
1.95	5.413			5.976	**5.695**	**4.9**
2.00			5.729		**5.729**	
2.10		6.379			**6.379**	
Ave(Total)	**5.681**	**7.586**	**6.362**	**6.482**	**6.257**	**7.8{32.5*}**

* DR = 1.553

www.manaraa.com

Table 4.8 Comparison of added resistance for KCS in head waves at Fr=0.26

Institute	FORCE[1]	FORCE[2]	FORCE[3]	IIHR (Aug.)	IIHR (Nov.)	All Facilities		Without 2.7m model	
λ/L	σ_{aw}					Ave ($\overline{D}$)	SD% $\overline{D}$ {SD%DR}	Ave ($\overline{D}$)	SD% $\overline{D}$ {SD%DR}
0.50	2.40	3.63		3.96	2.67	**3.16**	**20.4**	**3.01**	**20.4**
0.65		3.52			2.88	**3.20**	**10.1**	**3.52**	
0.75		4.13		4.27	8.99	**5.80**	**38.9**	**4.13**	
0.85		6.08			8.80	**7.44**	**18.3**	**6.08**	
0.95		8.60			8.92	**8.76**	**1.8**	**8.60**	
1.00				10.34		**10.34**			
1.05		9.64	11.76		8.37	**9.92**	**14.1**	**9.64**	
1.15	10.80	9.95	12.03		9.84	**10.66**	**8.2**	**10.38**	**4.1**
1.25		9.21	10.26	9.44	8.60	**9.38**	**6.4**	**9.21**	
1.37	8.50	6.52	9.01		7.20	**7.81**	**12.7**	**7.51**	**13.2**
1.50	5.50	4.56	6.08	5.04	5.42	**5.32**	**9.5**	**5.03**	**9.3**
1.65		3.02	4.15		3.18	**3.45**	**14.5**	**3.02**	
1.80		2.20			2.69	**2.44**	**10.0**	**2.20**	
1.95		1.94			1.86	**1.90**	**2.1**	**1.94**	
2.00				1.12		**1.12**			
2.10	1.80		1.87			**1.84**	**1.9**	**1.80**	
Ave(Total)	**5.80**	**5.62**	**7.88**	**5.70**	**6.11**	**5.78**	**12.8{15.6*}**	**5.43**	**11.7{14.9*}**

* DR = 4.767
+ DR = 4.288

www.manaraa.com

Table 4.9 Comparison of 0th harmonic amplitudes of heave for KCS in head waves at Fr=0.26

Institute	FORCE[2]	FORCE[3]	IIHR (Aug.)	IIHR (Nov.)	All Facilities	
λ/L	z_0/A				Ave ($\overline{D}$)	SD% $\overline{D}$ {SD%DR}
0.50	-0.486		-0.420	-0.402	**-0.436**	**8.3**
0.65	-0.405			-0.296	**-0.350**	**15.4**
0.75	-0.310		-0.252	-0.254	**-0.272**	**9.9**
0.85	-0.314			-0.204	**-0.259**	**21.2**
0.95	-0.226			-0.164	**-0.195**	**15.7**
1.00			-0.165		**-0.165**	
1.05	-0.181	-0.170		-0.130	**-0.160**	**13.8**
1.15	-0.139	-0.145		-0.101	**-0.128**	**15.3**
1.25	-0.139	-0.129	-0.104	-0.080	**-0.113**	**20.3**
1.37	-0.118	-0.124		-0.080	**-0.107**	**18.1**
1.50	-0.115	-0.102	-0.097	-0.077	**-0.098**	**14.1**
1.65	-0.100	-0.094		-0.074	**-0.089**	**12.7**
1.80	-0.096			-0.067	**-0.082**	**17.7**
1.95	-0.100			-0.065	**-0.082**	**21.6**
2.00			-0.078		**-0.078**	
2.10		-0.089			**-0.089**	
Ave(Total)	**-0.210**	**-0.122**	**-0.186**	**-0.153**	**-0.169**	**15.7{14.8*}**

* DR = 0.179

www.manaraa.com

Table 4.10 Comparison of 0th harmonic amplitudes of pitch for KCS in head waves at Fr=0.26

Institute	FORCE[2]	FORCE[3]	IIHR (Aug.)	IIHR (Nov.)	All Facilities	
λ/L	θ_0/Ak				Ave ($\overline{D}$)	SD% $\overline{D}$ {SD%DR}
0.50	-0.0518		0.0533	0.003	**0.0016**	**2723.5**
0.65	-0.0539			0.003	**-0.0254**	**112.3**
0.75	-0.0435		0.0505	0.002	**0.0031**	**1251.0**
0.85	-0.0651			0.020	**-0.0228**	**185.5**
0.95	-0.0272			0.036	**0.0043**	**727.7**
1.00			0.1635		**0.1635**	
1.05	-0.0152	0.0263		0.056	**0.0224**	**130.5**
1.15	-0.0008	0.0542		0.073	**0.0420**	**74.3**
1.25	-0.0038	-0.0062	0.1251	0.079	**0.0485**	**115.4**
1.37	-0.0034	-0.0022		0.053	**0.0160**	**166.0**
1.50	-0.0112	-0.0081	0.1119	0.041	**0.0334**	**149.3**
1.65	-0.0156	-0.0157		0.022	**-0.0031**	**580.3**
1.80	-0.0200			0.017	**-0.0014**	**1340.6**
1.95	-0.0281			0.020	**-0.0042**	**562.1**
2.00			0.0571		**0.0571**	
2.10		-0.0282			**-0.0282**	
Ave(Total)	**-0.0261**	**0.0029**	**0.9360**	**0.0327**	**0.0192**	**624.5{124.9*}**

* DR = 0.0958

www.manaraa.com

The 1st harmonic resistance and motion results from FORCE and IIHR are compared. Figure 4.17 shows the 1st harmonic amplitudes and phases of the wave amplitude, total resistance coefficient, heave, pitch, and heave and pitch without the 2.70 m model. Figure 4.17 includes the individual facility results and a mean line with standard deviation. Table 4.11 shows the 1st harmonic amplitudes of wave elevation and the percent difference from the desired wave amplitude. Tables 4.12 through 4.18 show the 1st harmonic amplitudes and phases of wave amplitude, total resistance coefficient, heave, pitch. The tables include the mean and standard deviation between all facilities along with the mean and standard deviation between facilities excluding the 2.70 m model.

The 1st harmonic amplitude of wave amplitude showed very good agreement between facilities and model sizes, with very little deviation from the desired amplitude, < 6.0 %D average deviation for all facilities. The 1st harmonic phase of wave amplitude showed small amounts of scatter. The 1st harmonic amplitude and phase of total resistance coefficient shows large scatter due to the removal of the inertial force in the IIHR data. Both heave and pitch show good agreement between facilities and model sizes. The standard deviations of amplitudes are < 9 %D with and without 2.70 m model. The heave amplitude shows smaller scatter with all models, while pitch shows smaller scatter excluding 2.70 m model. The 1st harmonic phases of heave and pitch show large scatter overall, but larger wavelength cases show good agreement.

www.manaraa.com

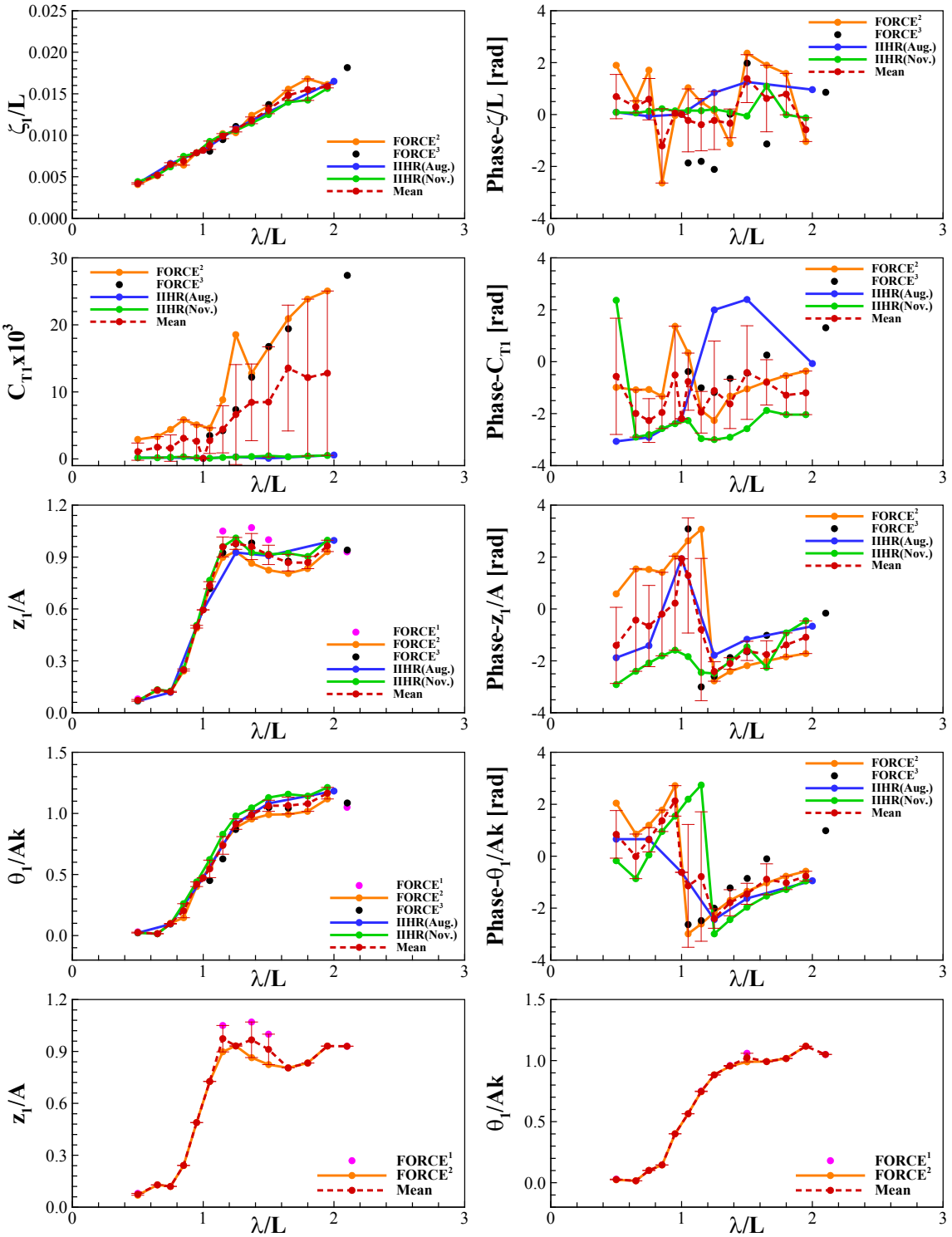

Figure 4.17 Comparison of and 1st harmonic of amplitude and phase of wave amplitude, resistance and motions, at Fr=0.26, for FORCE, IIHR (August and November), and mean and standard deviation of the facilities

www.manaraa.com

Table 4.11 Comparison of 1st harmonic amplitudes of wave elevation at FP for KCS in head waves at Fr=0.26 where theoretical ζ_1/L values are based on $H/\lambda=1/60$ (ζ_1 is used as A to non-dimensionalize the motion variables)

Institute	FORCE[2]		FORCE[3]		IIHR (Aug.)		IIHR (Nov.)		All Facilities	
λ/L	ζ_1/L	E%D	ζ_1/L	E%D	ζ_1/L	E%D	ζ_1/L	E%D	Ave ($\overline{D}$)	SD% $\overline{D}$ {SD%DR}
0.50	0.0041	2.2			0.0042	1.7	0.0044	6.1	**0.0042**	**3.3**
0.65	0.0051	5.3					0.0052	4.1	**0.0052**	**0.6**
0.75	0.0066	5.9			0.0066	4.8	0.0062	0.6	**0.0065**	**2.8**
0.85	0.0064	9.5					0.0075	5.5	**0.0069**	**7.7**
0.95	0.0079	0.2					0.0079	0.4	**0.0079**	**0.1**
1.00					0.0082	1.7			**0.0082**	
1.05	0.0092	4.7	0.0081	7.6			0.0093	5.8	**0.0088**	**6.0**
1.15	0.0102	6.4	0.0095	1.1			0.0101	5.0	**0.0099**	**3.1**
1.25	0.0103	1.0	0.0111	6.2	0.0108	3.8	0.0106	1.6	**0.0107**	**2.6**
1.37	0.0124	8.6	0.0116	1.5			0.0115	0.3	**0.0118**	**3.6**
1.50	0.0135	8.3	0.0137	9.6	0.0128	2.7	0.0125	0.1	**0.0131**	**3.8**
1.65	0.0155	13.1	0.0148	7.8			0.0140	1.7	**0.0148**	**4.3**
1.80	0.0168	12.0					0.0142	5.1	**0.0155**	**8.2**
1.95	0.0161	0.8					0.0156	3.8	**0.0159**	**1.5**
2.00					0.0165	0.9			**0.0165**	
2.10			0.0181	3.7					**0.0181**	
Ave(Total)	**0.0103**	**6.0**	**0.0124**	**5.6**	**0.0085**	**2.9**	**0.0100**	**3.1**	**0.0109**	**3.7 {5.7*}**

* DR = 0.007

www.manaraa.com

Table 4.12 Comparison of 1st harmonic amplitudes of total resistance coefficient for KCS in head waves at Fr=0.26

Institute	FORCE[2]	FORCE[3]	IIHR (Aug.)	IIHR (Nov.)	All Facilities	
λ/L	C_{T1} x 10^3				Ave ($\overline{D}$)	SD% $\overline{D}$ {SD%DR}
0.50	2.90		0.17	0.16	**1.08**	**119.8**
0.65	3.32			0.17	**1.74**	**90.5**
0.75	4.39		0.18	0.24	**1.60**	**123.1**
0.85	5.84			0.31	**3.07**	**89.8**
0.95	5.09			0.15	**2.62**	**94.1**
1.00			0.07		**0.07**	
1.05	4.58	3.48		0.10	**2.72**	**70.2**
1.15	8.82	4.22		0.21	**4.42**	**79.6**
1.25	18.55	7.35	0.30	0.27	**6.62**	**112.9**
1.37	12.78	12.19		0.34	**8.44**	**67.9**
1.50	16.64	16.78	0.08	0.45	**8.49**	**96.9**
1.65	20.93	19.42		0.31	**13.55**	**69.3**
1.80	23.84			0.42	**12.13**	**96.5**
1.95	25.07			0.51	**12.79**	**96.0**
2.00			0.56		**0.56**	
2.10		3.48			**3.48**	
Ave(Total)	**11.75**	**9.56**	**0.23**	**0.28**	**5.21**	**92.8{71.8*}**

* DR = 6.740

www.manaraa.com

Table 4.13Comparison of 1st harmonic amplitudes of heave for KCS in head waves at Fr=0.26

Institute	FORCE[1]	FORCE[2]	FORCE[3]	IIHR (Aug.)	IIHR (Nov.)	All Facilities		Without 2.7m model	
λ/L	z_1/A					Ave ($\overline{D}$)	SD% $\overline{D}$ {SD%DR}	Ave ($\overline{D}$)	SD% $\overline{D}$ {SD%DR}
0.50	0.080	0.069		0.067	0.069	**0.071**	**7.2**	**0.075**	**7.2**
0.65		0.129			0.133	**0.131**	**1.7**	**0.129**	
0.75		0.120		0.118	0.125	**0.121**	**2.4**	**0.120**	
0.85		0.241			0.253	**0.247**	**2.4**	**0.241**	
0.95		0.489			0.505	**0.497**	**1.6**	**0.489**	
1.00				0.595		**0.595**			
1.05		0.727	0.717		0.765	**0.736**	**2.8**	**0.727**	
1.15	1.050	0.898	0.925		0.960	**0.958**	**6.0**	**0.974**	**7.8**
1.25		0.932	0.976	0.926	1.010	**0.961**	**3.6**	**0.932**	
1.37	1.070	0.864	0.981		0.926	**0.960**	**7.9**	**0.967**	**10.6**
1.50	1.000	0.824	0.914	0.907	0.916	**0.912**	**6.1**	**0.912**	**9.7**
1.65		0.805	0.876		0.921	**0.868**	**5.5**	**0.805**	
1.80		0.833			0.903	**0.868**	**4.0**	**0.833**	
1.95		0.931			0.997	**0.964**	**3.4**	**0.931**	
2.00				0.996		**0.996**			
2.10	0.930		0.940			**0.935**	**0.5**	**0.930**	
Ave(Total)	**0.826**	**0.605**	**0.904**	**0.601**	**0.653**	**0.677**	**3.9{5.8*}**	**0.647**	**8.8{12.7*}**

* DR = 0.462
\+ DR = 0.450

www.manaraa.com

Table 4.14 Comparison of 1st harmonic amplitudes of pitch for KCS in head waves at Fr=0.26

Institute	FORCE[1]	FORCE[2]	FORCE[3]	IIHR (Aug.)	IIHR (Nov.)	All Facilities		Without 2.7m model	
λ/L	θ_1/Ak					Ave ($\overline{D}$)	SD% $\overline{D}$ {SD%DR}	Ave ($\overline{D}$)	SD% $\overline{D}$ {SD%DR}
0.50	0.030	0.024		0.022	0.022	**0.024**	**13.6**	**0.027**	**10.7**
0.65		0.016			0.014	**0.015**	**6.0**	**0.016**	
0.75		0.101		0.094	0.095	**0.097**	**3.0**	**0.101**	
0.85		0.146			0.261	**0.203**	**28.4**	**0.146**	
0.95		0.401			0.439	**0.420**	**4.6**	**0.401**	
1.00				0.472		**0.472**			
1.05		0.565	0.451		0.622	**0.546**	**5.3**	**0.565**	
1.15	0.750	0.745	0.628		0.829	**0.738**	**5.2**	**0.748**	**0.3**
1.25		0.883	0.869	0.917	0.979	**0.912**	**4.3**	**0.883**	
1.37	0.960	0.954	0.992		1.045	**0.988**	**4.2**	**0.957**	**0.3**
1.50	1.060	0.990	1.049	1.082	1.129	**1.062**	**4.7**	**1.025**	**3.4**
1.65		0.992	1.044		1.157	**1.065**	**7.8**	**0.992**	
1.80		1.017			1.142	**1.080**	**5.8**	**1.017**	
1.95		1.118			1.213	**1.165**	**4.0**	**1.118**	
2.00				1.183		**1.183**			
2.10	1.050		1.085			**1.068**		**1.050**	
Ave(Total)	**0.770**	**0.612**	**0.874**	**0.628**	**0.688**	**0.690**	**7.8{9.2*}**	**0.646**	**3.7{4.3*}**

* DR = 0.584
\+ DR = 0.551

www.manaraa.com

Table 4.15 Comparison of 1st harmonic phases of wave elevation at FP for KCS in head waves at Fr=0.26

Institute	FORCE[2]	FORCE[3]	IIHR (Aug.)	IIHR (Nov.)	All Facilities	
λ/L	Phase - ζ_1/L [rad]				Ave ($\overline{D}$)	SD% $\overline{D}$ {SD%DR}
0.50	1.898		0.089	0.086	**0.691**	**123.5**
0.65	0.525			0.060	**0.293**	**79.4**
0.75	1.709		-0.067	0.130	**0.590**	**134.7**
0.85	-2.641			0.224	**-1.208**	**118.6**
0.95	-0.037			0.142	**0.052**	**171.0**
1.00			0.006		**0.006**	
1.05	1.032	-1.866		0.153	**-0.227**	**534.7**
1.15	0.483	-1.804		0.146	**-0.392**	**257.4**
1.25	0.150	-2.115	0.844	0.206	**-0.229**	**490.7**
1.37	-1.123	0.012		0.091	**-0.340**	**163.0**
1.50	2.364	1.979	1.256	-0.059	**1.385**	**66.7**
1.65	1.900	-1.136		1.091	**0.619**	**207.5**
1.80	1.584			-0.011	**0.787**	**101.4**
1.95	-1.040			-0.128	**-0.584**	**78.2**
2.00			0.958		**0.958**	
2.10		0.855			**0.855**	
Ave(Total)	**0.523**	**-0.582**	**0.514**	**0.164**	**0.204**	**194.4{30.5*}**

* DR = 1.297

www.manaraa.com

Table 4.16 Comparison of 1st harmonic phases of total resistance coefficient for KCS in head waves at Fr=0.26

Institute	FORCE[2]	FORCE[3]	IIHR (Aug.)	IIHR (Nov.)	All Facilities	
λ/L	Phase- C_{T1} [rad]				Ave ($\overline{D}$)	SD% $\overline{D}$ {SD%DR}
0.50	-0.988		-3.068	2.367	**-0.563**	**397.8**
0.65	-1.084			-2.903	**-1.993**	**45.6**
0.75	-1.072		-2.913	-2.811	**-2.265**	**37.3**
0.85	-1.331			-2.576	**-1.953**	**31.8**
0.95	1.366			-2.386	**-0.510**	**368.0**
1.00			-2.197		**-2.197**	
1.05	0.345	-0.379		-2.266	**-0.767**	**143.5**
1.15	-1.872	-1.005		-2.960	**-1.946**	**41.1**
1.25	-2.263	-1.184	1.995	-3.000	**-1.113**	**171.4**
1.37	-1.322	-0.644		-2.910	**-1.626**	**58.4**
1.50	-1.050	-0.436	2.397	-2.580	**-0.417**	**432.4**
1.65	-0.764	0.257		-1.877	**-0.795**	**109.6**
1.80	-0.537			-2.039	**-1.288**	**58.3**
1.95	-0.359			-2.038	**-1.198**	**70.1**
2.00			-0.071		**-0.071**	
2.10		1.309			**1.309**	
Ave(Total)	**-0.841**	**-0.297**	**-0.643**	**-2.152**	**-1.087**	**151.2{92.0*}**

* DR = 1.787

www.manaraa.com

Table 4.17 Comparison of 1st phases of heave for KCS in head waves at Fr=0.26

Institute	FORCE[2]	FORCE[3]	IIHR (Aug.)	IIHR (Nov.)	All Facilities	
λ/L	Phase- z_1/A [rad]				Ave ($\overline{D}$)	SD% $\overline{D}$ {SD%DR}
0.50	0.581		-1.879	-2.915	**-1.404**	**104.4**
0.65	1.540			-2.402	**-0.431**	**457.5**
0.75	1.521		-1.412	-2.084	**-0.658**	**237.8**
0.85	1.409			-1.808	**-0.199**	**807.1**
0.95	2.033			-1.588	**0.223**	**812.2**
1.00			-1.932		**-1.932**	
1.05	2.624	3.083		-1.837	**1.290**	**172.0**
1.15	3.067	-3.003		-2.447	**-0.794**	**344.8**
1.25	-2.773	-2.594	-1.782	-2.488	**-2.409**	**15.6**
1.37	-2.406	-1.873		-2.026	**-2.102**	**10.7**
1.50	-2.183	-1.649	-1.168	-1.462	**-1.616**	**22.9**
1.65	-2.003	-1.019		-2.250	**-1.757**	**30.3**
1.80	-1.847			-0.925	**-1.386**	**33.3**
1.95	-1.721			-0.459	**-1.090**	**57.9**
2.00			-0.666		**-0.666**	
2.10		-1.019			**-1.019**	
Ave(Total)	**-0.012**	**-1.154**	**-0.829**	**-1.899**	**-0.755**	**239.0{83.2*}**

* DR = 1.850

www.manaraa.com

Table 4.18 Comparison of 1st harmonic phases of pitch for KCS in head waves at Fr=0.26

Institute	FORCE[2]	FORCE[3]	IIHR (Aug.)	IIHR (Nov.)	All Facilities	
λ/L	Phase- θ_1/Ak [rad]				Ave ($\overline{D}$)	SD% $\overline{D}$ {SD%DR}
0.50	2.0430		0.6545	-0.1781	**0.8398**	**109.1**
0.65	0.8492			-0.8685	**-0.0096**	**8908.8**
0.75	1.1916		0.6556	0.0470	**0.6314**	**74.1**
0.85	1.7769			0.9496	**1.3632**	**30.3**
0.95	2.7171			1.5418	**2.1294**	**27.6**
1.00			-0.6214		**-0.6214**	
1.05	-2.9916	-2.6348		2.1939	**-1.1442**	**206.7**
1.15	-2.6117	-2.4839		2.7385	**-0.7857**	**317.2**
1.25	-2.1679	-2.0063	-2.4435	-2.9940	**-2.4029**	**15.6**
1.37	-1.7077	-1.2250		-2.4460	**-1.7929**	**28.0**
1.50	-1.3542	-0.8599	-1.6267	-1.9656	**-1.4516**	**27.9**
1.65	-1.0280	-0.1045		-1.5357	**-0.8894**	**66.6**
1.80	-0.7745			-1.2859	**-1.0302**	**24.8**
1.95	-0.5811			-0.9583	**-0.7697**	**24.5**
2.00			-0.9474		**-0.9474**	
2.10		0.9820			**0.9820**	
Ave(Total)	**-0.3568**	**-1.1903**	**-0.7215**	**-0.3663**	**-0.3687**	**758.6{12.3.4*}**

* DR = 2.385

www.manaraa.com

The 2nd harmonic resistance and motion results from FORCE and IIHR are compared. Figure 4.18 shows the 2nd harmonic amplitudes and phases of the total resistance coefficient, heave, and pitch. Figure 4.18 includes the individual facility results and a mean line with standard deviation. Tables 4.19 through 4.24 show the 2nd harmonic amplitudes and phases of total resistance coefficient, heave, pitch. The tables include the mean and standard deviation between all facilities along with the mean and standard deviation between facilities excluding the 2.70 m model.

The 2nd harmonic amplitude of the total resistance coefficient shows very large scatter between facilities and models. The variation between IIHR and FORCE 2nd harmonic amplitude of total resistance coefficient is due to the removal of the inertial force from the IIHR data. The large variations in the 2nd harmonic of phases of the total resistance coefficient is due to the removal of inertial force as well. The 2nd harmonic amplitudes of heave and pitch show a general agreement in trends, but have large scatter in results for intermediate wavelengths. The 2nd harmonic phases of heave and pitch show similar trends overall, but show large scatter throughout all wavelengths.

www.manaraa.com

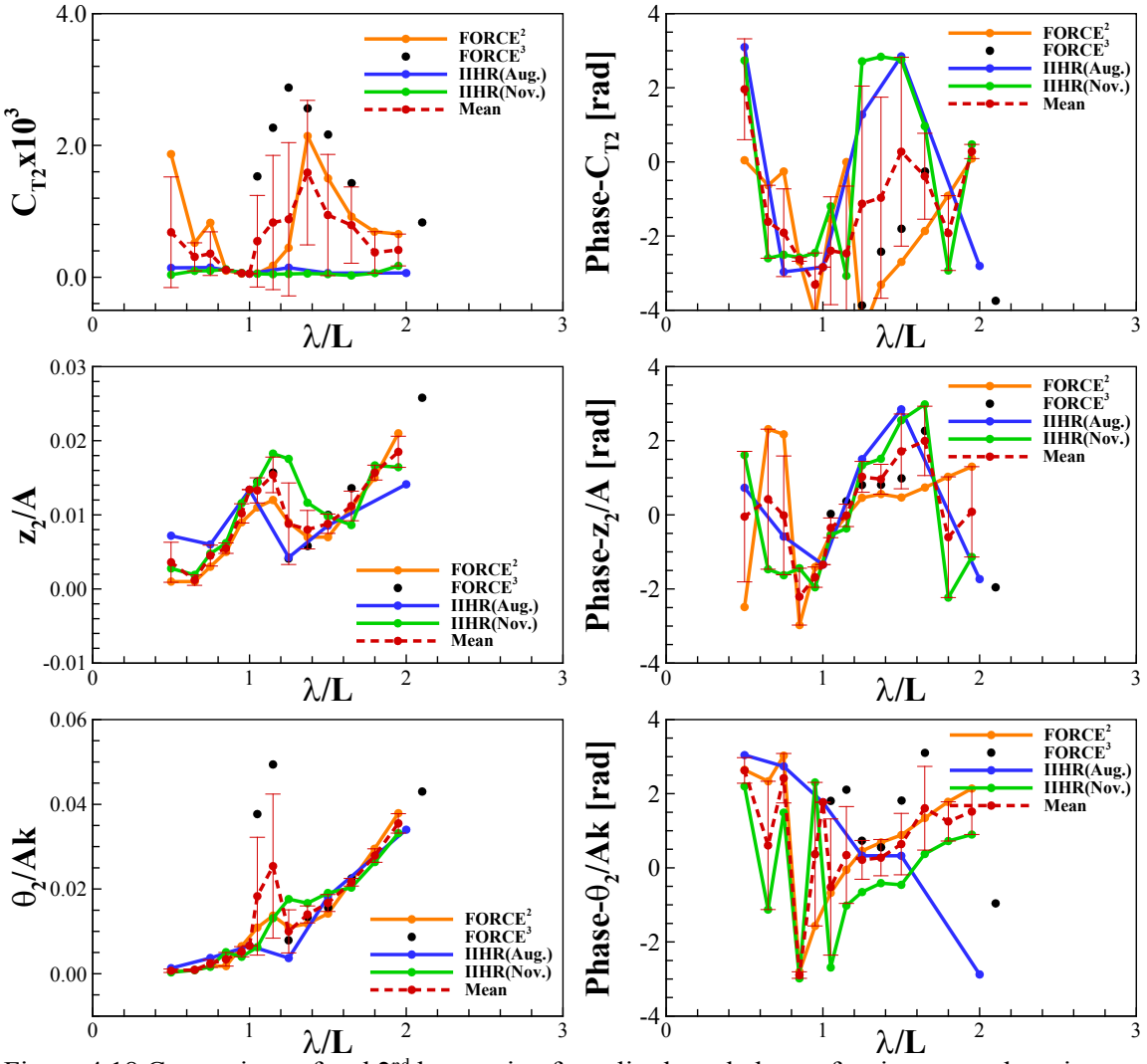

Figure 4.18 Comparison of and 2nd harmonic of amplitude and phase of resistance and motions, at Fr=0.26, for FORCE, IIHR (August and November), and mean and standard deviation of the facilities

www.manaraa.com

Table 4.19 Comparison of 2nd harmonic amplitudes of total resistance coefficient for KCS in head waves at Fr=0.26

Institute	FORCE[2]	FORCE[3]	IIHR (Aug.)	IIHR (Nov.)	All Facilities	
λ/L	C_{T2} x 10^3				Ave ($\overline{D}$)	SD% $\overline{D}$ {SD%DR}
0.50	1.868		0.141	0.037	**0.682**	**123.1**
0.65	0.522			0.096	**0.309**	**69.0**
0.75	0.826		0.147	0.099	**0.358**	**92.9**
0.85	0.100			0.120	**0.110**	**8.8**
0.95	0.055			0.065	**0.060**	**8.5**
1.00			0.054		**0.054**	
1.05	0.059	1.530		0.052	**0.547**	**127.0**
1.15	0.175	2.269		0.046	**0.830**	**122.8**
1.25	0.446	2.877	0.146	0.049	**0.879**	**132.2**
1.37	2.142	2.563		0.055	**1.587**	**69.1**
1.50	1.500	2.165	0.062	0.048	**0.944**	**97.4**
1.65	0.919	1.428		0.026	**0.791**	**73.3**
1.80	0.691			0.063	**0.377**	**83.3**
1.95	0.654			0.173	**0.414**	**58.2**
2.00			0.063		**0.063**	
2.10		0.831			**0.831**	
Ave(Total)	**0.766**	**1.952**	**0.102**	**0.071**	**0.552**	**82.0{59.1*}**

* DR = 0.766

www.manaraa.com

Table 4.20 Comparison of 2nd harmonic amplitudes of heave for KCS in head waves at Fr=0.26

Institute	FORCE[2]	FORCE[3]	IIHR (Aug.)	IIHR (Nov.)	All Facilities	
λ/L	z_2/A				Ave ($\overline{D}$)	SD% $\overline{D}$ {SD%DR}
0.50	0.0008		0.0072	0.003	**0.0036**	**73.6**
0.65	0.0005			0.002	**0.0012**	**57.5**
0.75	0.0027		0.0060	0.005	**0.0045**	**30.5**
0.85	0.0048			0.006	**0.0055**	**12.9**
0.95	0.0089			0.012	**0.0102**	**12.9**
1.00			0.0134		**0.0134**	
1.05	0.0109	0.0145		0.014	**0.0133**	**12.5**
1.15	0.0124	0.0157		0.018	**0.0154**	**15.6**
1.25	0.0091	0.0041	0.0043	0.018	**0.0088**	**62.4**
1.37	0.0066	0.0058		0.012	**0.0080**	**32.5**
1.50	0.0067	0.0100	0.0086	0.010	**0.0088**	**14.8**
1.65	0.0114	0.0136		0.009	**0.0112**	**18.1**
1.80	0.0146			0.017	**0.0157**	**6.5**
1.95	0.0206			0.016	**0.0185**	**11.2**
2.00			0.0141		**0.0141**	
2.10		0.0258			**0.0258**	
Ave(Total)	**0.0085**	**0.0128**	**0.0089**	**0.0108**	**0.0111**	**27.8{25.1*}**

* DR = 0.012

www.manaraa.com

Table 4.21 Comparison of 2nd harmonic amplitudes of pitch for KCS in head waves at Fr=0.26

Institute	FORCE[2]	FORCE[3]	IIHR (Aug.)	IIHR (Nov.)	All Facilities	
λ/L	θ_2/Ak				Ave ($\overline{D}$)	SD% $\overline{D}$ {SD%DR}
0.50	0.0005		0.0013	0.0003	**0.0007**	**57.5**
0.65	0.0009			0.0009	**0.0009**	**2.3**
0.75	0.0018		0.0037	0.0016	**0.0024**	**39.0**
0.85	0.0018			0.0051	**0.0034**	**47.7**
0.95	0.0065			0.0040	**0.0052**	**23.5**
1.00			0.0066		**0.0066**	
1.05	0.0109	0.0377		0.0063	**0.0183**	**75.9**
1.15	0.0137	0.0494		0.0131	**0.0254**	**66.7**
1.25	0.0110	0.0079	0.0037	0.0176	**0.0100**	**50.6**
1.37	0.0118	0.0134		0.0167	**0.0140**	**14.4**
1.50	0.0142	0.0156	0.0182	0.0191	**0.0167**	**11.6**
1.65	0.0219	0.0225		0.0203	**0.0216**	**4.2**
1.80	0.0295			0.0264	**0.0279**	**5.6**
1.95	0.0379			0.0332	**0.0355**	**6.6**
2.00			0.0340		**0.0340**	
2.10		0.0430			**0.0430**	
Ave(Total)	**0.0125**	**0.0244**	**0.0248**	**0.0248**	**0.0166**	**31.2{24.5*}**

* DR = 0.021

www.manaraa.com

Table 4.22 Comparison of 2nd harmonic phases of total resistance coefficient for KCS in head waves at Fr=0.26

Institute	FORCE[2]	FORCE[3]	IIHR (Aug.)	IIHR (Nov.)	All Facilities	
λ/L	Phase- C_{T2} [rad]				Ave ($\overline{D}$)	SD% $\overline{D}$ {SD%DR}
0.50	0.045		3.097	2.737	**1.960**	**69.5**
0.65	-0.631			-2.600	**-1.615**	**60.9**
0.75	-0.257		-2.967	-2.506	**-1.910**	**62.0**
0.85	-2.682			-2.580	**-2.631**	**2.0**
0.95	-4.166			-2.456	**-3.311**	**25.8**
1.00			-2.841		**-2.321**	
1.05	-1.546	-4.444		-1.199	**-2.396**	**60.7**
1.15	-0.005	-4.325		-3.074	**-2.468**	**73.6**
1.25	-4.631	-3.873	1.276	2.713	**-1.129**	**281.4**
1.37	-3.313	-2.424		2.836	**-0.967**	**280.6**
1.50	-2.698	-1.804	2.847	2.755	**0.275**	**926.3**
1.65	-1.865	-0.259		0.966	**-0.386**	**300.2**
1.80	-0.914			-2.931	**-1.922**	**52.5**
1.95	0.089			0.473	**0.281**	**68.3**
2.00			-2.808		**-2.808**	
2.10		-0.259			**-0.259**	
Ave(Total)	**-1.736**	**-2.484**	**-0.232**	**-0.374**	**-1.383**	**174.1{91.4*}**

* DR = 2.635

www.manaraa.com

Table 4.23 Comparison of 2nd phases of heave for KCS in head waves at Fr=0.26

Institute	FORCE[2]	FORCE[3]	IIHR (Aug.)	IIHR (Nov.)	All Facilities	
λ/L	Phase- z_2/A [rad]				Ave ($\overline{D}$)	SD% $\overline{D}$ {SD%DR}
0.50	-2.487		0.730	1.613	**-0.048**	**3678.3**
0.65	2.313			-1.468	**0.422**	**447.6**
0.75	2.172		-0.586	-1.628	**-0.014**	**11608.2**
0.85	-2.975			-1.440	**-2.208**	**34.8**
0.95	-1.408			-1.954	**-1.681**	**16.2**
1.00			-1.342		**-1.342**	
1.05	-0.530	0.026		-0.547	**-0.350**	**76.0**
1.15	-0.043	0.367		-0.367	**-0.014**	**2133.0**
1.25	0.461	0.806	1.504	1.338	**1.027**	**40.5**
1.37	0.562	0.811		1.513	**0.962**	**41.9**
1.50	0.469	0.985	2.848	2.553	**1.714**	**58.9**
1.65	0.739	2.268		2.980	**1.996**	**46.8**
1.800	1.028			-2.231	**-0.601**	**270.9**
1.95	1.301			-1.136	**0.082**	**1477.7**
2.00			-1.732		**-1.732**	
2.10		2.268			**2.268**	
Ave(Total)	**0.123**	**1.076**	**0.496**	**-0.060**	**0.030**	**1533.1{20.6*}**

* DR = 2.238

www.manaraa.com

Table 4.24 Comparison of 2nd harmonic phases of pitch for KCS in head waves at Fr=0.26

Institute	FORCE[2]	FORCE[3]	IIHR (Aug.)	IIHR (Nov.)	All Facilities	
λ/L	Phase θ_2/Ak [rad]				Ave ($\overline{D}$)	SD% $\overline{D}$ {SD%DR}
0.50	2.642		3.042	2.201	**2.628**	**13.1**
0.65	2.334			-1.126	**0.604**	**286.3**
0.75	3.026		2.738	1.490	**2.418**	**27.6**
0.85	-2.804			-2.983	**-2.894**	**3.1**
0.95	-1.568			2.304	**0.368**	**526.6**
1.00			1.770		**1.770**	
1.05	-0.676	1.806		-2.688	**-0.519**	**353.9**
1.15	-0.053	2.108		-1.019	**0.345**	**378.7**
1.25	0.455	0.732	0.327	-0.655	**0.215**	**243.4**
1.37	0.684	0.553		-0.414	**0.274**	**178.6**
1.50	0.884	1.816	0.324	-0.460	**0.641**	**129.4**
1.65	1.347	3.102		0.375	**1.608**	**70.2**
1.80	1.780			0.723	**1.251**	**42.2**
1.95	2.139			0.897	**1.518**	**40.9**
2.00			-2.878		**-2.878**	
2.10		-0.959			**-0.959**	
Ave(Total)	**0.784**	**1.308**	**0.887**	**-0.104**	**0.399**	**176.5{25.5*}**

* DR = 2.760

www.manaraa.com

4.3 Oblique Waves

4.3.1 Individual Wave Encounter Angles

Added Resistance and 4 DOF motion tests were completed for head, quartering, beam, and following wave conditions with Fr = 0.2601, H/λ = 1/60, and wave numbers, λ/L, from 0.25 to 2.00. Time history results of wave height at forward perpendicular, stationary wave height, measured X-force, hydrodynamic X-force, measured surge, modified surge, heave, roll, and pitch were obtained. The time histories for the waves, X-force, and motions are shown in Appendix C, Figures C.16 through C.42.

Repeatability analysis was completed for $\chi = 45°$ tests. Figure 4.19 shows the mean, individual test, and standard deviation of the 0^{th} harmonic amplitudes of total resistance coefficient, added resistance, and 4 degrees of freedom motions with a wave encounter angle of 45°. For the $\chi = 45°$ tests, the 0^{th} harmonic amplitudes show acceptable scatter. The largest deviations occur at the smallest and largest wavelengths. Figure 4.20 shows the mean, individual test, and standard deviation of the 1^{st} harmonic amplitudes and phases of wave amplitude, total resistance coefficient, and 4 degrees of freedom motions with a wave encounter angle of 45°. Figure 4.21 shows the mean, individual test, and standard deviation of the 2^{nd} harmonic amplitudes and phases of total resistance coefficient and 4 degrees of freedom motions with a wave encounter angle of 45°. The 1^{st} and 2^{nd} harmonic amplitudes and phases for tests at $\chi = 45°$ show very good agreement for waves, resistance, and motions.

Repeatability analysis was completed for $\chi = 90°$ tests. Similar Figures to Figures 4.19 through 4.21 are shown for the wave encounter angle 90°, Figures 4.22 through 4.24. The 0^{th} harmonic amplitudes show very little scatter for wavelengths larger than $\lambda/L = 0.50$, but the smaller wavelengths show large scatter. The 1^{st} harmonic amplitudes and phases for resistances and motions show a generally good agreement between repeated tests. The 2^{nd} harmonic amplitudes and phases show good agreement throughout, except for the small wavelength cases for surge and roll. The wavelengths, $\lambda/L < 0.50$, are small for the L = 2.70 m model. Considering the scale of the 2.70 m model, these wavelength conditions yield wave amplitudes less than 1.8 cm. These small amplitudes make accurate predictions difficult to obtain.

www.manaraa.com

Repeatability analysis was completed for $\chi = 135°$ tests. Like the $\chi = 90°$ data set, the $\chi = 135°$ data set included wavelengths of $\lambda/L < 0.50$. Similar Figures to Figures 4.19 through 4.21 are shown for the wave encounter angle 135°, Figures 4.25 through 4.27. Following the same trends as $\chi = 90°$, the 0^{th} harmonic amplitudes of $\chi = 135°$ results show good repeatability except for the small wavelengths. The 1^{st} harmonic amplitudes and phases show reasonable repeatability, except the surge and heave of $\lambda/L = 0.25$. Likewise, the 2^{nd} harmonic amplitudes and phases show reasonable repeatability, except the surge and heave of $\lambda/L = 0.25$. As with the $\chi = 90°$ tests, the magnitude of the desired wave amplitude in small wavelengths makes accurate predictions difficult to obtain.

Repeatability analysis was completed for $\chi = 180°$ tests. Similar to Figures 4.19 through 4.21 are shown for the wave encounter angle 135°, Figures 4.28 through 4.30. The 0^{th} harmonic amplitudes show a good agreement between repeated tests for all wavelengths. The 1^{st} harmonic amplitudes and phases show very good agreement between repeated tests for all wavelengths. The 2^{nd} harmonic amplitudes show a good agreement between repeated tests for all wavelengths.

In general, acceptable repeatability is shown throughout the test cases. The standard deviation values as percentages of mean results are shown in Tables 3.7 through 3.23. For values with small mean amplitudes or phases the random uncertainty as a percentage of the mean is not a good representation of the actual variance. This is the case for many of the 0^{th} and 2^{nd} harmonic amplitudes of resistance and motions. Figures 4.5 through 4.10 and Figures 4.19 through 4.30, show that the cases with repeated tests show good repeatability.

www.manaraa.com

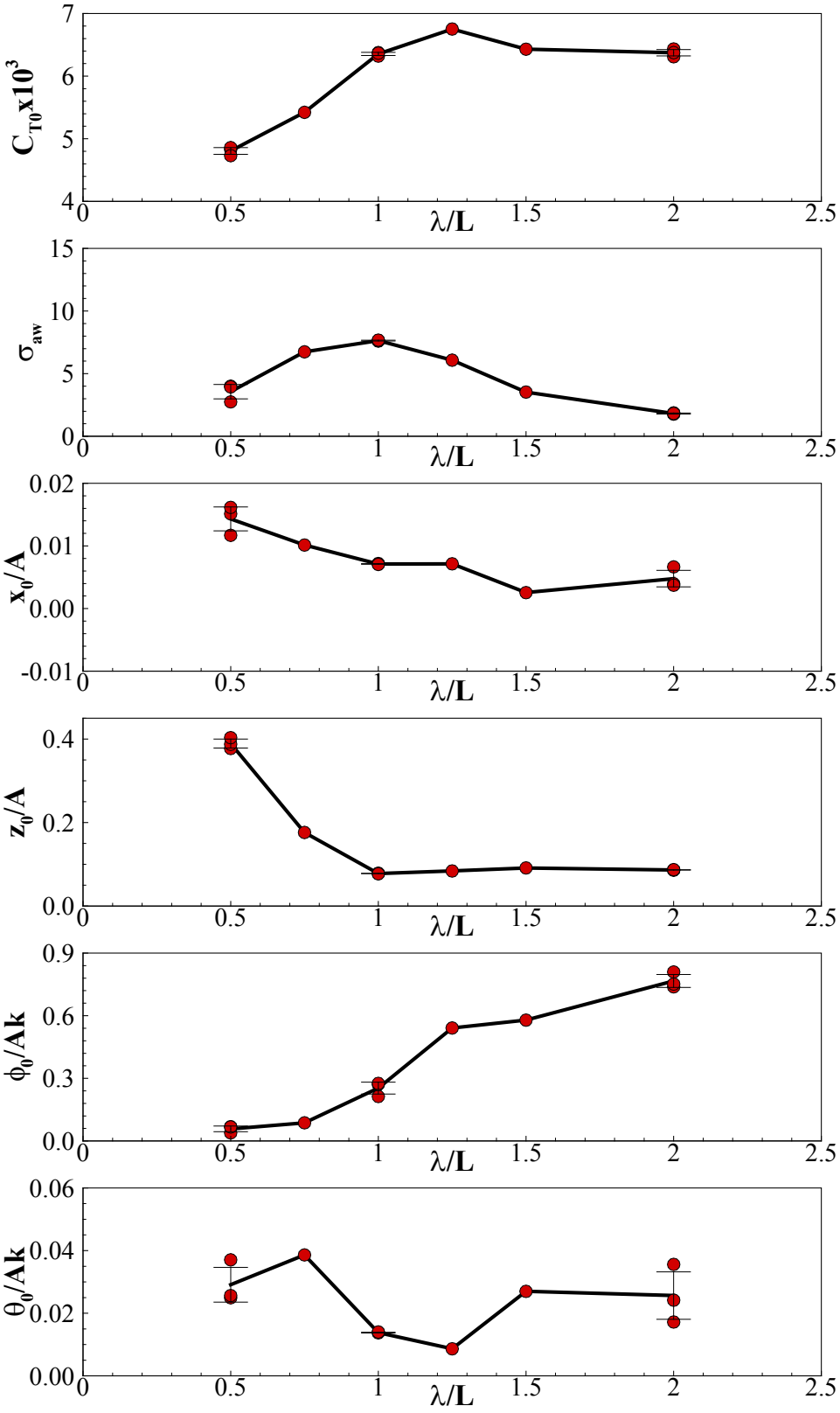

Figure 4.19 Mean, individual results, and standard deviation for 0th harmonic amplitudes of resistance and 4 DOF for $\chi = 45°$ test cases

www.manaraa.com

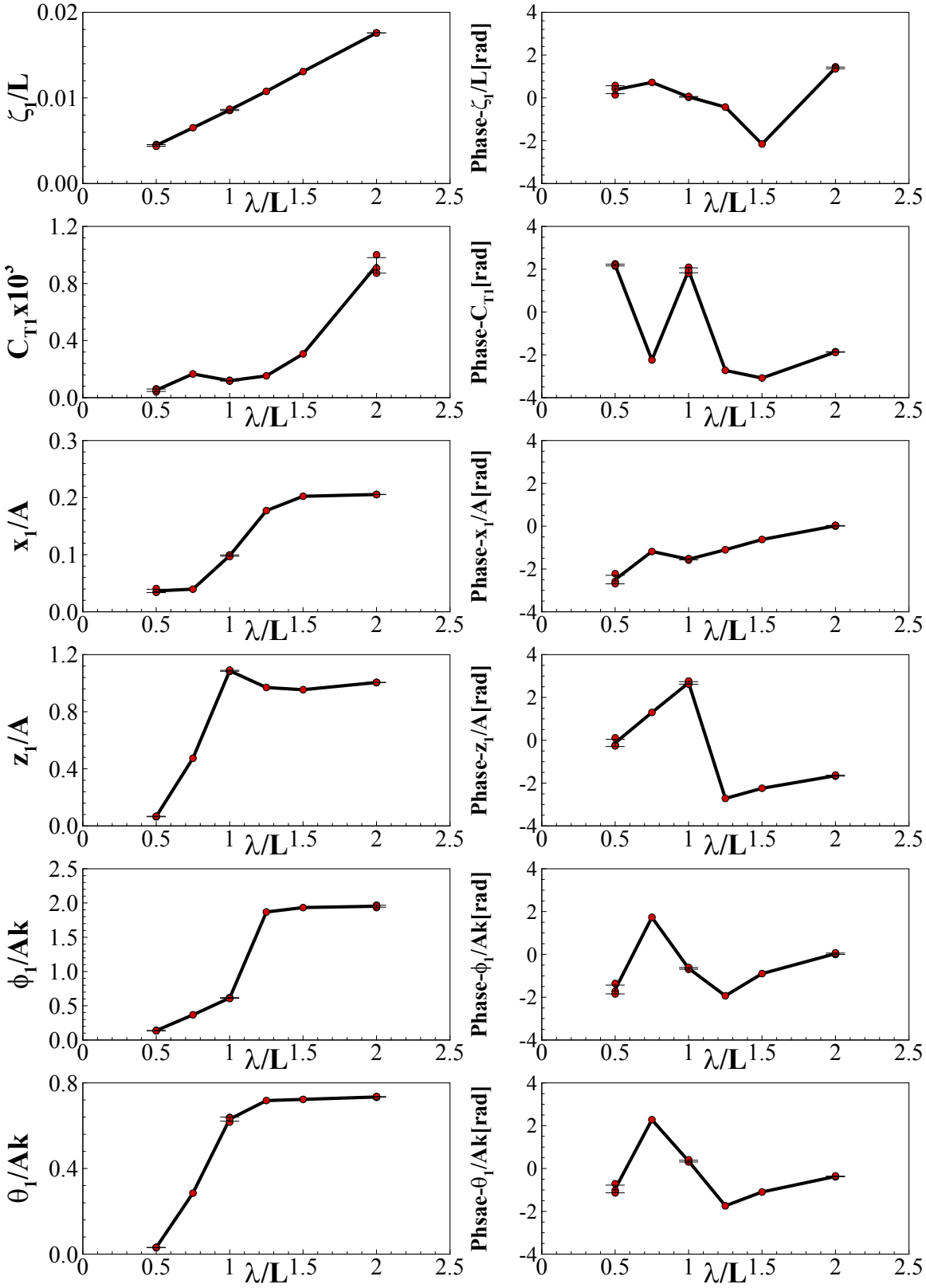

Figure 4.20 Mean, individual results, and standard deviation for 1st harmonic amplitudes and phases of resistance and 4 DOF for $\chi = 45°$ test cases

www.manaraa.com

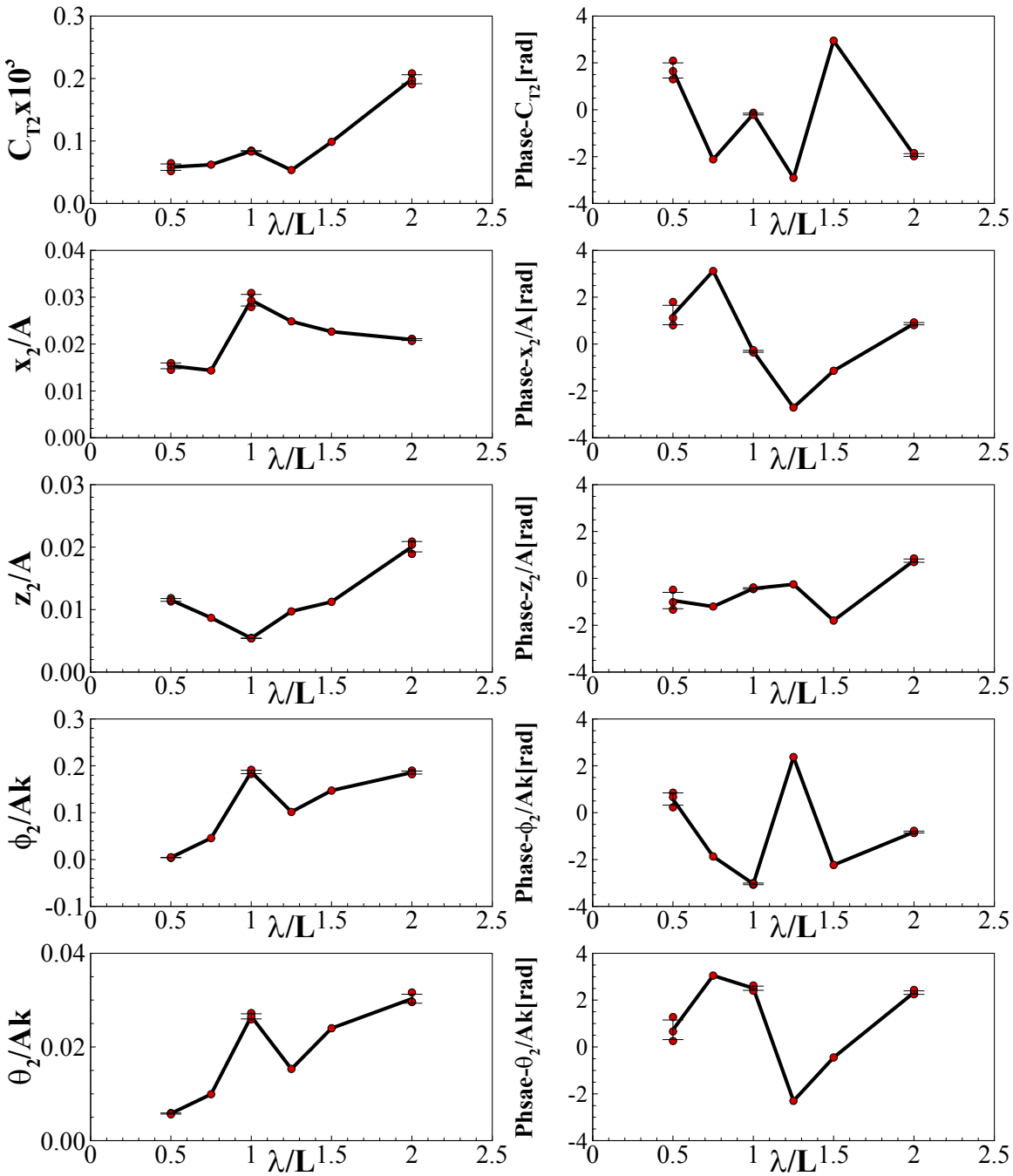

Figure 4.21 Mean, individual results, and standard deviation for 2nd harmonic amplitudes and phases of resistance and 4 DOF for $\chi = 45°$ test cases

www.manaraa.com

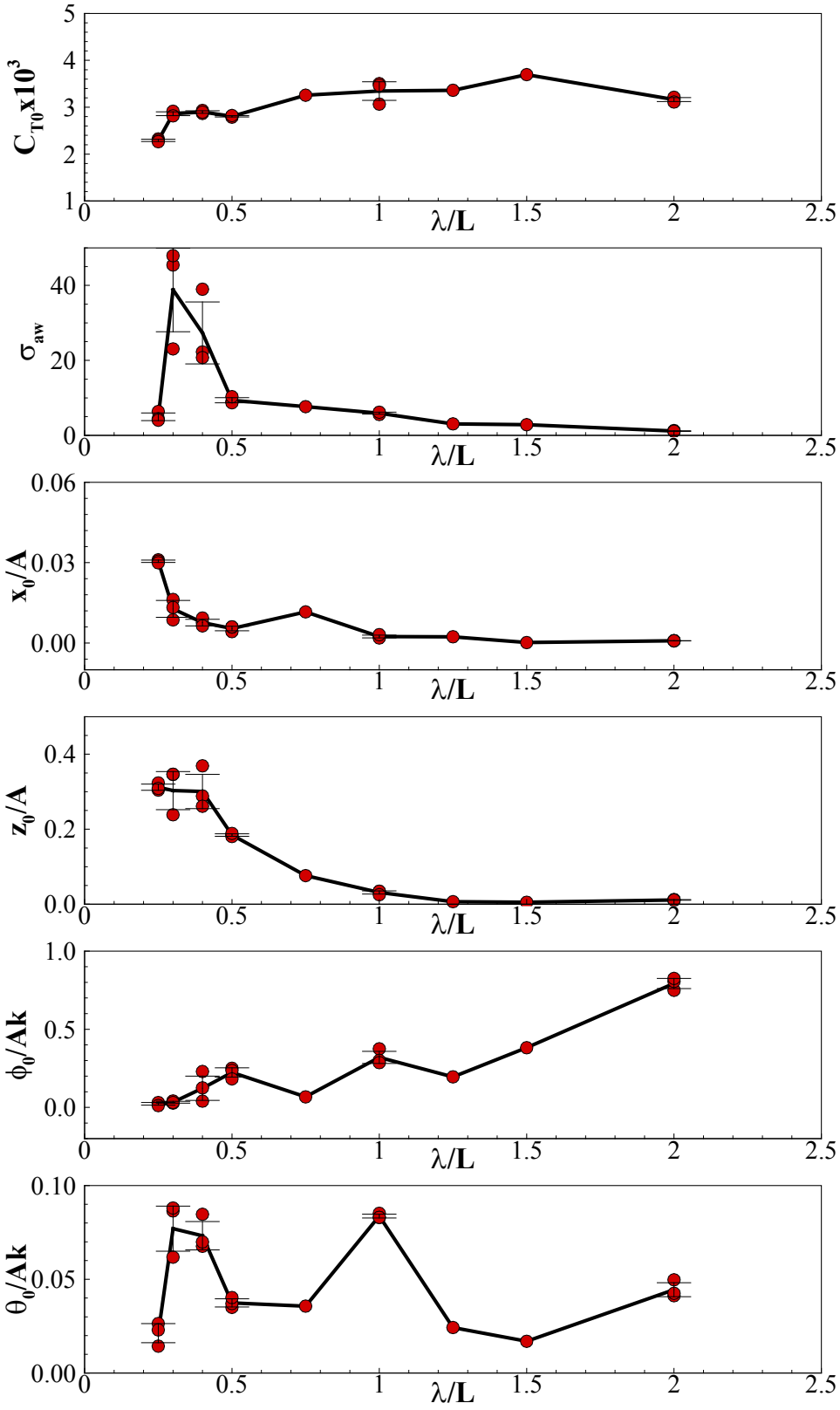

Figure 4.22 Mean, individual results, and standard deviation for 0th harmonic amplitudes of resistance and 4 DOF for $\chi = 90°$ test cases

www.manaraa.com

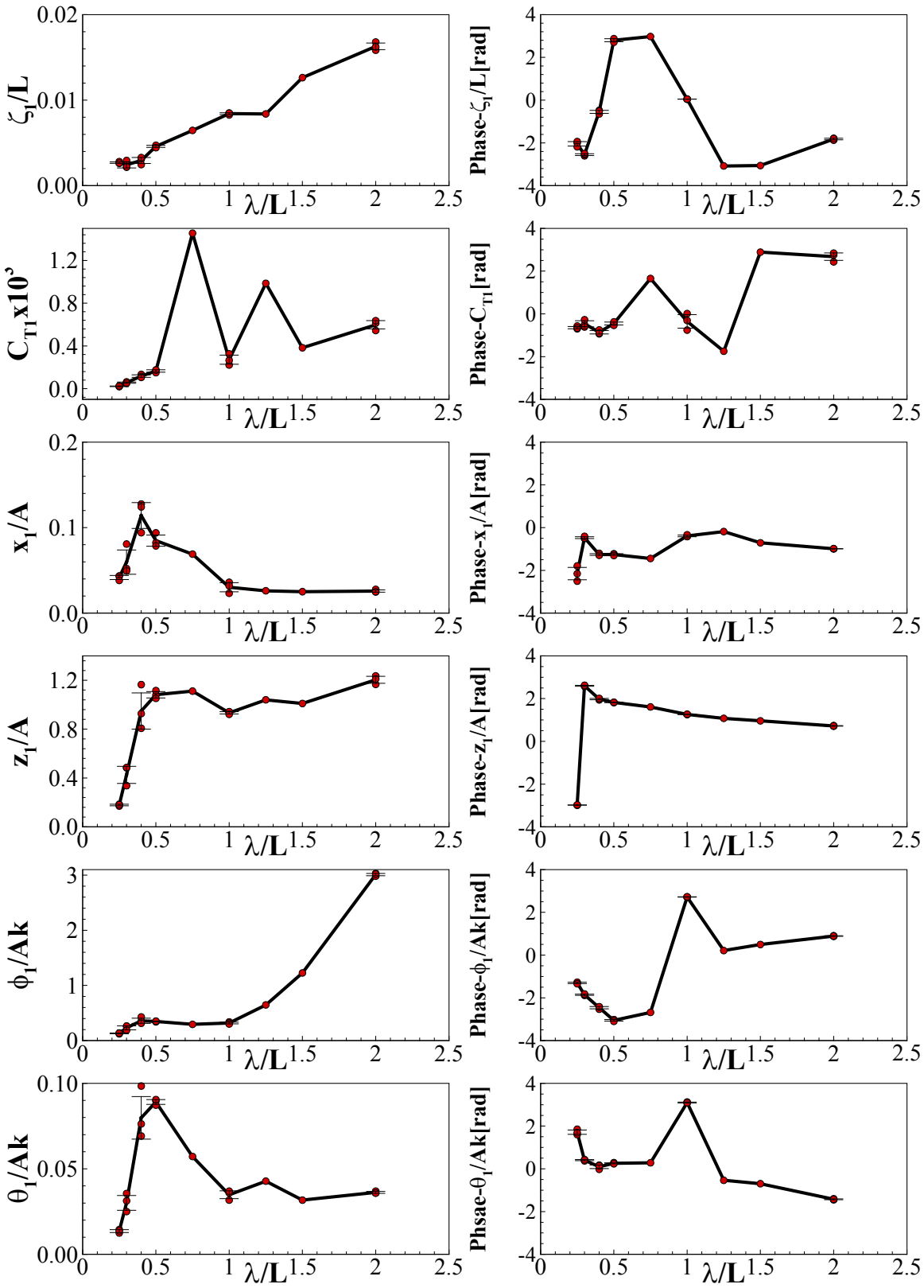

Figure 4.23 Mean, individual results, and standard deviation for 1st harmonic amplitudes and phases of resistance and 4 DOF for $\chi = 90°$ test cases

www.manaraa.com

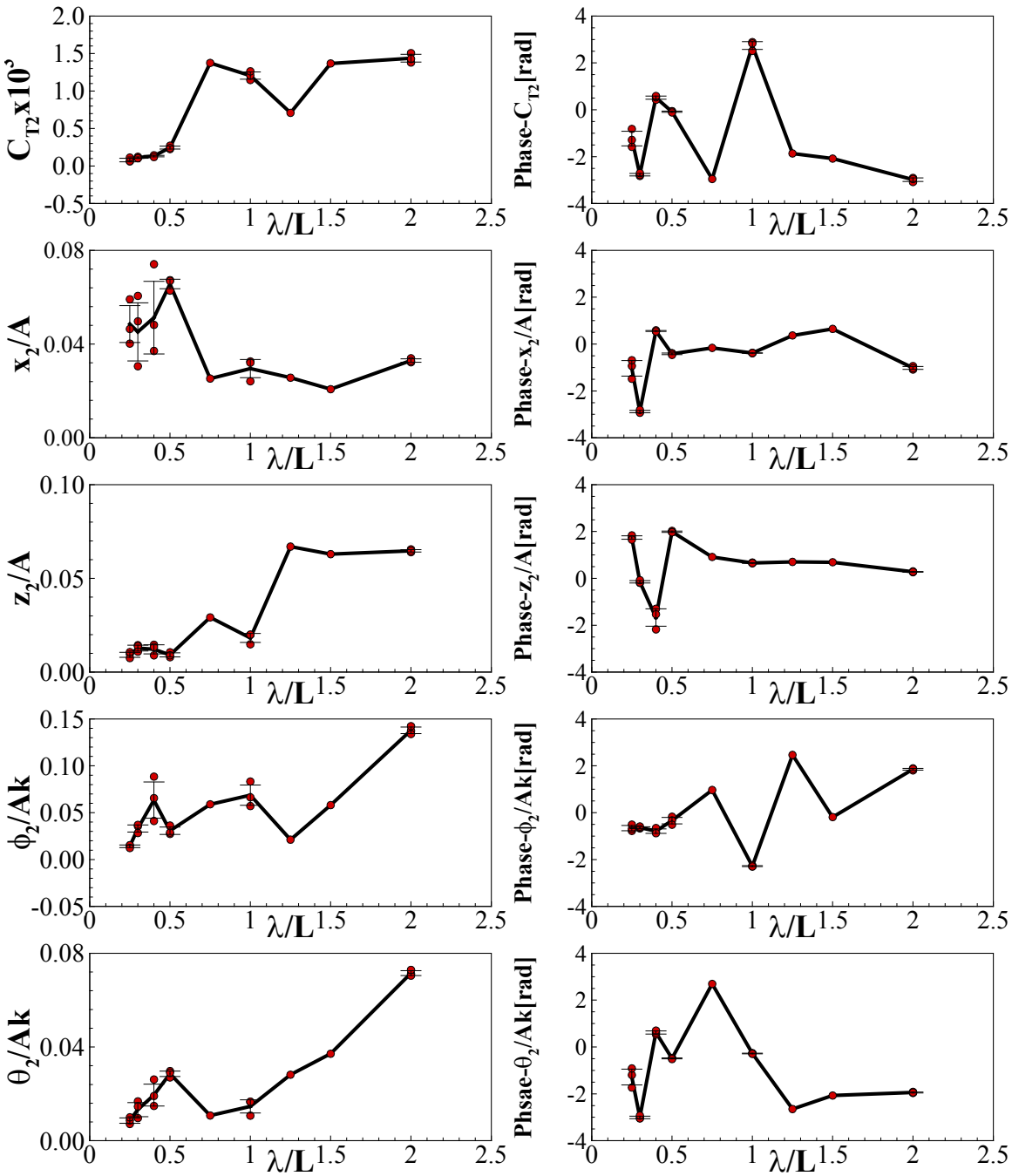

Figure 4.24 Mean, individual results, and standard deviation for 2nd harmonic amplitudes and phases of resistance and 4 DOF for $\chi = 90°$ test cases

www.manaraa.com

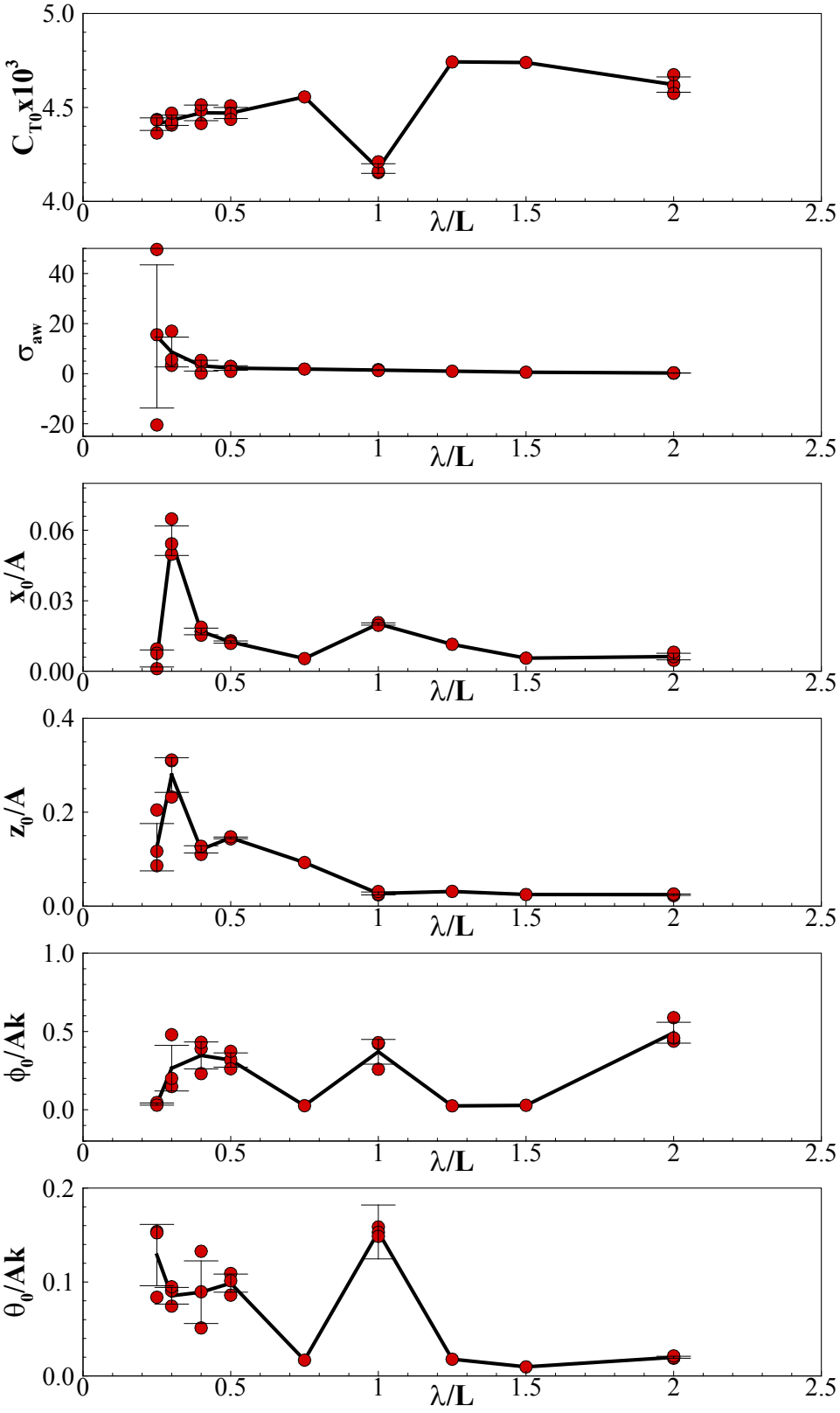

Figure 4.25 Mean, individual results, and standard deviation for 0th harmonic amplitudes of resistances and 4 DOF for $\chi = 135°$ test cases

www.manaraa.com

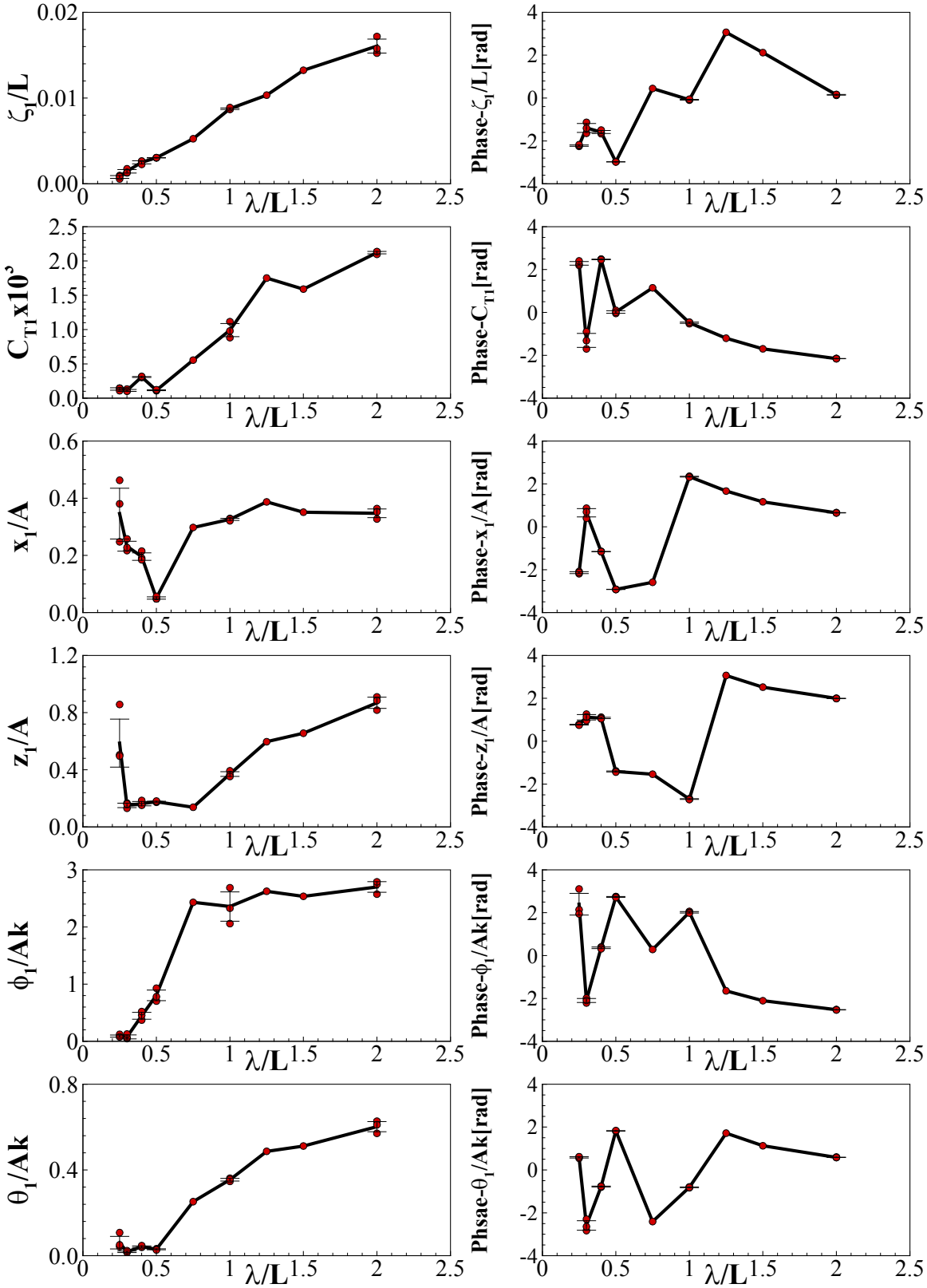

Figure 4.26 Mean, individual results, and standard deviation for 1st harmonic amplitudes and phases of resistance and 4 DOF for $\chi = 135°$ test cases

www.manaraa.com

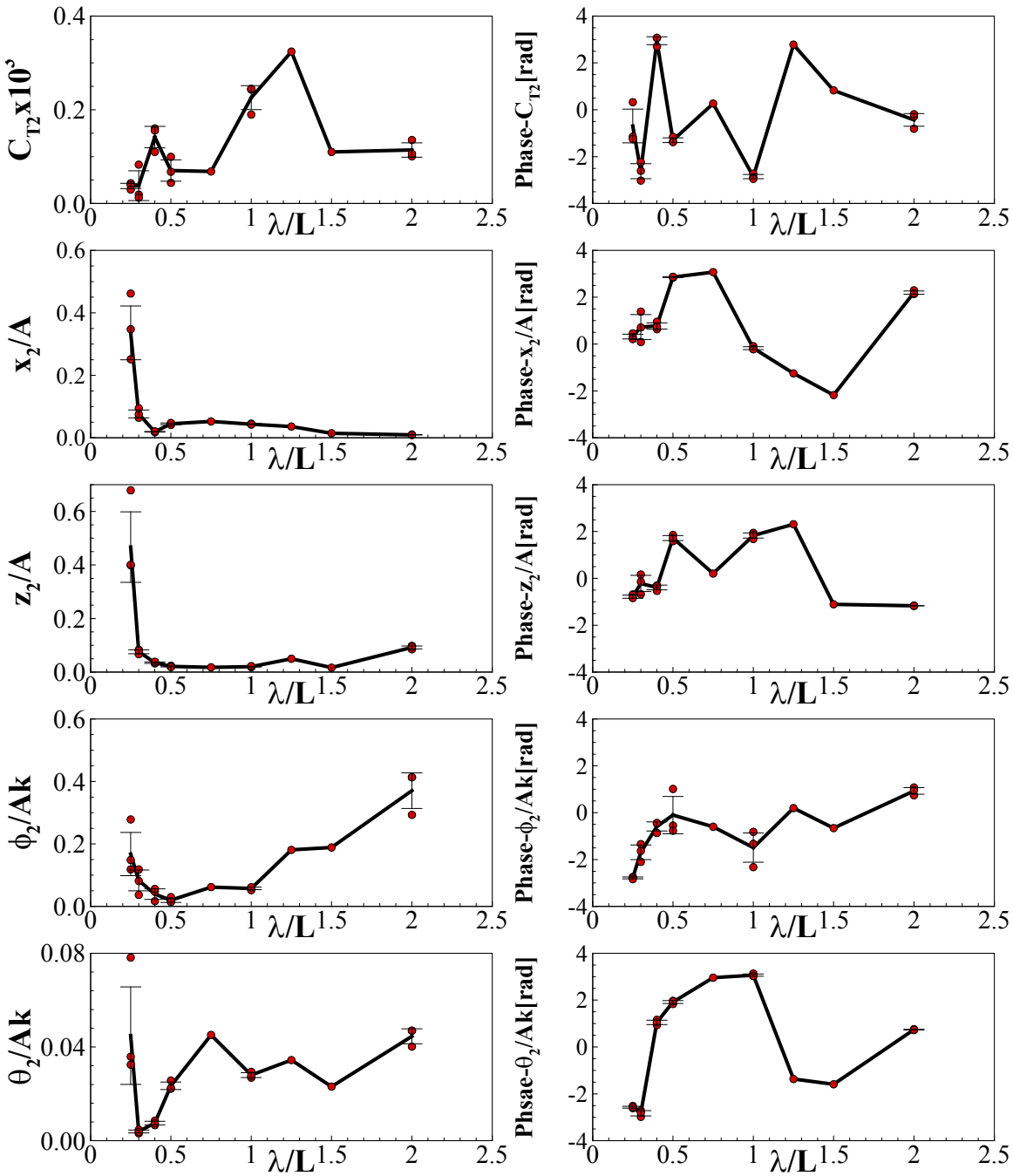

Figure 4.27 Mean, individual results, and standard deviation for 2nd harmonic amplitudes and phases of resistance and 4 DOF for $\chi = 135°$ test cases

www.manaraa.com

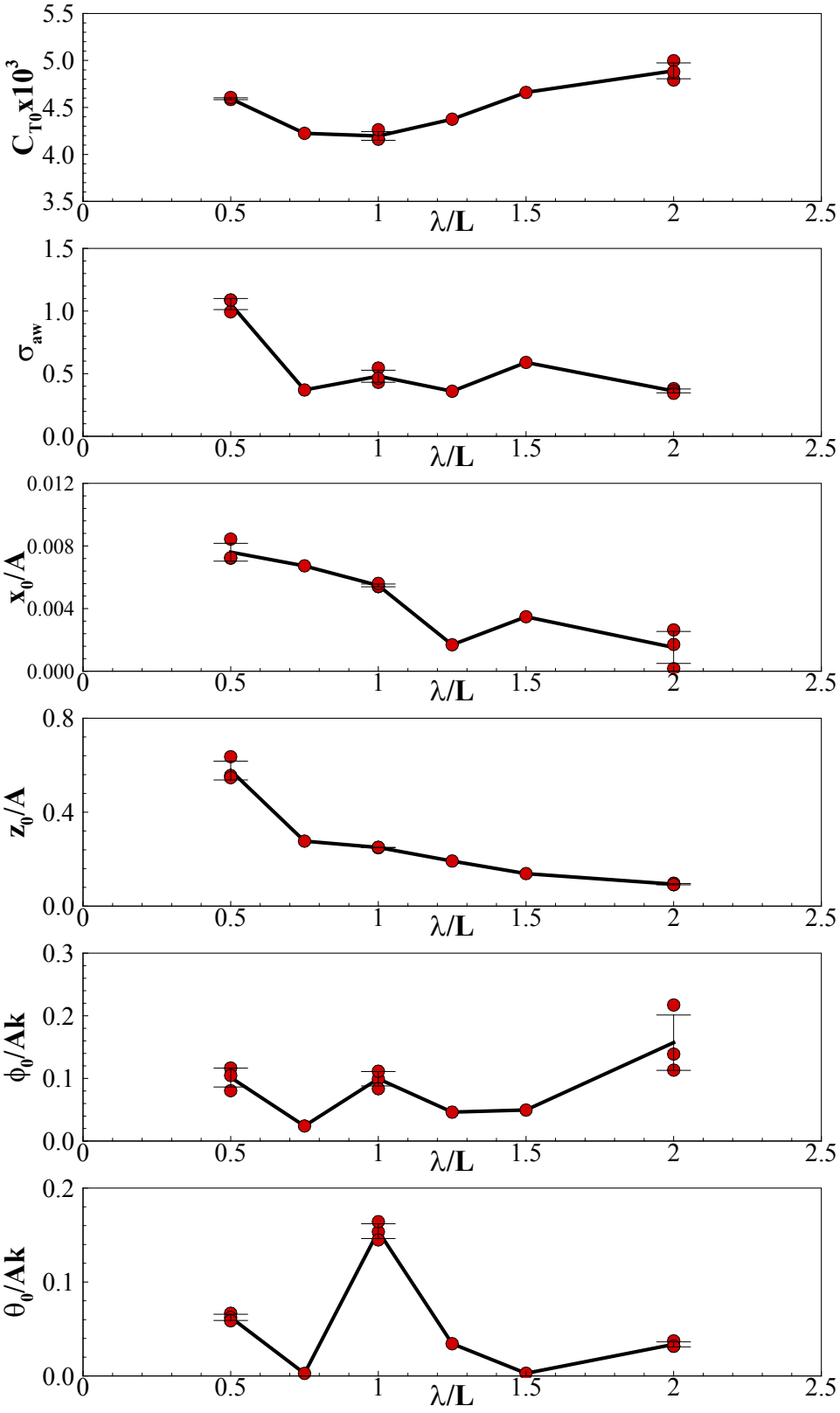

Figure 4.28 Mean, individual results, and standard deviation for 0th harmonic amplitudes of resistance and 4 DOF for $\chi = 180°$ test cases

www.manaraa.com

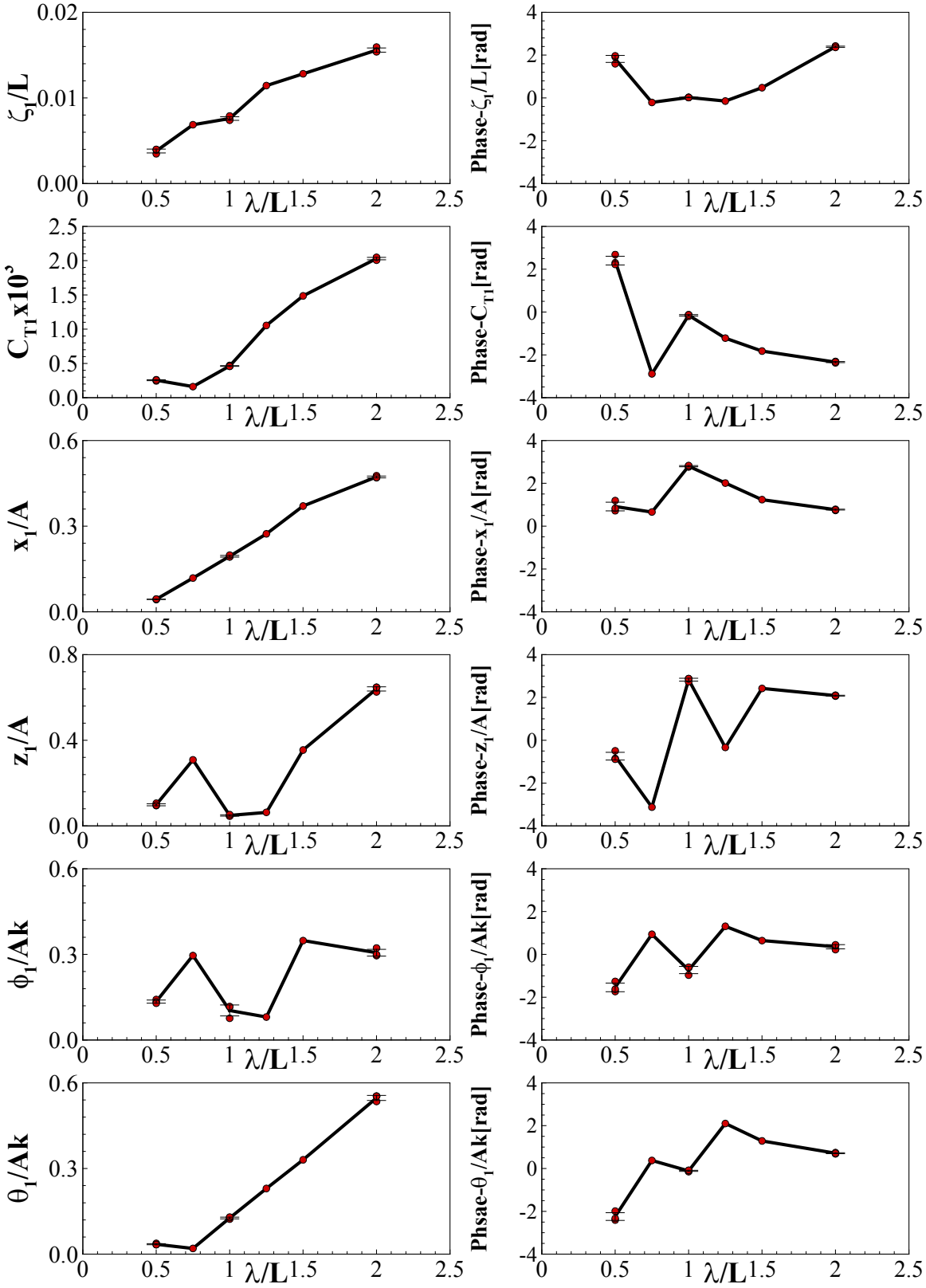

Figure 4.29 Mean, individual results, and standard deviation for 1st harmonic amplitudes and phases of resistance and 4 DOF for $\chi = 180°$ test cases

www.manaraa.com

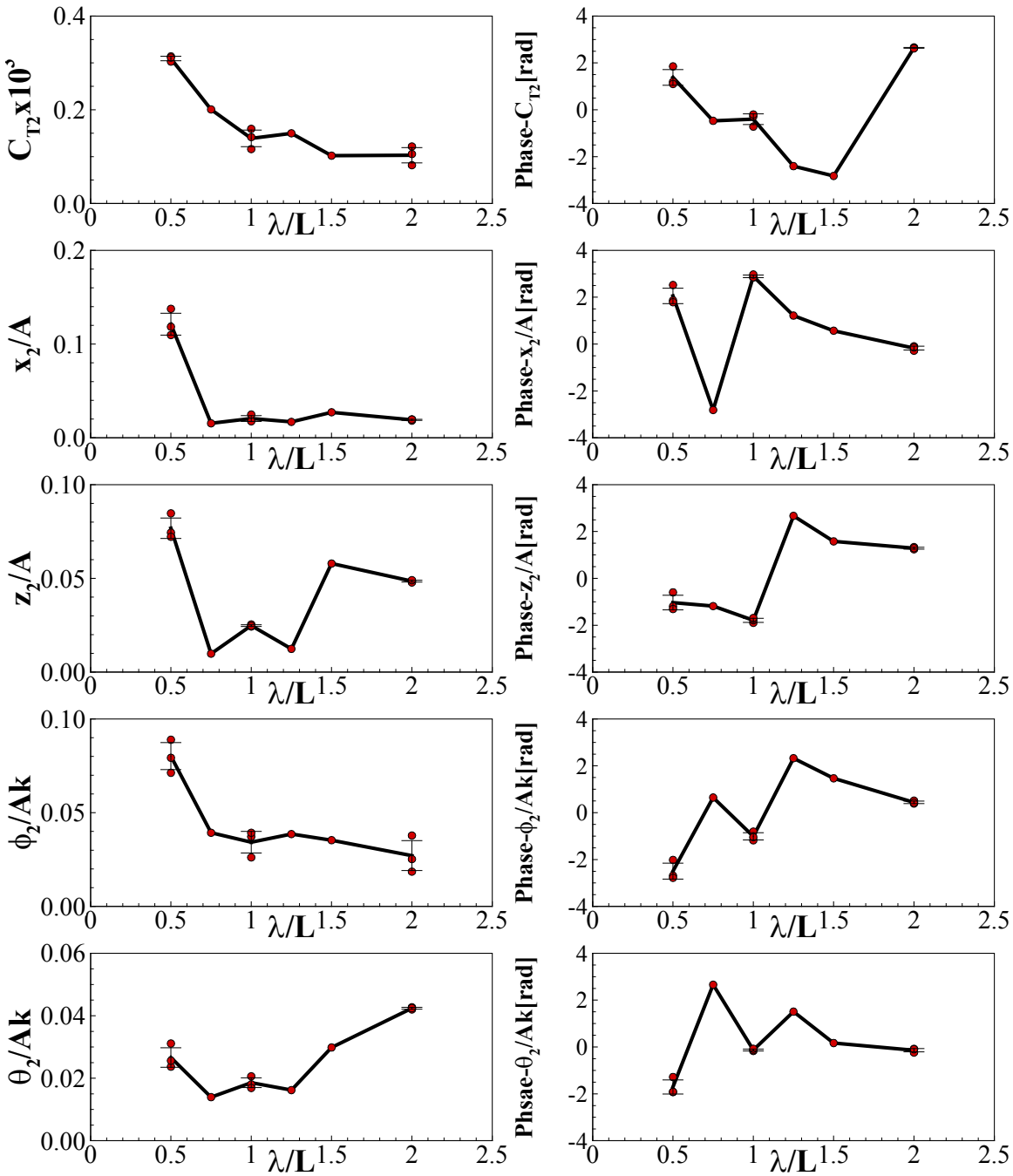

Figure 4.30 Mean, individual results, and standard deviation for 2nd harmonic amplitudes and phases of resistance and 4 DOF for $\chi = 180°$ test cases

www.manaraa.com

4.3.2 Comparison of Wave Encounter Angles

The 0^{th} harmonic frequencies for each wave encounter angle are compared to find trends with varying wave encounter angles. Figure 4.31 shows the 0^{th} harmonic amplitudes of total resistance coefficient, added resistance, surge, heave, roll and pitch for all five wave encounter angles. Figure 4.31 also includes the expanded standard uncertainties shown in Tables 3.7 through 3.12. Table 4.25 shows the 0^{th} harmonic amplitudes of total resistance coefficient, added resistance, surge, heave, roll, and pitch for all five wave encounter angles.

The peak amplitude of the 0^{th} harmonic of total resistance coefficient decreases from head to stern waves. The stern quartering, following, and beam conditions show a 0^{th} harmonic total resistance coefficient near the magnitude of the calm water resistance coefficient for that specific wave encounter angle. The peak added resistance shows a decrease from head to stern waves. The added resistance peak location moves toward the shorter wavelength conditions from head to stern waves since the heave/pitch resonance occurs at a shorter wavelength as in Figure 2.14. The data and uncertainty is cut off for some cases of $\lambda/L < 0.5$. Though the actual force value is small compared to other cases, as made evident by the C_{T0} values, the wave amplitude is very small is squared in the denominator leading to a very large value. The presented data set is cut in order for the trends to be visible for the medium and large wave lengths. The 0^{th} harmonic amplitude of surge shows the largest peak occurring in stern quartering. A decrease in the magnitude with increasing wavelength is shown for every wave heading besides head waves. The presented does not show the entire uncertainty bands in order to show trend, the uncertainty bands appear large due to very small harmonic amplitudes. The 0^{th} harmonic of heave shows a decrease in amplitude with an increase in wavelength. Head and stern waves show the largest 0^{th} harmonic amplitudes. Higher wavelengths of stern quartering and beam waves show a zero or negative 0^{th} harmonic amplitude of heave. The 0^{th} harmonic of roll increases with an increase in wavelength. Quartering has the largest 0^{th} harmonic amplitude of roll for most wavelengths. The 0^{th} harmonic amplitude of pitch has little variability between headings besides head waves. Head wave conditions show a larger 0^{th} harmonic amplitude of pitch than the other headings and have a negative amplitude.

www.manaraa.com

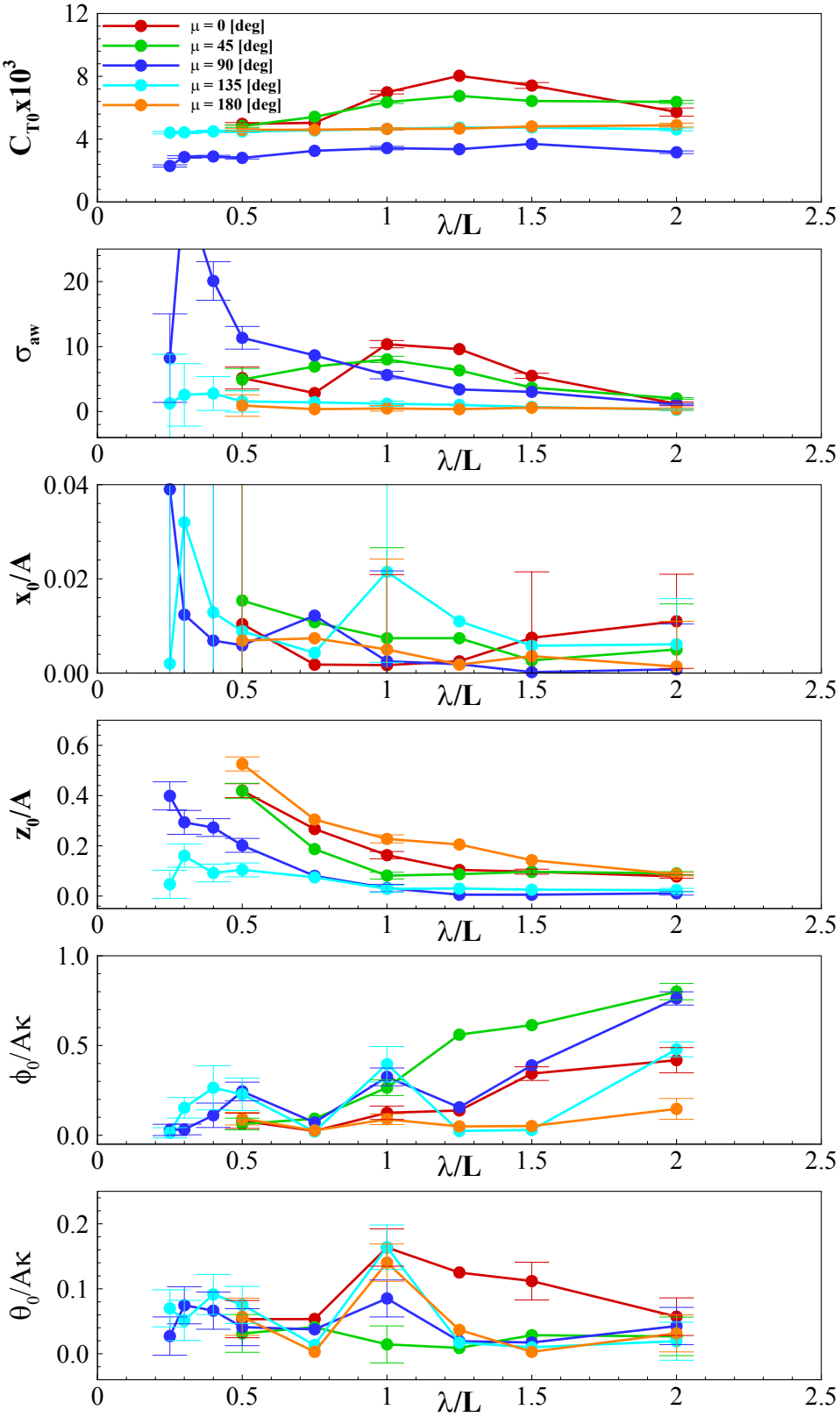

Figure 4.31 0th harmonic amplitudes of total resistance coefficient, added resistance, and 4 DOF for all five wave encounter angle

www.manaraa.com

Table 4.25 0th harmonic amplitudes of resistance and motions for all wave encounter angles

χ [°]	λ/L	$C_{T0}*10^3$	σ_{aw}	x_0/A	z_0/A	ϕ_0/Ak	θ_0/Ak
0	calm	4.66	-	-	-	-	-
	0.50	4.97	5.16	0.010	0.420	0.080	0.053
	0.75	5.04	2.84	0.002	0.267	0.024	0.054
	1.00	6.98	10.36	0.002	0.163	0.125	0.164
	1.25	8.04	9.60	0.003	0.104	0.138	0.125
	1.50	7.41	5.50	0.007	0.097	0.343	0.112
	2.00	5.73	1.18	0.011	0.078	0.418	0.057
45	calm	4.58	-	-	-	-	-
	0.50	4.83	4.92	0.015	0.419	0.062	0.031
	0.75	5.42	6.93	0.011	0.187	0.092	0.041
	1.00	6.35	8.02	0.007	0.082	0.265	0.014
	1.25	6.75	6.33	0.007	0.087	0.560	0.009
	1.50	6.43	3.67	0.003	0.097	0.614	0.029
	2.00	6.37	2.02	0.005	0.090	0.800	0.027
90	calm	2.18	-	-	-	-	-
	0.25	2.29	8.22	0.039	0.399	0.030	0.027
	0.30	2.86	34.28	0.012	0.294	0.032	0.075
	0.40	2.90	20.10	0.007	0.273	0.111	0.066
	0.50	2.81	11.34	0.006	0.202	0.244	0.041
	0.75	3.26	8.65	0.012	0.080	0.071	0.038
	1.00	3.43	5.62	0.002	0.032	0.326	0.085
	1.25	3.36	3.41	0.002	0.005	0.156	0.019
	1.50	3.70	3.03	0.000	0.005	0.390	0.017
	2.00	3.16	1.11	0.001	0.011	0.762	0.043
135	calm	4.39	-	-	-	-	-
	0.25	4.41	1.25	0.002	0.047	0.014	0.070
	0.30	4.43	2.57	0.032	0.161	0.153	0.051
	0.40	4.50	2.78	0.013	0.092	0.264	0.091
	0.50	4.49	1.55	0.009	0.104	0.228	0.075
	0.75	4.56	1.42	0.004	0.074	0.021	0.014
	1.00	4.65	1.20	0.022	0.029	0.396	0.164
	1.25	4.74	1.02	0.011	0.030	0.024	0.017
	1.50	4.74	0.70	0.006	0.025	0.029	0.010
	2.00	4.62	0.27	0.006	0.024	0.479	0.019
180	calm	4.55	-	-	-	-	-
	0.50	4.59	0.92	0.007	0.526	0.092	0.057
	0.75	4.60	0.37	0.007	0.305	0.027	0.003
	1.00	4.65	0.48	0.005	0.228	0.089	0.140
	1.25	4.67	0.36	0.002	0.205	0.049	0.037
	1.50	4.81	0.59	0.004	0.143	0.051	0.003
	2.00	4.89	0.39	0.001	0.087	0.147	0.031

www.manaraa.com

The 1st harmonic frequencies for each wave encounter angle are compared to find trends with varying encounter angles. Figure 4.32 shows the 1st harmonic amplitudes and phases of wave amplitude, total resistance coefficient, surge, heave, roll, and pitch for all five wave encounter angles. Figure 4.32 also includes the expanded total standard uncertainties shown in Tables 3.13 through 3.18. Table 4.26 shows the 1st harmonic amplitudes of wave amplitude, total resistance coefficient, surge, heave, roll, and pitch for all five wave encounter angles as well as the % error of wave amplitude compared to the desired wave amplitude. Table 4.27 shows the 1st harmonic phases of wave amplitude, total resistance coefficient, surge, heave, roll, and pitch for all five wave encounter angles.

The first harmonic wave amplitude shows very little deviation from the linear relationship of λ/L for every wave encounter angle and λ/L. This shows that the magnitude of the waves matched the desired wave amplitude well. Because the surge inertial force is removed from the total force, the 1st harmonic amplitude and phase of the total force coefficient are small compared to the expected magnitude. The 1st harmonic amplitudes of surge show an amplitude increase with increase in wavelength for all wave headings except for beam heading which shows a decrease. The 1st harmonic amplitudes of surge in stern waves show the largest peak of the wave headings. The peak 1st harmonic amplitude of surge for head and stern waves occur at the maximum wavelength tested. The 1st harmonic amplitude peak occurs at a decreasing wavelength from head to beam waves and then increases from beam to stern waves. The 1st harmonic amplitudes of heave increase with an increase in wavelength for every heading. The 1st harmonic amplitudes of heave are smallest in stern waves and increase from stern to beam waves. From beam waves to head waves the 1st harmonic amplitudes of heave slightly decrease. Head and bow quartering have a peak 1st harmonic amplitude of heave near λ/L = 1.25 and 1.00, respectively which are close to the resonance conditions for those headings as shown in Figure 2.14. The peak 1st harmonic amplitude of heave in beam waves occurs at λ/L = 0.50, which was predicted in Figure 2.14. The 1st harmonic amplitudes of roll increase with an increase in wavelength for every heading. The 1st harmonic amplitudes of roll in stern quartering have the largest amplitude for most wavelengths. This increase is due to the wave encounter frequency being close to the parametric rolling frequency of the model, as shown in Figure 2.14. Similarly, the 1st harmonic amplitudes of roll in beam waves increases significantly with

www.manaraa.com

increasing wavelength at longer wavelengths due to the wave encounter frequencies near parametric roll frequency. The 1st harmonic amplitudes of pitch increase with an increase in wavelength for every heading. The 1st harmonic amplitudes of pitch decrease from head to stern waves, excluding the beam waves that have a small magnitude compared to the other headings.

www.manaraa.com

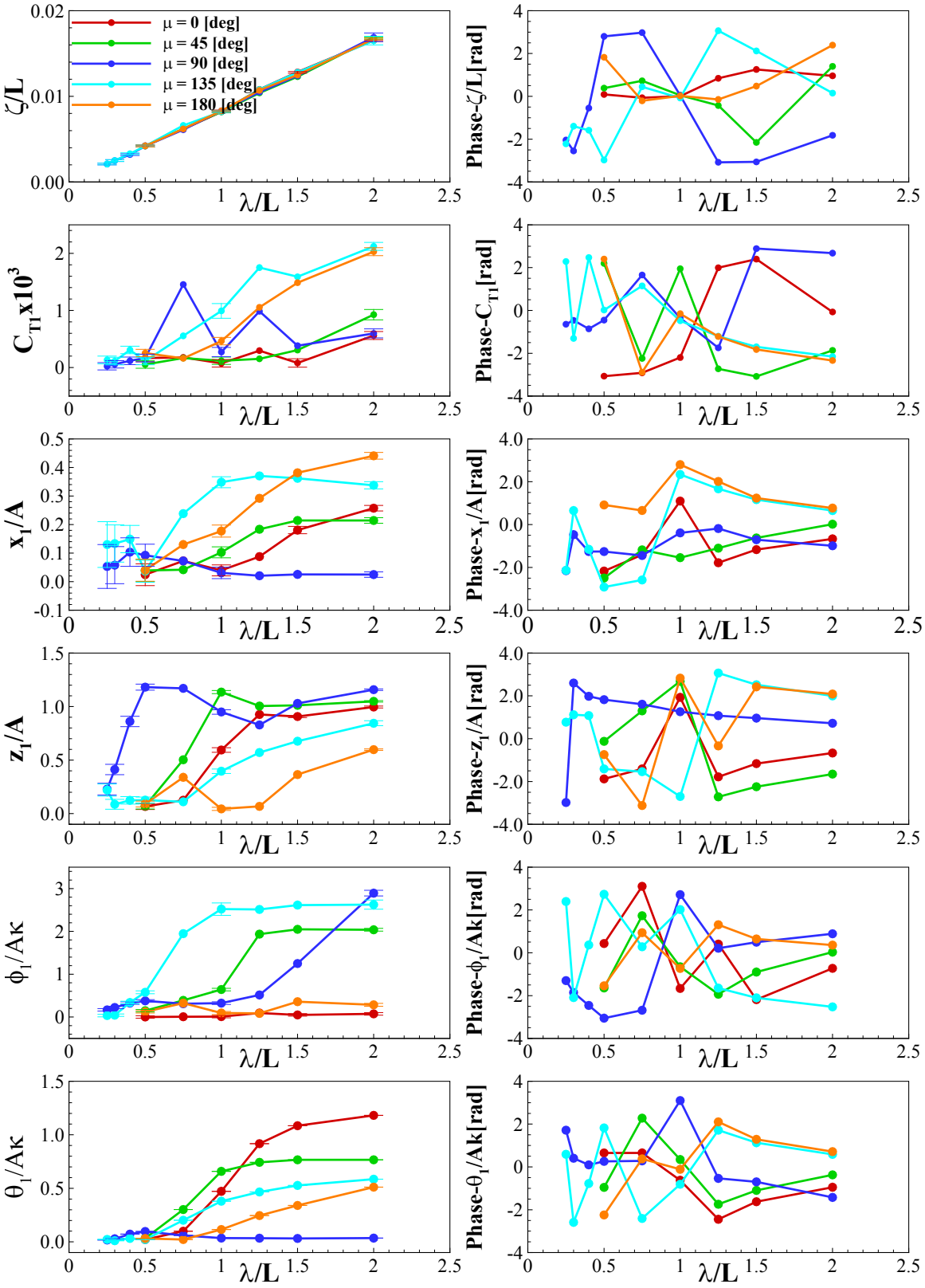

Figure 4.32 1st harmonic amplitudes and phases of wave amplitude, total resistance coefficient, and 4 DOF for all five wave encounter angle

www.manaraa.com

Table 4.26 1st harmonic amplitudes of wave amplitude, resistance, and motions for all wave encounter angles including percent error of ζ_1 compared to desired amplitude

χ [°]	λ/L	ζ_1/L	$E_{\zeta 1}$%A	$C_{T1}*10^3$	x_1/A	z_1/A	ϕ_1/Ak	θ_1/Ak
0	0.50	0.00424	1.67	0.17	0.024	0.067	0.002	0.021
	0.75	0.00618	1.13	0.18	0.073	0.125	0.007	0.100
	1.00	0.00819	1.71	0.07	0.040	0.595	0.009	0.472
	1.25	0.01081	3.78	0.30	0.088	0.926	0.095	0.917
	1.50	0.01284	2.71	0.08	0.181	0.907	0.050	1.085
	2.00	0.01652	0.88	0.56	0.258	0.996	0.074	1.182
45	0.50	0.00415	0.40	0.05	0.039	0.071	0.148	0.034
	0.75	0.00615	1.53	0.17	0.042	0.503	0.390	0.302
	1.00	0.00822	1.30	0.12	0.103	1.136	0.642	0.659
	1.25	0.01040	0.15	0.15	0.184	1.005	1.936	0.743
	1.50	0.01234	1.28	0.31	0.215	1.012	2.049	0.766
	2.00	0.01685	1.09	0.93	0.214	1.049	2.039	0.767
90	0.25	0.00210	0.98	0.02	0.053	0.228	0.167	0.017
	0.30	0.00251	0.44	0.06	0.058	0.412	0.224	0.029
	0.40	0.00324	2.78	0.12	0.104	0.861	0.326	0.072
	0.50	0.00420	0.89	0.17	0.093	1.181	0.378	0.097
	0.75	0.00614	1.78	1.45	0.073	1.170	0.310	0.060
	1.00	0.00828	0.67	0.27	0.031	0.950	0.325	0.035
	1.25	0.01054	1.16	0.99	0.021	0.828	0.515	0.034
	1.50	0.01239	0.89	0.38	0.026	1.030	1.251	0.032
	2.00	0.01694	1.67	0.60	0.025	1.157	2.893	0.035
135	0.25	0.00212	1.78	0.13	0.130	0.220	0.034	0.023
	0.30	0.00254	1.48	0.11	0.134	0.087	0.045	0.011
	0.40	0.00329	1.22	0.31	0.149	0.124	0.340	0.032
	0.50	0.00424	1.67	0.12	0.037	0.127	0.578	0.021
	0.75	0.00655	4.80	0.56	0.238	0.110	1.948	0.202
	1.00	0.00819	1.71	0.99	0.348	0.396	2.520	0.379
	1.25	0.01081	3.78	1.75	0.370	0.571	2.512	0.466
	1.50	0.01284	2.71	1.59	0.362	0.676	2.615	0.527
	2.00	0.01652	0.88	2.12	0.337	0.845	2.625	0.585
180	0.50	0.00417	0.12	0.25	0.040	0.090	0.123	0.032
	0.75	0.00624	0.12	0.16	0.130	0.339	0.326	0.022
	1.00	0.00834	0.10	0.46	0.177	0.045	0.094	0.116
	1.25	0.01070	2.74	1.05	0.292	0.068	0.086	0.246
	1.50	0.01245	0.40	1.49	0.382	0.365	0.359	0.340
	2.00	0.01670	0.22	2.03	0.441	0.597	0.286	0.511

www.manaraa.com

Table 4.27 1st harmonic phases of wave amplitude, resistance, and motions for all wave encounter angles

χ [°]	λ/L	ζ_1/L	$C_{T1}*10^3$	x_1/A	z_1/A	ϕ_1/Ak	θ_1/Ak
0	0.50	0.09	-3.07	-2.17	-1.88	0.43	0.65
	0.75	-0.07	-2.91	-1.41	-1.41	3.10	0.66
	1.00	0.01	-2.20	1.10	1.93	-1.66	-0.62
	1.25	0.84	2.00	-1.78	-1.78	0.41	-2.44
	1.50	1.26	2.40	-1.17	-1.17	-2.19	-1.63
	2.00	0.96	-0.07	-0.67	-0.67	-0.72	-0.95
45	0.50	0.39	2.20	-2.50	-0.12	-1.64	-0.96
	0.75	0.73	-2.24	-1.18	1.30	1.73	2.28
	1.00	0.05	1.95	-1.54	2.68	-0.65	0.35
	1.25	-0.43	-2.73	-1.10	-2.72	-1.93	-1.74
	1.50	-2.15	-3.08	-0.62	-2.24	-0.90	-1.10
	2.00	1.40	-1.86	0.02	-1.65	0.03	-0.37
90	0.25	-2.04	-0.64	-2.15	-2.98	-1.30	1.72
	0.30	-2.55	-0.46	-0.47	2.60	-1.86	0.41
	0.40	-0.55	-0.86	-1.26	1.98	-2.46	0.10
	0.50	2.80	-0.45	-1.26	1.82	-3.05	0.26
	0.75	2.98	1.66	-1.44	1.61	-2.68	0.28
	1.00	0.05	-0.35	-0.39	1.26	2.72	3.10
	1.25	-3.08	-1.75	-0.18	1.08	0.21	-0.54
	1.50	-3.06	2.89	-0.71	0.96	0.49	-0.70
	2.00	-1.82	2.68	-0.99	0.72	0.89	-1.43
135	0.25	-2.22	2.29	-2.14	0.77	2.40	0.59
	0.30	-1.39	-1.31	0.66	1.12	-2.09	-2.59
	0.40	-1.58	2.47	-1.16	1.08	0.36	-0.77
	0.50	-2.97	0.02	-2.92	-1.41	2.73	1.82
	0.75	0.45	1.15	-2.59	-1.54	0.28	-2.41
	1.00	-0.08	-0.48	2.34	-2.70	2.02	-0.81
	1.25	3.07	-1.20	1.67	3.07	-1.65	1.72
	1.50	2.12	-1.70	1.17	2.52	-2.11	1.13
	2.00	0.15	-2.15	0.65	1.99	-2.53	0.59
180	0.50	1.82	2.40	0.92	-0.74	-1.54	-2.24
	0.75	-0.21	-2.89	0.66	-3.12	0.94	0.38
	1.00	0.02	-0.15	2.80	2.83	-0.73	-0.11
	1.25	-0.15	-1.22	2.01	-0.34	1.31	2.10
	1.50	0.48	-1.82	1.24	2.42	0.65	1.29
	2.00	2.39	-2.34	0.77	2.08	0.36	0.71

www.manaraa.com

The 2nd harmonic frequencies for each wave encounter angle are compared to find trends with varying encounter angles. Figure 4.33 shows the 2nd harmonic amplitudes of total resistance coefficient, surge, heave, roll, and pitch for all five wave encounter angles. Figure 4.33 also includes the expanded total standard uncertainties shown in Tables 3.19 through 3.23. Table 4.28 shows the 2nd harmonic amplitudes of total resistance coefficient, surge, heave, roll, and pitch for all five wave encounter angles. Table 4.29 shows the 2nd harmonic phases of total resistance coefficient, surge, heave, roll, and pitch for all five wave encounter angles. The 2nd harmonic amplitude and phase for the resistance coefficients are shown they are less significant because the large fluctuations from the inertial forces were removed when calculating the hydrodynamic force.

The 2nd harmonic amplitude and phase of the total resistance coefficient are a smaller magnitude than expected in a typical resistance test because of the the inertial force was removed from the total resistance. The 2nd harmonic amplitudes of surge increase with increasing wave encounter angle, except following cases where the amplitudes are at intermediate values. The 2nd harmonic amplitudes of heave increase with an increase in wavelength from head to beam waves and then begin to decrease from beam to following waves. The 2nd harmonic amplitudes of roll increase with an increase in wavelength for each heading. Head and bow quartering have the largest 2nd harmonic amplitudes of roll. The 2nd harmonic amplitudes of pitch increase with an increase in wavelength for each heading. The largest 2nd harmonic amplitudes of pitch occur in beam waves.

www.manaraa.com

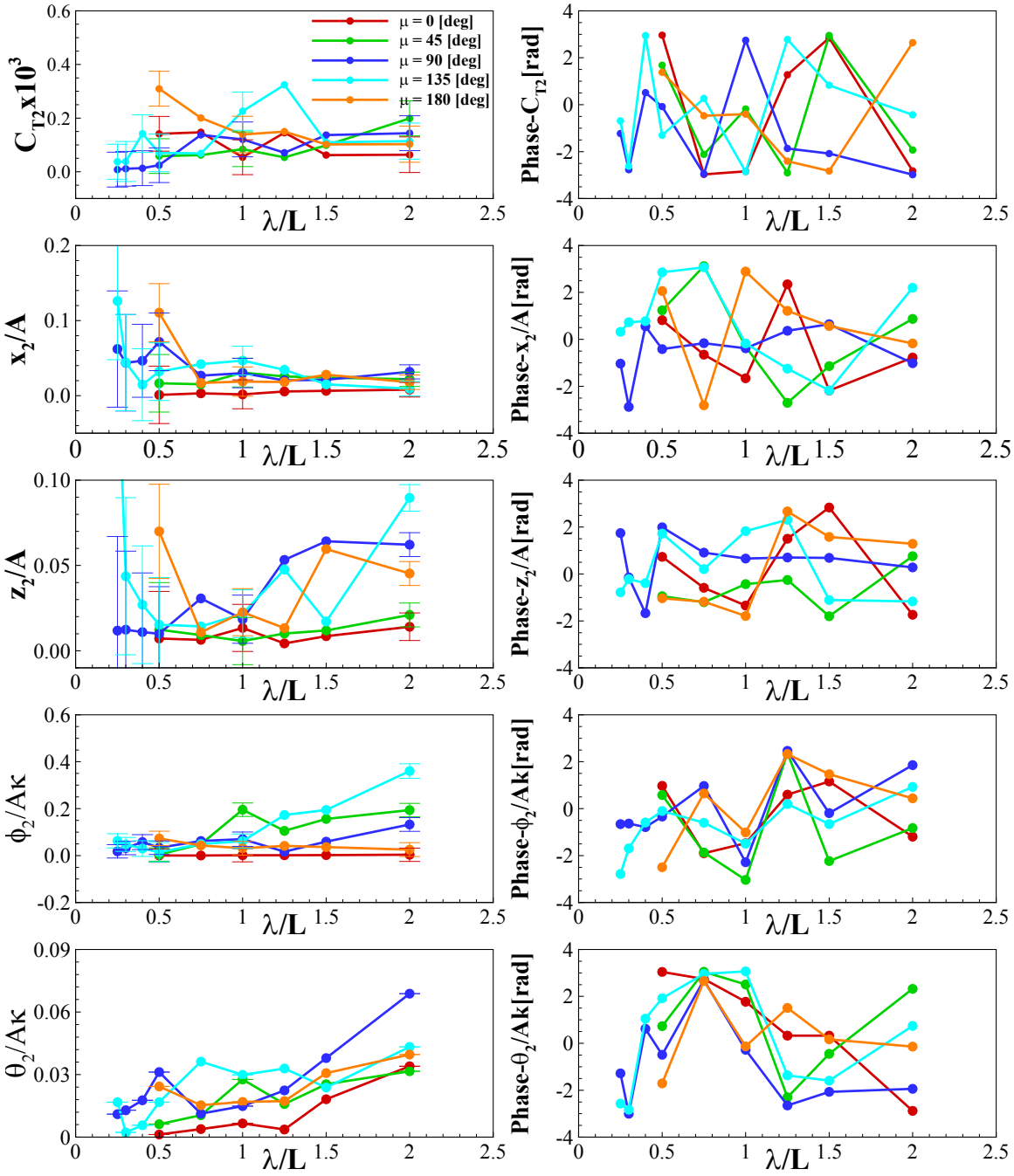

Figure 4.33 2nd harmonic amplitudes and phases of total resistance coefficient, and 4 DOF for all five wave encounter angle

www.manaraa.com

Table 4.28 2nd harmonic amplitudes of resistance, and motions for all wave encounter angles

χ [°]	λ/L	$C_{T2}*10^3$	x_2/A	z_2/A	ϕ_2/Ak	θ_2/Ak
0	0.50	0.141	0.001	0.007	0.000	0.001
	0.75	0.147	0.003	0.006	0.000	0.004
	1.00	0.054	0.002	0.013	0.002	0.007
	1.25	0.146	0.006	0.004	0.002	0.004
	1.50	0.062	0.006	0.009	0.002	0.018
	2.00	0.063	0.008	0.014	0.003	0.034
45	0.50	0.058	0.017	0.012	0.005	0.006
	0.75	0.062	0.015	0.009	0.049	0.011
	1.00	0.084	0.031	0.006	0.195	0.028
	1.25	0.054	0.026	0.010	0.105	0.016
	1.50	0.099	0.024	0.012	0.156	0.025
	2.00	0.199	0.022	0.021	0.194	0.032
90	0.25	0.008	0.062	0.012	0.018	0.011
	0.30	0.011	0.044	0.012	0.032	0.013
	0.40	0.013	0.047	0.011	0.058	0.018
	0.50	0.025	0.072	0.010	0.034	0.031
	0.75	0.137	0.027	0.031	0.062	0.011
	1.00	0.121	0.030	0.019	0.070	0.015
	1.25	0.071	0.020	0.053	0.017	0.022
	1.50	0.137	0.021	0.064	0.059	0.038
	2.00	0.144	0.032	0.062	0.133	0.069
135	0.25	0.037	0.126	0.175	0.063	0.017
	0.30	0.038	0.044	0.044	0.048	0.002
	0.40	0.142	0.015	0.027	0.030	0.006
	0.50	0.070	0.032	0.015	0.014	0.017
	0.75	0.068	0.042	0.014	0.049	0.036
	1.00	0.226	0.047	0.022	0.062	0.030
	1.25	0.324	0.034	0.048	0.173	0.033
	1.50	0.110	0.015	0.017	0.195	0.024
	2.00	0.114	0.009	0.090	0.360	0.043
180	0.50	0.309	0.111	0.070	0.073	0.024
	0.75	0.201	0.017	0.011	0.043	0.015
	1.00	0.139	0.019	0.023	0.031	0.017
	1.25	0.150	0.018	0.013	0.041	0.017
	1.50	0.102	0.028	0.060	0.036	0.031
	2.00	0.103	0.018	0.045	0.025	0.040

www.manaraa.com

Table 4.29 2nd harmonic phases of resistance, and motions for all wave encounter angles

χ [°]	λ/L	$C_{T2}*10^3$	x_2/A	z_2/A	ϕ_2/Ak	θ_2/Ak
0	0.50	2.96	0.82	0.73	0.97	3.04
	0.75	-2.97	-0.65	-0.59	-1.90	2.74
	1.00	-2.84	-1.66	-1.34	-1.47	1.77
	1.25	1.28	2.35	1.50	0.60	0.33
	1.50	2.85	-2.18	2.84	1.16	0.32
	2.00	-2.82	-0.77	-1.74	-1.19	-2.88
45	0.50	1.68	1.24	-0.95	0.58	0.73
	0.75	-2.12	3.12	-1.20	-1.87	3.05
	1.00	-0.18	-0.31	-0.43	-3.04	2.51
	1.25	-2.90	-2.71	-0.25	2.38	-2.30
	1.50	2.95	-1.14	-1.80	-2.23	-0.45
	2.00	-1.93	0.87	0.76	-0.83	2.32
90	0.25	-1.23	-1.03	1.74	-0.66	-1.28
	0.30	-2.77	-2.88	-0.15	-0.64	-3.00
	0.40	0.52	0.56	-1.67	-0.79	0.62
	0.50	-0.08	-0.42	1.99	-0.34	-0.49
	0.75	-2.96	-0.16	0.91	0.97	2.69
	1.00	2.74	-0.38	0.66	-2.28	-0.28
	1.25	-1.86	0.37	0.70	2.46	-2.65
	1.50	-2.08	0.65	0.69	-0.19	-2.07
	2.00	-2.98	-1.02	0.28	1.85	-1.94
135	0.25	-0.69	0.32	-0.78	-2.78	-2.57
	0.30	-2.62	0.73	-0.22	-1.69	-2.83
	0.40	2.95	0.77	-0.39	-0.59	1.05
	0.50	-1.30	2.86	1.72	-0.10	1.92
	0.75	0.27	3.07	0.21	-0.60	2.96
	1.00	-2.85	-0.17	1.83	-1.49	3.07
	1.25	2.78	-1.25	2.31	0.20	-1.37
	1.50	0.83	-2.18	-1.11	-0.66	-1.59
	2.00	-0.43	2.20	-1.17	0.93	0.74
180	0.50	1.38	2.06	-1.03	-2.49	-1.71
	0.75	-0.47	-2.81	-1.18	0.65	2.66
	1.00	-0.40	2.89	-1.79	-1.01	-0.13
	1.25	-2.41	1.22	2.67	2.33	1.51
	1.50	-2.82	0.57	1.58	1.47	0.17
	2.00	2.64	-0.17	1.29	0.44	-0.14

www.manaraa.com

4.3.3 Oblique Wave Facility Comparison

There are very few facilities with the capability to do oblique wave added resistance tests. This requires a wave basin with the capability of towing a ship model in multiple directions or the capability of generating multidirectional waves. (Fujii & Takahashi 1975) completed regular oblique wave added resistance testing for a container ship model in Fr = 0.15 and Fr = 0.25.

Figure 4.34 shows the added resistance results for all angles and all λ/L, 0.5 to 2.00, for the KCS at IIHR, Fr = 0.26, and (Fujii & Takahashi 1975) Fr = 0.15 and Fr = 0.25. The three data sets show very similar results for head wave conditions. There is an expected magnitude decrease between the higher velocity data sets and the data set Fr = 0.15. All three have similar amplitude peaks and agree in trend overall, with the similar velocities showing the most similar trend. Figure 4.35 (a) shows the comparison of the three data sets in head wave conditions. The head wave results agree between IIHR and (Fujii & Takahashi 1975). For wave encounter angles 0° to 90°, a similar trend is shown for all data sets. The peak value when going from wave encounter angle 0° to 90° decreases in the magnitude and the λ/L where it is located. As predicted from the resonance chart, the 90° wave encounter angle should show a peak magnitude at λ/L less than 0.5. All 3 data sets show this trend with a decreasing magnitude for all λ/L greater than 0.5. Figure 4.35 (b) shows the beam wave added resistances for all three data sets. The trends agree for all 3. The results from (Fujii & Takahashi 1975) show magnitude agreement, but the IIHR data has a much larger magnitude. There is an added resistance magnitude discrepancy because the sway motion is fixed at IIHR as opposed to a soft spring sway motion on the (Fujii & Takahashi 1975) mount. The wave encounter angles added resistance results from 90° to 180° show similar trends between all three data sets. With increasing wave encounter angle, the peak magnitude decreases significantly and moves toward smaller wave lengths. The results also show a decrease in added resistance as the wave lengths increase for these wave encounter angles. All three data sets show a very small magnitude of added resistance for χ = 180°, with decreasing magnitudes as λ/L increases. Figure 4.35 (a) shows good agreement between IIHR and (Fujii & Takahashi 1975) for following wave cases. Overall, the trends agree when comparing the results of this study to the container ship model studied in (Fujii & Takahashi 1975).

www.manaraa.com

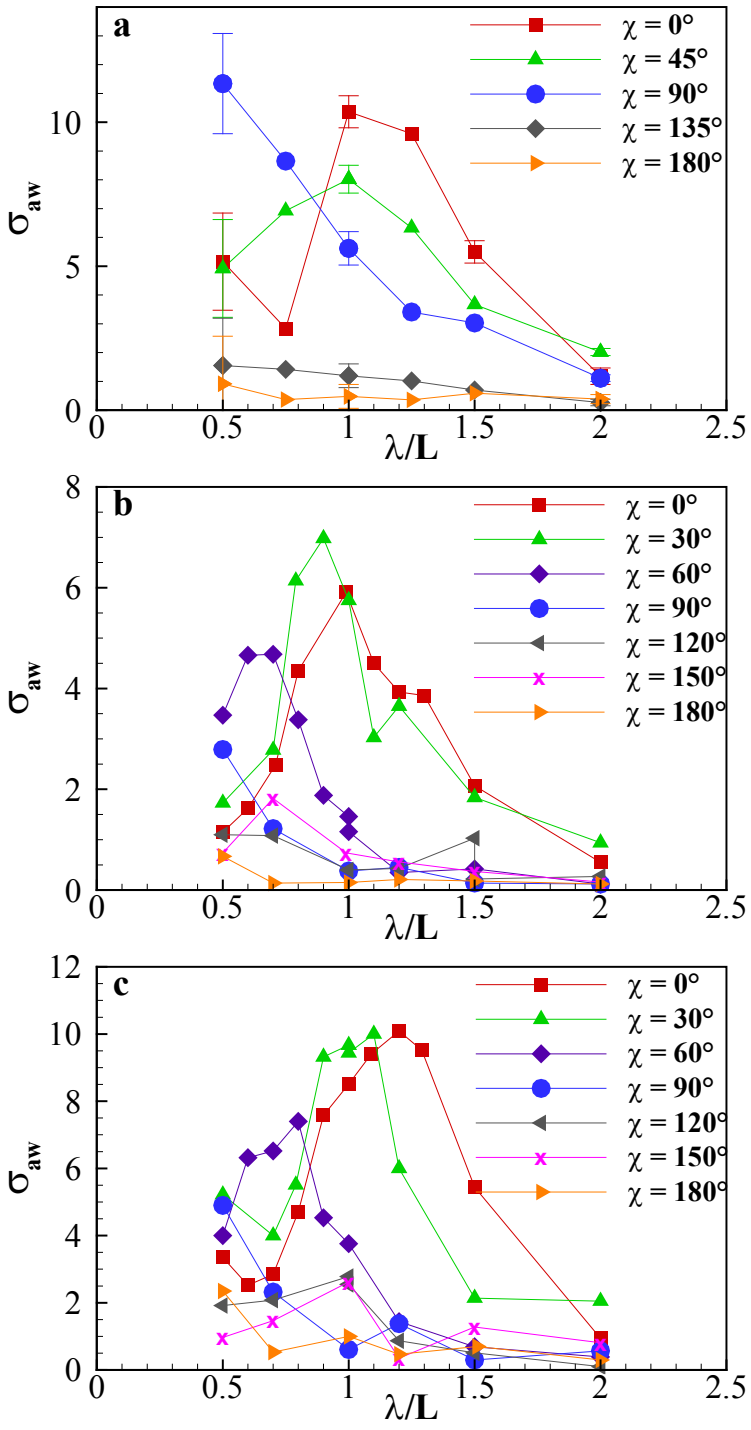

Figure 4.34 Added Resistance results for all wave encounter angles for the KCS model at IIHR, Fr=0.26 (a) and Container ship model, Fr=0.15 (b) and Fr=0.25 (c) (Fujii & Takahashi 1975)

www.manaraa.com

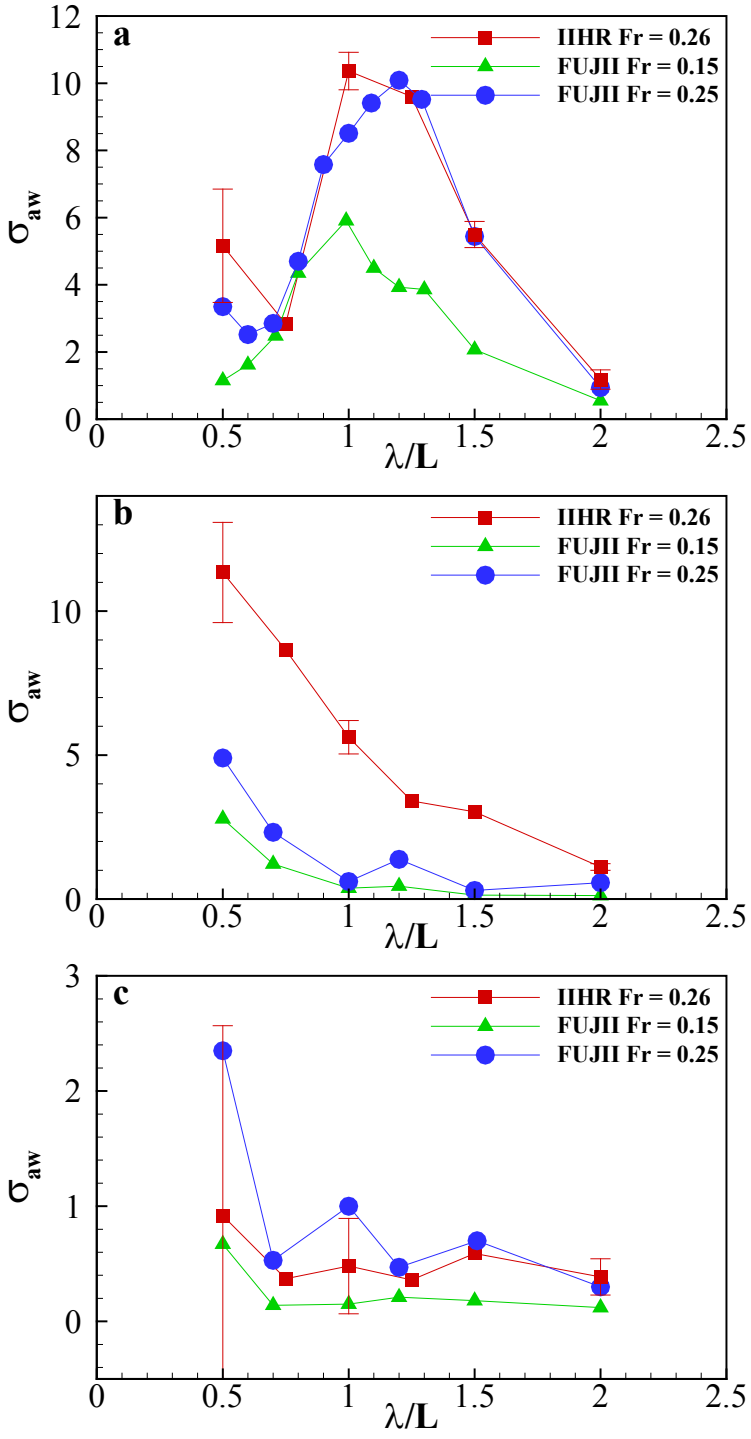

Figure 4.35 Added Resistance results for χ = 0°(a), 90°(b), and 180°(c) for KCS at IIHR, Fr=0.26, Container ship model, Fr=0.15 and Fr=0.25 (Fujii & Takahashi 1975)

www.manaraa.com

CHAPTER 5 CONCLUSION AND FUTURE WORK

Added Resistance and motion testing was completed for the KRISO container ship model in calm water and oblique wave encounter conditions. The IIHR wave basin is utilized for these tests due to the uncommon ability to conduct towing tests in oblique wave encounter conditions. The oblique wave encounter is achievable because of the three carriage system, made up of the main carriage (x-direction), sub carriage (y-direction), and turntable (θ-direction). A 4 DOF mounting system is attached to the carriage system, including a spring mass damper system in the surge direction. In this study the IIHR wave basin is utilized to conduct surge, heave, roll, and pitch free towing tests in calm water and a range of oblique wave encounter conditions to study the effect that the wave encounter angle has on the added resistance and motions. Repeated runs and uncertainty analysis were completed for certain test cases to assess the quality of the data. Another objective of this study is to provide data for validation of for the simulation based design method. Specifically, this data is used as benchmark data for potential flow studies and IIHR computation fluid dynamics validation.

Added resistance towing tests with 4 DOF were conducted in calm water conditions with varying Froude numbers. Hydrodynamic resistance, sinkage, and trim time histories were all recorded for all calm water cases. The total and residual resistance coefficients were calculated, with and without using the Prohaska form factor method. Repeated tests were conducted for several Froude number cases and the repeated resistance coefficients and motions have good agreement. Uncertainty analysis was completed for Froude number cases with repeated tests. The IIHR results were compared to results at other facilities with varying model size. The comparison showed that good agreement is achieved when the smaller model, L = 2.70 m, results are excluded.

Added resistance towing tests in head waves were conducted in a wide range of λ/L in order to compare the experimental results at IIHR with the experimental results at FORCE. Wave amplitude at forward perpendicular, stationary wave amplitude, total resistance, hydrodynamic resistance, measured surge, modified surge, heave, pitch, and roll time histories were recorded for all tests. Repeated tests were conducted for several wavelengths. Uncertainty analysis was completed for cases with repeated tests. The results of conditions with repeated tests show good agreement. The results of IIHR and FORCE

www.manaraa.com

agree for most 0^{th}, 1^{st}, and 2^{nd} harmonic amplitudes. Like calm water, excluding the smaller L = 2.70 m model showed less scatter than including all models. The phases showed large variations between data sets.

Oblique wave encounter tests were conducted at $\chi = 45^0$, 90^0, 135^0, and 180^0. Resistance, wave amplitude, surge, heave, roll, and pitch time histories were recorded for all tests. Repeated tests were conducted for several wavelengths. Uncertainty analysis was completed for cases with repeated tests. The results of conditions with repeated tests show good agreement. The added resistance and motions of KCS in oblique wave encounter condition were obtained for establishing benchmark data for CFD validation. The results are validated by comparing to (Fujii & Takahashi 1975), the only other added resistance study performed in oblique waves. The results show an agreement in trends between the current study and (Fujii & Takahashi 1975).

In order to achieve better simulation based design, further work is necessary to improve the predictability of the added resistance and motions. To achieve this, further research will focus on validating results with repeated tests and in depth analysis of added resistance and motions in conditions near the resonance conditions. The further testing will use a modified set up to improve the quality of the results. The primary modifications are to reduce the noise in the resistance measurement. This is achieved by eliminating electrical noise from the facility and lowering the location of the surge free rail in order to shorten the heaving rod. Shortening the heaving rod will reduce the mechanical vibrations between the heaving rod and the lightweight carriage. In addition, the wave gauge at the forward perpendicular will be mounted to the surge free mount, allowing a more accurate phase and initial position of wave peak calculation, for better comparison with other facilities. Also, an accelerometer will be used to measure the surge acceleration and more accurately predict the hydrodynamic force. A system identification is necessary to determine the actual mass spring damper coefficients for better predication of hydrodynamic force and its uncertainty. Once confirmation of the added resistance results are completed, the KCS model will be fitted with a propeller powering system and free running added powering tests will be completed.

www.manaraa.com

APPENDIX A ATMOSPHERIC AND WATER TEMPERATURE

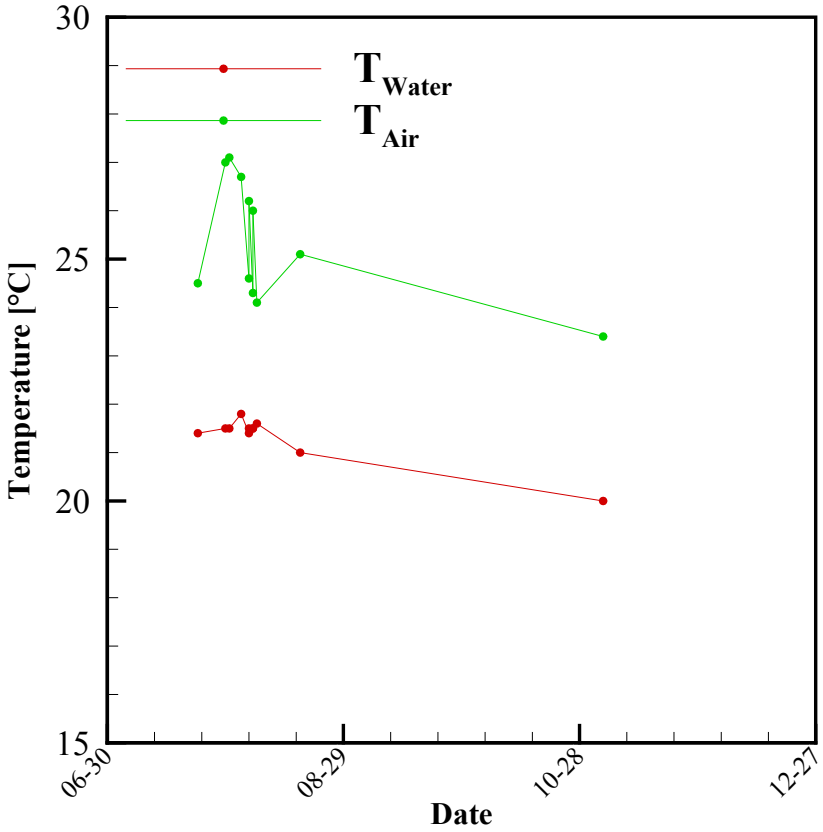

Figure A.1 Temperature tendencies for testing days

Table A.1 Recorded temperatures on testing days

Date	Time	Water Temperature [°C]	Atmosphere Temperature [°C]
7/23/2015	10:00 a.m.	21.4	24.5
7/30/2015	6:30 p.m.	21.5	27
7/31/2015	4:30 p.m.	21.5	27.1
8/3/2015	4:00 p.m.	21.8	26.7
8/5/2015	10:40 a.m.	21.4	24.6
8/5/2015	16:00 p.m.	21.5	26.2
8/6/2015	8:00 a.m.	21.5	24.3
8/6/2015	1:00 p.m.	21.5	26.0
8/7/2015	6:30 a.m.	21.6	24.1
8/18/2015	4:30 p.m.	21.0	25.1
11/3/2015	10:30 a.m.	20.0	23.4

www.manaraa.com

APPENDIX B SYSTEMATIC UNCERTIANTY OF MEASUREMENTS

Table B.1 lists the systematic standard uncertainty of measurements. The summary of values are shown in Table 3.1.

Table B.1 Values with evaluated individual systematic uncertainty

Variable	Name	Bias Limit	Units
T_w	Water Temperature	$b\rho$	kg/m3
L	Length Between Perpendiculars	b_L	m
B	Beam	b_B	m
T	Draft	b_T	m
S	Wetted Surface	b_S	m2
M	Model Mass	b_M	kg
X_T	Measured X-Force	b_{XT}	N
V	Carriage Velocity	b_V	m/s
x	Surge	b_x	mm
z,σ	Heave	b_z	mm
ϕ	Roll	b_ϕ	deg
θ,τ	Pitch	b_θ	deg
χ	Wave Encounter Angle	b_χ	deg
A	Desired Wave Amplitude	b_A	m
ζ	Wave Amplitude	b_ζ	mm
λ	Wavelength	b_λ	mm
T_e	Period of Encounter	b_{Te}	s
XG	Longitudinal Center of Gravity	b_{XG}	m
GM	Metacentric Height	b_{GM}	m
KG	Vertical Center of Gravity	b_{KG}	m
k_{yy}/L	Longitudinal Radius of Gyration	$b_{kyy/L}$	-
k_{xx}/B	Horizontal Radius of Gyration	$b_{kxx/B}$	-
T_{hz}, $T_{h\phi}$, $T_{h\theta}$	Natural Heave, Roll, and Pitch Period	b_{Thz}, $b_{Th\phi}$, $b_{Th\theta}$	s

www.manaraa.com

B.1 Water Temperature, T_w °C

The water temperature is measured with a thermocouple thermometer. The thermometer has a resolution of ± 0.1 °C. The systematic standard uncertainty for the temperature is calculated by finding the variance of the temperature measurement assuming a normal distribution following (ASME 2013). Equation B.1 is used to calculate the variance. Table B.2 lists the total systematic standard uncertainty of the water temperature measurement.

$$b_2 = 0.1°C / 2 \tag{B.1}$$

Table B.2 Systematic standard uncertainty for water temperature

b_T	m	0.05

B.2 Length, L m

The 2.70 m ship model tested at IIHR is the same model that is the topic of uncertainty analysis of Otzen (2015). The accuracy of the ship length depends on the precision of the mill used to create the ship model. The mill has a tolerance of ± 1 mm in all directions. Therefore, the length of the KCS model is 2.70 m with a range of ± 0.002 m. Equation B.2 is used to calculate the systematic standard uncertainty of the ship length, assuming a the length is somewhere in between the range and that statistical distribution is normal. Table B.3 shows the total systematic standard uncertainty of the ship length measurement.

$$b_L = 0.002m / 2 \tag{B.2}$$

Table B.3 Systematic standard uncertainty for ship's length

b_L	m	0.001

B.3 Beam, B m^2

Like the accuracy of the ship's length, the accuracy of the ship's beam is also attributed to the precision of the milling machine. The tolerance of the milling machine is ± 1 mm. Therefore, the beam of the KCS model is 0.3780 m with a range of ± 0.002 m. Equation B.3 is used to calculate the systematic standard uncertainty of the beam, assuming

www.manaraa.com

the beam is somewhere in between the range and that statistical distribution is normal. Table B.4 shows the total systematic standard uncertainty of the beam measurement.

$$b_B = 0.002m/2 \tag{B.3}$$

Table B.4 Systematic standard uncertainty for ship's beam

b_B	m	0.001

B.4 Draft, T m

Like the accuracy of the ship's length and beam, the accuracy of the ship's draft is also attributed to the precision of the milling machine. The tolerance of the milling machine is ± 1 mm. Therefore, the draft of the KCS model is 0.1268 m with a range of ± 0.001 m. Equation B.4 is used to calculate the systematic standard uncertainty of the draft, assuming the draft is somewhere in between the range and that statistical distribution is square. Table B.5 shows the total systematic standard uncertainty of the ship's draft measurement.

$$b_T^2 = 0.001m/2 \tag{B.4}$$

Table B.5 Systematic standard uncertainty for ship's draft

b_T	m	0.0005

B.5 Wetted Surface, S m^2

The systematic standard uncertainty is calculated as in Otzen, (2015). The wetted surface depends on the markings on the ship. Therefore, the total systematic standard uncertainty of the wetted surface is calculated by the root mean sum square of the bias limits related to the manufacturing process and the accuracy of the marks. Equation B.5 is used to calculate the systematic standard uncertainty of the wetted surface.

$$b_S = \left[B_{S_{Manufacturing}}^2 + B_{S_{Marking}}^2 \right]^{1/2} \Big/ 2 \tag{B.5}$$

As with L and B, the tolerance of the mill contributes to the manufacturing systematic standard uncertainty of the wetted surface. The mill has a tolerance of ± 1 mm in all directions. This means that the beam of the ship may be ± 2 mm and the draft may be ± 1 mm. To assess the tolerance effect on systematic standard uncertainty, the wetted surface coefficient it used. Equation B.6 is used to calculate the wetted surface coefficient.

www.manaraa.com

$$C_S = \frac{S_{manufacturing}}{\sqrt{\nabla L}} \tag{B.6}$$

The wetted surface coefficient is assumed constant at all times. Given this assumption, Equation B.7 is used to calculate the bias limit of $S_{manufacturing}$.

$$\frac{B_{S_{manufacturing}}}{S_{manufacturing}} = \sqrt{\left(\frac{0.5}{\nabla} B_{\nabla}\right)^2 + \left(\frac{0.5}{L} B_L\right)^2} \tag{B.7}$$

A constant block coefficient is assumed as well. This allows the systematic standard uncertainty of the displacement to be expressed in terms of draft, Beam, and length values and uncertainties. Equation B.8 is used to calculate the block coefficient. Equation B.9 is used to calculate the systematic uncertainty of displacement. Table B.6 shows the bias limit of the manufacturing along with the bias limits used in the calculation of Equation B.9.

$$C_B = \frac{\nabla}{TBL} \tag{B.8}$$

$$\frac{B_{\nabla}}{\nabla} = \sqrt{\left(\frac{B_T}{T}\right)^2 + \left(\frac{B_B}{B}\right)^2 + \left(\frac{B_L}{L}\right)^2} \tag{B.9}$$

Table B.6 Systematic uncertainty for the manufactured wetted surface

B_T	m	0.001
B_B	m	0.002
B_L	m	0.002
B_{∇}	m^3	0.001
$B_{Smanufacturing}$	m^2	0.0036

The systematic uncertainty related to the marking of the wetted surface depends on the accuracy of the placement of the makings on the model. The procedure from Otzen (2015) is followed to estimate the small differences in the marking. Equation B.10 is used to define the small differences in the marking, assuming that the water plane area is described as an ellipse.

$$\Delta S_{marking} = \Delta T_{marking} 2\pi \sqrt{0.5\left(\left(\frac{L}{2}\right)^2 + \left(\frac{B}{2}\right)^2\right)} \tag{B.10}$$

The small change in draft marking, $\Delta T_{marking,}$ is assumed to be in a range of ±1mm. Therefore, $\Delta T_{marking}$ is 2mm. The systematic uncertainty of $S_{marking}$ is set to $\Delta S_{marking,}$

www.manaraa.com

assuming the true wetted surface is in the range of $S \pm \Delta S_{marking}$. Table B.7 shows the bias limit analysis for the wetted surface.

Table B.7 Systematic standard uncertainty for wetted surface

$B_{Smanufacturing}$	m^3	0.004
$B_{Smarking}$	m^3	0.007
b_S	m^3	0.004

B.6 Model Mass, M kg

The source of uncertainty of the total model mass is the base model mass, mass of the instrumentation, and the mass of the weights used for ballasting the model. The systematic uncertainty of the model mass is associated with the variance of the resolution of the scale, ± 0.1 kg. The ballasting weight all follow the precision specifications from (ASME 2013). Table B.8 shows the mass and systematic uncertainty of each of the masses contributing to the ship mass.

Table B.8 Systematic uncertainty for individual masses

i		M_i [kg]	b_{Mi} [kg]	Number Used
1	Model	37	0.05	1
2	Instrumentation	6.5	0.003	1
3-5	Ballast	0.5	0.002	3
6-15	Ballast	1	0.003	10
16-21	Ballast	2	0.004	6
22-25	Ballast	5	0.0005	4

The systematic uncertainty of each of the individual masses is calculated using the root sum square. Equation B.11 is used to calculate the systematic standard uncertainty of the total mass. Table B.9 shows the systematic standard uncertainty analysis of the model mass.

$$b_M = \left[\sum_{i=1}^{N} B_{M_i}^2\right]^{1/2} \Big/ 2 \tag{B.11}$$

Table B.9 Systematic standard uncertainty of the model mass

b_M	kg	0.05

www.manaraa.com

B.7 Measured X Force, X_T N

The systematic standard uncertainty of the measured X-force consists of the uncertainty associated with the load cell data acquisition during calibration, X_{SEE}, and the uncertainty associated with the masses used to complete the calibration, X_m. Equation B.12 is used to calculate the systematic standard uncertainty of the total measured X-force.

$$b_{X_T} = \sqrt{B_{X_{SEE}}{}^2 + B_{X_m}{}^2} \Big/ 2 \tag{B.12}$$

The bias limit associated with the masses is calculated by summing the bias limit of each individual mass used, as in equation B.13. The bias limit for each mass, B_m, is the manufacturer uncertainty for the masses used. These uncertainties are found in (ASTM 2010) standards.

$$B_{X_m} = \sum_{i=1}^{N} B_{m_i} \tag{B.13}$$

The uncertainty of the gravitational constant is zero because it is not measured. Therefore, the uncertainty of the masses in Newtons is the mass systematic uncertainty times the gravitational constant. Table B.10 shows the mass and systematic uncertainty of each of the calibration masses.

Table B.10 Systematic uncertainty for calibration masses

i	m_i [kg]	B_{mi} [kg]
1	0.5	0.0002
2	0.5	0.0002
3	0.5	0.0002
4	0.5	0.0002

The volt-force conversion during data acquisition also contributes to the measured X-force systematic standard uncertainty. The conversion bias limit, SEE, is calculated using linear regression analysis following (ASME 2013). Equation B.14 is used to calculate the SEE of the X-force.

$$B_{X_{SEE}} = \sqrt{\sum_{i=1}^{N} \frac{(X_i - X_{measi})^2}{N-2}} \tag{B.14}$$

Where X_{measi} is the measured X-force and X_i is the applied X-force. The calibration curve of an instrument is normally linear. Table B.11 shows the linear regression analysis. Table B.12 shows the results of the X-force bias limit analysis.

www.manaraa.com

Table B.11 X-force Linear Regression Analysis

i	M_i [kg]	$X_{applied}$ [N]	$X_{measured}$ [N]
1	0.0	0.00	0.00
2	0.5	4.91	4.90
3	1.0	9.81	9.81
4	1.5	14.72	14.71
5	2.0	19.62	19.61
6	1.5	14.72	14.71
7	1.0	9.81	9.81
8	0.5	4.91	4.90
9	0.0	0.00	0.00

Table B.12 Systematic standard uncertainty analysis for X-force

B_{Xm}	N	0.0004
B_{XSEE}	N	0.076
b_{XT}	N	0.04

B.8 Carriage Velocity, V m/s

Equation B.15 is used to calculate the carriage velocity following (ITTC 2002). There are systematic uncertainties associated with the diameter of the wheel, D, the size of divisions, Δt, and the number of pulse counts. Equation B.16 is used to calculate the systematic standard uncertainty of the carriage velocity.

$$V = \frac{n\pi D}{N\Delta t} \tag{B.15}$$

$$b_V = \left[\left(\theta_n b_n\right)^2 + \left(\theta_D b_D\right)^2 + \left(\theta_{\Delta t} b_{\Delta t}\right)^2 \right]^{1/2} \Big/ 2 \tag{B.16}$$

The sensitivity coefficients for calculating the systematic standard uncertainty of carriage velocity are calculated using Equations B.17 through B.19.

$$\frac{\partial U_c}{\partial D} = \frac{n\pi}{N\Delta t} \tag{B.17}$$

$$\frac{\partial U_c}{\partial \Delta t} = -\frac{n\pi D}{N\Delta t^2} \tag{B.18}$$

$$\frac{\partial U_c}{\partial n} = \frac{\pi D}{N\Delta t} \tag{B.19}$$

www.manaraa.com

The manufacturer states the systematic standard uncertainty associated with the diameter of the wheel is ± 0.03 mm. The manufacturer provided the minimum precision in the size of the divisions as ± 0.009 s. The resolution of the pulse count and the DAQ board systematic uncertainty is used to calculate the systematic uncertainty of the pulse c_{out}, as in Equation B.20. The manufacturer states the systematic standard uncertainty of the DAQ board is ± 0.004 mm. Table B.13 shows the systematic standard uncertainty of the pulse count from the encoder. Table B.14 shows the systematic standard uncertainty analysis for carriage speed.

$$b_n = \sqrt{b_{n_{res}}^2 + b_{n_{DAQ}}^2} \tag{B.20}$$

Table B.13 Systematic uncertainty analysis for pulse count

b_{nres}	bit	0.6
b_{nDAQ}	bit	0.000004
b_n	bit	0.6

Table B.14 Systematic standard uncertainty analysis for carriage speed

b_n	bit	1
b_D	m	0.0003
$b_{\Delta t}$	s	0.009
b_V	m/s	0.0007

B.9 Surge, x mm

A potentiometer is used to measure the surge motion. Like the load cell used for the X-force measurement, the potentiometer has two sources of uncertainty. There is uncertainty in the surge measurement due to the accuracy of the calibration standard and there is uncertainty associated with the volt-surge conversion during data acquisition. Equation B.21 is used to calculate the total bias limit of surge.

$$b_x = \left[B_{x_m} + B_{x_{SEE}} \right]^{1/2} \Big/ 2 \tag{B.21}$$

The uncertainty of the standard length used to calibrate the surge potentiometer is associated with the resolution of the ruler used to measure the gauge location. The bias limit of the ruler is ± 0.0005 m. The bias limit of the volt-surge conversion is calculated using linear regression techniques following (ASME 2013). Equation B.22 is used to

www.manaraa.com

calculate the bias limit of the volt-surge conversion. Table B.15 shows the systematic standard uncertainty of surge motions.

$$B_{x_{SEE}} = \sqrt{\sum_{i=1}^{n} \frac{(x_i - x_{meas,i})^2}{n-2}} \tag{B.22}$$

Table B.15 Systematic standard uncertainty analysis for surge motion

B_{xm}	mm	0.32
B_{xSEE}	mm	0.29
b_x	mm	0.22

B.10 Heave, z mm

A potentiometer is used to measure the heave motion. The potentiometer has two sources of systematic uncertainty. There is systematic uncertainty in the heave measurement due to the accuracy of the calibration standard and there is systematic uncertainty associated with the volt-heave conversion during data acquisition. Equation B.23 is used to calculate the total systematic standard uncertainty of heave.

$$b_z = \left[B_{z_m} + B_{z_{SEE}} \right]^{1/2} / 2 \tag{B.23}$$

The systematic uncertainty of the standard length used to calibrate the heave potentiometer is associated with the resolution of the ruler used to measure the gauge location. The bias limit of the ruler is ± 0.0005 m. The bias limit of the volt-heave conversion is calculated using linear regression techniques following (ASME 2013). Equation B.24 is used to calculate the systematic uncertainty of the volt-heave conversion. Table B.16 shows the systematic standard uncertainty of heave motions.

$$B_{z_{SEE}} = \sqrt{\sum_{i=1}^{n} \frac{(z_i - z_{meas,i})^2}{n-2}} \tag{B.24}$$

Table B.16 Systematic standard uncertainty analysis for heave motion

B_{zm}	mm	0.11
B_{zSEE}	mm	0.29
b_z	mm	0.16

www.manaraa.com

B.11 Roll, ϕ deg

A potentiometer is used to measure the roll motion. The potentiometer has two sources of systematic uncertainty. There is systematic uncertainty in the roll measurement due to the accuracy of the calibration standard and there is systematic uncertainty associated with the volt-roll conversion during data acquisition. Equation B.25 is used to calculate the systematic standard uncertainty of roll.

$$b_{\phi} = \left[B_{\phi_m} + B_{\phi_{SEE}} \right]^{1/2} / 2 \tag{B.25}$$

A digital protractor was used to calibrate the potentiometer. The manufacturer reports the systematic uncertainty of the digital protractor as a repeatability and resolution of ± 0.05°. Assuming a square distribution, the variance of the repeatability and resolution is ± 0.029°. The bias limit of the protractor is calculated to be 0.04° by calculating the root mean square of the of the repeatability and resolution. The systematic uncertainty of the volt-roll conversion is calculated using linear regression techniques following (ASME 2013). Equation B.26 is used to calculate the bias limit of the volt-roll conversion. Table B.17 shows the systematic standard uncertainty roll motions.

$$B_{\phi_{SEE}} = \sqrt{\sum_{i=1}^{n} \frac{(\phi_i - \phi_{meas,i})^2}{n-2}} \tag{B.26}$$

Table B.17 Systematic standard uncertainty analysis for roll motion

$B_{\phi m}$	deg	0.05
$B_{\phi SEE}$	deg	0.07
b_{ϕ}	deg	0.04

B.12 Pitch, θ deg

A potentiometer is used to measure the roll motion. The potentiometer has two sources of systematic uncertainty. There is systematic uncertainty in the roll measurement due to the accuracy of the calibration standard and there is systematic uncertainty associated with the volt-pitch conversion during data acquisition. Equation B.27 is used to calculate systematic standard uncertainty of roll.

$$b_{\theta} = \left[B_{\theta_m} + B_{\theta_{SEE}} \right]^{1/2} / 2 \tag{B.27}$$

www.manaraa.com

The digital protractor used to calibrate the roll motion was used to calibrate the potentiometer. The systematic uncertainty of the protractor is calculated to be 0.05° by calculating the root mean square of the systematic uncertainty of the repeatability and resolution. The uncertainty of the volt-roll conversion is calculated using linear regression techniques. Equation B.28 is used to calculate the bias limit of the volt-roll conversion. Table B.18 shows the systematic standard uncertainty of heave motions.

$$B_{\theta_{SEE}} = \sqrt{\sum_{i=1}^{n} \frac{(\theta_i - \theta_{meas,i})^2}{n-2}} \tag{B.28}$$

Table B.18 Systematic standard uncertainty analysis for pitch motion

$B_{\theta m}$	deg	0.07
$B_{\theta SEE}$	deg	0.05
b_{θ}	deg	0.04

B.13 Wave Encounter Angle, χ deg

The systematic uncertainty associated with the wave encounter angle is based on the resolution of the reported value of carriage wave encounter angle. The resolution of the reported wave encounter angle is ± 0.01°. The variance, based on a normal distribution, is ± 0.005°. Table B.19 shows the systematic standard uncertainty for wave encounter angle.

Table B.19 Systematic standard uncertainty for wave encounter angle

b_{χ}	deg	0.005

B.14 Desired Wave Amplitude, A m

The desired wave amplitude has no systematic uncertainty. This value represents the wave condition that is that the wave maker amplitude and frequency is set to replicate. Table B.20 shows the systematic standard for the desired wave amplitude.

Table B.20 Systematic standard uncertainty for desired wave amplitude

b_A	m	0.00

www.manaraa.com

B.15 Measured Wave Amplitude, ζ mm

An ultrasound wave gauge is used to measure the wave amplitude at the Forward Perpendicular of the ship and at a fixed location 15 m from the wave gauge. The ultrasound wave gauge has two sources of systematic uncertainty. There is systematic uncertainty in the wave amplitude measurement due to the accuracy of the calibration standard and there is systematic uncertainty associated with the volt-wave amplitude conversion during data acquisition. Equation B.29 is used to calculate the systematic standard uncertainty of wave amplitude.

$$b_\zeta = \left[B_{\zeta_m} + B_{\zeta_{SEE}} \right]^{1/2} / 2 \tag{B.29}$$

The uncertainty of the standard used to calibrate the ultrasound wave gauge comes from the standard ruler used to measure the height of the gauge while calibrating. The ultrasound wave gauge was set to various amplitudes and the voltage read is recorded. The accuracy of the ruler, ± 0.0005 m, is the systematic uncertainty. The systematic uncertainty of the volt-wave amplitude conversion is calculated using linear regression techniques following (ASME 2013). Equation B.30 is used to calculate the systematic uncertainty of the volt-heave conversion. Table B.21 shows the systematic standard uncertainty of wave amplitude.

$$B_{\zeta_{SEE}} = \sqrt{\sum_{i=1}^{n} \frac{(\zeta_i - \zeta_{meas,i})^2}{n-2}} \tag{B.30}$$

Table B.21 Systematic standard uncertainty analysis for wave amplitude

$B_{\xi m}$	mm	0.05
$B_{\xi SEE}$	mm	0.2
b_ξ	mm	0.1

www.manaraa.com

In order to determine the accuracy of the waves throughout the wave basin extra tests were done to determine the deterioration of waves throughout the basin. A calibration is done for several wave conditions at five positions along the wave basin's x direction. To begin the wave amplitude calibration, a transfer function, wave height divided by plunger stroke (H/S), is used to attempt and replicate the desired wave height. According to (IMO 2006), the wave quality can must be assessed with at least three wave gauges along the length of the basin. (IMO 2006) states that the measured wave height should be within ± 5% of the desired wave height. To assess the IIHR Wave Basin waves, three wave gauge locations, North, center, and South were used for calibration at five different locations, 10, 15, 20, 25, and 30 meters from wave maker, with varying desired wave amplitudes. Figure B.1 shows the results of the stationary calibration for the north, central, south, and mean of all three wave gauges. From Figure B.1 it is evident that the IIHR Wave Basin satisfies the IMO wave quality criteria for most of the wavelengths in this research.

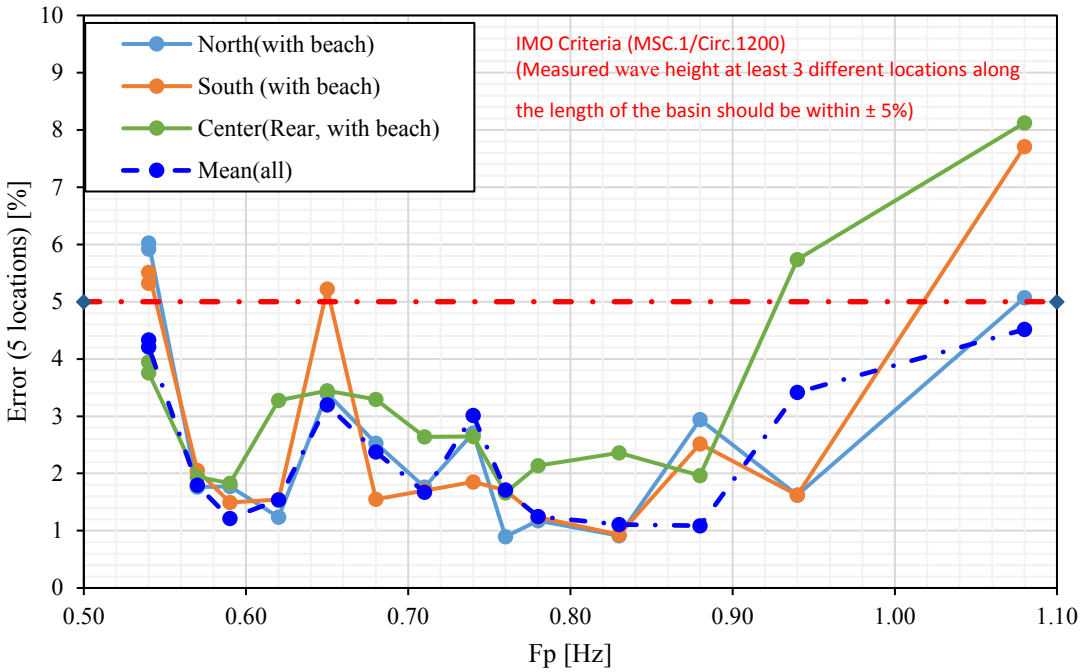

Figure B.1 Percent error of 5 wave gauge locations vs. the prescribed plunger frequency for North, South, Center, and Mean longitudinal wave gauge locations at H/λ = 1/60

www.manaraa.com

B.16 Wavelength, λ mm

The length between the wave peaks determines the wavelength. Therefore, the systematic uncertainty of the wavelength is the uncertainty of the wave height. Following Otzen (2015), the wavelengths are assumed constant at every position because no decay in wavelength is observed. The waves have a set nominal steepness of H/λ=1/60. The wave elevation is assumed to follow a sinusoidal function. Equation B.31 is used to calculate the slope near the wave crest.

$$\frac{\partial \zeta}{\partial t} = \frac{H}{2}\sqrt{\frac{2\pi g}{\lambda}} = \frac{1}{2}\sqrt{\frac{2\pi g}{60}} = 0.507 \tag{B.31}$$

This slope calculation is used as the sensitivity coefficient for calculating the systematic uncertainty of the wavelength in regards to the uncertainty of the wave amplitude. Equation B.32 is used to calculate the systematic uncertainty of the wavelength following Otzen (2015). Table B.22 shows the Systematic standard uncertainty analysis for the wavelength.

$$b_\lambda = \left(\frac{\partial \zeta}{\partial t}\right)^{-1} b_\zeta \tag{B.32}$$

Table B.22 Systematic standard uncertainty analysis for wavelength

b_ζ	mm	0.1
b_λ	mm	0.2

B.17 Period of Wave Encounter, Te s

Following Otzen (2015), the systematic uncertainty of the period of wave encounter is calculated by finding the slope of the wave crest from the perspective of the carriage. The wave slope will appear steeper due to the carriage velocity. The slope will be different for every wave encounter angle. Therefore, the systematic uncertainty of the period of encounter will be different for every wave encounter angle as well. Equation B.33 is used to calculate the slope near the wave crest.

$$\frac{\partial \zeta}{\partial t} = \frac{H}{2}\left(\sqrt{\frac{2\pi g}{\lambda}} - \frac{2\pi V}{\lambda}\cos(\chi + 180)\right) = \frac{1}{2}\left(\sqrt{\frac{2\pi g}{60}} - \frac{2\pi V}{60}\cos(\chi + 180)\right) \tag{B.33}$$

Using the wave slope near the wave crest, the systematic uncertainty of the length between wave encounters can be expressed in terms of the wave amplitude uncertainty.

www.manaraa.com

Equation B.34 is used to calculate the bias limit of the length between wave encounters. Table B.23 shows the Systematic standard uncertainty analysis of the length between the carriage wave encounters.

$$b_{\lambda_e} = \left[\left(\frac{\partial \zeta}{\partial t} \right)^{-1} B_{\zeta_e} \right] \Big/ 2 \tag{B.34}$$

Table B.23 Systematic standard uncertainty for length between carriage wave encounters

χ [°]	dζ/dt [m/s]	B_ζ [m]	$b_{\lambda e}$ [m]
0	0.577	0.0002	0.0002
45	0.556	0.0002	0.0002
90	0.507	0.0002	0.0002
135	0.457	0.0002	0.0003
180	0.437	0.0002	0.0003

The uncertainty of the wave encounter period is attributed to the uncertainty of the wavelength. As in Otzen (2015) Equation B.35 is used to calculate the systematic uncertainty of the wave encounter period. Table B.24 shows the bias limit analysis of encounter period.

$$b_{T_e} = b_{\lambda_e} \sqrt{\frac{\pi}{2g\lambda_e}} \tag{B.35}$$

Table B.24 Systematic standard uncertainty analysis for wave encounter period

	χ [°]				
	0	45	90	135	180
λ/L	b_{Te} [s]				
0.50	0.00007	0.00008	0.00008	0.00009	0.00010
0.65	0.00006	-	-	-	-
0.75	0.00006	0.00006	0.00007	0.00008	0.00008
0.85	0.00006	-	-	-	-
0.95	0.00005	-	-	-	-
1.00	0.00005	0.00005	0.00006	0.00007	0.00007
1.05	0.00005	-	-	-	-
1.15	0.00005	-	-	-	-
1.25	0.00005	0.00005	0.00005	0.00006	0.00006
1.37	0.00004	-	-	-	-
1.50	0.00004	0.00004	0.00005	0.00005	0.00006
1.65	0.00004	-	-	-	-
1.80	0.00004	-	-	-	-
1.95	0.00004	-	-	-	-
2.00	0.00004	0.00004	0.00004	0.00005	0.00005

www.manaraa.com

B.18 Longitudinal Center of Gravity, XG m

The longitudinal center of gravity is the distance between the amidship positions. There are two sources of the systematic uncertainty of the longitudinal center of gravity. The systematic uncertainty comes from the accuracy of the mounting set up, B_{XG1}, and the accuracy of the location of the center of gravity, B_{XG2}. The accuracy of the mounting is accurate to ± 1 mm in either direction. Therefore, the uncertainty from mounting set up is ± 2 mm. Because the model studied at IIHR is the model studied in Otzen (2015) the uncertainty in center of gravity location is assumed to be the same. Therefore the location of the center of gravity is accurate to ± 5 mm. Equation B.36 is used to calculate the Systematic standard uncertainty of the longitudinal center of gravity. Table B.25 shows the systematic standard uncertainty of longitudinal center of gravity.

$$b_{X_G} = \left[B_{X_{G1}} + B_{X_{G2}} \right]^{1/2} \Big/ 2 \tag{B.36}$$

Table B.25 Systematic standard uncertainty analysis for longitudinal center of gravity

B_{XG1}	m	0.002
B_{XG2}	m	0.005
b_{XG}	m	0.003

B.19 Metacentric Height, GM m

The metacentric height was calculated using the incline test. The ship was placed on the water, a ballasting mass, m, was set to port and the incline angle was measured. The mass was then set to the starboard side and the incline angle was measured with a digital level. The GM is calculated using Equation B.37. The variables used are the ballasting mass, m, the length from port side to starboard side, D, the mass of the ship, M, and the change in roll angle between ballasting weight position, φ. The total systematic standard uncertainty is calculated using Equation B.38. The ballasting position origin is located at the port side position and the position decreases as the ballasting weight moves to the starboard side. The roll angle is negative when starboard is down.

$$GM = \frac{mD}{M \tan(\varphi)} \tag{B.37}$$

$$b_{GM} = \left[\left(\theta_\varphi b_\varphi\right)^2 + \left(\theta_D b_D\right)^2 + \left(\theta_m b_m\right)^2 + \left(\theta_M b_M\right)^2 \right]^{1/2} \tag{B.38}$$

www.manaraa.com

Equations B.39 through B.42 represent the sensitivity coefficients for the bias limit of metacentric height.

$$\theta_{\varphi} = \frac{\partial GM}{\partial \varphi} = -\frac{mD}{M \sin^2(\varphi)} \tag{B.39}$$

$$\theta_{D} = \frac{\partial GM}{\partial D} = \frac{m}{M \tan(\varphi)} \tag{B.40}$$

$$\theta_{m} = \frac{\partial GM}{\partial m} = \frac{D}{M \tan(\varphi)} \tag{B.41}$$

$$\theta_{M} = \frac{\partial GM}{\partial M} = -\frac{mD}{M^2 \tan(\varphi)} \tag{B.42}$$

Equation B.43 is used to calculate the systematic uncertainty of the change in incline angle, φ. This systematic uncertainty is associated with the manufacturer's specifications of the digital protractor. The manufacturer reports a repeatability of ± 0.05°, a resolution of ± 0.05°, and an accuracy of ± 0.1°. Equation B.44 is used to calculate the bias limits for the port and starboard measurement.

$$b_{\varphi} = \sqrt{\left(\theta_{\varphi_{port}} b_{\varphi_{port}}\right)^2 + \left(\theta_{\varphi_{Starboard}} b_{\varphi_{Starboard}}\right)^2} \tag{B.43}$$

$$b_{\varphi_{port}} = b_{\varphi_{starboard}} = \sqrt{\left(B_{\varphi_{repeat}}\right)^2 + \left(B_{\varphi_{resolution}}\right)^2 + \left(B_{\varphi_{accuracy}}\right)^2} \Big/ 2 \tag{B.44}$$

The bias limit of the ballasting mass is consistent with the calculations above. The systematic uncertainty in length between the two side positions is the variance of the resolution of the measuring tape, ± 1 mm, assuming normal distribution. The systematic standard uncertainty of the ship mass is ± 0.05 kg, as above. Table B.26 shows the systematic standard uncertainty analysis for metacentric height.

Table B.26 Systematic standard uncertainty analysis for metacentric height

b_{φ}	rad	0.001
b_D	m	0.0005
b_m	kg	0.0015
b_M	kg	0.05
b_{GM}	mm	0.06

www.manaraa.com

B.20 Swing Test Set up and Variables Used in Sections A.21, A.22, and A.23

A swing test is used to measure the Kyy/L, and K_{xx}/B, and KG. Figure B.1 shows the schematic of the swing set up.

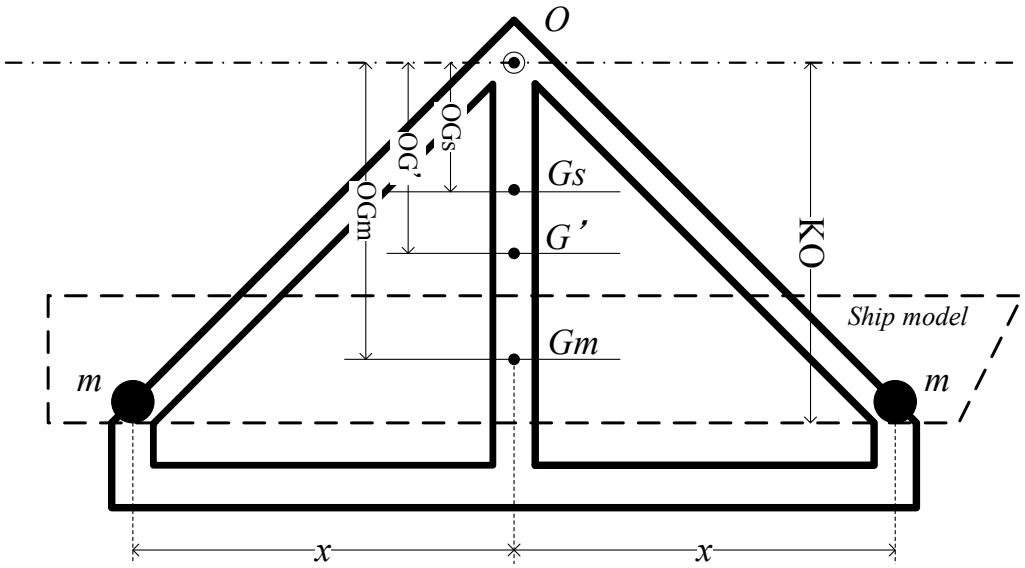

Figure B.2 Schematic of swing test set up

B.21 Vertical Center of gravity, KG_m m

Equation B.45 is used to calculate the vertical center of gravity. Systematic uncertainty is introduced by the mass of the swing, Ms, the mass of ballasting weights, m, the distance from the gravity center of the swing, counter weights and the ship model, OG', the gravity center of the swing and counter weights, OGs, and the mass of the model, M, effect the uncertainty of $KG_{m..}$ Table B.20 shows the bias limits of measured values that contribute to the systematic standard uncertainty of KG_m.

$$\overline{KG_m} = \overline{KO} - \overline{OG_m} = \overline{KO} - \frac{\left(\left(M_s + 2m\right) + M\right)\overline{OG'} - \left(M_s + 2m\right)\overline{OG_s}}{M} \qquad \text{(B.45)}$$

www.manaraa.com

Table B.27 Bias limits of measurements used in KG_m bias limit analysis

B_{Ms}	kg	0.1
B_M	kg	0.1
B_m	kg	0.001
B_x	m	0.001
B_{Ts0}	s	0.001
B_{Ts1}	s	0.001
B_{Tm0}	s	0.001
B_{Tm1}	s	0.001

Equation B.46 is used to calculate the gravity center of the swing and counter weights, OGs. Equation B.47 is used to calculate the systematic uncertainty of OGs. Equations B.48 through B.52 are used to calculate the sensitivity coefficients in Equation B.47.

$$\overline{OG_s} = \frac{2mx^2}{\frac{(M_s + 2m)g}{4\pi^2}\left(T_{s1}^{\ 2} - T_{s0}^{\ 2}\right)} \tag{B.46}$$

$$b_{\overline{OG_S}} = \left[\left(\theta_{T_{s0}} b_{T_{s0}}\right)^2 + \left(\theta_{T_{s1}} b_{T_{s1}}\right)^2 + \left(\theta_m b_m\right)^2 + \left(\theta_x b_x\right)^2 + \left(\theta_{M_s} b_{M_s}\right)^2\right]^{1/2} \Big/ 2 \tag{B.47}$$

$$\theta_{T_{s0}} = \frac{\partial \overline{OG_s}}{\partial T_{s0}} = \frac{4mx^2 T_{s0}}{\frac{(M_s + 2m)g}{4\pi^2}\left(T_{s1}^{\ 2} - T_{s0}^{\ 2}\right)^2} \tag{B.48}$$

$$\theta_{T_{s1}} = \frac{\partial \overline{OG_s}}{\partial T_{s1}} = -\frac{4mx^2 T_{s1}}{\frac{(M_s + 2m)g}{4\pi^2}\left(T_{s1}^{\ 2} - T_{s0}^{\ 2}\right)^2} \tag{B.49}$$

$$\theta_m = \frac{\partial \overline{OG_s}}{\partial m} = \frac{2M_s x^2}{\frac{(M_s + 2m)^2 g}{4\pi^2}\left(T_{s1}^{\ 2} - T_{s0}^{\ 2}\right)} \tag{B.50}$$

$$\theta_x = \frac{\partial \overline{OG_s}}{\partial x} = \frac{4mx}{\frac{(M_s + 2m)g}{4\pi^2}\left(T_{s1}^{\ 2} - T_{s0}^{\ 2}\right)} \tag{B.51}$$

$$\theta_{M_s} = \frac{\partial \overline{OG_s}}{\partial M_s} = -\frac{2mx^2}{\frac{(M_s + 2m)^2 g}{4\pi^2}\left(T_{s1}^{\ 2} - T_{s0}^{\ 2}\right)} \tag{B.52}$$

www.manaraa.com

Equation B.53 is used to calculate the gravity center of the swing and counter weights, OG'. Equation B.54 is used to calculate the systematic uncertainty of OG'. Equations B.55 through B.60 are used to calculate the sensitivity coefficients in Equation B.54.

$$\overline{OG'} = \frac{2mx^2}{\frac{\left(\left(M_s + 2m\right) + M\right)g}{4\pi^2}\left(T_{m1}{}^2 - T_{m0}{}^2\right)} \tag{B.53}$$

$$b_{\overline{OG'}} = \left[\left(\theta_m B_m\right)^2 + \left(\theta_x B_x\right)^2 + \left(\theta_{M_s} B_{M_s}\right)^2 + \left(\theta_M B_M\right)^2 + \left(\theta_{T_{m0}} B_{T_{m0}}\right)^2 + \left(\theta_{T_{m1}} B_{T_{m1}}\right)^2\right]^{1/2} \Big/ 2 \tag{B.54}$$

$$\theta_m = \frac{\partial \overline{OG'}}{\partial m} = \frac{2x^2(M_s + M)}{\frac{\left(\left(M_s + 2m\right) + M\right)^2 g}{4\pi^2}\left(T_{m1}{}^2 - T_{m0}{}^2\right)} \tag{B.55}$$

$$\theta_x = \frac{\partial \overline{OG'}}{\partial x} = \frac{4xm}{\frac{\left(\left(M_s + 2m\right) + M\right)g}{4\pi^2}\left(T_{m1}{}^2 - T_{m0}{}^2\right)} \tag{B.56}$$

$$\theta_{M_s} = \frac{\partial \overline{OG'}}{\partial M_s} = -\frac{2x^2 m}{\frac{\left(\left(M_s + 2m\right) + M\right)^2 g}{4\pi^2}\left(T_{m1}{}^2 - T_{m0}{}^2\right)} \tag{B.57}$$

$$\theta_{M_m} = \frac{\partial \overline{OG'}}{\partial M} = -\frac{2x^2 m}{\frac{\left(\left(M_s + 2m\right) + M\right)^2 g}{4\pi^2}\left(T_{m1}{}^2 - T_{m0}{}^2\right)} \tag{B.58}$$

$$\theta_{T_{m0}} = \frac{\partial \overline{OG'}}{\partial T_{m0}} = \frac{4x^2 m T_{m0}}{\frac{\left(\left(M_s + 2m\right) + M\right)^2 g}{4\pi^2}\left(T_{m1}{}^2 - T_{m0}{}^2\right)^2} \tag{B.59}$$

$$\theta_{T_{m1}} = \frac{\partial \overline{OG'}}{\partial T_{m1}} = -\frac{4x^2 m T_{m1}}{\frac{\left(\left(M_s + 2m\right) + M\right)^2 g}{4\pi^2}\left(T_{m1}{}^2 - T_{m0}{}^2\right)^2} \tag{B.60}$$

Equation B.61 is used to calculate the gravity center of the ship model, OG_m. The equation B.62 is used to calculate the bias limit of OG_m. Equations B.63 through B.67 are used to calculate the sensitivity coefficients in Equation B.62.

www.manaraa.com

$$\overline{OG_{\mathrm{m}}} = \frac{\left(\left(M_{\mathrm{s}} + 2m\right) + M\right)\overline{OG'} - \left(M_{\mathrm{s}} + 2m\right)\overline{OG_{\mathrm{s}}}}{M} \tag{B.61}$$

$$b_{\overline{OG_m}} = \left[\left(\theta_{M_s} B_{M_s}\right)^2 + \left(\theta_M B_M\right)^2 + \left(\theta_m B_m\right)^2 + \left(\theta_{\overline{OG'}} B_{\overline{OG'}}\right)^2 + \left(\theta_{\overline{OG_s}} B_{\overline{OG_s}}\right)^2\right]^{1/2} \Big/ 2 \tag{B.62}$$

$$\theta_{M_s} = \frac{\partial \overline{OG_{\mathrm{m}}}}{\partial M_s} = \frac{\overline{OG'} - \overline{OG_{\mathrm{s}}}}{M} \tag{B.63}$$

$$\theta_{M_m} = \frac{\partial \overline{OG_{\mathrm{m}}}}{\partial M} = -\frac{\left(M_{\mathrm{s}} + 2m\right)\left(\overline{OG'} - \overline{OG_{\mathrm{s}}}\right)}{M^2} \tag{B.64}$$

$$\theta_m = \frac{\partial \overline{OG_{\mathrm{m}}}}{\partial m} = 2\frac{\overline{OG'} - \overline{OG_s}}{M} \tag{B.65}$$

$$\theta_{\overline{OG'}} = \frac{\partial \overline{OG_{\mathrm{m}}}}{\partial \overline{OG'}} = \frac{\left(\left(M_{\mathrm{s}} + 2m\right) + M\right)}{M} \tag{B.66}$$

$$\theta_{\overline{OG_s}} = \frac{\partial \overline{OG_{\mathrm{m}}}}{\partial \overline{OG_s}} = \frac{-(M_{\mathrm{s}} + 2m)}{M} \tag{B.67}$$

Equation B.68 is used to calculate the total systematic standard uncertainty of KG_m. Table B.28 shows the systematic standard uncertainty analysis for the vertical center of gravity.

$$b_{\overline{KG_m}} = \left[\left(b_{\overline{OG_m}}\right)^2 + \left(b_{\overline{KO}}\right)^2\right]^{1/2} \tag{B.68}$$

Table B.28 Systematic standard uncertainty analysis for the vertical center of gravity

b_{OGs}	m	0.01
$b_{OG'}$	m	0.02
b_{KO}	m	0.0005
b_{OGm}	m	0.0015
b_{KG}	m	0.002

B.22 Radius of Gyration about the y axis K_{yy}/L

Equation B.69 is used to calculate the moment of inertia about the y axis. Equation B.70 is used to calculate the mass moment of inertia, Im. The systematic uncertainty of OG', M, Ms, m, and L are the same as for the standard uncertainty of KG. Equation B.71 is used to calculate the mass moment of inertia about the swing, Is.

www.manaraa.com

$$\frac{k_{yy}}{L} = \frac{\sqrt{\mathrm{I_m}/M}}{L} \tag{B.69}$$

$$I_{\mathrm{m}} = \left(\left(M_{\mathrm{s}} + 2m\right) + M\right) g\overline{OG'}\left(\frac{T_{m0}}{2\pi}\right)^2 - \left(\left(M_{\mathrm{s}} + 2m\right) + M\right)\overline{OG'}^2 - I_{\mathrm{s}} \tag{B.70}$$

$$I_{\mathrm{s}} = \left(M_{\mathrm{s}} + 2m\right) g\overline{OG_{\mathrm{s}}}\left(\frac{T_{s0}}{2\pi}\right)^2 - \left(M_{\mathrm{s}} + 2m\right)\overline{OG_{\mathrm{s}}}^2 \tag{B.71}$$

Equation B.72 is used to calculate the systematic uncertainty of the mass moment of inertia about the swing. Equations B.73 through B.76 were used to calculate the sensitivity coefficients for equation B.72.

$$b_{I_s} = \left[\left(\theta_{M_s} B_{M_s}\right)^2 + \left(\theta_m B_m\right)^2 + \left(\theta_{\overline{OG_s}} B_{\overline{OG_s}}\right)^2 + \left(\theta_{T_{s0}} B_{T_{s0}}\right)^2\right]^{1/2} \Big/ 2 \tag{B.72}$$

$$\theta_{M_s} = \frac{\partial I_{\mathrm{s}}}{\partial M_{\mathrm{s}}} = g\overline{OG_{\mathrm{s}}}\left(\frac{T_{s0}}{2\pi}\right)^2 - \overline{OG_{\mathrm{s}}}^2 \tag{B.73}$$

$$\theta_m = \frac{\partial I_{\mathrm{s}}}{\partial m} = 2g\overline{OG_{\mathrm{s}}}\left(\frac{T_{s0}}{2\pi}\right)^2 - 2\overline{OG_{\mathrm{s}}}^2 \tag{B.74}$$

$$\theta_{\overline{OG_{\mathrm{s}}}} = \frac{\partial I_{\mathrm{s}}}{\partial \overline{OG_{\mathrm{s}}}} = (M_s + 2m)g\left(\frac{T_{s0}}{2\pi}\right)^2 - 2\overline{OG_{\mathrm{s}}} \tag{B.75}$$

$$\theta_{T_{s0}} = \frac{\partial I_{\mathrm{s}}}{\partial T_{s0}} = \frac{(M_s + 2m)g}{4\pi^2} 2T_{s0} \tag{B.76}$$

Equation B.77 is used to calculate the bias limit of the mass moment of inertia about the model, Im. Equations B.78 through B.83 are used to calculate the sensitivity coefficients for equation B.77.

$$b_{I_m} = \left[\left(\theta_{M_s} B_{M_s}\right)^2 + \left(\theta_M B_M\right)^2 + \left(\theta_m B_m\right)^2 + \left(\theta_{\overline{OG'}} B_{\overline{OG'}}\right)^2 + \left(\theta_{T_{s0}} B_{T_{s0}}\right)^2 + \left(\theta_{I_s} B_{I_s}\right)^2\right]^{1/2} \Big/ 2 \tag{B.77}$$

$$\theta_{M_s} = \frac{\partial I_{\mathrm{m}}}{\partial M_s} = g\overline{OG'}\left(\frac{T_{m0}}{2\pi}\right)^2 - \overline{OG'}^2 \tag{B.78}$$

$$\theta_{M_m} = \frac{\partial I_{\mathrm{m}}}{\partial M} = g\overline{OG'}\left(\frac{T_{m0}}{2\pi}\right)^2 - \overline{OG'}^2 \tag{B.79}$$

$$\theta_m = \frac{\partial I_{\mathrm{m}}}{\partial m} = 2g\overline{OG'}\left(\frac{T_{m0}}{2\pi}\right)^2 - 2\overline{OG'}^2 \tag{B.80}$$

www.manaraa.com

$$\theta_{\overline{OG'}} = \frac{\partial I_{\mathrm{m}}}{\partial \overline{OG'}} = \left(\left(M_{\mathrm{s}} + 2m\right) + M\right) g \left(\frac{T_{m0}}{2\pi}\right)^2 - 2\left(\left(M_{\mathrm{s}} + 2m\right) + M\right)\overline{OG'} \tag{B.81}$$

$$\theta_{T_{m0}} = \frac{\partial I_{\mathrm{m}}}{\partial T_{m0}} = \frac{\left(\left(M_{\mathrm{s}} + 2m\right) + M\right)\overline{OG'} g}{2\pi^2} T_{m0} \tag{B.82}$$

$$\theta_{I_s} = \frac{\partial I_{\mathrm{m}}}{\partial I_s} = -1 \tag{B.83}$$

Equation B.84 is used to calculate the systematic uncertainty of the moment of inertia about the y axis, k_{yy}/L. Equations B.85 through B.87 are used to calculate the sensitivity coefficients for Equation B.84. Table B.29 shows the systematic standard uncertainty of radius of gyration about the y axis.

$$b_{k_{yy}/L} = \left[\left(\theta_{I_m} B_{I_m}\right)^2 + \left(\theta_{M_m} B_M\right)^2 + \left(\theta_L B_L\right)^2\right]^{1/2} \Big/ 2 \tag{B.84}$$

$$\theta_{I_m} = \frac{\partial k_{yy} / L_{pp}}{\partial I_m} = -\frac{1}{2L\sqrt{M + I_m}} \tag{B.85}$$

$$\theta_M = \frac{\partial k_{yy} / L_{pp}}{\partial M} = -\frac{\sqrt{\mathrm{Im}}}{2LM^{3/2}} \tag{B.86}$$

$$\theta_L = \frac{\partial k_{yy} / L}{\partial L} = -\frac{\sqrt{\mathrm{I_m} / M}}{L^2} \tag{B.87}$$

Table B.29 Systematic standard uncertainty analysis for the radius of gyration about the y axis

b_{Is}	kgm^2	0.10
b_{Im}	kgm^2	0.04
$b_{kyy/L}$	-	0.001

B.23 Radius of gyration of inertia about the x axis K_{xx}/B

Equation B.88 is used to calculate the gravity center of the swing and counter weights, OGs. For the swing test about the x axis there are two mass positions due to space constraints. These constraints do not allow the weights to be in the same position Equation B.46. Equation B.89 is used to calculate the systematic uncertainty of OGs. Equations B.90 through B.95 are used to calculate the sensitivity coefficients in equation B.89.

$$\overline{OG_s} = \frac{2m\left(x_1^{\,2} - x_0^{\,2}\right)}{\frac{\left(M_{\mathrm{s}} + 2m\right) g}{4\pi^2}\left(T_{s1}^{\,2} - T_{s0}^{\,2}\right)} \tag{B.88}$$

www.manaraa.com

$$b_{\overline{OG_S}} = \left[\left(\theta_{T_{s0}} B_{T_{s0}}\right)^2 + \left(\theta_{T_{s1}} B_{T_{s1}}\right)^2 + \left(\theta_m B_m\right)^2 + \left(\theta_{x_1} B_{x_1}\right)^2 + \left(\theta_{x_0} B_{x_0}\right)^2 + \left(\theta_{M_s} B_{M_s}\right)^2 \right]^{1/2} \Big/ 2 \quad \text{(B.89)}$$

$$\theta_{T_{s0}} = \frac{\partial \overline{OG_s}}{\partial T_{s0}} = \frac{4m\left(x_1^{\,2} - x_0^{\,2}\right) T_{s0}}{\frac{\left(M_s + 2m\right) g}{4\pi^2}\left(T_{s1}^{\,2} - T_{s0}^{\,2}\right)^2} \quad \text{(B.90)}$$

$$\theta_{T_{s1}} = \frac{\partial \overline{OG_s}}{\partial T_{s1}} = -\frac{4m\left(x_1^{\,2} - x_0^{\,2}\right) T_{s1}}{\frac{\left(M_s + 2m\right) g}{4\pi^2}\left(T_{s1}^{\,2} - T_{s0}^{\,2}\right)^2} \quad \text{(B.91)}$$

$$\theta_m = \frac{\partial \overline{OG_s}}{\partial m} = \frac{2M_s\left(x_1^{\,2} - x_0^{\,2}\right)}{\frac{\left(M_s + 2m\right)^2 g}{4\pi^2}\left(T_{s1}^{\,2} - T_{s0}^{\,2}\right)} \quad \text{(B.92)}$$

$$\theta_{x_1} = \frac{\partial \overline{OG_s}}{\partial x_1} = \frac{4mx_1}{\frac{\left(M_s + 2m\right) g}{4\pi^2}\left(T_{s1}^{\,2} - T_{s0}^{\,2}\right)} \quad \text{(B.93)}$$

$$\theta_{x_0} = \frac{\partial \overline{OG_s}}{\partial x_0} = \frac{4mx_0}{\frac{\left(M_s + 2m\right) g}{4\pi^2}\left(T_{s1}^{\,2} - T_{s0}^{\,2}\right)} \quad \text{(B.94)}$$

$$\theta_{M_s} = \frac{\partial \overline{OG_s}}{\partial M_s} = -\frac{2m\left(x_1^{\,2} - x_0^{\,2}\right)}{\frac{\left(M_s + 2m\right)^2 g}{4\pi^2}\left(T_{s1}^{\,2} - T_{s0}^{\,2}\right)} \quad \text{(B.95)}$$

Equation B.96 is used to calculate the gravity center of the swing and counter weights, OG'. Equation B.97 is used to calculate the systematic uncertainty of OG'. Equations B.98 through B.104 are used to calculate the sensitivity coefficients for Equation B.97.

$$\overline{OG'} = \frac{2m\left(x_1^{\,2} - x_0^{\,2}\right)}{\frac{\left(\left(M_s + 2m\right) + M\right) g}{4\pi^2}\left(T_{m1}^{\,2} - T_{m0}^{\,2}\right)} \quad \text{(B.96)}$$

$$b_{\overline{OG'}} = \left[\left(\theta_m B_m\right)^2 + \left(\theta_{x_0} B_{x_0}\right)^2 + \left(\theta_{M_s} B_{M_s}\right)^2 + \left(\theta_M B_M\right)^2 + \left(\theta_{T_{m0}} B_{T_{m0}}\right)^2 + \left(\theta_{T_{m1}} B_{T_{m1}}\right)^2 \right]^{1/2} \Big/ 2 \quad \text{(B.97)}$$

$$\theta_m = \frac{\partial \overline{OG'}}{\partial m} = \frac{2\left(x_1^{\,2} - x_0^{\,2}\right)\left(M_s + M\right)}{\frac{\left(\left(M_s + 2m\right) + M\right)^2 g}{4\pi^2}\left(T_{m1}^{\,2} - T_{m0}^{\,2}\right)} \quad \text{(B.98)}$$

www.manaraa.com

$$\theta_{x_1} = \frac{\partial \overline{OG'}}{\partial x_1} = \frac{4x_1 m}{\frac{\left(\left(M_s + 2m\right) + M\right) g}{4\pi^2}\left(T_{m1}{}^2 - T_{m0}{}^2\right)} \tag{B.99}$$

$$\theta_{x_0} = \frac{\partial \overline{OG'}}{\partial x_0} = \frac{4x_0 m}{\frac{\left(\left(M_s + 2m\right) + M\right) g}{4\pi^2}\left(T_{m1}{}^2 - T_{m0}{}^2\right)} \tag{B.100}$$

$$\theta_{M_s} = \frac{\partial \overline{OG'}}{\partial M_s} = -\frac{2\left(x_1{}^2 - x_0{}^2\right) m}{\frac{\left(\left(M_s + 2m\right) + M\right)^2 g}{4\pi^2}\left(T_{m1}{}^2 - T_{m0}{}^2\right)} \tag{B.101}$$

$$\theta_{M} = \frac{\partial \overline{OG'}}{\partial M} = -\frac{2\left(x_1{}^2 - x_0{}^2\right) m}{\frac{\left(\left(M_s + 2m\right) + M\right)^2 g}{4\pi^2}\left(T_{m1}{}^2 - T_{m0}{}^2\right)} \tag{B.102}$$

$$\theta_{T_{m0}} = \frac{\partial \overline{OG'}}{\partial T_{m0}} = \frac{4\left(x_1{}^2 - x_0{}^2\right) m T_{m0}}{\frac{\left(\left(M_s + 2m\right) + M\right)^2 g}{4\pi^2}\left(T_{m1}{}^2 - T_{m0}{}^2\right)^2} \tag{B.103}$$

$$\theta_{T_{m1}} = \frac{\partial \overline{OG'}}{\partial T_{m1}} = -\frac{4\left(x_1{}^2 - x_0{}^2\right) m T_{m1}}{\frac{\left(\left(M_s + 2m\right) + M\right)^2 g}{4\pi^2}\left(T_{m1}{}^2 - T_{m0}{}^2\right)^2} \tag{B.104}$$

Equations B.72 through B.83 are used to calculate systematic uncertainties of I_s and I_m. The calculation is identical to the calculation for the mass moments of inertia about the y axis. Equation B.106 is used to calculate the systematic uncertainty of the radius of gyration of inertia about the x axis. Equations B.107 through B.109 are used to calculate the sensitivity coefficients for Equation B.106. Table B.30

Table B.30 Systematic standard uncertainty analysis for the radius of gyration of inertia about the x axisshows the systematic standard uncertainty analysis for the radius of

bIm	kgm2	0.6
bB	m	0.001
bM	kg	0.1
$bkxx_{/B}$	-	0.005

gyration about the x axis.

www.manaraa.com

$$\frac{k_{xx}}{B} = \frac{\sqrt{\mathrm{I_m}/M}}{B} \tag{B.105}$$

$$b_{k_{xx}/B} = \left[\left(\theta_{I_m} B_{I_m}\right)^2 + \left(\theta_M B_M\right)^2 + \left(\theta_B B_B\right)^2 \right]^{1/2} \Big/ 2 \tag{B.106}$$

$$\theta_B = \frac{\partial k_{xx}/B}{\partial B} = -\frac{\sqrt{\mathrm{I_m}/M}}{B^2} \tag{B.107}$$

$$\theta_M = \frac{\partial k_{xx}/B}{\partial M} = -\frac{\sqrt{\mathrm{Im}}}{2BM^{3/2}} \tag{B.108}$$

$$\theta_{\mathrm{I_m}} \frac{\partial k_{xx}/B}{\partial I_m} = -\frac{1}{2B\sqrt{M + I_m}} \tag{B.109}$$

Table B.30 Systematic standard uncertainty analysis for the radius of gyration of inertia about the x axis

b_{Im}	kgm^2	0.6
b_B	m	0.001
b_M	kg	0.1
$b_{kxx/B}$	-	0.005

B.24 Natural Heave, Roll, and Pitch Period

The natural heave, roll, and pitch frequencies are measured by affixing a tilt sensor to the center of gravity, in the x and y plane, of the ship model. The heave frequency is measured by displacing the ship several degrees in the negative heave direction and recording 10 swing periods, T_{hz}. The roll frequency is measured by displacing the ship several degrees in the negative direction and recording 10 swing periods, $T_{h\phi}$. The pitch frequency is measured by displacing the ship several degrees in the negative direction and recording 10 swing periods, $T_{h\theta}$. This procedure is important for finding the natural heave, roll, and pitch period with added inertial effects, as opposed to out of water swing tests.

The tilt sensor used is a Memsic CXTA01 model. The tilt sensor has a bias limit, B_{ts}, of ± 0.01 seconds. Equation B.110 shows the total systematic uncertainty for the natural heave, roll, and pitch period. Table B.31 shows the systematic standard uncertainty of natural heave, roll, and pitch period.

www.manaraa.com

$$b_{T_{hz}} = b_{T_{h\phi}} = b_{T_{h\theta}} = \left[B_{ts}\right]/\sqrt{3} \tag{B.110}$$

Table B.31 Systematic standard uncertainty of the natural heave, roll, and pitch period

B_{ts}	s	0.01
b_{Thz}, $b_{Th\phi}$, $b_{Th\theta}$	s	0.006

www.manaraa.com

APPENDIX C TIME HISTORIES OF FORCES AND MOTIONS

C.1 Time Histories of Wave Cases, χ=0°

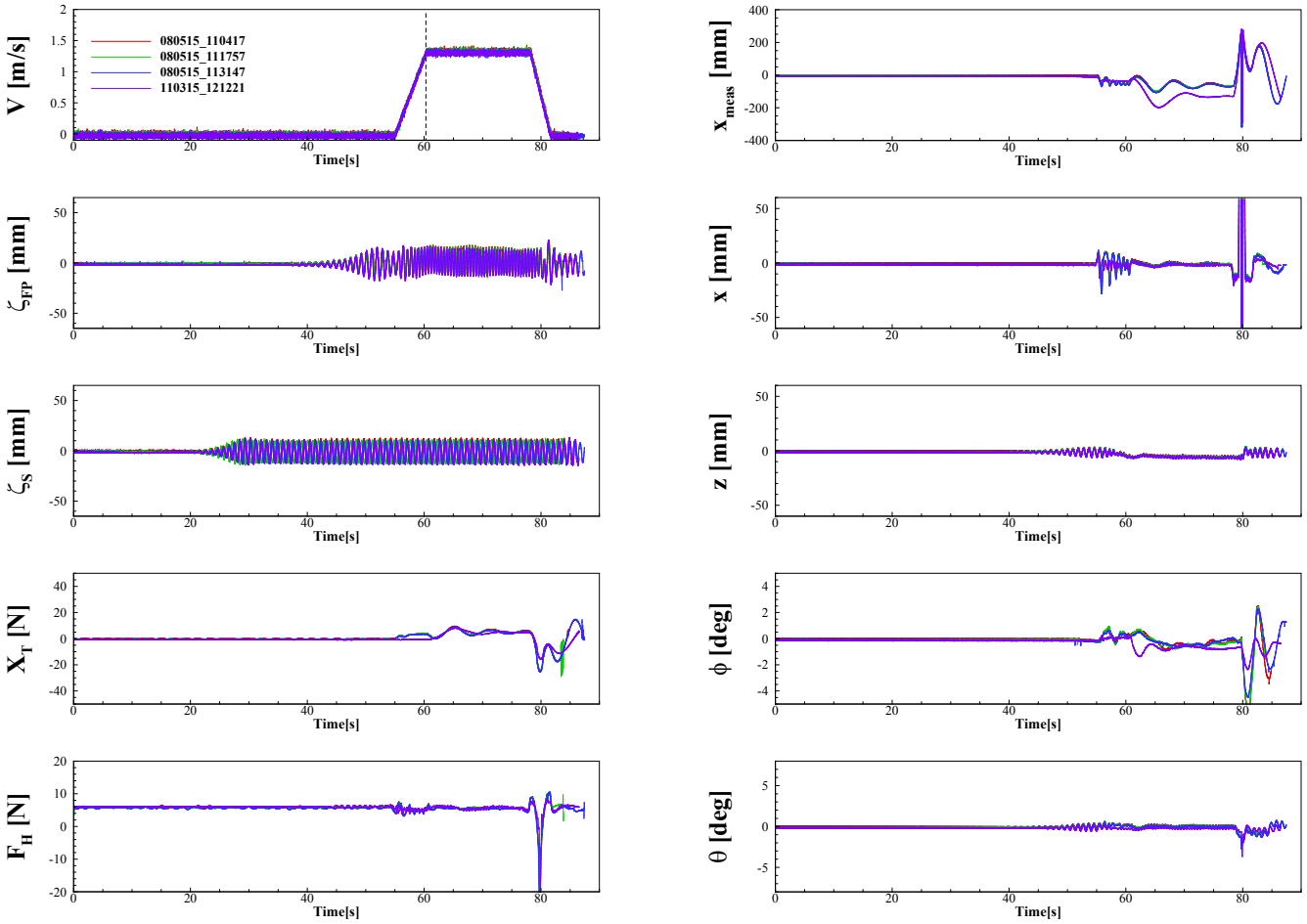

Figure C.1 Time Histories of measured and modified variables at Fr = 0.26, λ/L = 0.50, and χ = 0.0°

www.manaraa.com

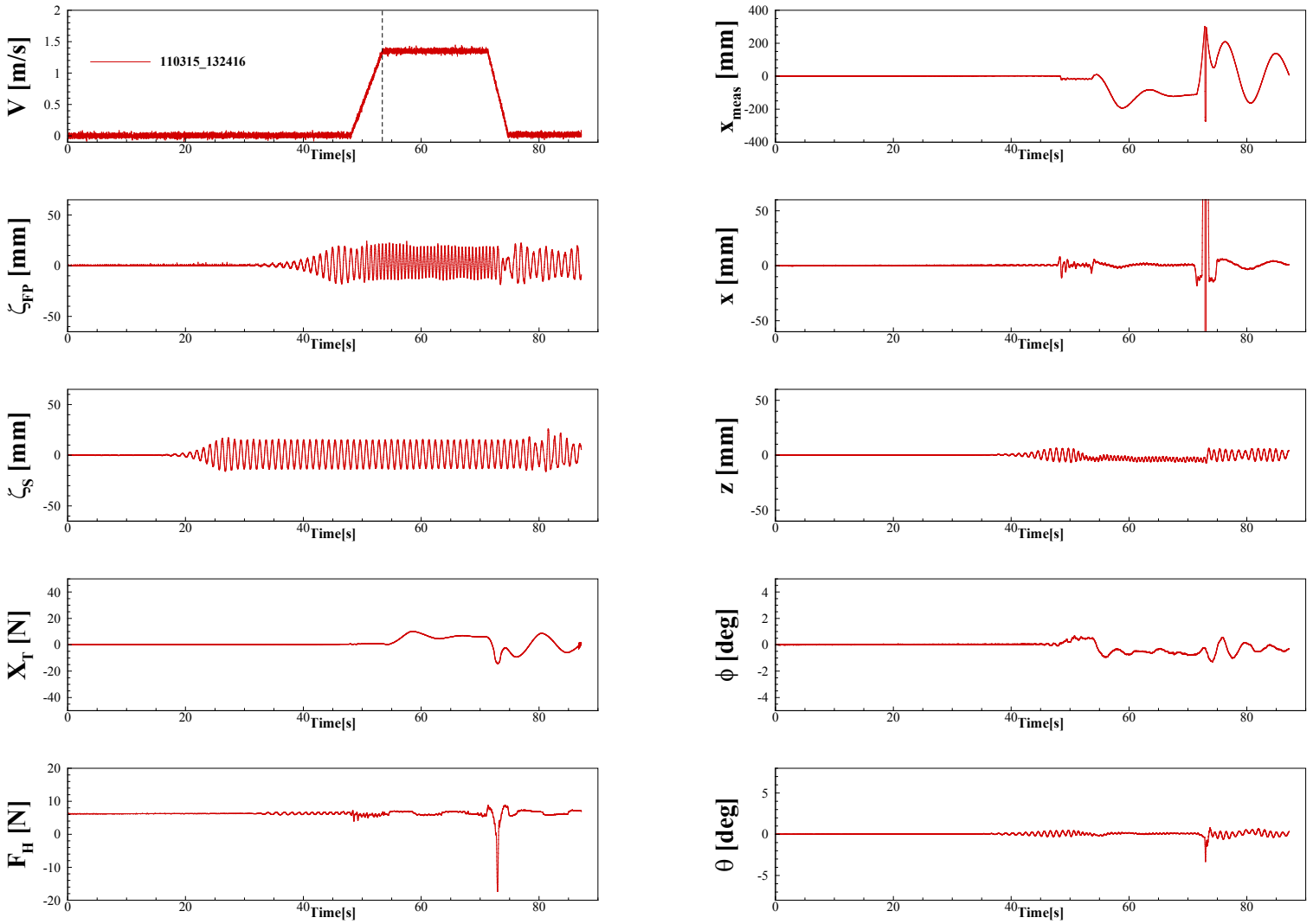

Figure C.2 Time Histories of measured and modified variables at Fr = 0.26, λ/L = 0.65, and χ = 0.0°

www.manaraa.com

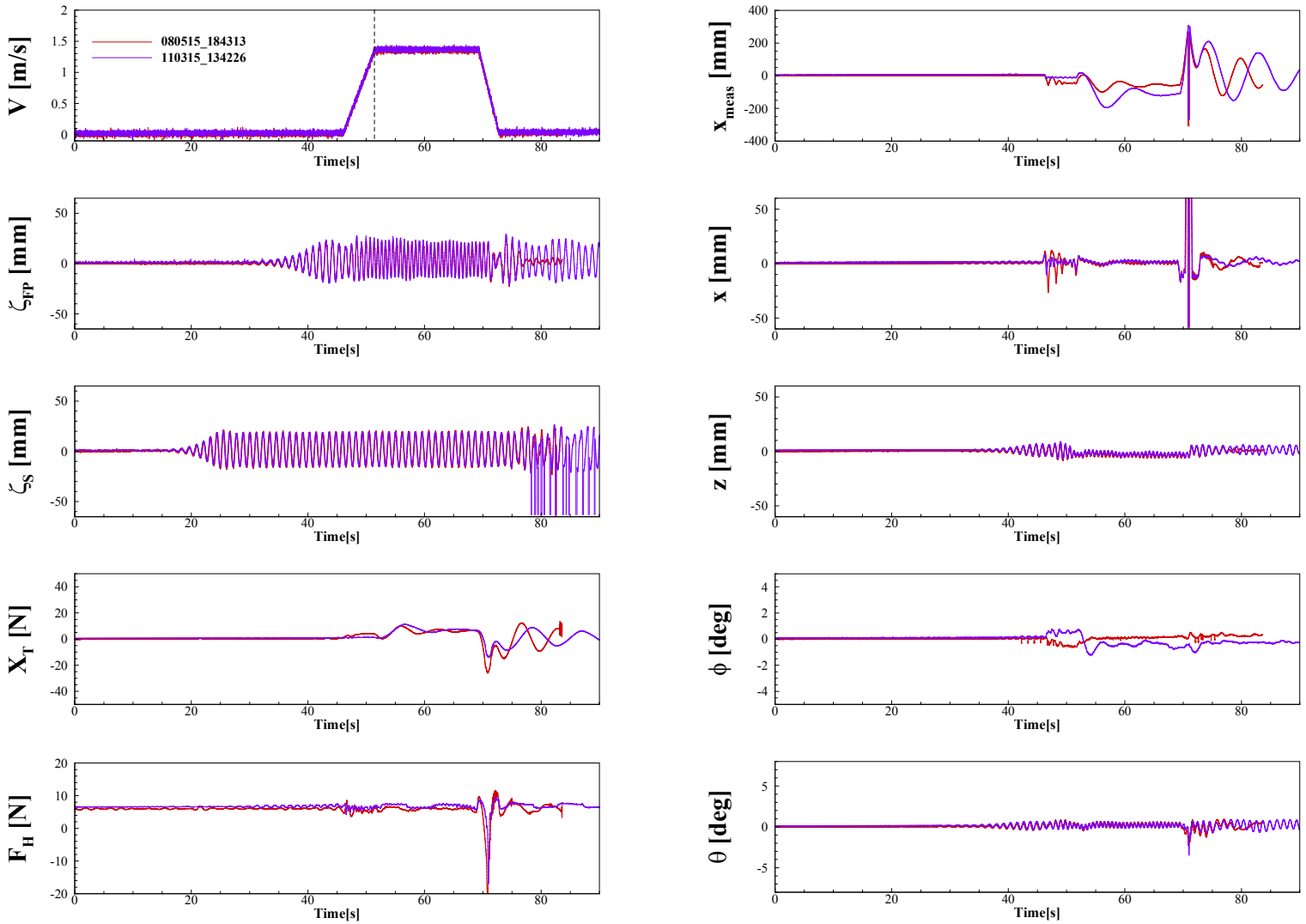

Figure C.3 Time Histories of measured and modified variables at Fr = 0.26, λ/L = 0.75, and χ = 0.0°

www.manaraa.com

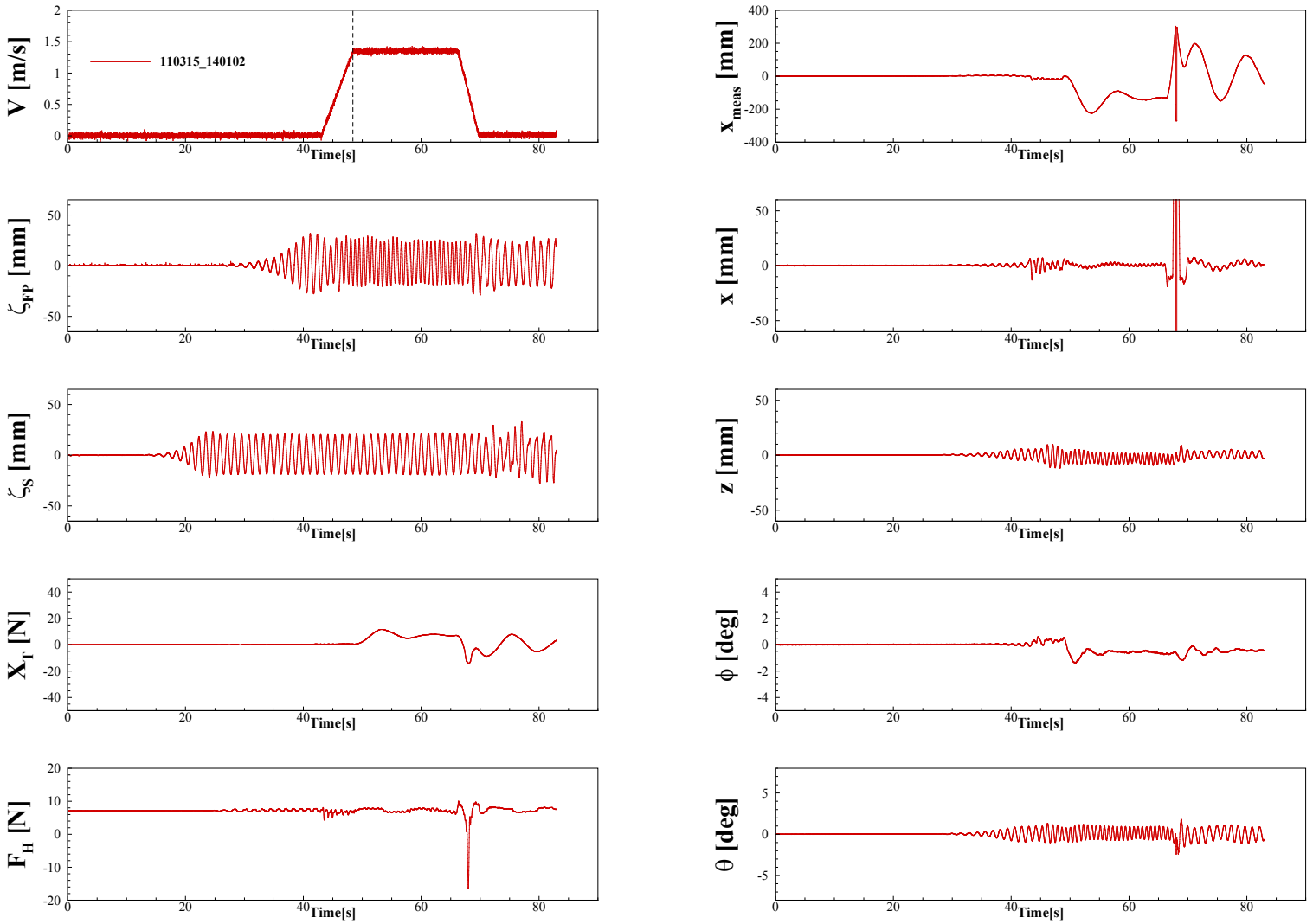

Figure C.4 Time Histories of measured and modified variables at Fr = 0.26, λ/L = 0.85, and χ = 0.0°

www.manaraa.com

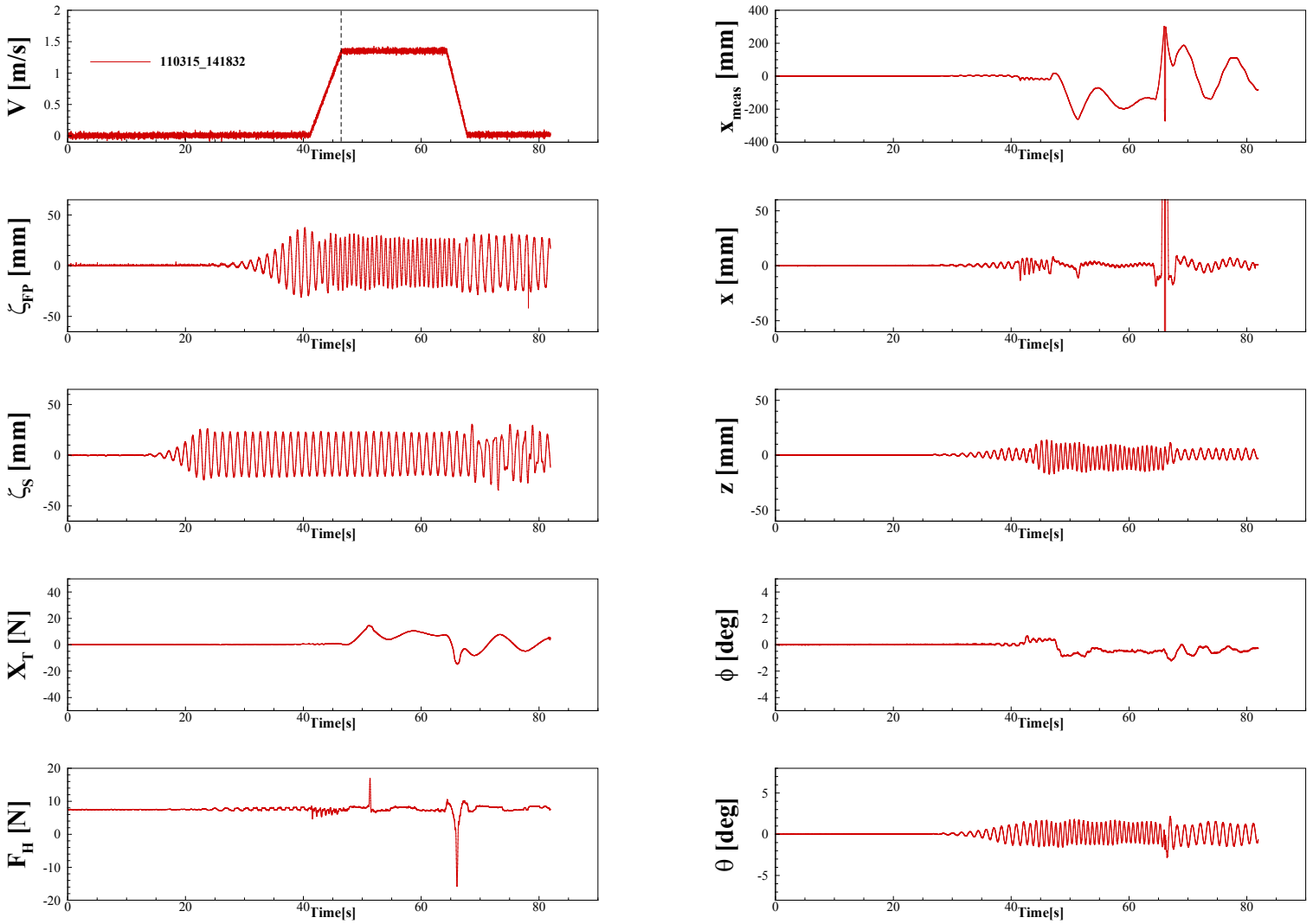

Figure C.5 Time Histories of measured and modified variables at Fr = 0.26, λ/L = 0.95, and χ = 0.0°

www.manaraa.com

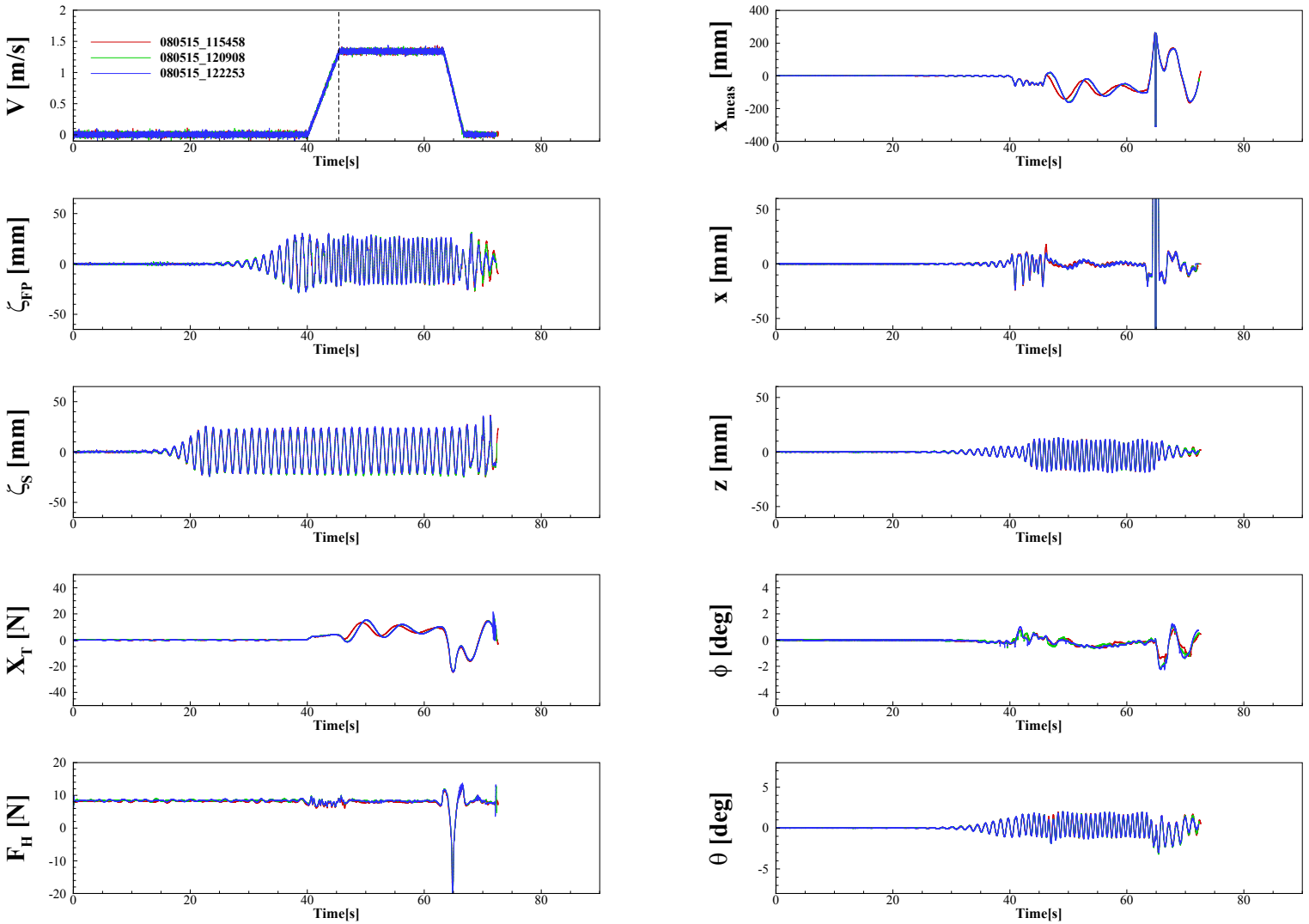

Figure C.6 Time Histories of measured and modified variables at Fr = 0.26, λ/L = 1.00, and χ = 0.0°

www.manaraa.com

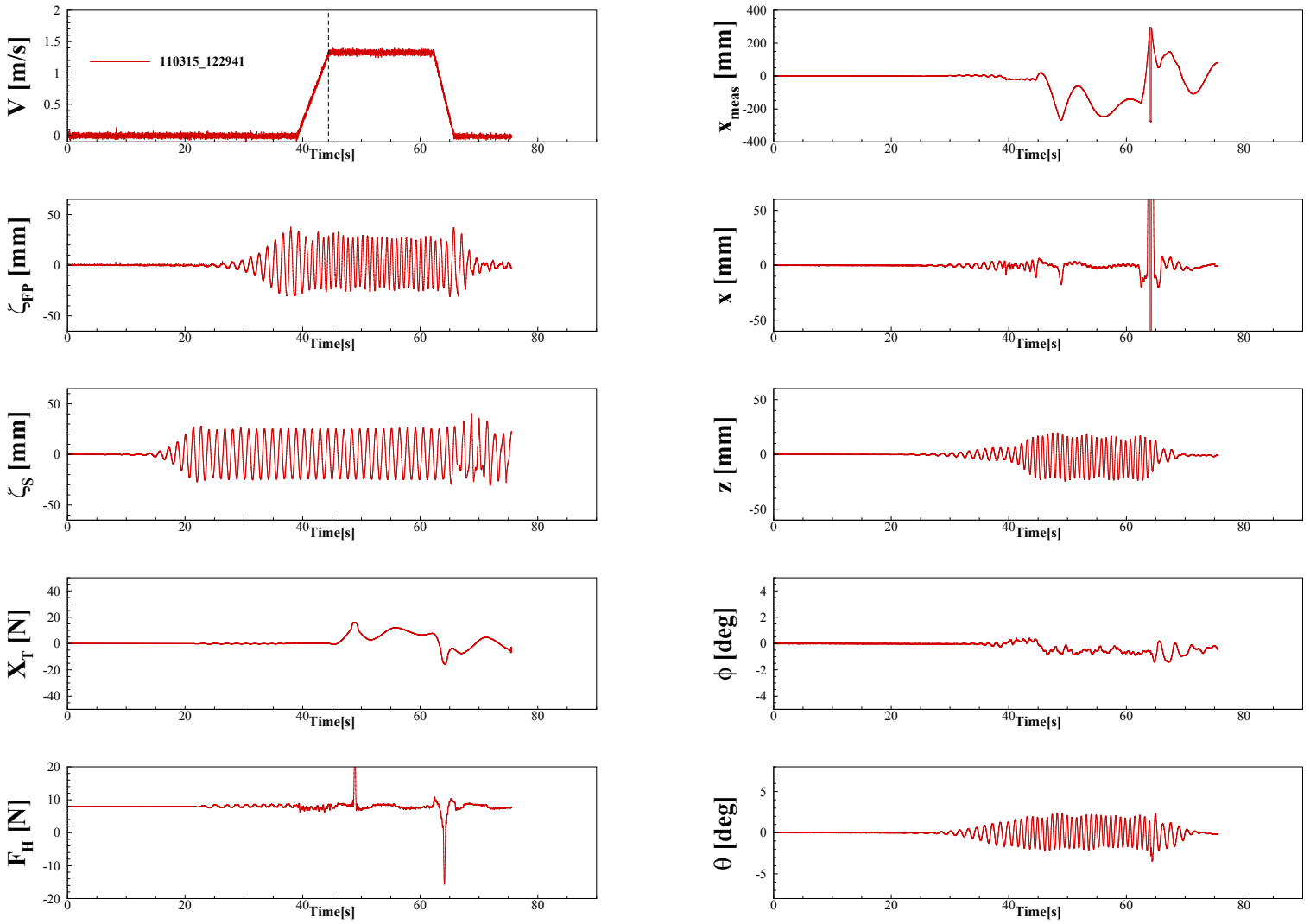

Figure C.7 Time Histories of measured and modified variables at Fr = 0.26, λ/L = 1.05, and χ = 0.0°

www.manaraa.com

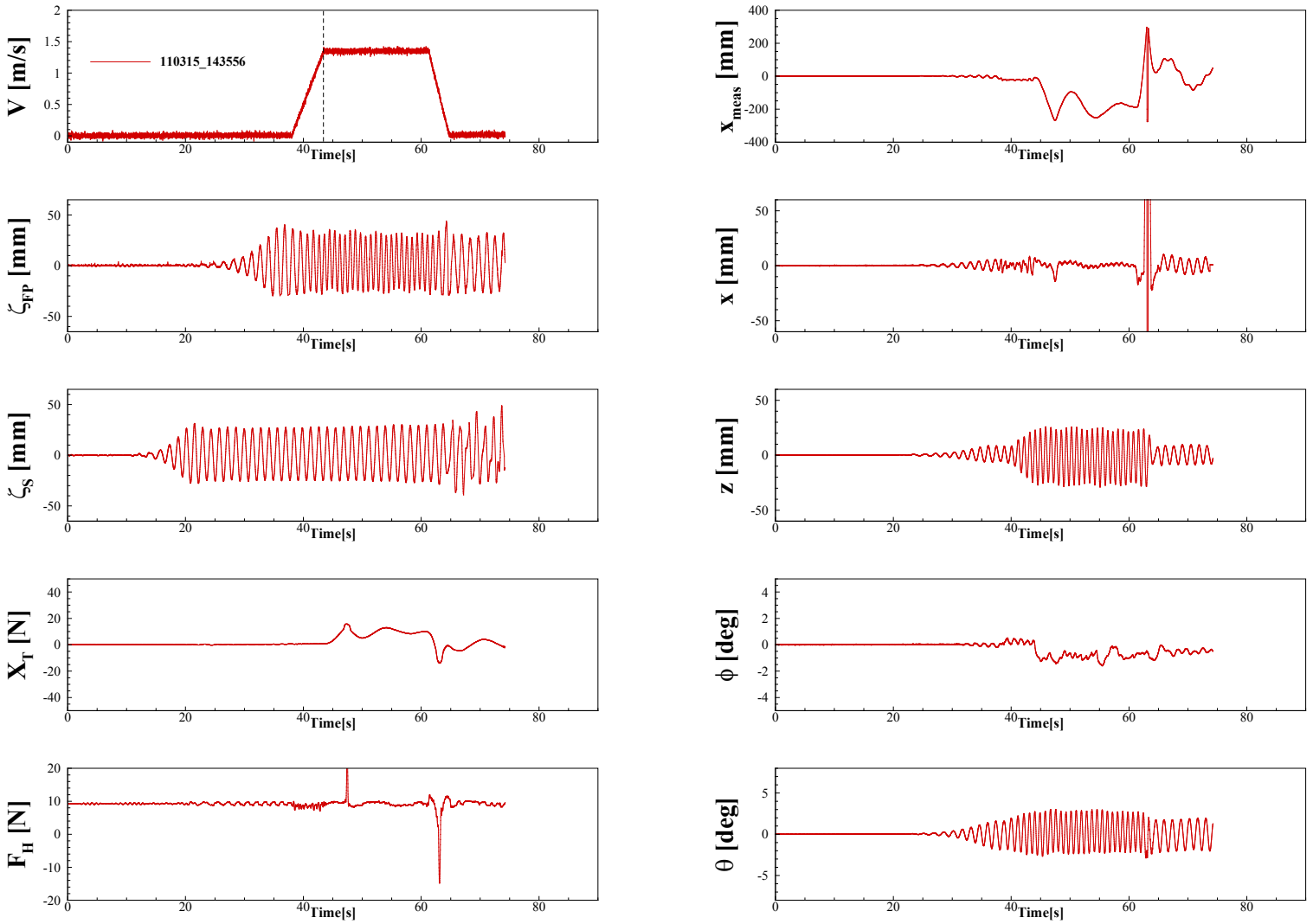

Figure C.8 Time Histories of measured and modified variables at Fr=0.26, λ/L=1.15, and χ=0.0°

www.manaraa.com

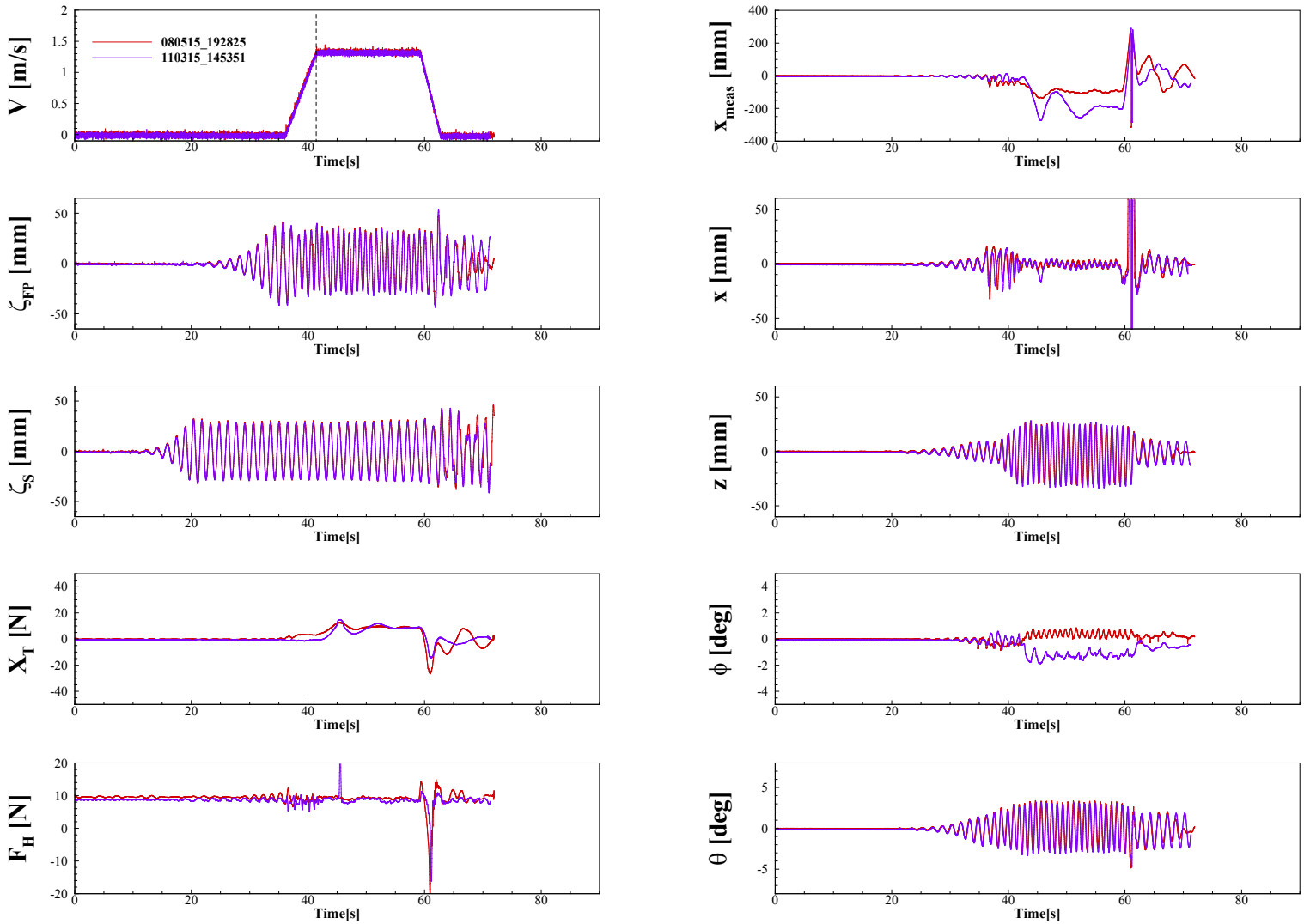

Figure C.9 Time Histories of measured and modified variables at Fr = 0.26, λ/L = 1.25, and χ = 0.0°

www.manaraa.com

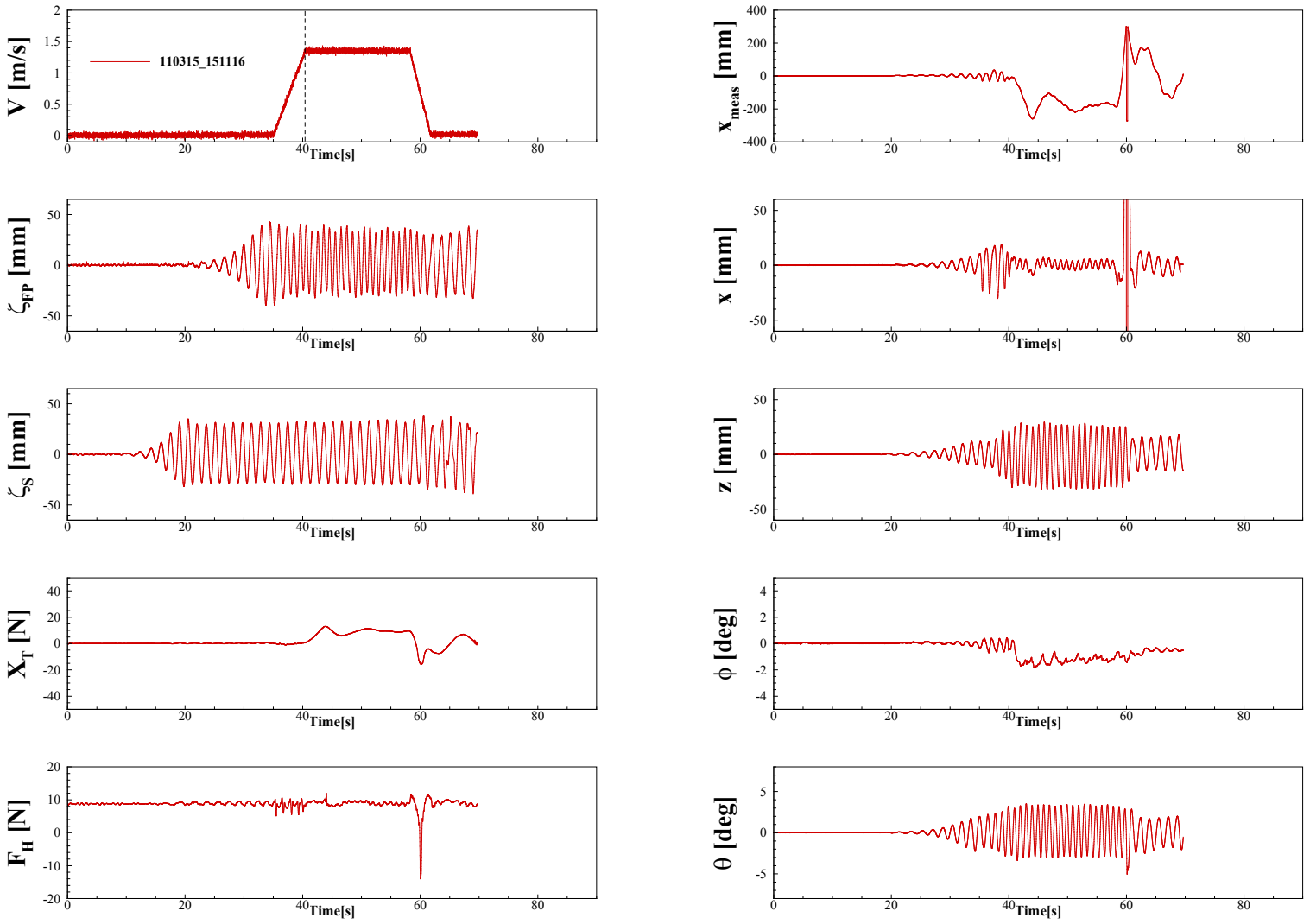

Figure C.10 Time Histories of measured and modified variables at Fr = 0.26, λ/L = 1.37, and χ = 0.0°

www.manaraa.com

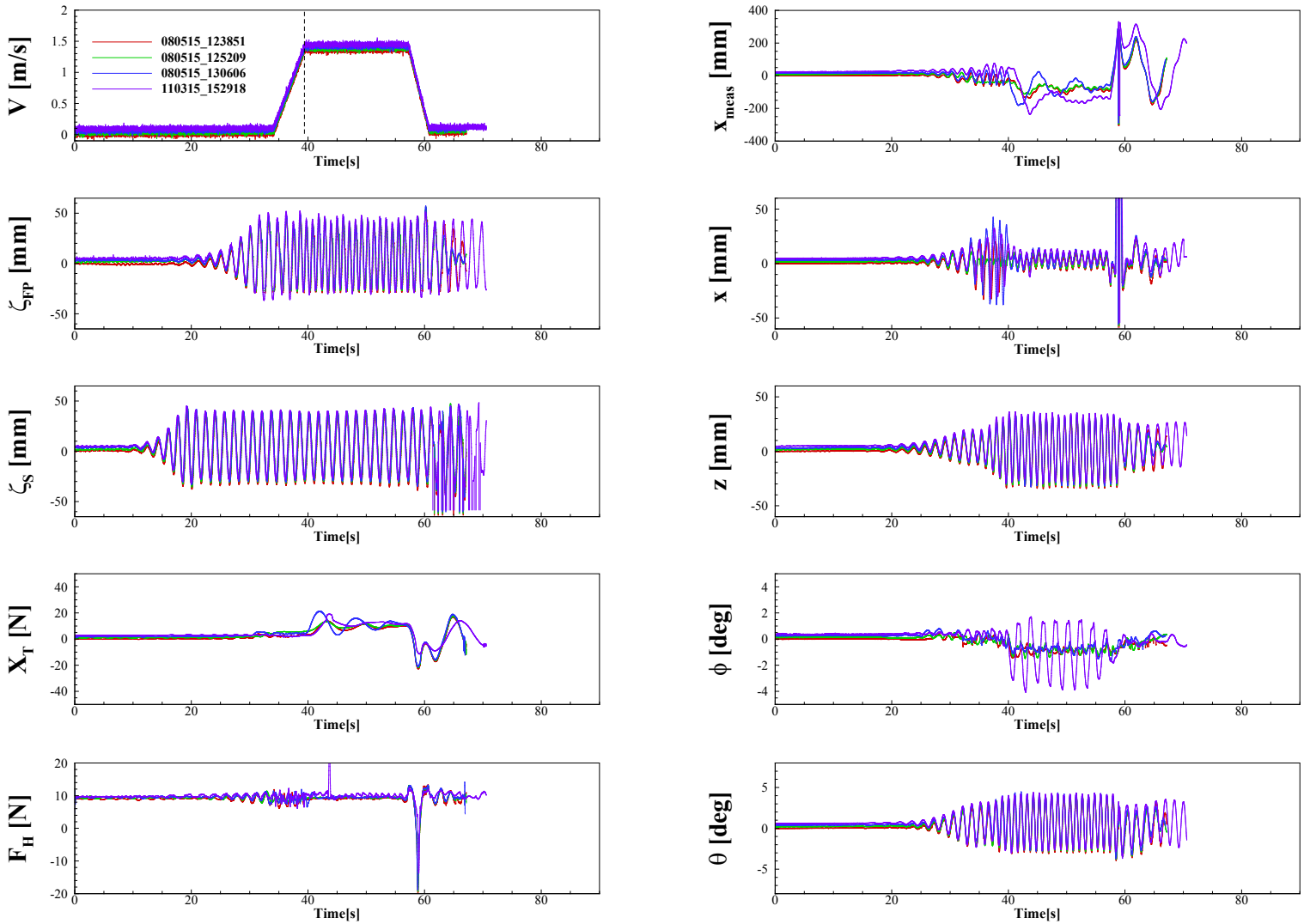

Figure C.11 Time Histories of measured and modified variables at Fr = 0.26, λ/L = 1.50, and χ = 0.0°

www.manaraa.com

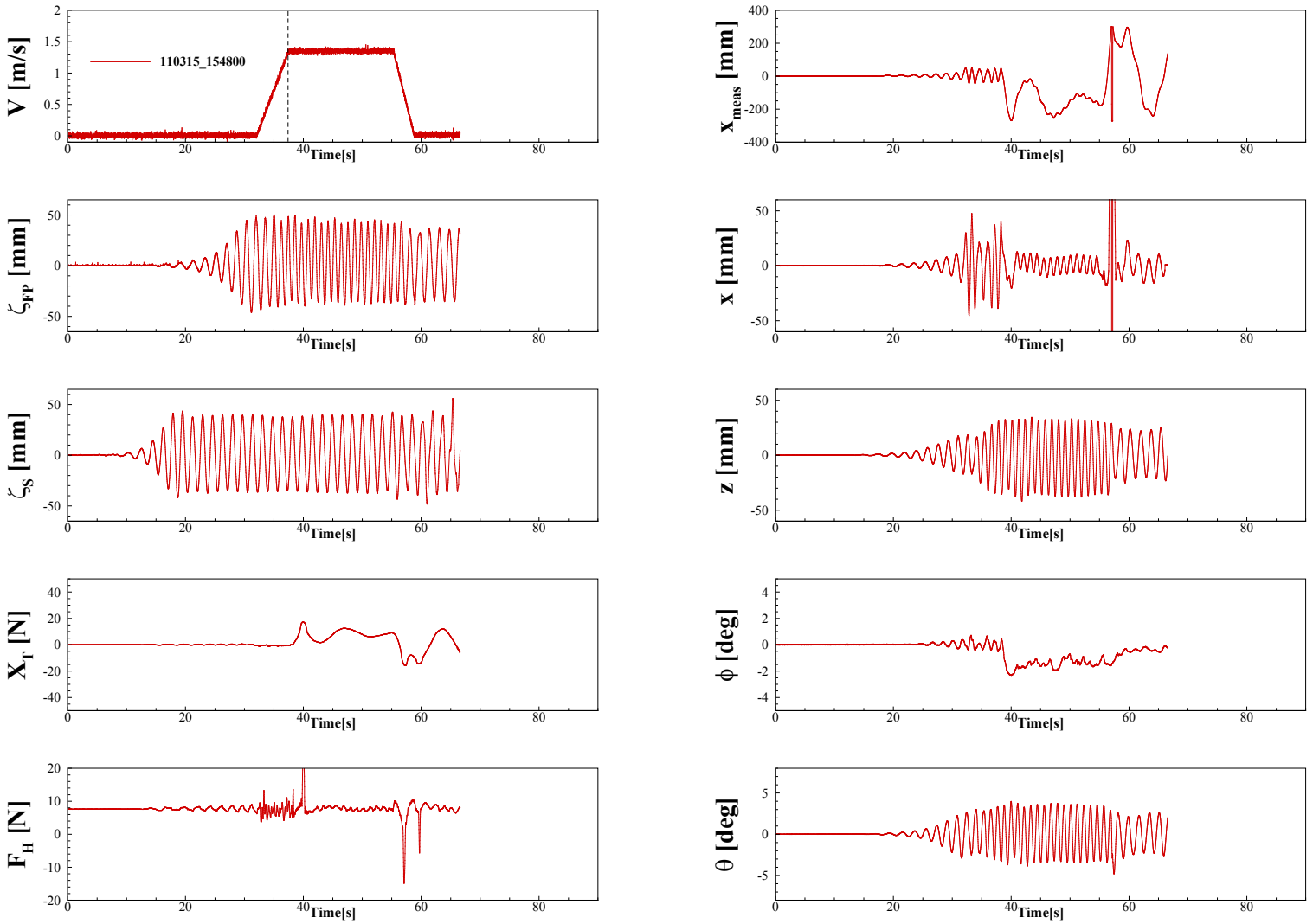

Figure C.12 Time Histories of measured and modified variables at Fr = 0.26, λ/L = 1.65, and χ = 0.0°

www.manaraa.com

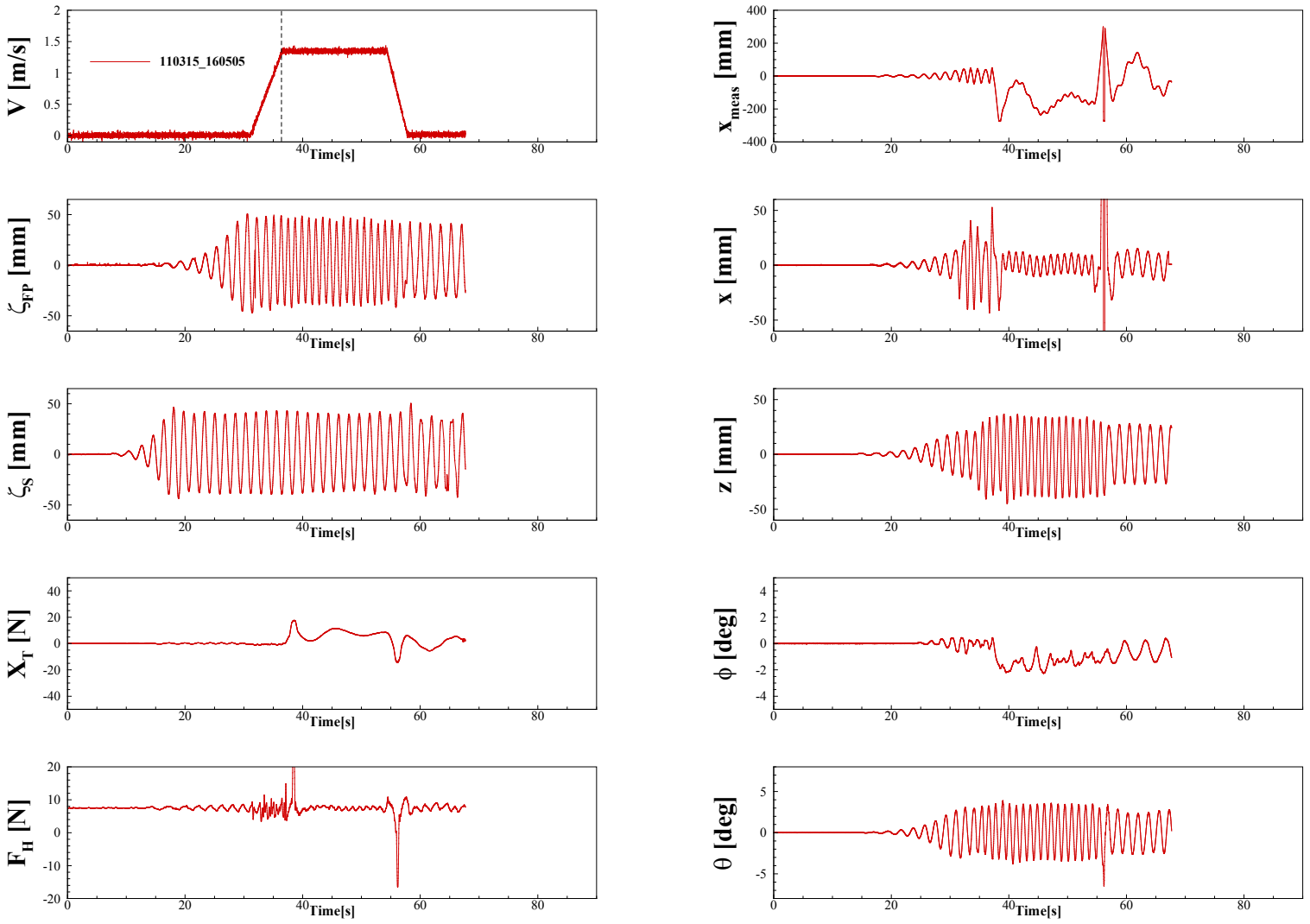

Figure C.13 Time Histories of measured and modified variables at Fr = 0.26, λ/L = 1.80, and χ = 0.0°

www.manaraa.com

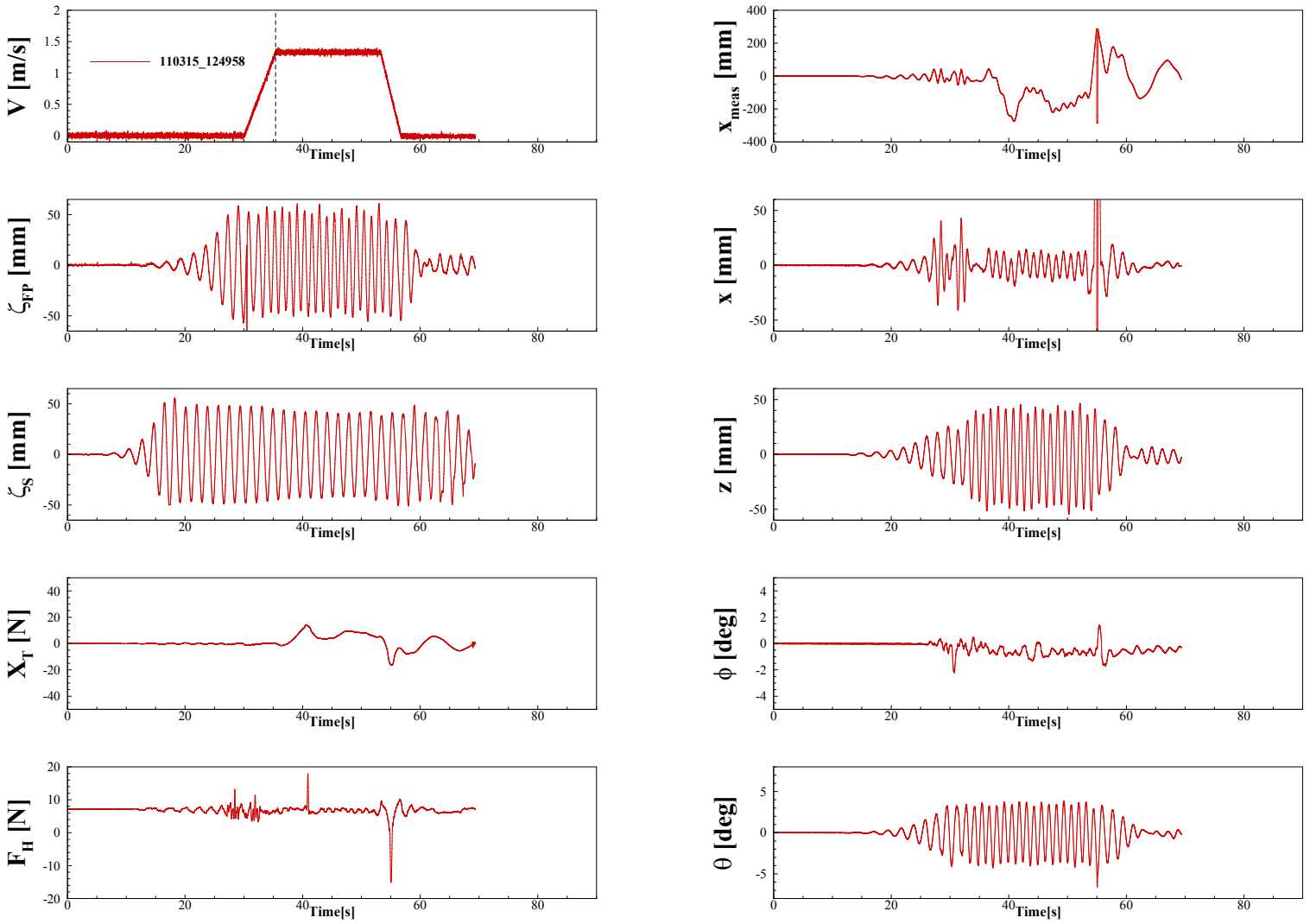

Figure C.14 Time Histories of measured and modified variables at Fr = 0.26, λ/L = 1.95, and χ = 0.0°

www.manaraa.com

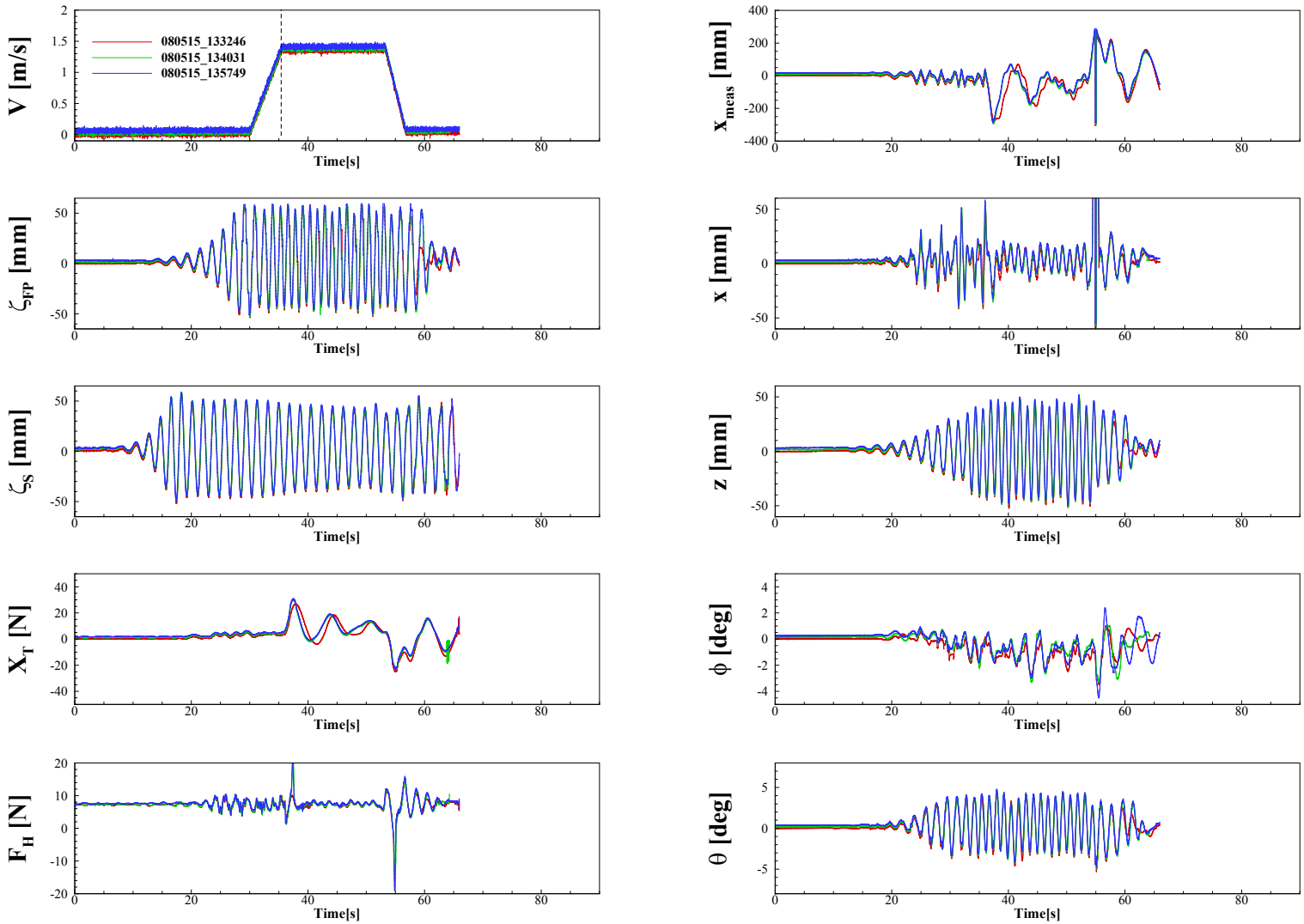

Figure C.15 Time Histories of measured and modified variables at Fr = 0.26, λ/L = 2.00, and χ = 0.0°

www.manaraa.com

C.2 Time Histories of Wave Cases, $\chi = 45^{o}$

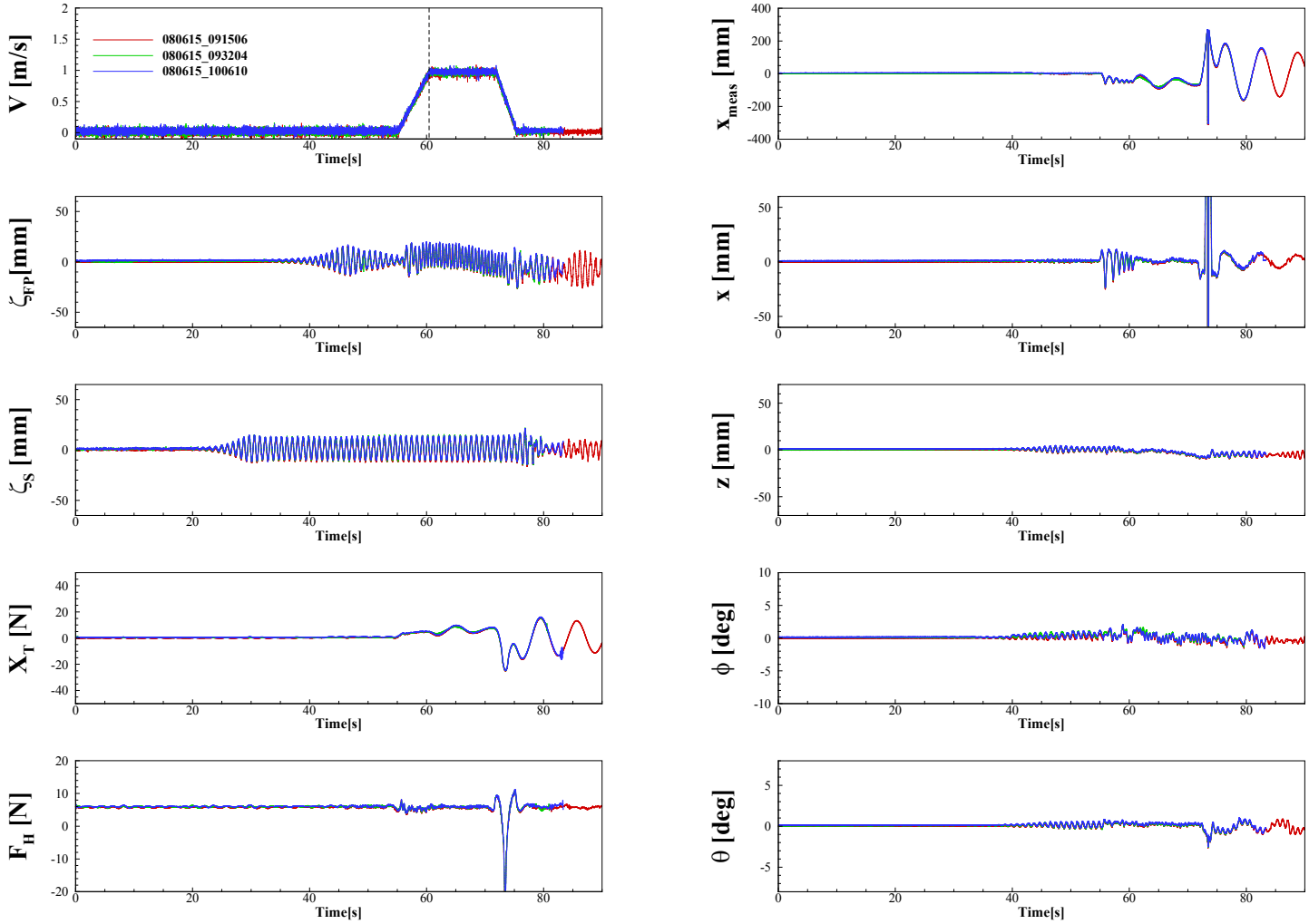

Figure C.16 Time Histories of measured and modified variables at Fr = 0.26, λ/L = 0.50, and $\chi = 45.0°$

www.manaraa.com

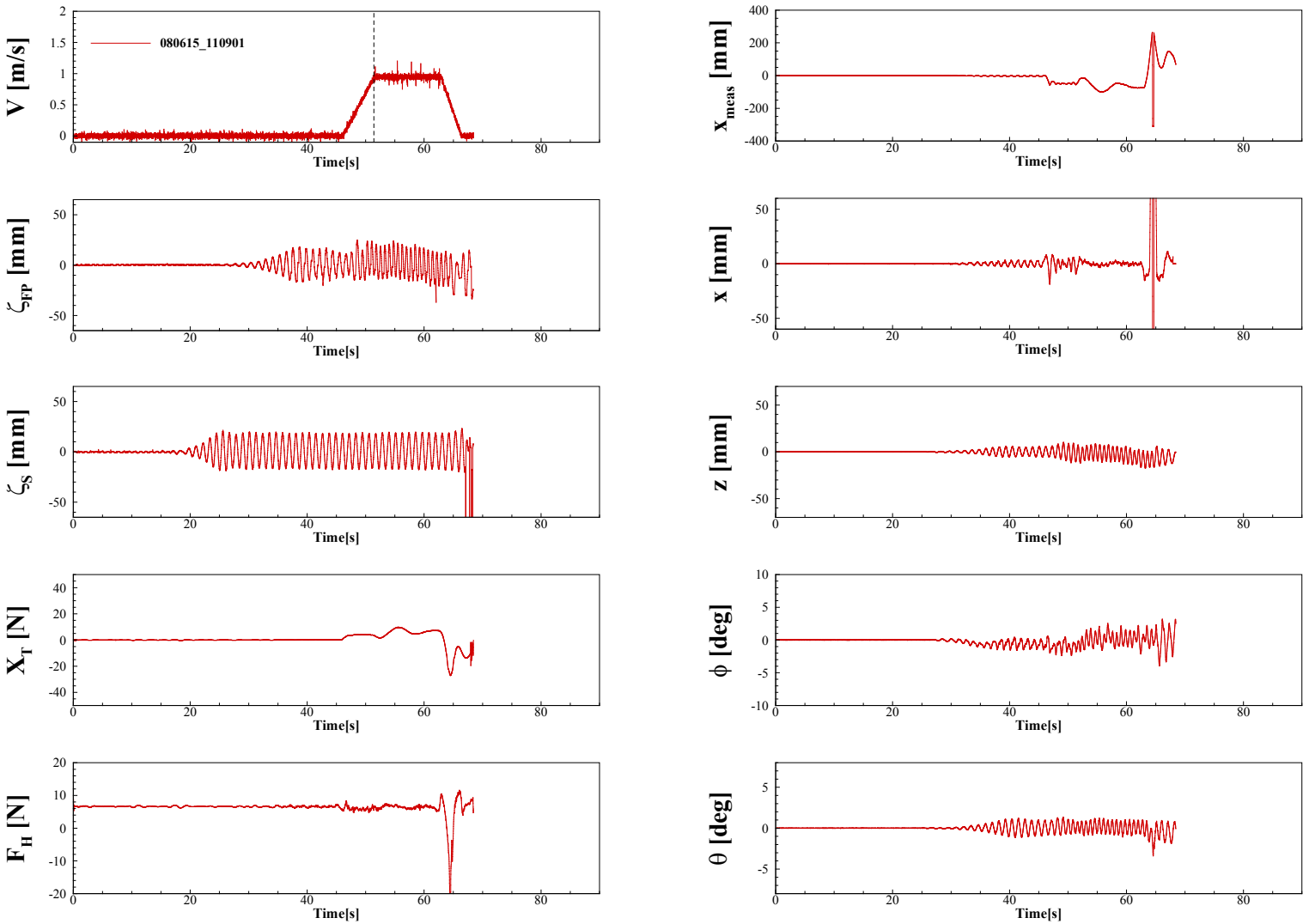

Figure C.17 Time Histories of measured and modified variables at Fr = 0.26, λ/L = 0.75, and χ = 45.0°

www.manaraa.com

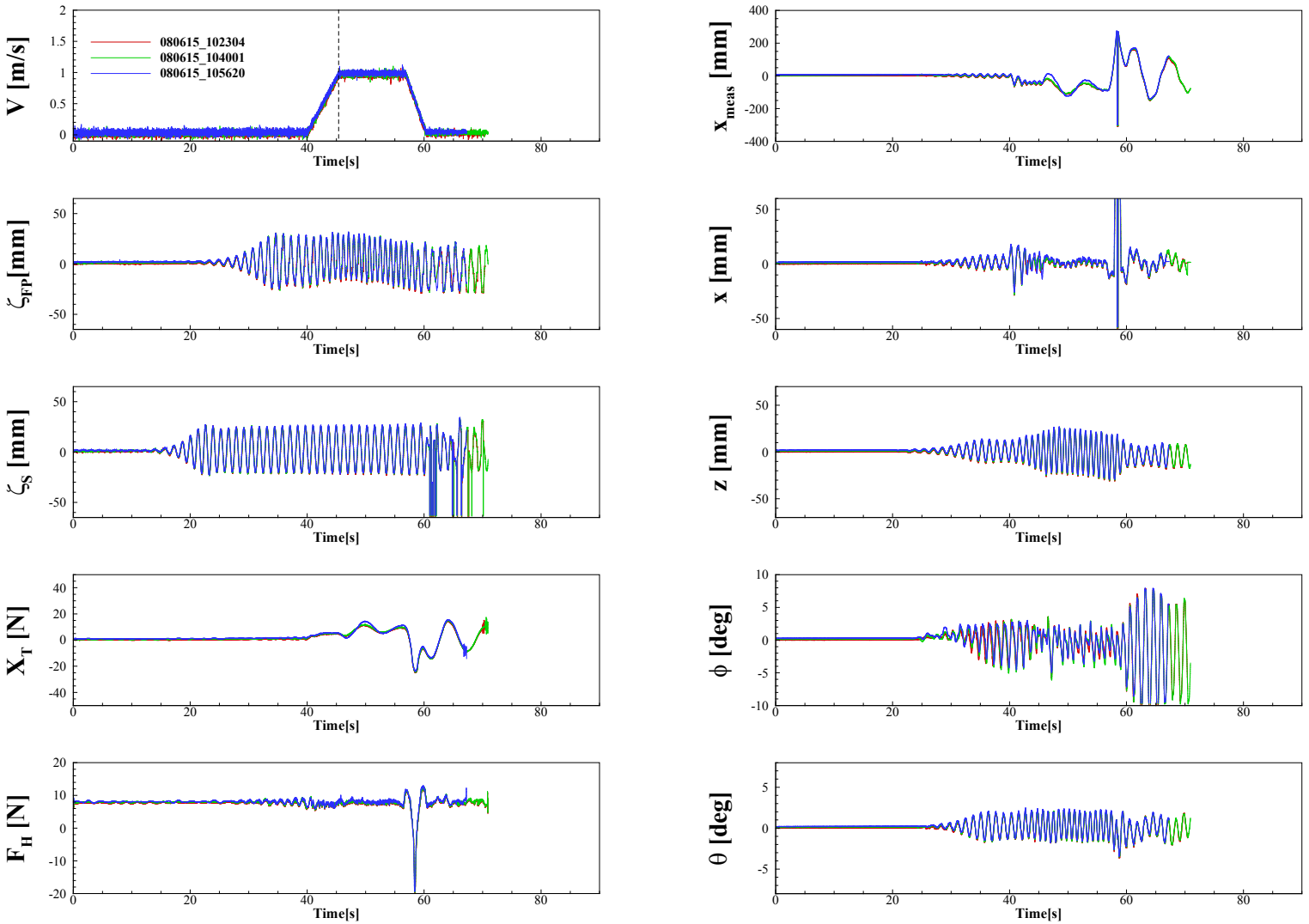

Figure C.18 Time Histories of measured and modified variables at Fr = 0.26, λ/L = 1.00, and χ = 45.0°

www.manaraa.com

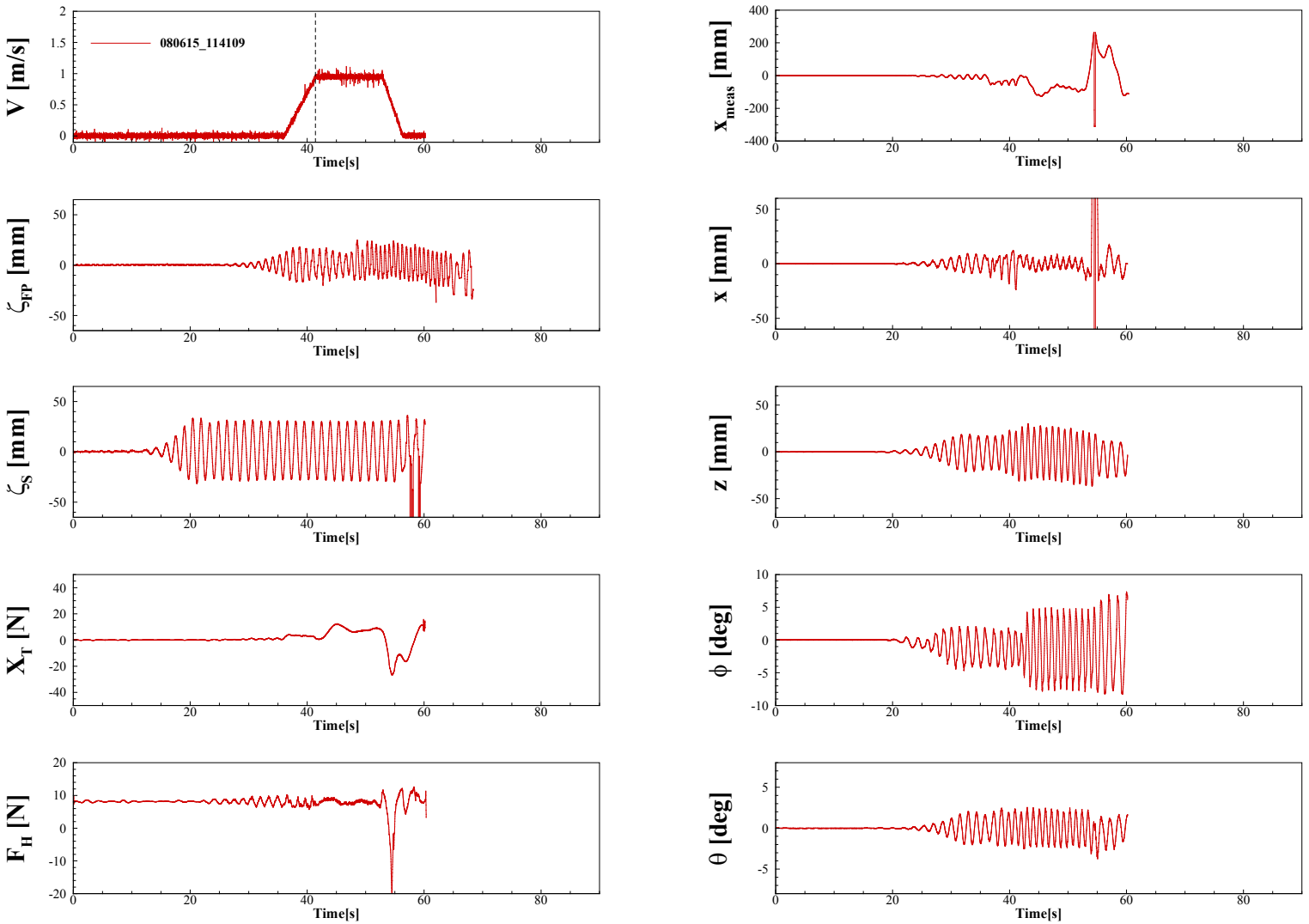

Figure C.19 Time Histories of measured and modified variables at Fr = 0.26, λ/L = 1.25, and χ = 45.0°

www.manaraa.com

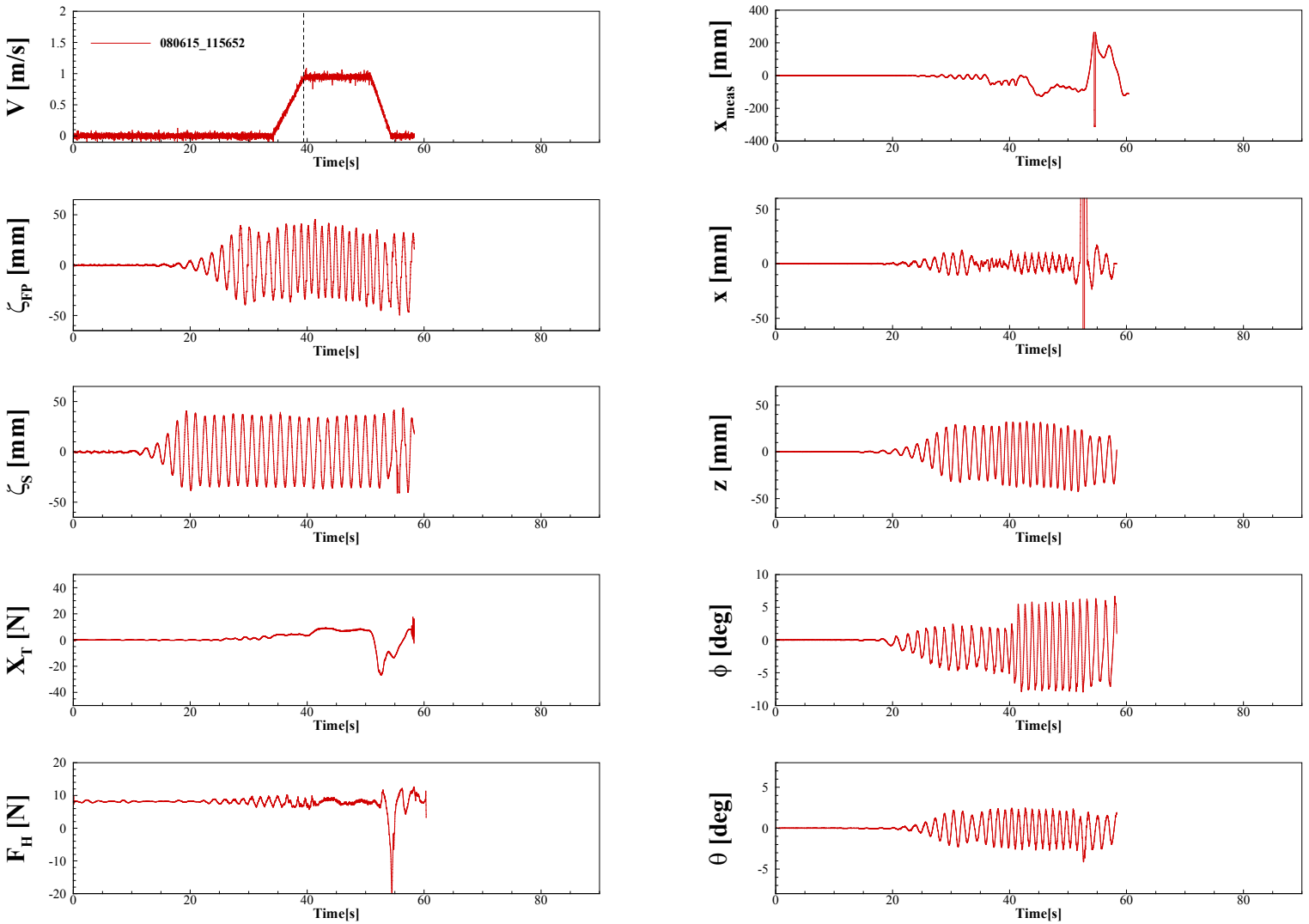

Figure C.20 Time Histories of measured and modified variables at Fr = 0.26, λ/L = 1.50, and χ = 45.0°

www.manaraa.com

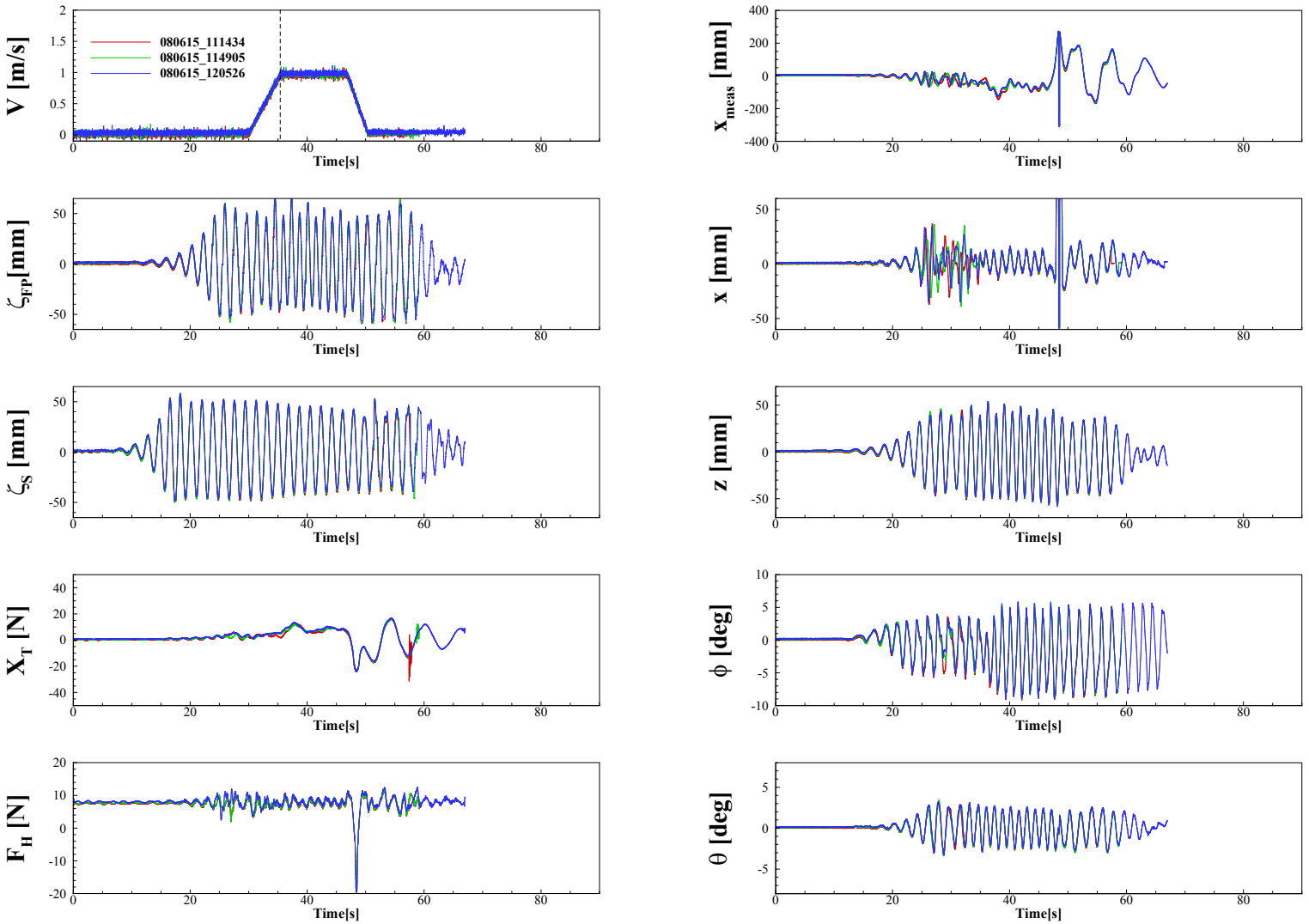

Figure C.21 Time Histories of measured and modified variables at Fr = 0.26, λ/L = 2.00, and χ = 45.0°

www.manaraa.com

C.3 Time Histories of Wave Cases, $\chi = 90^{o}$

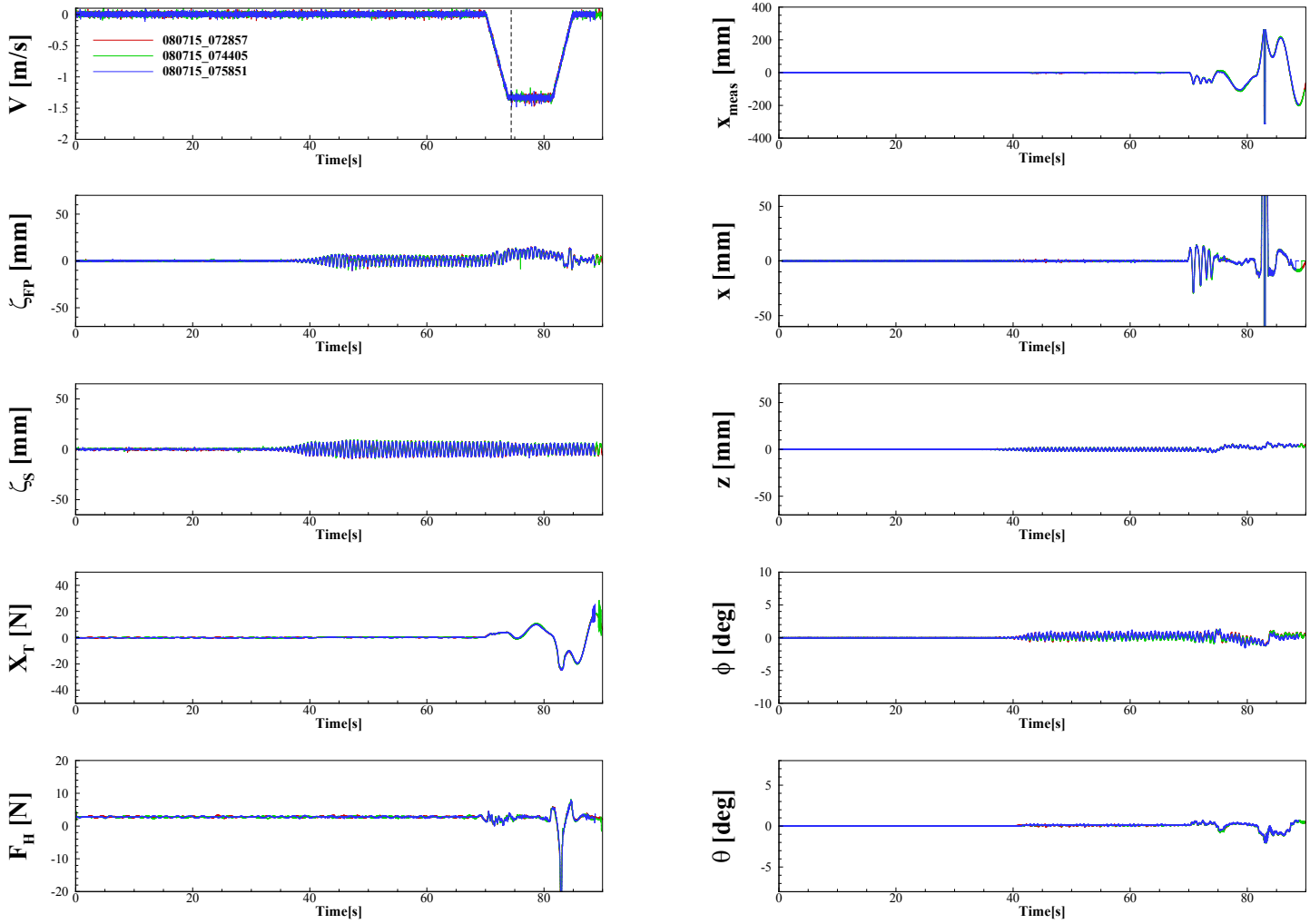

Figure C.22 Time Histories of measured and modified variables at Fr = 0.26, λ/L = 0.25, and $\chi = 90.0°$

www.manaraa.com

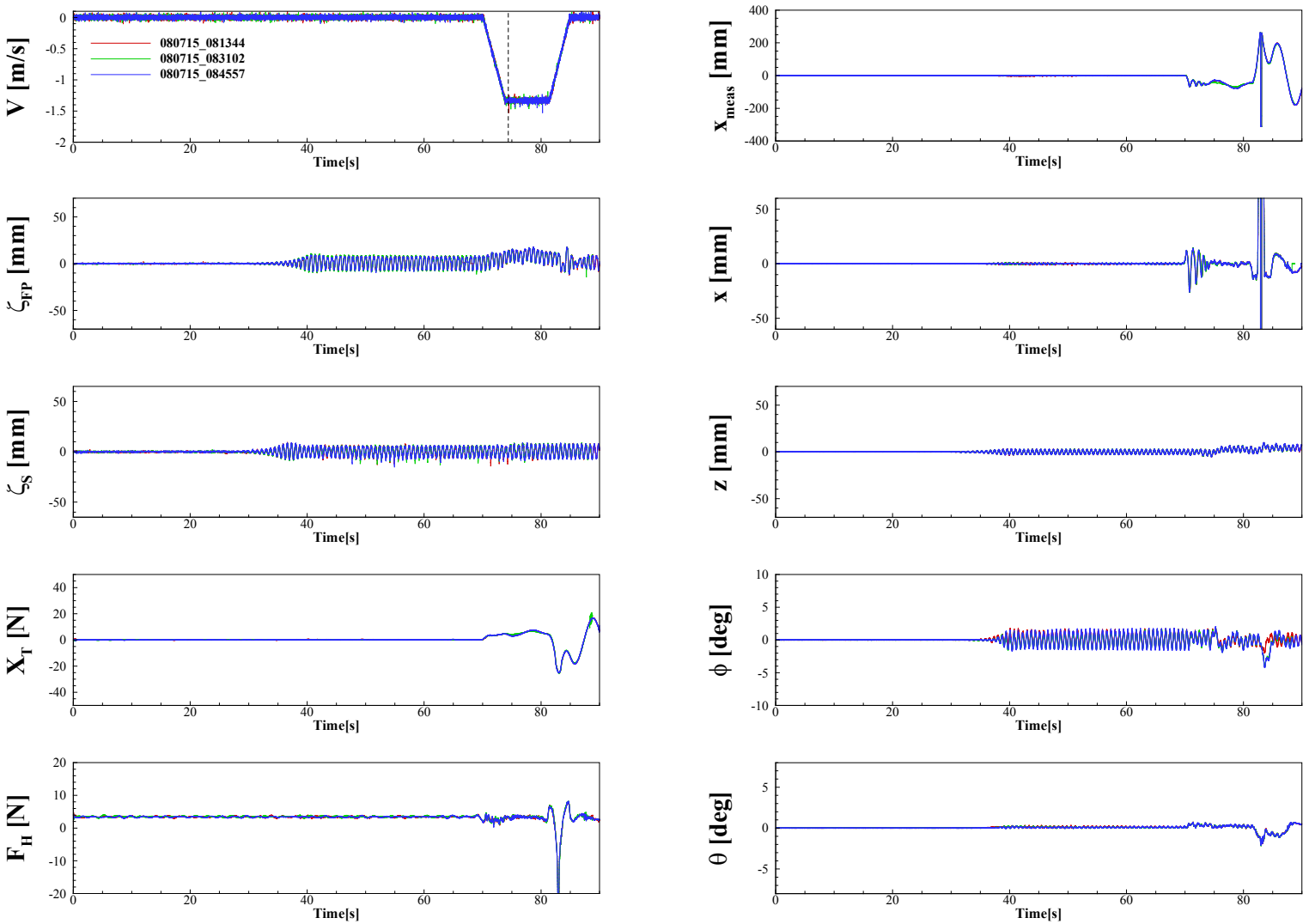

Figure C.23 Time Histories of measured and modified variables at Fr = 0.26, λ/L = 0.30, and χ = 90.0°

www.manaraa.com

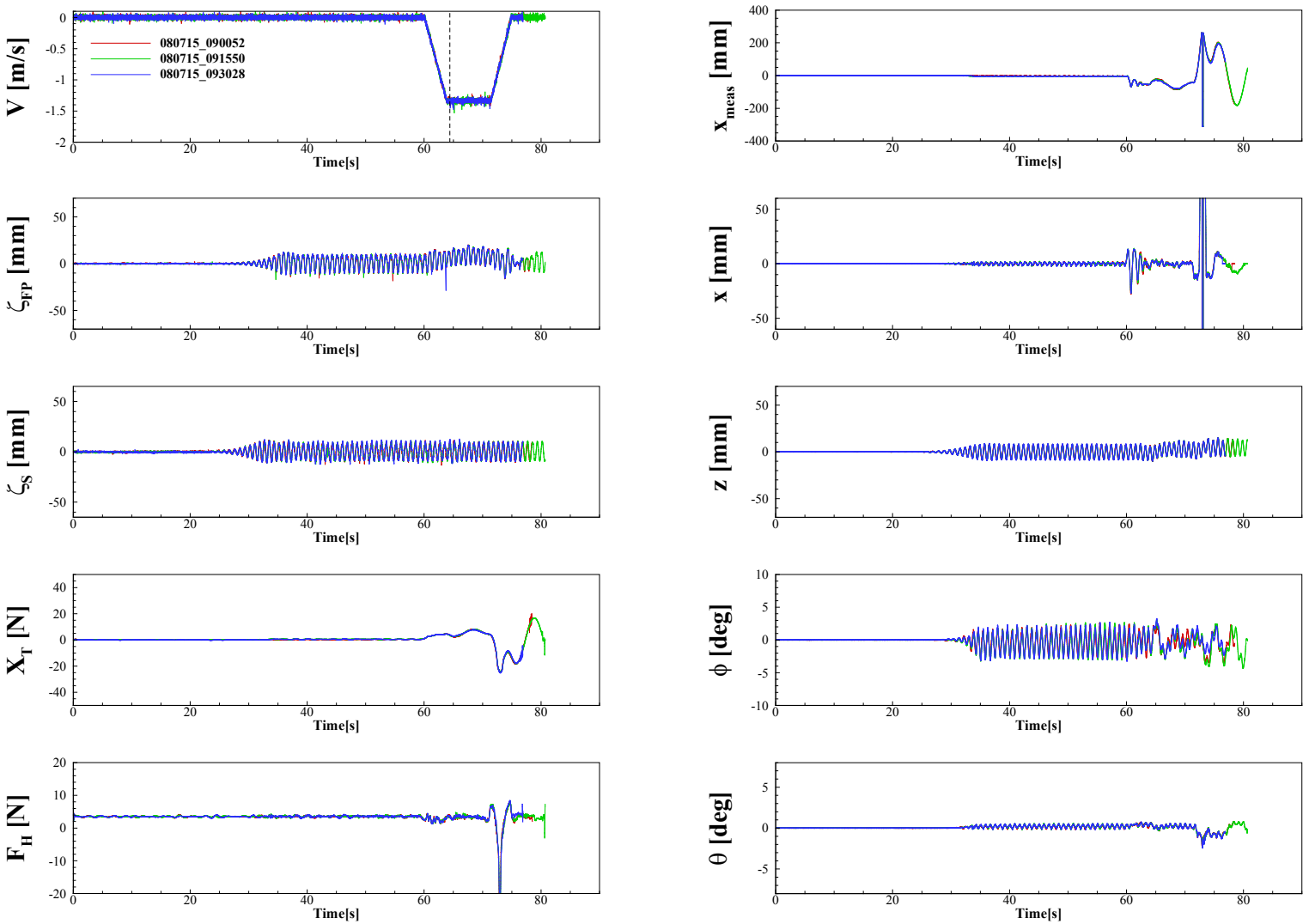

Figure C.24 Time Histories of measured and modified variables at Fr = 0.26, λ/L = 0.40, and χ = 90.0°

www.manaraa.com

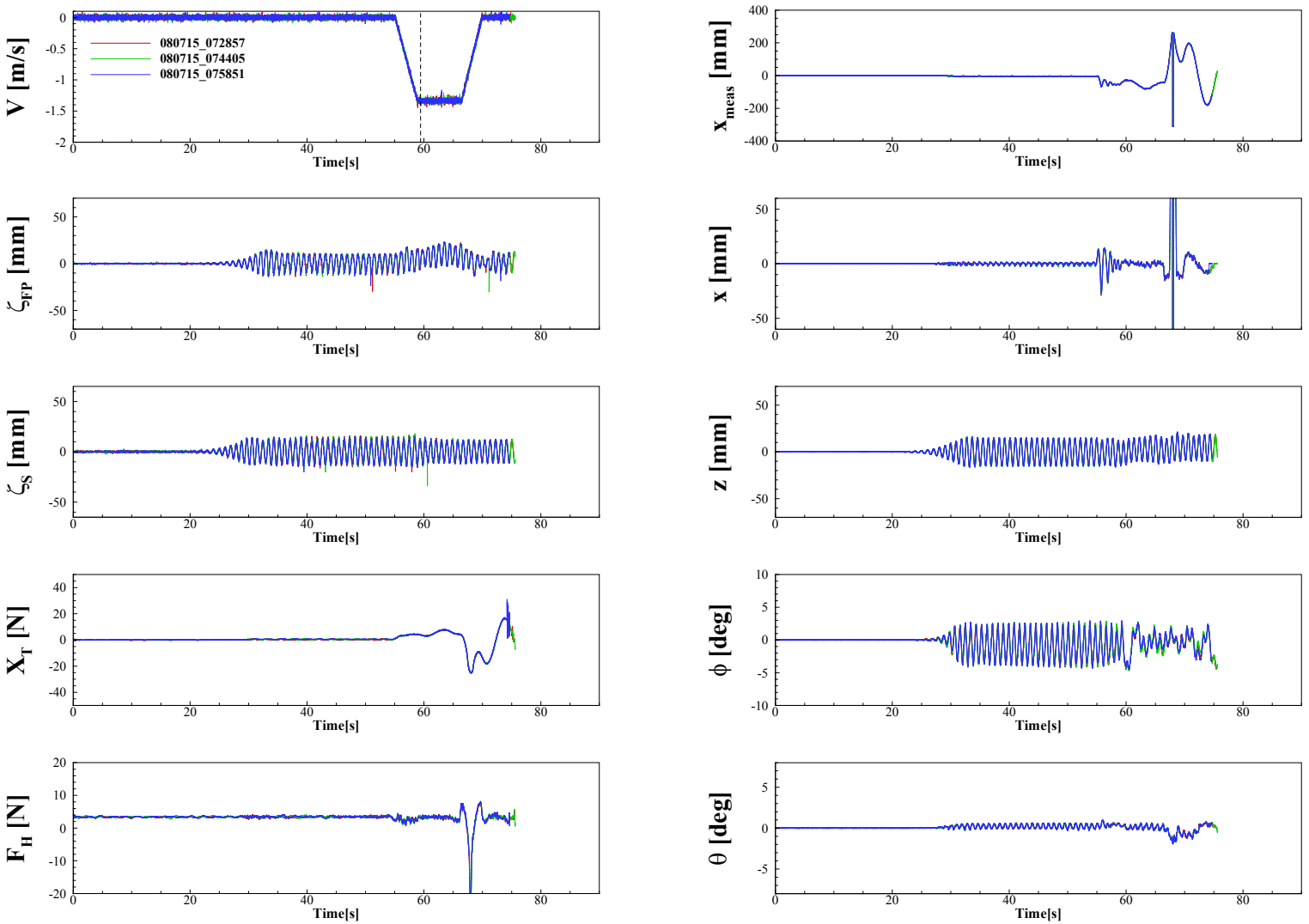

Figure C.25 Time Histories of measured and modified variables at Fr = 0.26, λ/L = 0.50, and χ = 90.0°

www.manaraa.com

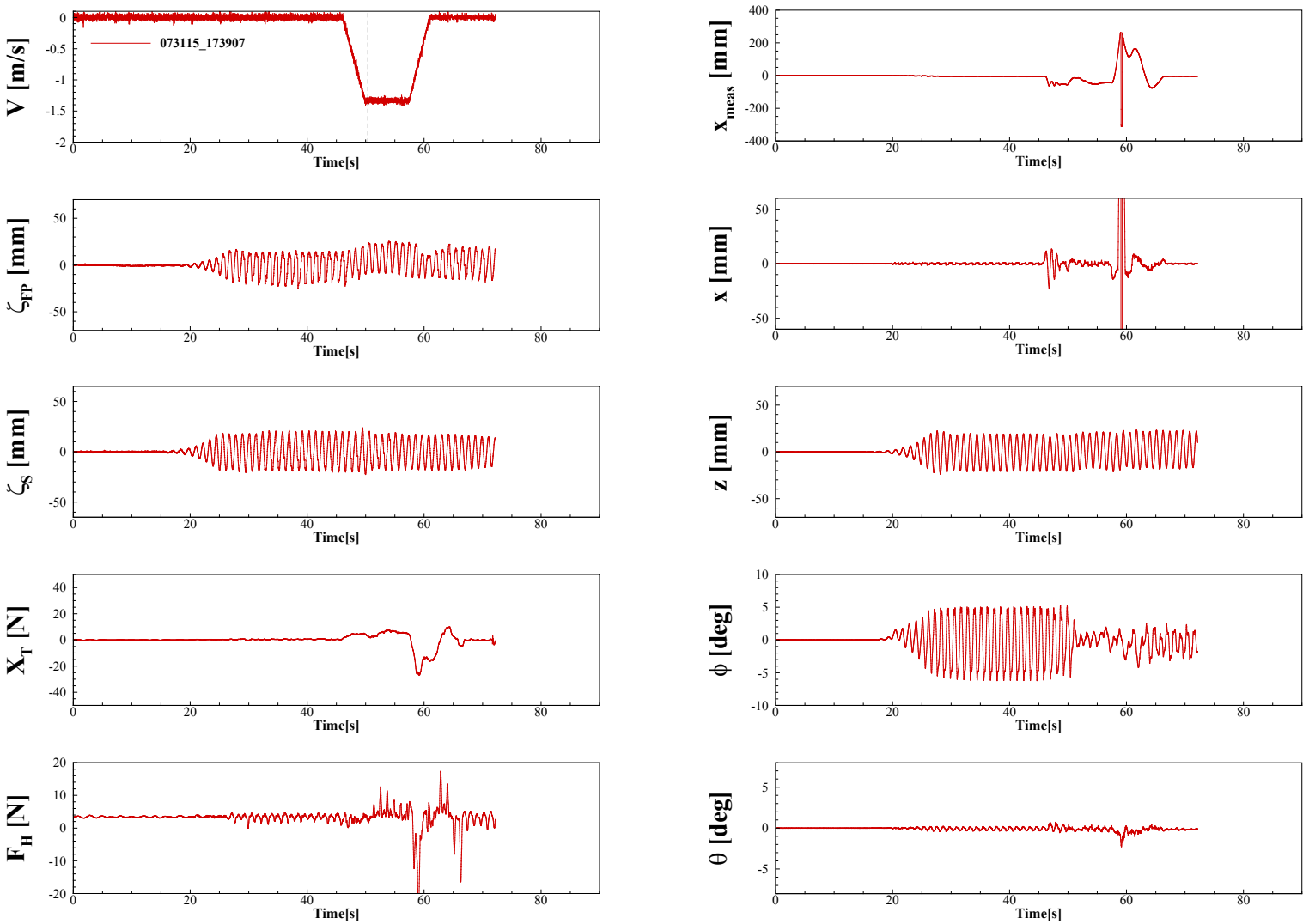

Figure C.26 Time Histories of measured and modified variables at Fr = 0.26, λ/L = 0.75, and χ = 90.0°

www.manaraa.com

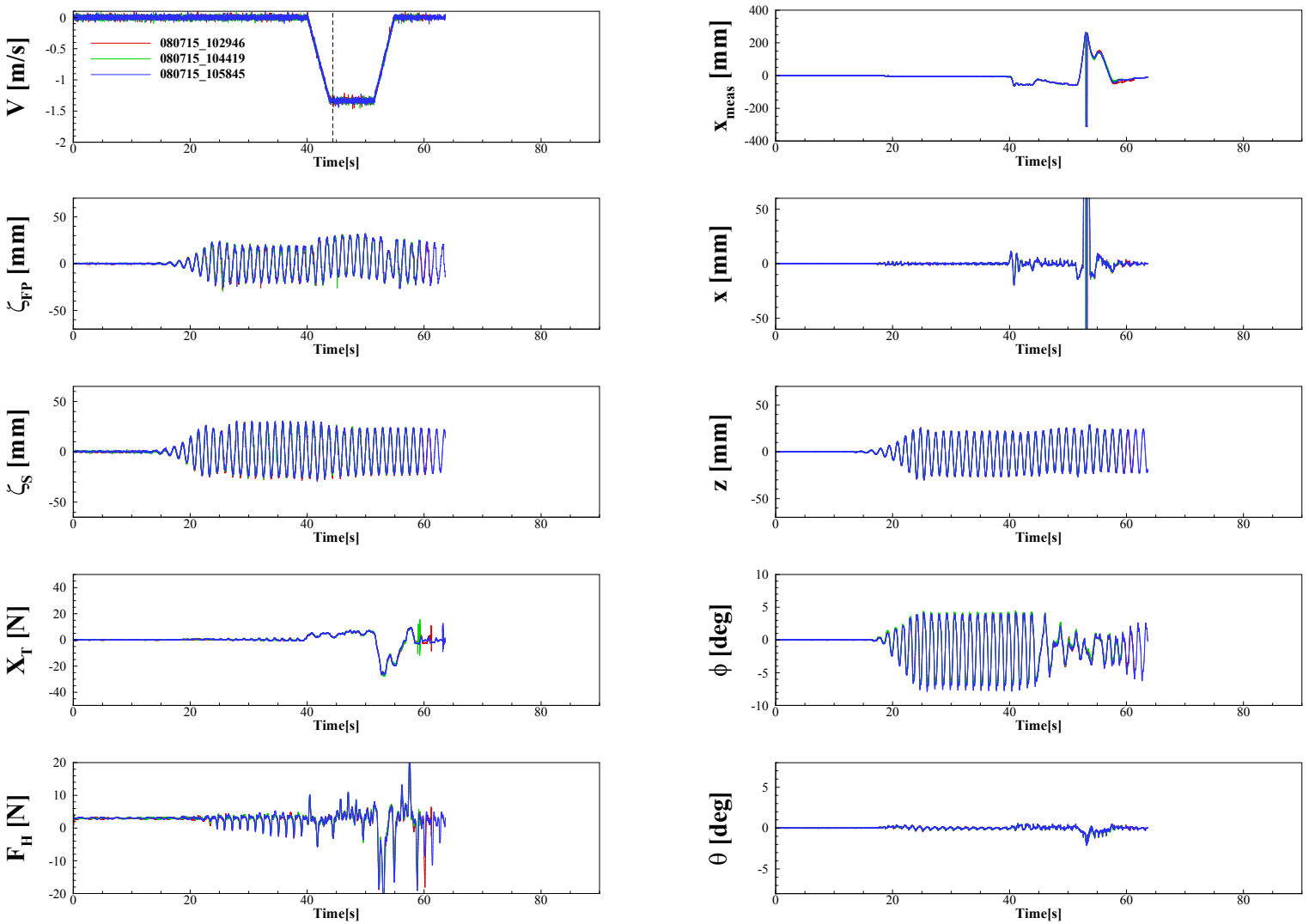

Figure C.27 Time Histories of measured and modified variables at Fr = 0.26, λ/L = 1.00, and χ = 90.0°

www.manaraa.com

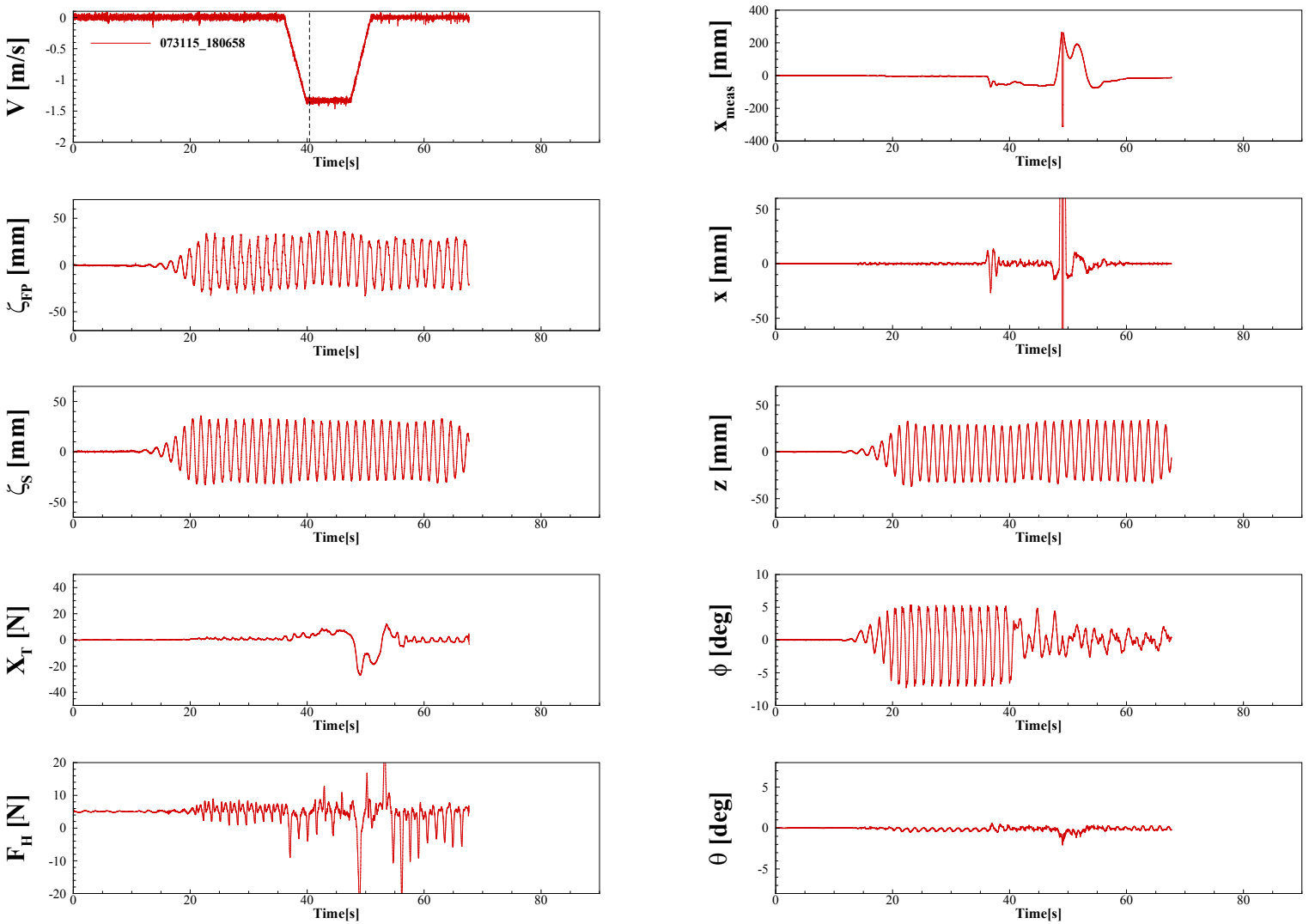

Figure C.28 Time Histories of measured and modified variables at Fr = 0.26, λ/L = 1.25, and χ = 90.0°

www.manaraa.com

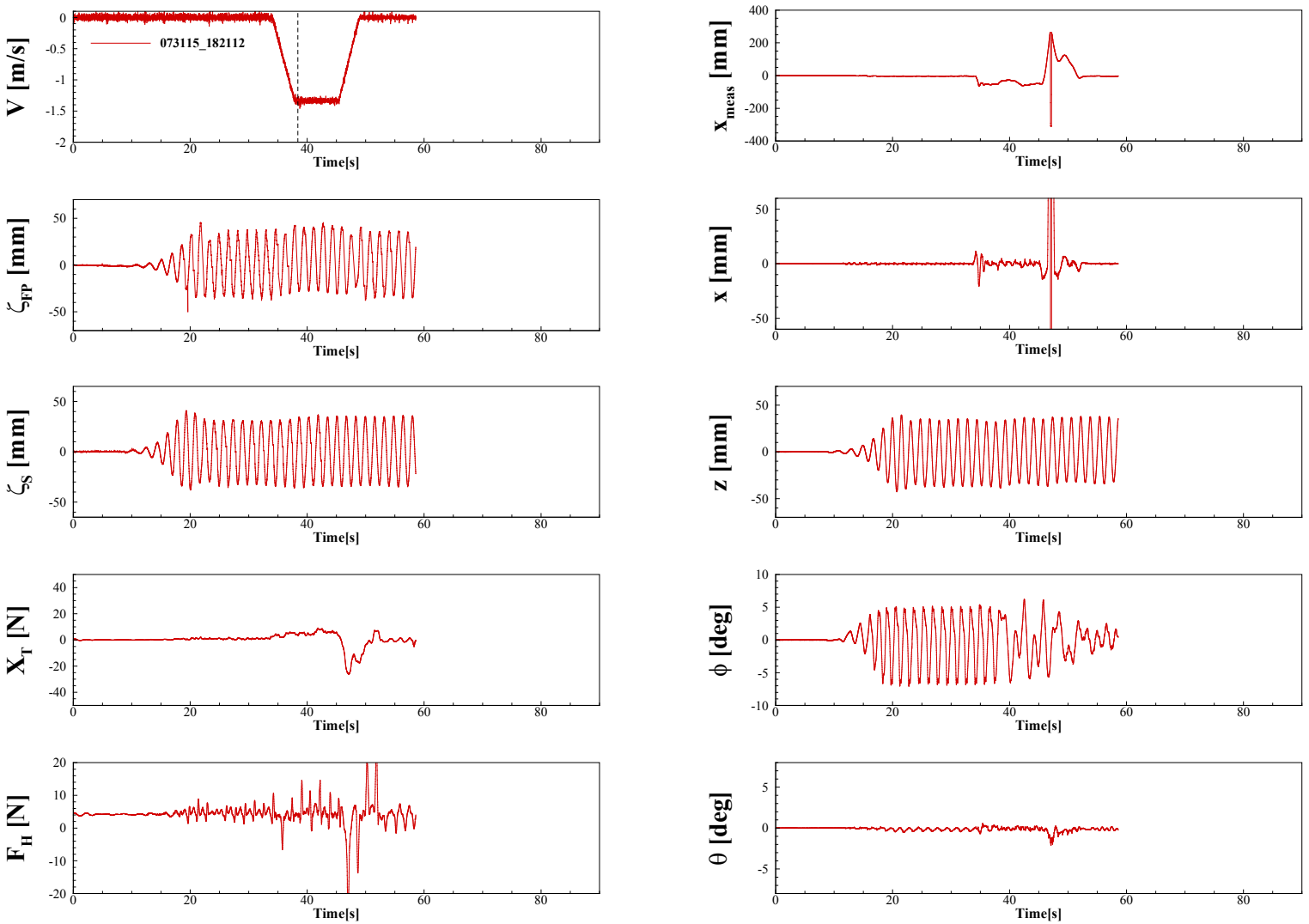

Figure C.29 Time Histories of measured and modified variables at Fr = 0.26, λ/L = 1.50, and χ = 90.0°

www.manaraa.com

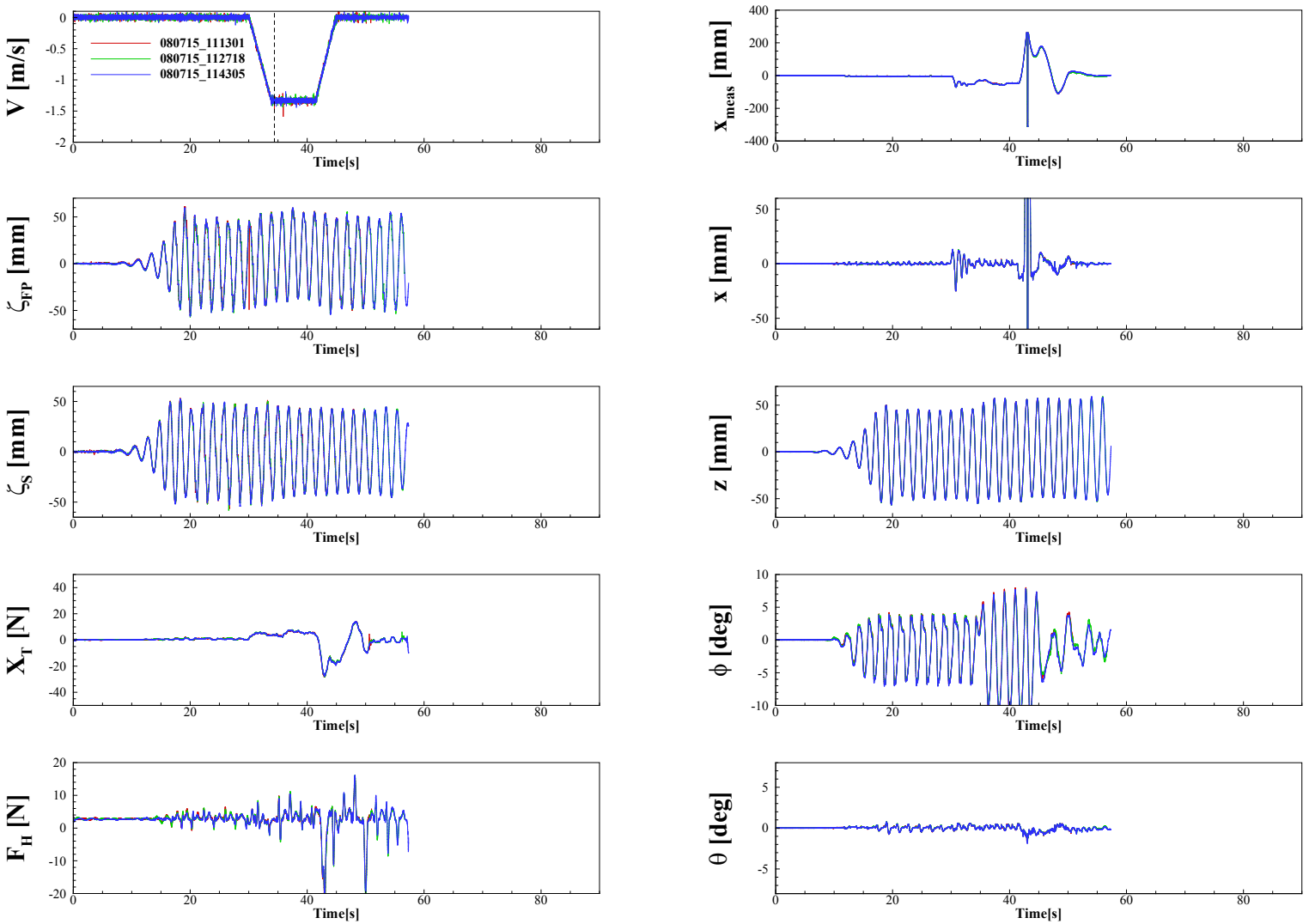

Figure C.30 Time Histories of measured and modified variables at Fr = 0.26, λ/L = 2.00, and χ = 90.0°

www.manaraa.com

C.4 Time Histories of Wave Cases, $\chi = 135^{o}$

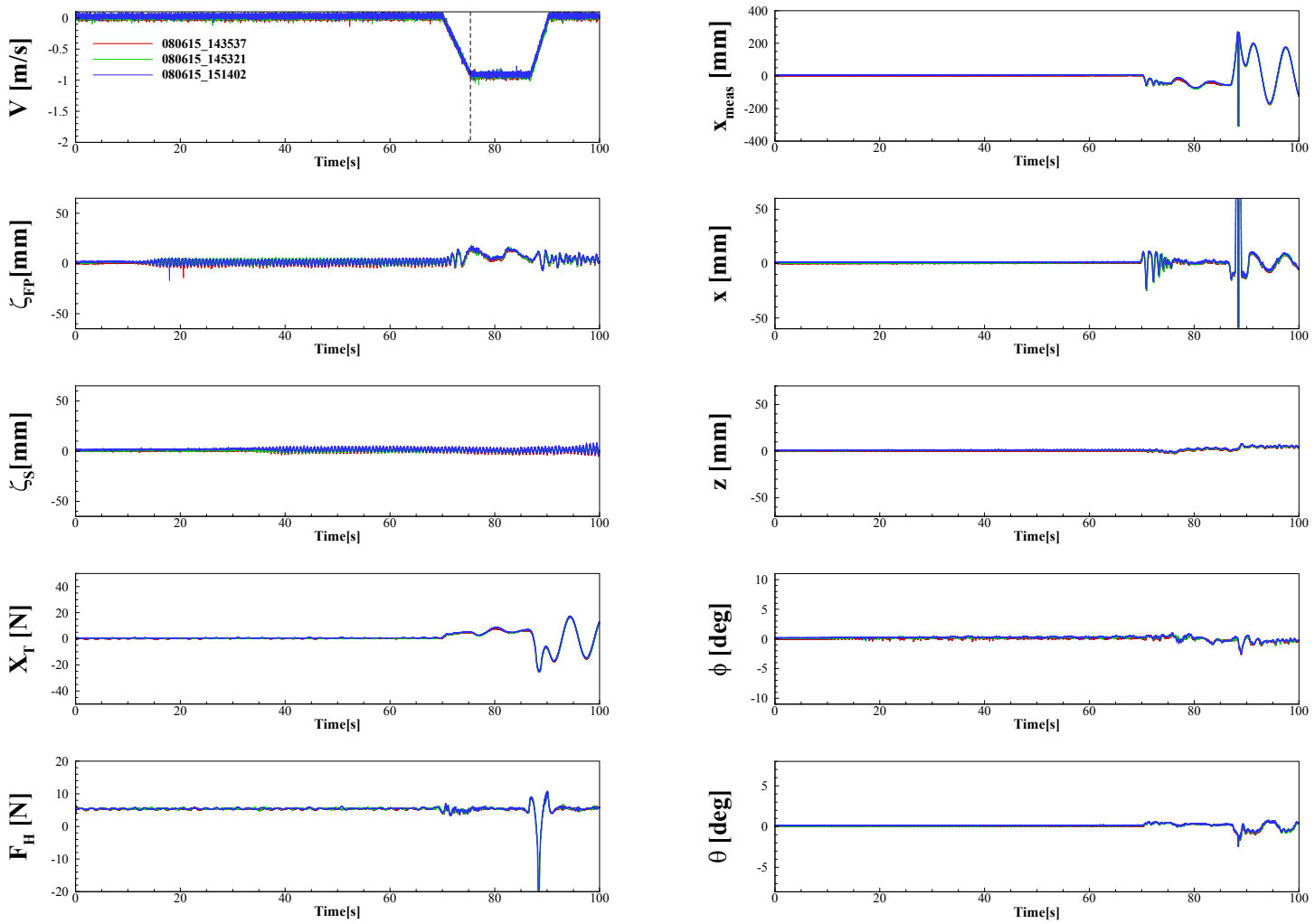

Figure C.31 Time Histories of measured and modified variables at Fr = 0.26, λ/L = 0.25, and $\chi = 135.0°$

www.manaraa.com

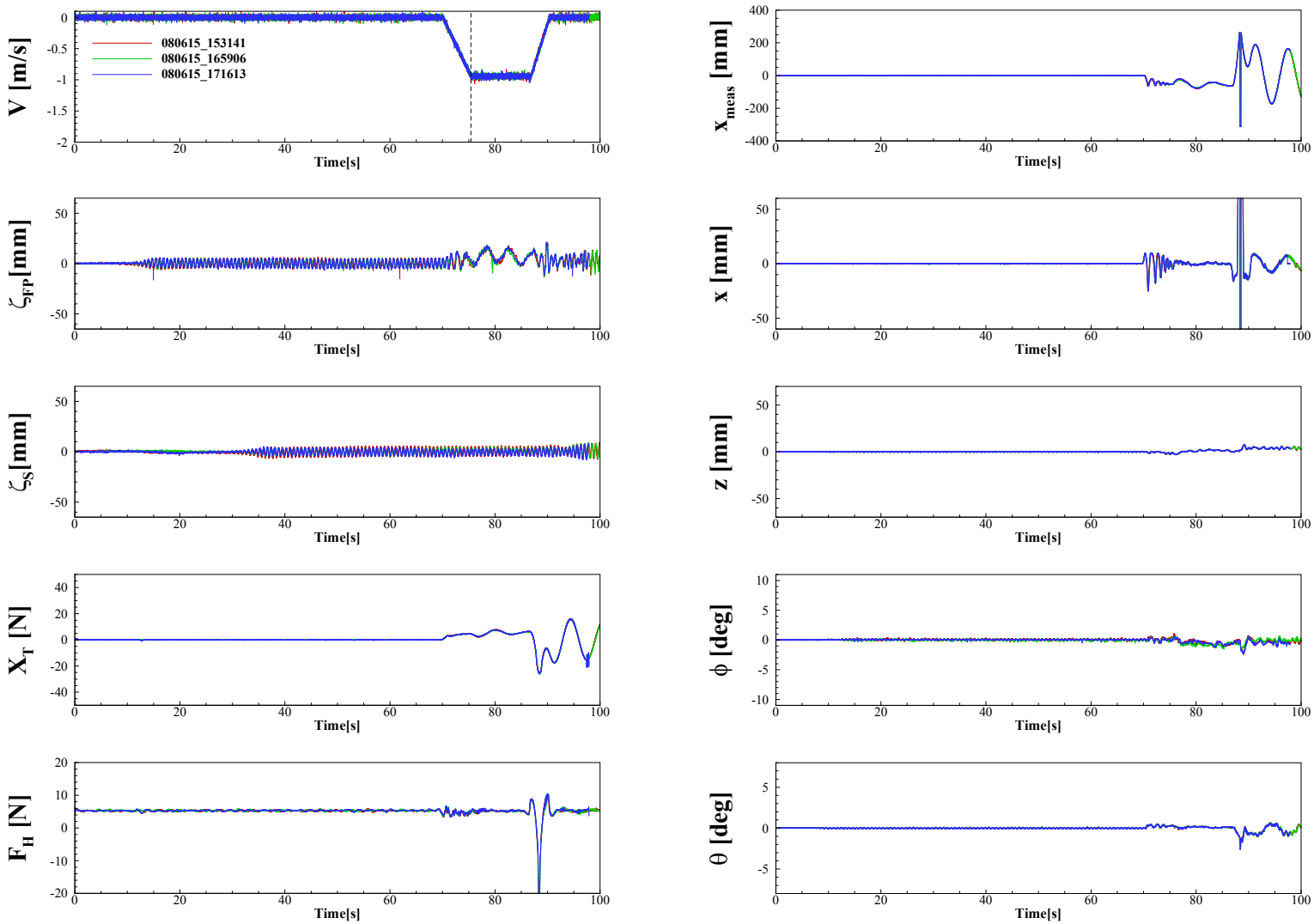

Figure C.32 Time Histories of measured and modified variables at Fr = 0.26, λ/L = 0.30, and χ = 135.0°

www.manaraa.com

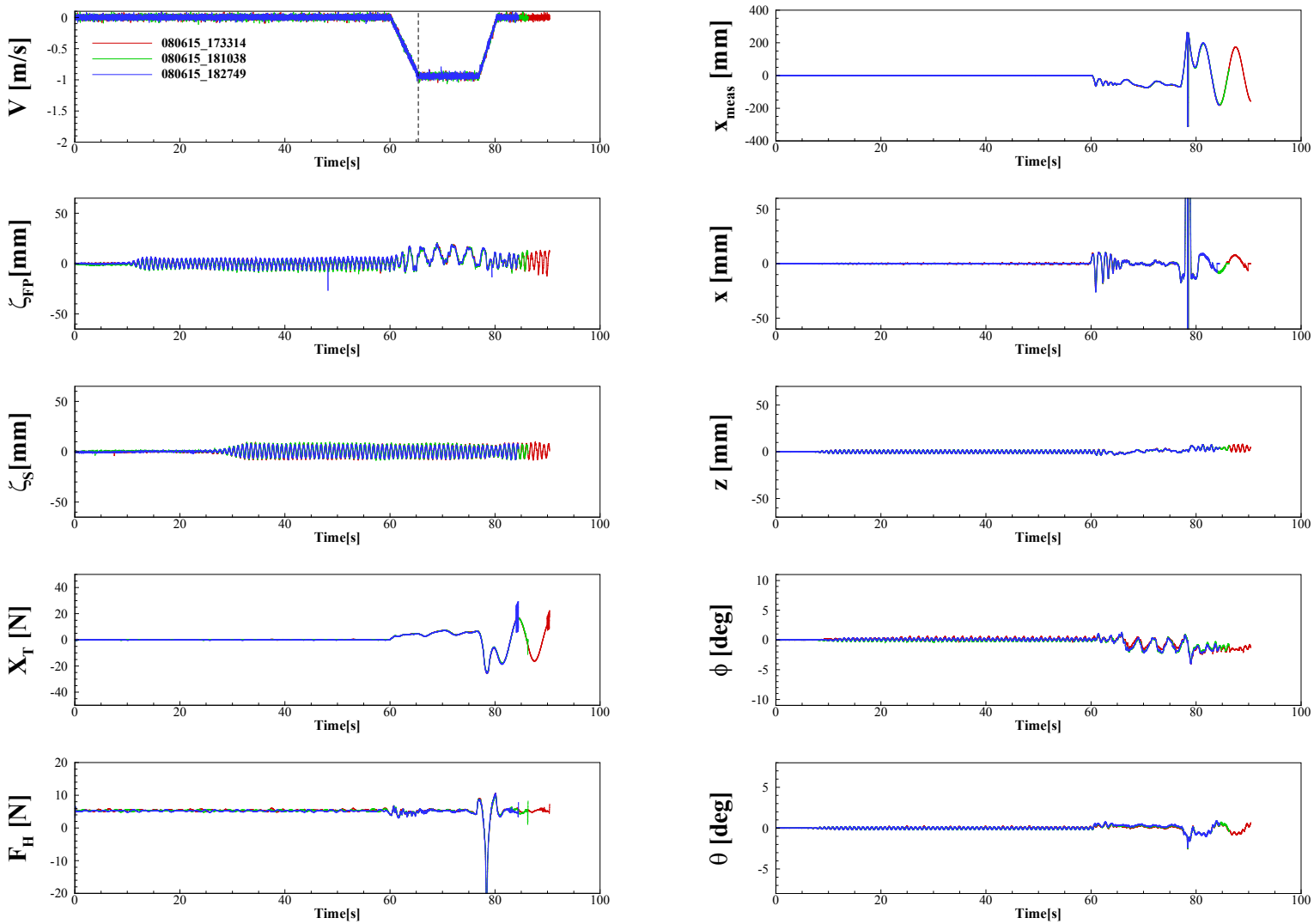

Figure C.33 Time Histories of measured and modified variables at Fr = 0.26, λ/L = 0.40, and χ = 135.0°

www.manaraa.com

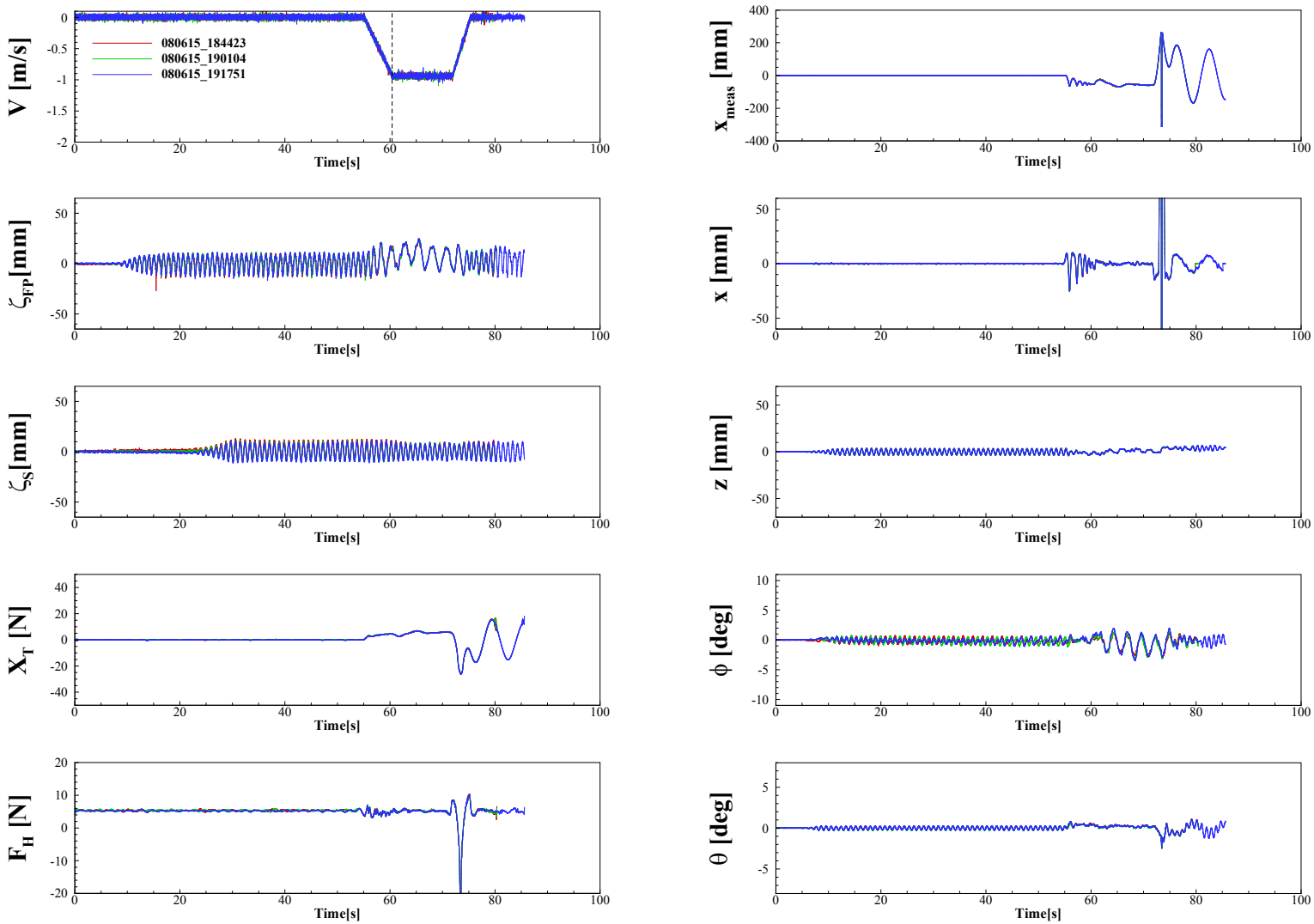

Figure C.34 Time Histories of measured and modified variables at Fr = 0.26, λ/L = 0.50, and χ = 135.0°

www.manaraa.com

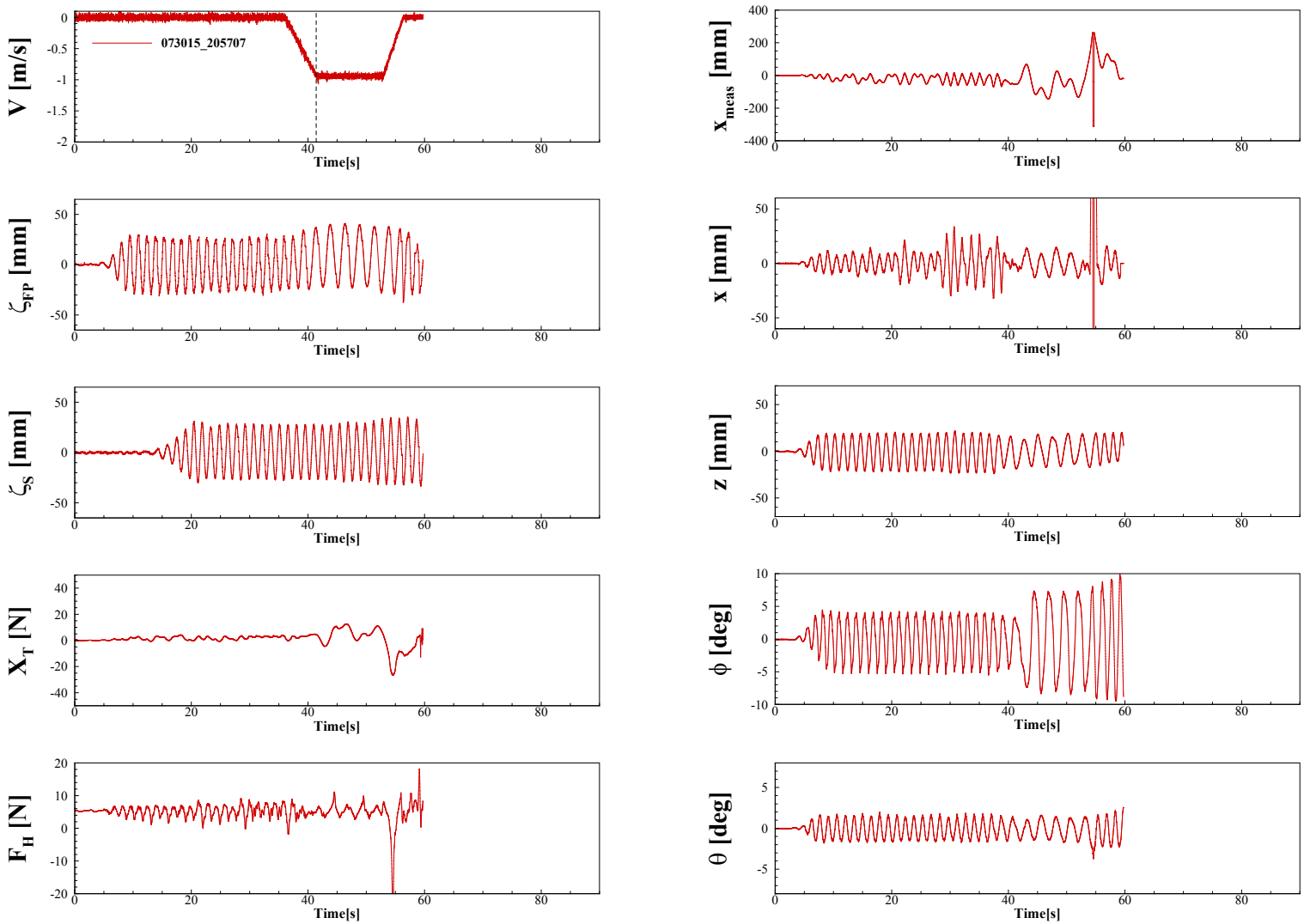

Figure C.35 Time Histories of measured and modified variables at Fr = 0.26, λ/L = 0.75, and χ = 135.0°

www.manaraa.com

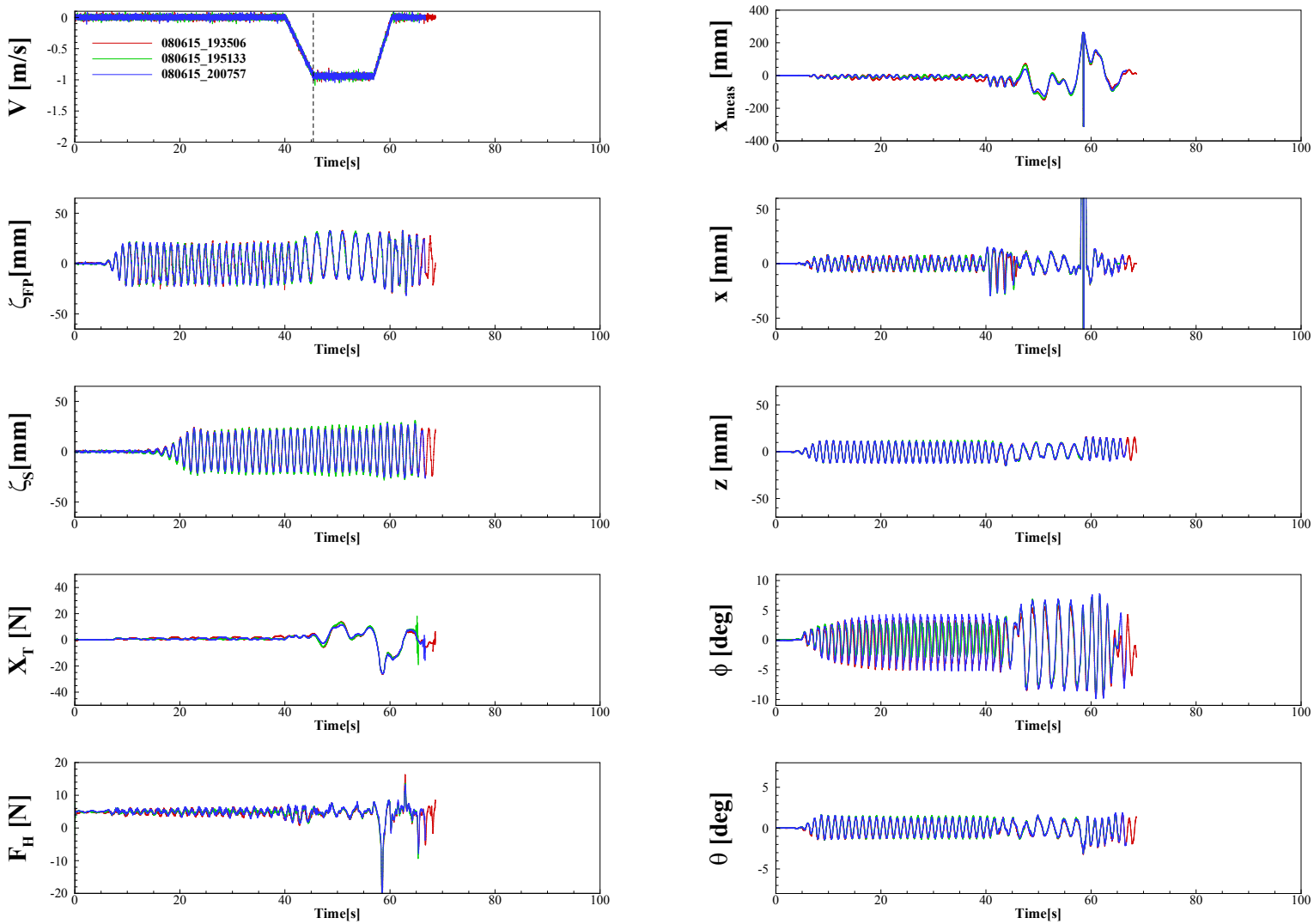

Figure C.36 Time Histories of measured and modified variables at Fr = 0.26, λ/L = 1.00, and χ = 135.0°

www.manaraa.com

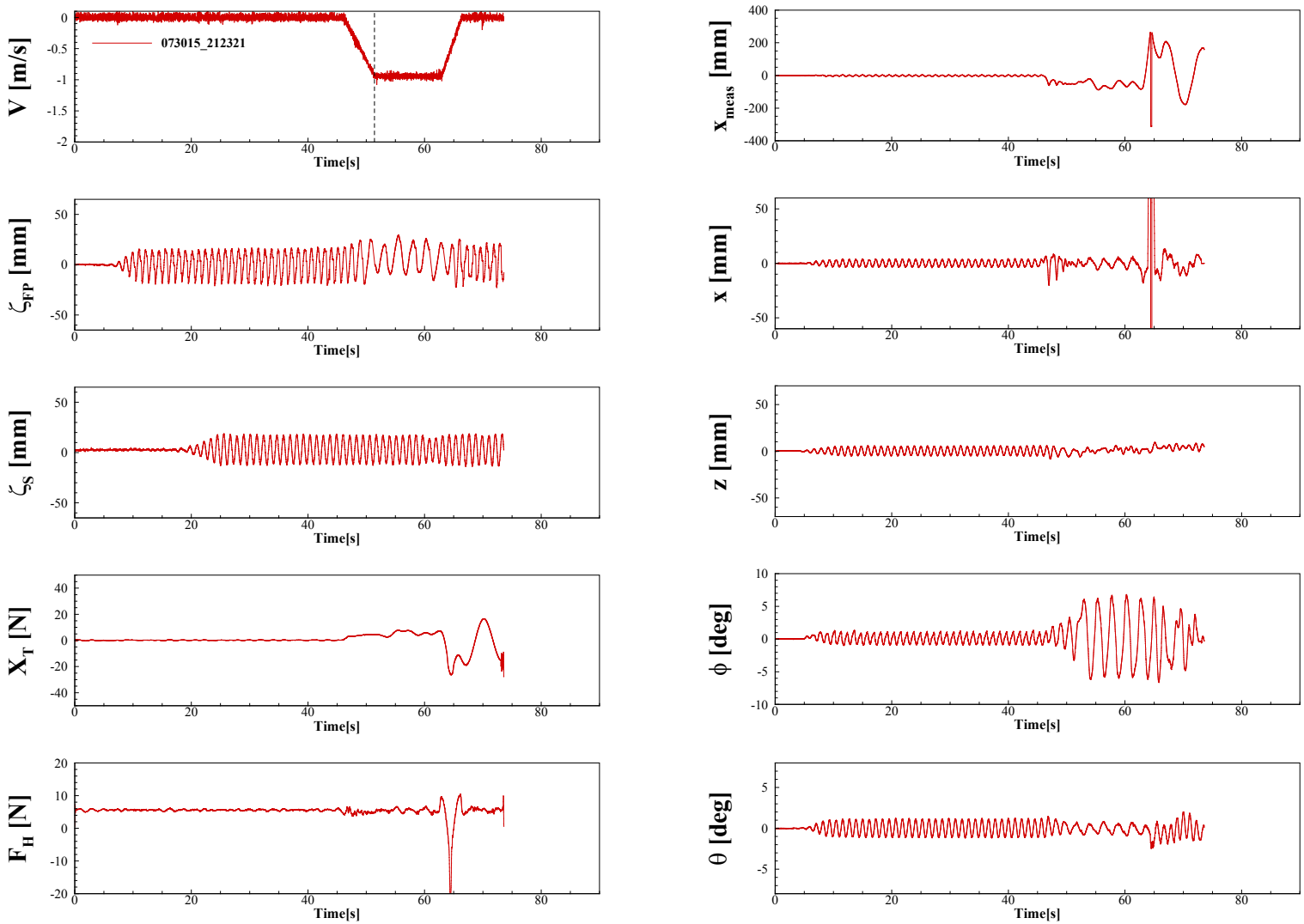

Figure C.37 Time Histories of measured and modified variables at Fr = 0.26, λ/L = 1.25, and χ = 135.0°

www.manaraa.com

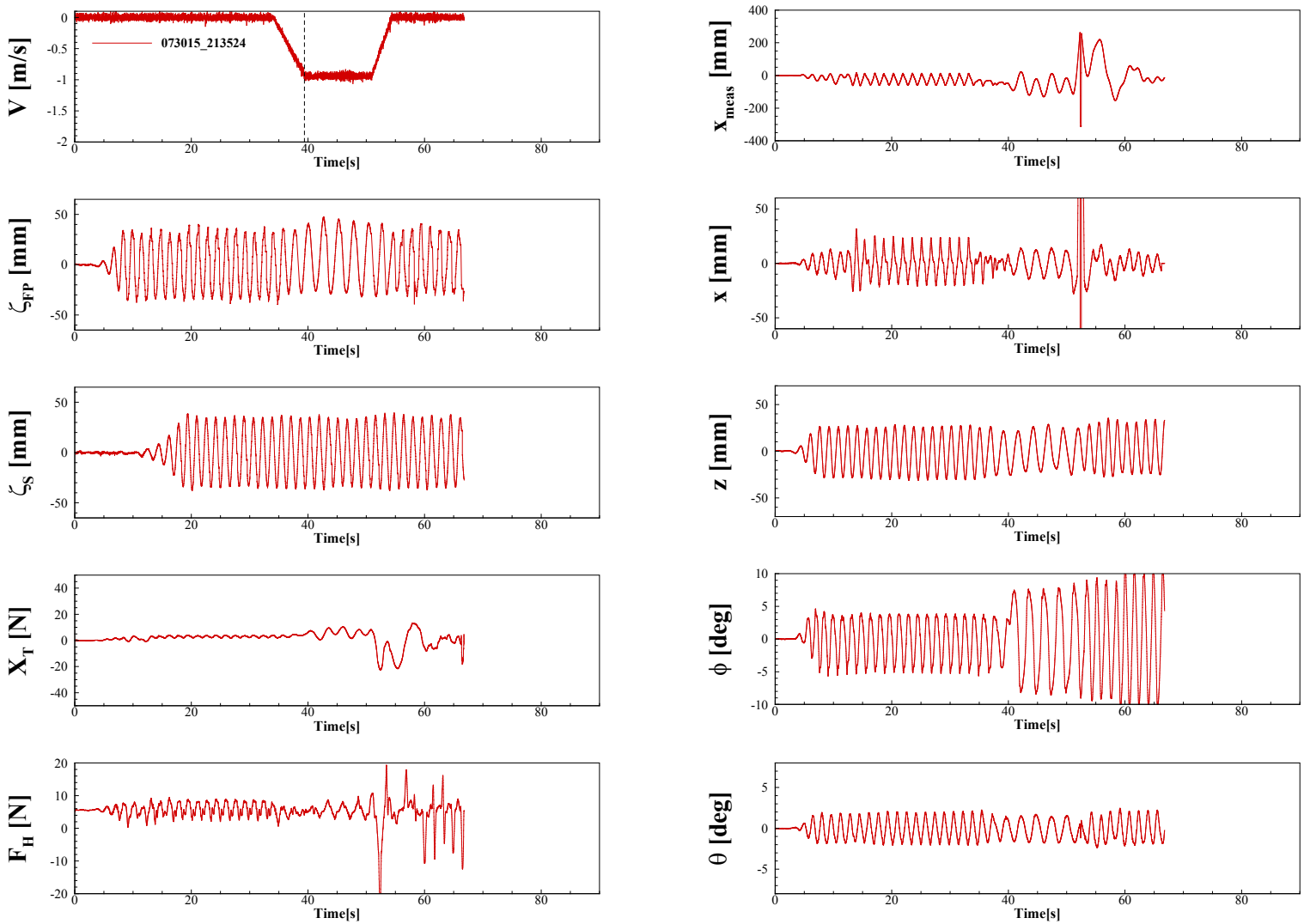

Figure C.38 Time Histories of measured and modified variables at Fr = 0.26, λ/L = 1.50, and χ = 135.0°

www.manaraa.com

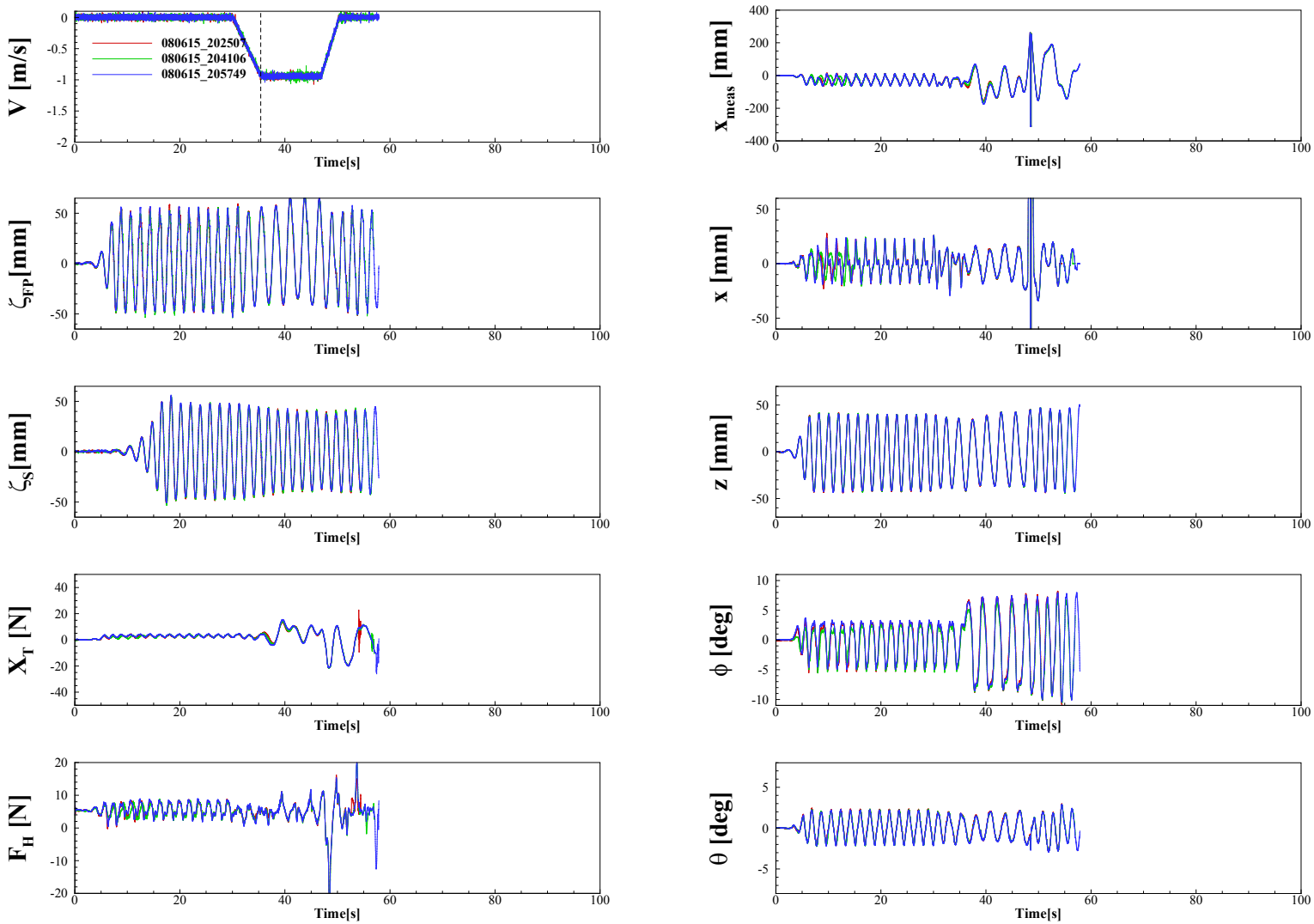

Figure C.39 Time Histories of measured and modified variables at Fr = 0.26, λ/L = 2.00, and χ = 135.0°

www.manaraa.com

C.5 Time Histories of Wave Cases, $\chi = 180^{o}$

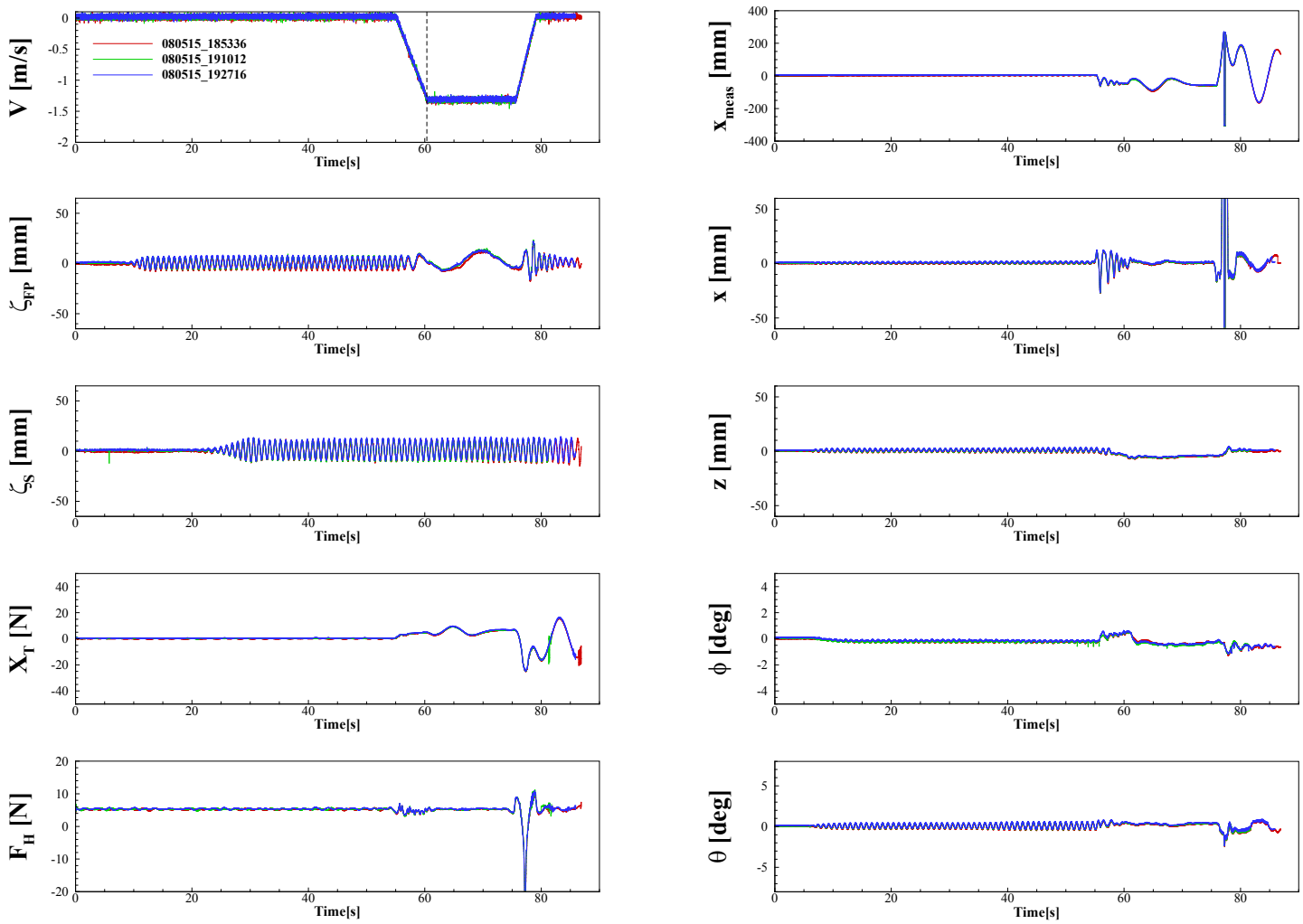

Figure C.40 Time Histories of measured and modified variables at Fr = 0.26, λ/L = 0.50, and $\chi = 180.0°$

www.manaraa.com

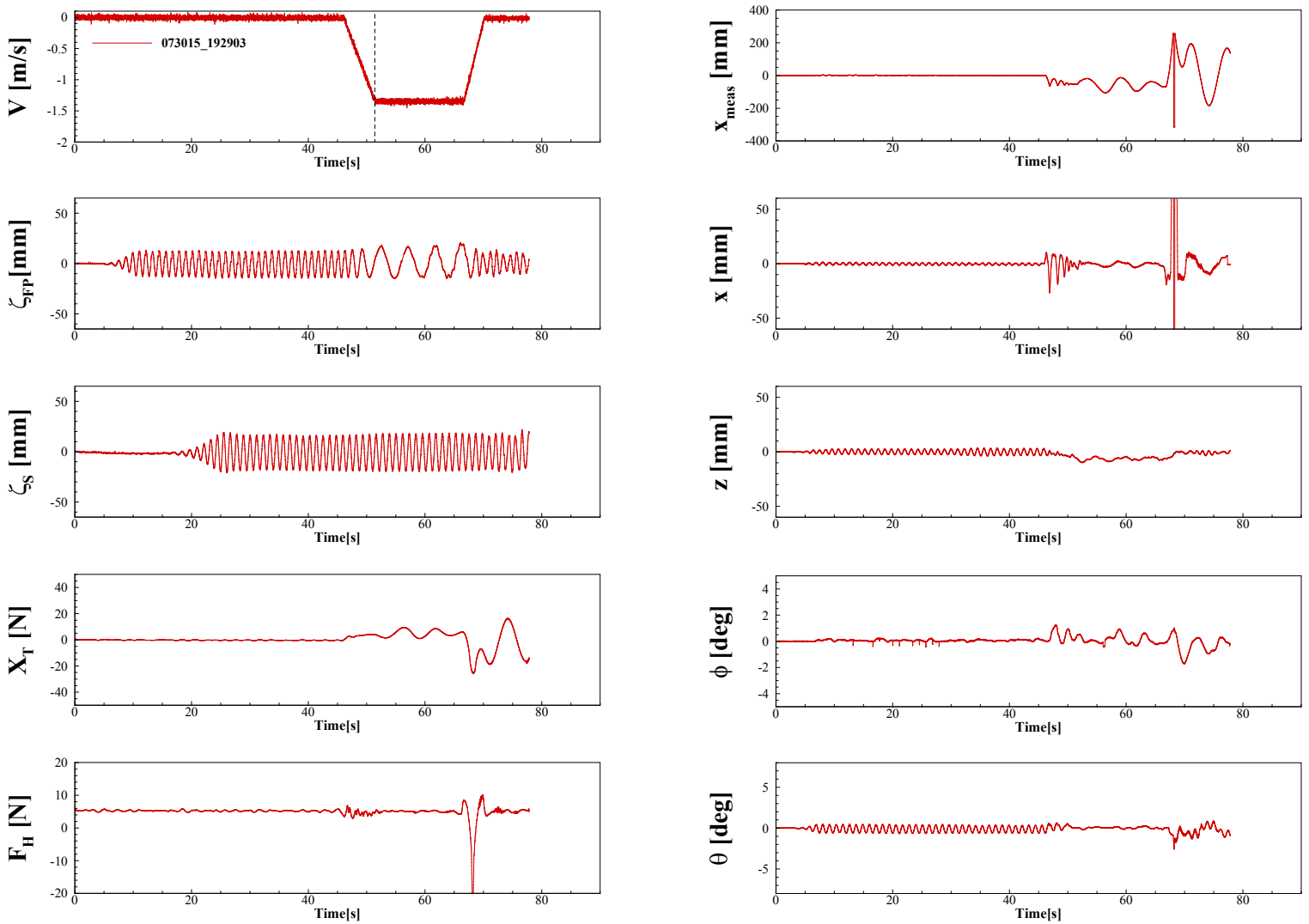

Figure C.41 Time Histories of measured and modified variables at Fr = 0.26, λ/L = 0.75, and χ = 180.0°

www.manaraa.com

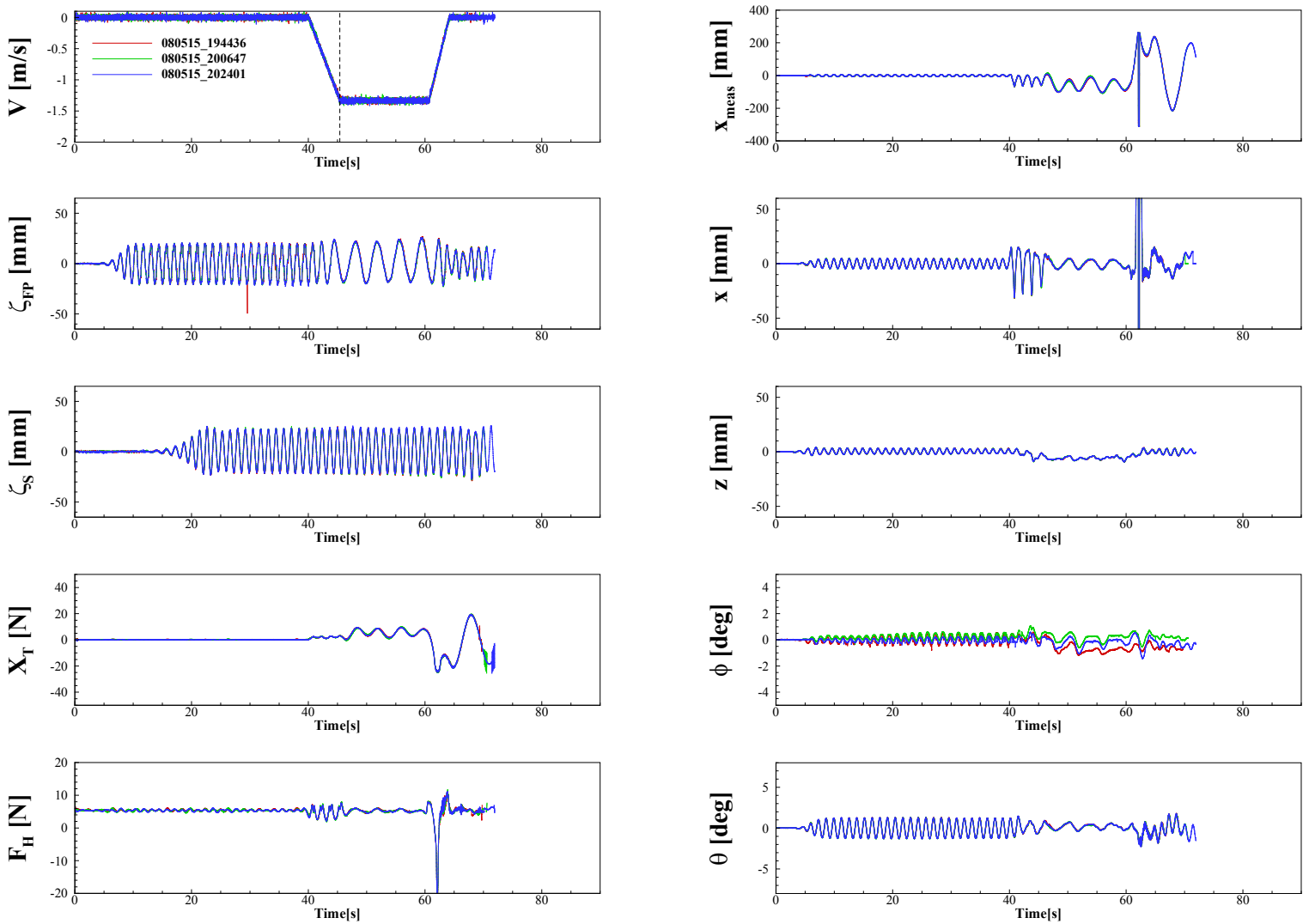

Figure C.42 Time Histories of measured and modified variables at Fr = 0.26, λ/L = 1.00, and χ = 180.0°

www.manaraa.com

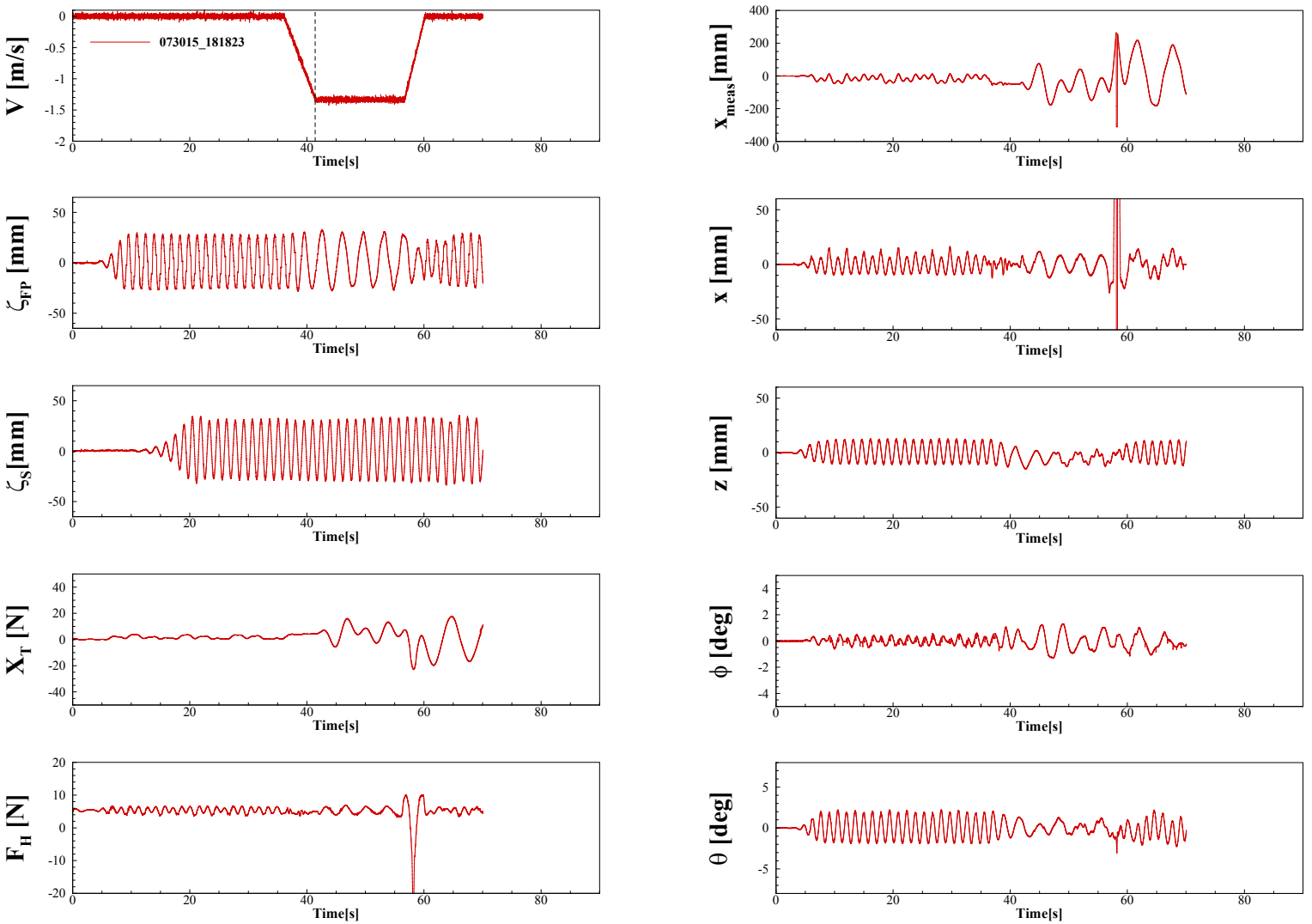

Figure C.43 Time Histories of measured and modified variables at Fr = 0.26, λ/L = 1.25, and χ = 180.0°

www.manaraa.com

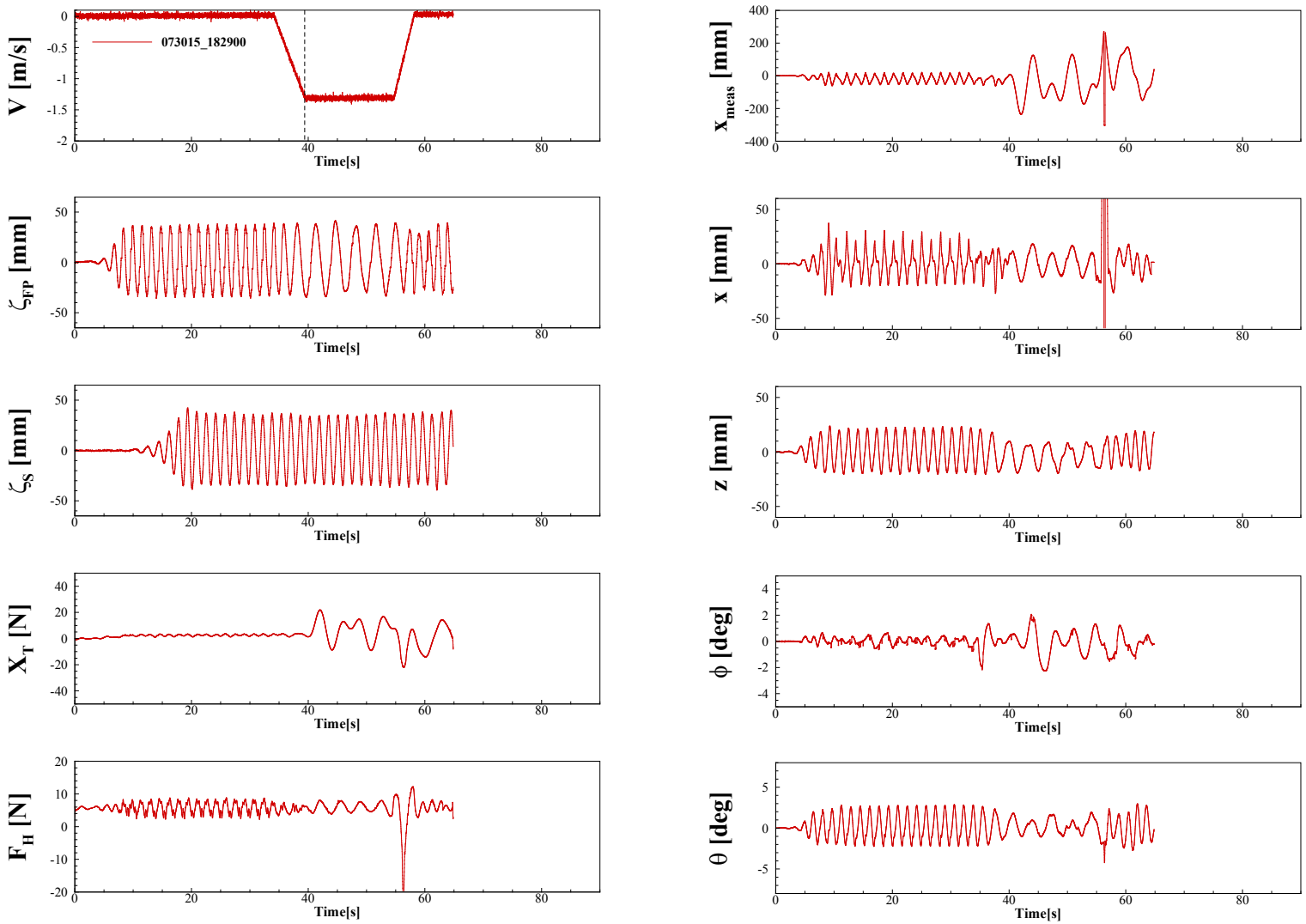

Figure C.44 Time Histories of measured and modified variables at Fr = 0.26, λ/L = 1.50, and χ = 180.0°

www.manaraa.com

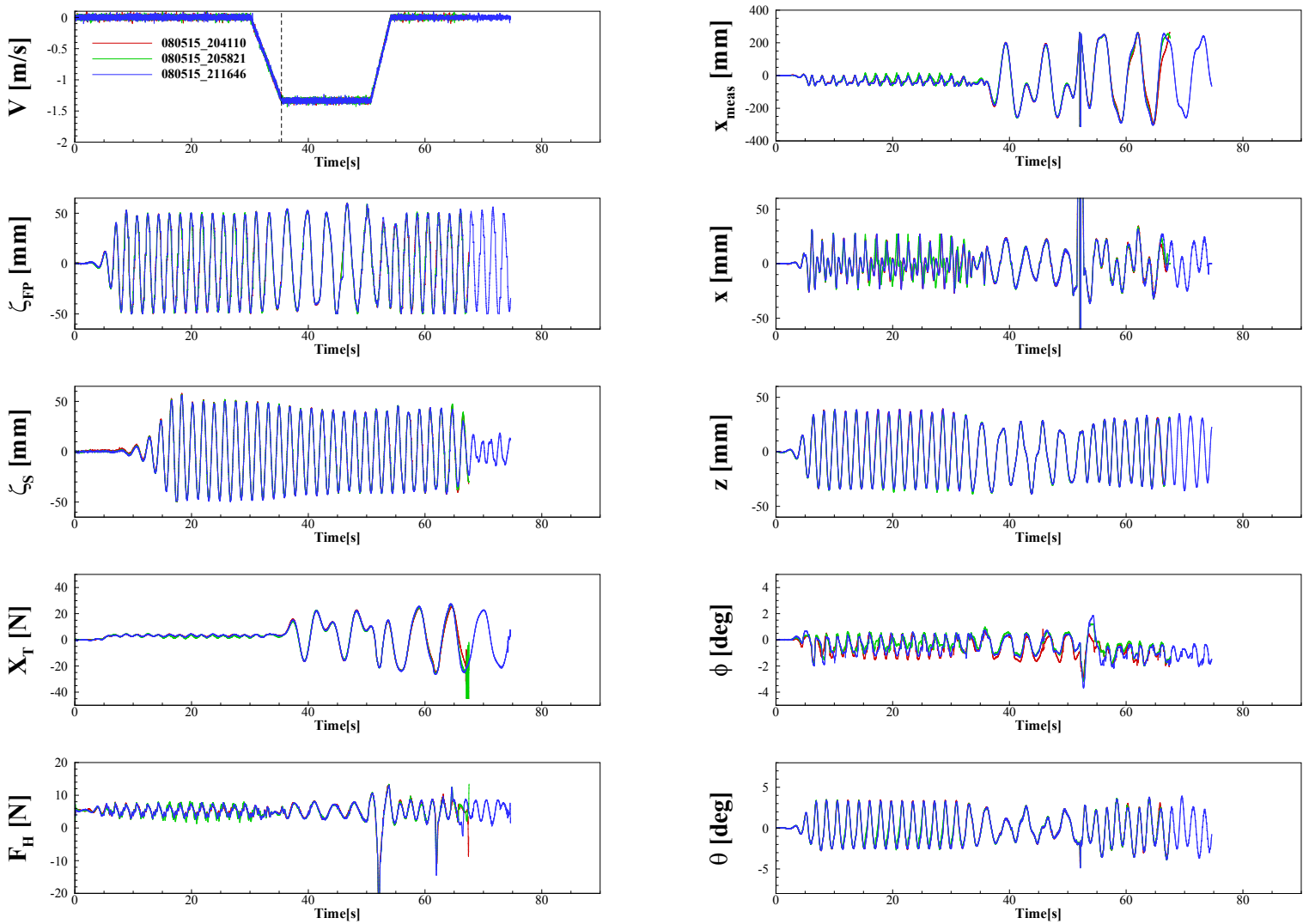

Figure C.45 Time Histories of measured and modified variables at Fr=0.26, λ/L=2.00, and χ=180.0°

www.manaraa.com

REFERENCES

AIAA Standard, 1999, Assessment of Experimental Uncertainty with Application to Wind Tunnel Testing, AIAA S-071A-1999, Washington, DC.

ASME, 1998, Test Uncertainty: Instruments and Apparatus, PTC 19.1-1998.

ASME, 2005, Test Uncertainty: Instruments and Apparatus, PTC 19.1-2005.

ASME, 2013, Test Uncertainty: Instruments and Apparatus, PTC 19.1-2013.

Abernethy, R. B., Benedict, R. P., and Dowdell, R. B., 1985, ASME Measurement Uncertainty, Journal of Fluids Engineering, 107, pp. 161-164.

Coleman, H., and Steele, G., 1989, Experimentation and Uncertainty Analysis for Engineers, Wiley, New York.

Elshiekh, Haitham Abdalla, 2014, Maneuvering characteristics in calm water and regular waves for ONR Tumblehome, MS (Master of Science) thesis, University of Iowa.

Fuji, H., Takahashi, T., 1975, Experimental Study on the Resistance Increase of a Ship in Regular Oblique Waves, Proceedings 14th ITTC, Vol. 4, pp. 351-360, Ottowa, Canada.

Fujisawa, J., Ukon, Y., Kume, K., and Takeshi, H., 2000, Local Velocity Measurements Around the KCS Model (SRI M.S. No. 631) in the SRI 400m Towing Tank, Ship Perf. Div. Rep. No. 00-003-2, SRI, Tokyo, Japan.

Otzen, J. F., 2013, Uncertainty Assessment for KCS Added Resistance in Waves, Force Technology Report No. 112-31859, report 1B, Lyngby, Denmark

Otzen, J. F., 2015, Uncertainty Assessment for KCS Added Resistance in Waves, Force Technology Report No. 112-31859, report 2A, Lyngby, Denmark.

IMO, 2006, Interim Guidelines for Alternative Assessment of Weather Criterion, International Maritime Organization, MSC.1/Circ.1200.

IMO, 2014, Third IMO Greenhouse Gas Study 2014 Executive Summary and Final Report, Suffolk, UK.

Irvine, M., Longo, J. and Stern, F., 2008, Pitch and Heave Tests and Uncertainty Assessment for a Surface Combatant in Regular Head Waves, Journal of Ship Research, 52, pp.146-163.

www.manaraa.com

JCGM 100:2008, 2008, Evaluation of Measurement Data – Guide to the Expression of Uncertainty in Measurements, Working Group 1 of the Joint Committee for Guides in Metrology (JCGM/WG1).

Kline, S. J., and McClintock, F. A., 1953, Describing Uncertainties in Single-Sample Experiments, Mechanical Engineering.

ITTC, 2008a, Testing and Extrapolation Methods, General Guidelines for Uncertainty Analysis in Resistance Towing Tank Tests, 7.5-02-02-02, pp. 1-16.

ITTC, 2008b, Uncertainty Analysis Instrument Calibration, ITTC – Recommended Procedures and Guidelines, 7.5-01-03-01, pp. 1-14.

ITTC, 2011, Seakeeping Experiments, 7.5-02-07-02.1, pp. 1-22.

ITTC, 2014, Example for Uncertainty Analysis of Resistance Tests in Towing Tanks, 7.5-02-02-02.1, pp.1-11.

Longo, J. and Stern, F., 2005, Uncertainty Assessment for Towing Tank Tests with Example for Surface Combatant DTMB Model 5415, Journal of Ship Research, 49, pp.55-68.

Sadat-Hosseini, Hamid et. al. Experiments and Computations for KCS Added Resistance for Variable Heading, 2015 World Maritime Technology Conference, Providence, Rhode Island, USA, 2015.

Sanada, Y., Tanimoto, K., Takaagi, K., Gui, L., Toda, Y., and Stern, F., 2013, Trajectories for ONR Tumblehome Maneuvering in Calm Water and Waves, Ocean Engineering Vol. 72, pp. 45-65.

Simonsen, C., Otzen, J., and Stern, F., 2008, EFD and CFD for KCS Heaving and Pitching in Regular Head Waves, Proc. 27th Symp. Naval Hydrodynamics, Seoul, Korea.

Simonsen, C. D., Otzen, J. F., Joncquez, S. and Stern, F., 2013, EFD and CFD for KCS Heaving and Pitching in Regular Head Waves, Journal of Marine Science and Technology, Vol. 18, pp 435-459.

Simonsen, C. D., Otzen, J.F., Nielson, C. and Stern F., 2014, CFD Prediction of Added Resistance of the KCS in Regular Head and Oblique Waves, 30th SNH, Hobart, Australia.

www.manaraa.com

Stern, F., Olivieri, A., Shao, J., Longo, J. and Ratcliffe, T., 2005, Statistical Approach for Estimating Intervals of Certification or biases of Facilities or Measurement Systems Including Uncertainties, ASME J. Fluids Eng., 127, pp. 604-610.

Stern, F., Sadat-Hosseini, H., Mousaviraad, M., Bhushan, S., 2014, Chapter 4: Evaluation of Seakeeping, Numerical Ship Hydrodynamics: An Assessment of the Gothenburg 2010 Workshop, Springer.

Yoon, H. Simonsen, C. D., Benedetti, L., Longo, J., Toda, Y., Stern, F., 2015, Benchmark CFD Validation Data for Surface Combatant 5415 in PMM Maneuvers – Part 1: Force/moment/motion Measurements, Ocean Eng. 109, pp. 705-734.

Wu, P., Okawa, Kim, H., Akamatsu, K., Sadat-Hosseini, H., Stern, F., Toda, Y., 2014, "Added Resistance and Nominal Wake in Waves of KVLCC2 Model Ship in Ballast Condition," 30th Symposium on Naval Hydrodynamics.

Zou, L. and Larsson, L., 2014, "Additional Data for Resistance, Sinkage and Trim", in Larsson et al.: "Numerical Ship Hydrodynamics - An Assessment of the Gothenburg 2010 Workshop," Springer Business Media, Dordrecht.

www.manaraa.com